1

2

3

4

5

Mechanisms of spinal cord degeneration and repair in multiple sclerosis: A 3T MRI study of the spinal cord.

8

Khaled Abdel-Aziz

10

11

12

13

14

15

16

17

18

19

NMR Research Unit,

Queen Square MS Centre

UCL Institute of Neurology,

Queen Square,

London, WC1N 3BG

25

Abstract

The spinal cord is a clinically eloquent structure, commonly affected in multiple sclerosis (MS) and spinal neuroaxonal loss is an important cause of non-remitting, disability progression. Neuroaxonal loss in MS is likely to be multifactorial and caused by several disease pathways. In contrast, repair and adaptive mechanisms can ameliorate disability following clinical relapses. This thesis has explored some of these clinically relevant disease mechanisms by combining single-voxel proton spectroscopy (MRS) and Q-space imaging (QSI), two advanced MRI techniques, which have increased pathological specificity for neurodegeneration and myelin, and allow quantification of metabolites that reflect biological mechanisms, to study spinal neurodegeneration and repair in MS.

In persons with early primary progressive MS (PPMS), spinal MRS and QSI exhibited increased sensitivity for detection of early disease changes than more conventional measures such as spinal cord atrophy and correlated with clinical disability measures suggesting these measures are functionally relevant. Region of interest analysis of the relationship between QSI indices in spinal white matter tracts and clinical scores which reflect the motor or sensory functions conveyed within those tracts, suggests a strong structure-function relationship exists between axonal integrity and disability.

In persons with relapsing remitting MS (RRMS), with recent (within 4 weeks) symptoms suggestive of spinal cord relapse, serial imaging with spinal MRS and QSI over 6 months reflected clinical changes over that time. Specifically, rising spinal concentrations of total N-acetyl-aspartate (tNAA) and restriction of QSI-derived perpendicular diffusivity, which I

hypothesise reflect, restoration of mitochondrial function and remyelination, respectively, underlie clinical recovery.

Within the RRMS cohort, MRS and QSI measures at baseline were predictive of clinical outcomes at 6 months; elevated baseline spinal glutamate-glutamine (Glx), myo-inositol (Ins) and total creatine (tCr) concentrations and increased QSI-derived perpendicular diffusivity predicted poor outcomes and may reflect important mechanisms of disability progression such as; demyelination, neurodegeneration, astrogliosis and altered neuronal metabolism. Taken together the results suggest that mechanisms of disability following spinal cord relapse are complex and glutamate excitotoxicity, gliosis and axonal metabolic dysfunction may be important determinants of residual disability following relapses.

This work suggests that newer, quantitative MRI techniques when applied to the spinal cord are sensitive markers of disease activity and progression and could be useful in monitoring therapies that aim to prevent neurodegeneration and enhance remyelination in MS.

Declaration

I, Khaled Abdel-Aziz, confirm that the work presented in this thesis is my own. Where work has been adapted from other sources, this has been indicated within my thesis.

The experiments performed in Chapter 4.1 were performed jointly with Dr Solanky, NMR research unit, UCL Institute of Neurology. Dr Solanky performed the statistical analyses for this chapter.

The colour-coded QSI maps in Chapters 5 and 6 were prepared by Dr Torben Schneider, NMR research unit, UCL Institute of Neurology.

I had help from Dr Cawley, NMR research unit, UCL Institute of Neurology who performed the brain volume measurements in Chapter 6.

The scripts used for quantification of brain tissue volumes in Chapters 5 and 6 were written by Dr Daniel Tozer, NMR research unit, UCL Institute of Neurology..

The Matlab scripts used for analysis of the posturography data were written and provided by Professor Day, Sobell Unit, UCL Institute of Neurology.

I performed the statistical analysis for Chapters 4.2, 4.3 and baseline data in Chapter 6. Dr Daniel Altmann (London School of Hygiene and Tropical Medicine) performed the statistical analyses for Chapter 5 and the longitudinal data in Chapter 6.

Publications associated with this thesis

Abdel-Aziz K, Schneider T, Yiannakas MC, Altmann DR, Wheeler-Kingshott CAM, Peters AL, Day BL, Thompson AJ and Ciccarelli O. Evidence for early neurodegeneration in the cervical cord of patients with primary progressive multiple sclerosis. Brain. 2015; 138 (6): 1568 - 82.

Abdel-Aziz K, Solanky BS, Yiannakas MC, Wheeler-Kingshott CAM, Altmann DR, Thompson AJ and Ciccarelli O. Age-related changes in metabolite concentrations in the normal spinal cord. Plos One. 2014; 9 (10): e105774

Abdel-Aziz K and Ciccarelli O. Rationale for Quantitative MRI of the Human Spinal Cord and Clinical Applications. In: Cohen-Adad J, Wheeler-Kingshott CAM, eds. *Quantitative MRI of the Spinal Cord*. 2014:3–21.

Kearney H, Yiannakas MC, Abdel-Aziz K, Wheeler-Kingshott CA, Altmann DR, Ciccarelli O and Miller DH. Improved MRI quantification of spinal cord atrophy in multiple sclerosis. J Magn Reson Imaging. 2014; 39 (3): 617-23

Solanky BS, Abdel-Aziz K, Yiannakas MC, Berry AM, Ciccarelli O, and Wheeler-Kingshott CAM. In vivo magnetic resonance spectroscopy detection of combined glutamate-glutamine in healthy upper cervical cord at 3T. NMR Biomed. 2013; 26 (3): 357-366

1 **Table of contents**

2

1

2

3

Abbreviations

AD	Axial diffusivity
ADC	Apparent diffusion coefficient
ALS	Amyotrophic Lateral Sclerosis
AP	Anterior posterior direction
BBB	Blood brain barrier
CDMS	Clinically definite multiple sclerosis
CI	Confidence interval
CIS	Clinically isolated syndrome
CNS	Central nervous system
CHESS	CHEmical Shift Selective
COV	Coefficient of variation
CRLB	Cramér Rao lower bounds
CSA	Cord cross sectional area
CSF	Cerebrospinal fluid
CT	Computer tomography
DIR	Double inversion recovery
DMT	Disease modifying therapy
DT	Diffusion tensor
DTI	Diffusion tensor imaging
DWI	Diffusion weighted imaging
EAE	Experimental allergic encephalomyelitis
EC	Eyes closed
EDSS	Expanded disability status scale

EO	Eyes open	
EPI	Echo planar imaging	
ETL	Echo train length	
FA	Fractional anisotropy	
FFE	Fast field echo	
FID	Free induction decay	
FLAIR	Fluid attenuated inversion recovery	
FOV	Field of View	
FSE	Fast spin echo	
FWHM	Full width at half maximum	
DTPA	Diethylenetriamine pentaacetic acid	
GABA	Gamma-Aminobutyric acid	
Gln	Glutamine	
Glu	Glutamate	
Glx	Glutamate + glutamine	
GM	Grey matter	
GMVF	Grey matter volume fraction	
HPT	9 hole peg test	
Ins	Myo-inositol	
MAS	Modified Ashworth score	
MD	Mean diffusivity	
MOIST	Multiply optimized insensitive suppression train	
MRI	Magnetic resonance imaging	
MRS	Magnetic resonance spectroscopy	
MS	Multiple sclerosis	

MSWS	Multiple sclerosis walking scale	
MtDNA	Mitochondrial DNA	
MTR	Magnetisation transfer ratio	
NAA	N-acetylaspartate	
NAAG	N-acetylaspartyl-glutamic acid	
NAWM	Normal appearing white matter	
NICE	National institute for clinical excellence	
NMR	Nuclear magnetic resonance	
OVS	Outer volume suppression	
P0	Zero displacement probability	
PD	Proton density	
PDF	Probability density function	
PPM	Parts per million	
PPMS	Primary progressive multiple sclerosis	
PRESS	Point resolved spectroscopy	
PSIR	Phase sensitive inversion recovery	
QSI	Q-space imaging	
RD	Radial diffusivity	
RF	Radio frequency	
ROI	Region of interest	
RRMS	Relapsing remitting multiple sclerosis	
SE	Standard error	
SNR	Signal-to-noise ratio	
SPMS	Secondary progressive multiple sclerosis	
STEAM	Stimulated echo acquisition mode	

1	**STIR**	Short tau inversion recovery
2		
3	**tCho**	Choline containing compounds
4		
5	**tCr**	Total creatine
6		
7	**TCA**	Total cord area
8		
9	**TCV**	Total cord volume
10		
11	**TE**	Echo time
12		
13	**TGMA**	Total grey matter area
14		
15	**TGMV**	Total grey matter volume
16		
17	**tNAA**	total N-acetylaspartate
18		
19	**TR**	Repetition time
20		
21	**TWT**	Timed walk test
22		
23	**VOI**	Volume of interest
24		
25	**VPT**	Vibration perception threshold
26		
27	**WM**	White matter
28		
29	**ZOOM**	Zonal oblique multi-slice
30		
31		
32		

1 **Figures**

2

1

1 **Tables**

2

Chapter One

Introduction to multiple sclerosis

1.1 Introduction

Multiple Sclerosis (MS) is a debilitating, multifocal, central nervous system (CNS) disorder of unknown aetiology, but is widely believed to be an autoimmune disease arising as a consequence of genetic-environmental interaction in at-risk individuals, and is the most common cause of disability of young people in the developed world (Compston and Coles, 2008).

The UK prevalence of MS is estimated to be around 125,000 people (Mackenzie *et al.*, 2014). Over the past few decades, the incidence has risen around the world, increasing the burden on patients, carers and healthcare systems. The socioeconomic impact of the disease is significant; from a patient perspective, each clinical relapse is associated with loss of earnings and a decline in health related quality of life and functional ability (Oleen-Burkey *et al.*, 2012). There are also significant costs to the national economy associated with healthcare provision, social services, diminishing productivity at work and earlier retirement, with one study estimating that the total lifetime costs of MS are in excess of £1 million per patient in the UK (McCrone *et al.*, 2008).

This introductory chapter will introduce the reader to MS and briefly cover aetiology, epidemiology, pathology, clinical course and diagnosis.

1.2 Aetiology

1.2.1 Genetic Factors

Evidence for a pre-determined genetic susceptibility to MS comes from familial studies which have compared disease recurrence rates amongst relatives of MS patients to the background population. Studies of European and North American populations have consistently shown an increased risk of approximately 3-5% amongst first degree relatives (Sadovnick and Baird, 1988; Carton *et al.*, 1997; Ebers *et al.*, 2000; Montomoli *et al.*, 2002). Concordance between monozygotic twins is approximately 30% (Ebers *et al.*, 1986; Sadovnick *et al.*, 1993), whilst in dizygotic pairs, rates of 3-5% are typically seen, equal to non-twin first degree relatives (James, 1982; Kinnunen *et al.*, 1988; Mumford *et al.*, 1994). The marked drop in recurrence risks between monozygotic and other first degree relatives, strongly suggests that MS is a polygenic disorder. A study looking at familial risk in non-biological relatives, looked at 1201 relatives of patients with MS and found only a single case which might be expected in the general population, suggesting environment alone, without genetic susceptibility is insufficient to trigger the onset of MS (Ebers *et al.*, 1995). The human leukocyte antigen (HLA) DRB1*1501 has been consistently associated with MS and exerts the largest known genetic contribution to MS susceptibility in Caucasian, Northern Europeans (Martin *et al.*, 1992; Fukazawa *et al.*, 2000).

1.2.2 Environmental factors

The global distribution of MS cannot readily be explained by genetics alone. MS prevalence follows a latitude gradient suggesting environmental factors also play a role. An Australian study of disease prevalence in Australia and New Zealand shows MS prevalence increasing three-fold from the North (35°S) to the South (48°S) independently of ethnic background

(Taylor *et al.*, 2010). The latitude gradient for MS prevalence, where those living at higher latitude are at increased risk of MS has been demonstrated in both Northern and Southern hemispheres (Miller *et al.*, 1990; Vukusic *et al.*, 2007; Ramagopalan *et al.*, 2011) and MS risk is seen to drop on migration from high to low latitudes (Gale and Martyn, 1995).

The strong correlation between latitude and MS prevalence has increased interest in vitamin D, which is produced in the skin following sunlight exposure as an important environmental factor determining MS risk. This hypothesis might explain why the prevalence of MS in some communities living at higher latitudes but have a diet rich in fatty fish which are rich in vitamin D have lower than expected risk of MS (Ascherio *et al.*, 2010). Additionally variability in UVB exposure and vitamin D status during pregnancy may explain why season of birth effects MS risk (Disanto *et al.*, 2012). Vitamin D specifically interacts with HLA-DRB1*1501 to influence its expression which provides a potential explanation for the mechanisms by which vitamin D might modulate MS risk (Ramagopalan *et al.*, 2009).

An autoimmune response to a viral infection has also been proposed as an aetiological explanation for MS (Granieri and Casetta, 1997). Epstein Barr virus (EBV) is one of several infective agents that have been suggested to be linked with MS. Rates of EBV seropositivity approach 100% in MS patients compared to 90% in the general population (Bray *et al.*, 1983; Munch *et al.*, 1998; Wandinger *et al.*, 2000). Additionally, geographical incidence of hospital admissions for infectious mononucleosis (IM), which is caused by EBV compares to the incidence to that of admissions for MS found that geographical distributions of IM and MS are significantly correlated (Ramagopalan *et al.*, 2011).

There is now also a substantial body of evidence that suggests that tobacco smoking is a modifiable environmental risk factor in MS. The reported effects of smoking in MS vary with study design. In a small study looking at immediate effects of smoking on motor function, twenty one patients were exposed to cigarette smoke, and of those, sixteen patients experienced a transient deterioration in their motor function immediately after smoking, lasting for ten minutes (Emre and de Decker, 1992). Several retrospective studies have found an accelerated transition from RRMS to SPMS in ever smokers (Hernan *et al.*, 2005; Koch *et al.*, 2007) and accelerated cognitive decline in heavy smokers (Ozcan *et al.*, 2014). Whilst in a retrospectively designed study of Austrian CIS patients, smoking was associated with a higher risk of conversion to clinically definite MS (HR =1.8; C.I. 1.2-2.1) (Di Pauli *et al.*, 2008).

Fewer prospective studies have reported on smoking risk in MS. A study of 368 patients looking at the effects of smoking on MRI measures, smoking was associated with higher EDSS, more contrast enhancing brain lesions, larger T1 and T2 lesion volumes and lower brain parenchymal fractions in smokers than non-smokers, after adjusting for demographic factors and treatment duration (Zivadinov *et al.*, 2009). Another prospectively designed cohort study from Southern Tasmania, showed smoking was associated with increased progression of clinical disability (Pittas *et al.*, 2009).

1.3 Epidemiology

MS is a global disease with an estimated 2.5 million affected people worldwide. The lifetime risk is thought to be approximately 1 in 400, making MS the commonest cause of progressive neurological disability affecting young people (Compston and Coles, 2002), but as discussed earlier, distribution of MS globally is not even. Although comparison of prevalence studies from different parts of the world is limited by differences in the sophistication of medical and diagnostic services, highest disease prevalence is consistently seen in Europe between 65 ° and 45 ° North latitude, the Northern United States and Southern Canada, New Zealand, and Southern Australia. Southern European, Northern Australian and South American populations carry an intermediate risk, whilst MS prevalence in Africa and Asia is relatively low (Kurtzke, 1977).

1.4 Pathology of Multiple Sclerosis

The pathological hallmarks of MS are the multi-focal MS lesions which occur in the cerebral grey and white matter as well as the spinal cord and consist of focal demyelination, inflammation, gliosis, and variable axonal destruction (Popescu and Lucchinetti, 2012).

1.4.1 Inflammation

In health, the blood–brain barrier (BBB) separates the brain and spinal parenchyma from circulating leucocytes and their inflammatory mediators (Pachter *et al.*, 2003). It is composed of densely arranged endothelial cells with tight junctions along the length of the capillary network within the CNS. Endothelial cells are supported by astrocytes within the CNS (Minagar and Alexander, 2003) and the tight junctions act to prevent passage of large molecules into the parenchyma. In health, the tight junctions prevent the entry of immune cells from the periphery and there is limited risk of local immune reactions, which is thought

to be due to the low expression of major histocompatibility complex (MHC) molecules by antigen-presenting cells.

In MS, pro-inflammatory cytokines produced by activated auto-reactive CD4+ cells are able to activate adhesion molecules (ICAM-1 and VCAM-1) within the endothelial cells at the BBB. Activated auto-reactive CD4+ cells express the respective counter receptors (LFA-1 and VLA-4), which allows them to adhere to the endothelium of the BBB; following adhesion, they transmigrate into the brain parenchyma through cerebrovascular endothelial cells (Engelhardt and Ransohoff, 2005; Komiyama *et al.*, 2006). Production of proteolytic enzymes by CD4+ cells and other co-ordinating inflammatory cells causes a breach in the integrity of the BBB which allows entry of circulating CD8+ T-cells, B-cells monocytes and mast cells from the periphery. Once CD4+ have access to the CNS, they become locally re-activated (Flugel *et al.*, 2001) and release pro-inflammatory chemokines and cytokines which is thought to be the first step in the formation of a new MS lesion. Activation of astrocytes and microglia is then implicated in phagocytosis of myelin which serves to amplify the local inflammatory response, propagating further injury and setting up a pro-inflammatory loop (Compston and Coles, 2002).

B-cells can only cross the BBB at sites where its integrity has been disrupted by focal inflammation. Once they enter the CNS, there is some evidence that they are involved in the pathogenesis of MS. Firstly, intrathecal synthesis of clonal IgG in the CSF, but not the serum (which gives rise to oligoclonal bands), increases during MS exacerbations and is less frequently observed in patients who run a more benign disease course (Zeman *et al.*, 1996). Secondly, B-cell depletion with the anti-CD20 monoclonal antibody, Rituximab, reduces

relapse rates and formation of new gadolinium-enhancing lesions on MRI (both markers of disease activity) (Hauser *et al.*, 2008).

The acute MS lesion is characterised by marked perivenous infiltration of lymphocytes and large numbers of macrophages and clonally expanded memory B cells in lesions which suggests binding to a specific antigen (Baranzini *et al.*, 1999). Oligodendrocyte apoptosis and demyelination associated with microglia activation occurs early (Barnett and Prineas, 2004). During the months following lesion formation, the cellular composition of the plaque changes and chronic plaques may show 'smouldering inflammation', but are often devoid of inflammatory cells and characterised by loss of myelin and axons, with relative increases in astrocytes, and gliotic tissue changes.

An ongoing controversy within the MS research community relates to whether or not the inflammatory response seen in MS is a secondary phenomenon to a primarily neurodegenerative disease process (Trapp and Nave, 2008; Stys *et al.*, 2012). The "inside-out model" of MS (Stys *et al.*, 2012), that has been proposed, hypothesises that an initial degenerative process affects the myelin sheaths and oligodendrocytes and it is the host's immune response to the highly autoantigenic break down products (Kanter *et al.*, 2006; Moscarello *et al.*, 2007) that lead to the inflammatory attacks which are characteristic of MS.

1.4.2 Axonal Degeneration

Axonal injury in MS has been noted ever since the earliest descriptive pathological studies of the disease and is now known to occur early in the disease course (Brex *et al.*, 2000; Filippi *et al.*, 2003). In acute lesions, the number of infiltrated microglia, macrophages and CD8+ T

cells correlates with axonal injury (Bitsch *et al.*, 2000) but axonal injury continues to develop in chronic lesions, once inflammation ebbs (Kornek *et al.*, 2000) and in chronic established lesions axonal density is reduced on average by 60–70% (Mews *et al.*, 1998; Bjartmar *et al.*, 2000). Axonal injury in MS is size selective; small calibre axons are more vulnerable to injury compared to thicker axons. Thus, in inactive chronic MS lesions thick axons are better preserved than thin ones (Evangelou *et al.*, 2001). Histopathological studies have demonstrated that within NAWM, both axonal density and volume are also reduced by an average of 33% and 53% respectively, compared to aged matched controls (Evangelou *et al.*, 2000). Mechanisms of axonal loss in MS are discussed in greater detail in Section 1.5.

1.4.3 Normal Appearing White Matter and "Dirty appearing" white matter

The term 'normal appearing white matter' (NAWM) in imaging studies has been defined to mean the white matter closest to and surrounding an MS plaque that is not abnormal in signal intensity on T2-weighted images (Guo *et al.*, 2001). NAWM has assumed increased importance over the past 30 years as it is thought that damage at these sites might explain the poor correlation between the location and size of MS plaques and clinical disability (see 'clinico-radiological paradox', Section 3.2.5).

Macroscopically invisible pathology within these tissues can be detected using sophisticated quantitative MRI techniques including magnetization transfer imaging which shows reduced MTR thought to represent changes in myelination (Leary *et al.*, 1999). A decrease in NAA concentration seen on spectroscopy (Fu *et al.*, 1998) suggestive of axonal loss and changes seen in diffusion characteristics suggesting abnormalities in the microstructural integrity of the tracts in these regions (Werring *et al.*, 1999).

Histological examination of NAWM reveals demyelination, infiltration of macrophages filled with myelin, axonal spheroids, microglial cells with increased expression of MHC class I and II molecules, gliosis and some remyelination (Allen and McKeown, 1979; van Waesberghe *et al.*, 1999; Vos *et al.*, 2005). The axonal loss in NAWM can be variable and is thought to be partly explained by Wallerian degeneration following axonal transection in focal lesions (Evangelou *et al.*, 2000; Lassmann, 2003).

1.4.4 Spinal Cord

Spinal cord involvement in MS is almost absolute, with one post-mortem study of MS patients from the United States, reporting spinal cord plaques in 99% of spinal cord samples (Ikuta and Zimmerman, 1976). Demyelinating lesions within the spinal cord show preponderance for the cervical cord, with the upper thoracic segment being the second most likely to be involved (Kidd *et al.*, 1993). Lesions most frequently affect the lateral columns, followed by the posterior columns, with most cord atrophy occurring in the cervical cord (Oppenheimer, 1978; Bjartmar *et al.*, 2000; Gilmore *et al.*, 2006).

Pure grey matter lesions in the spinal cord account for approximately 22% of all spinal cord lesions, with pure white matter lesions making up 33% and mixed white matter/grey matter lesions making 45% (Gilmore *et al.*, 2006). The majority of atrophy seen in the cord is thought to be due to volume loss within the white matter compartment (Gilmore *et al.*, 2005), where up to 84% of axons within chronic lesions may be lost (Bjartmar *et al.*, 2000). Interestingly, Gilmore *et al* reported no difference in grey matter volumes in the spinal cord between MS patients and healthy controls (Gilmore *et al.*, 2005).

1.5 Mechanisms of Neurodegeneration

1.5.1 Inflammatory demyelination and axonal damage

Within the active MS lesion, high numbers of transected axons can be seen (Trapp *et al.*, 1998). Trapp *et al* found that inflammatory infiltrates consisting of macrophages and activated microglia are seen in close contact with axons, that show signs of injury and that axonal loss correlated with inflammation and demyelination. It is therefore likely that one mechanism of axonal loss in MS is the consequence of direct immunologic attack on axons, from soluble inflammatory mediators, or from secondary effects of chronic demyelination (Trapp *et al.*, 1998). In acute lesions, the number of infiltrated microglia, macrophages and CD8+ T cells correlates closely with the degree of axonal injury (Bitsch *et al.*, 2000).

1.5.2 Glutamatergic neurotransmission and excitotoxic axonal damage

The amino acid, L-glutamate is the most abundant excitatory neurotransmitter in the mammalian nervous system. Glutamate has many important roles; synaptic plasticity at glutamatergic synapses is thought to underlie many aspects of regulated cortical function, including memory and learning (Headley and Grillner, 1990). Glutamate does not cross the blood brain barrier and therefore needs to be synthesised in neurones from precursors. The predominant precursor is glutamine which is released by glial cells and taken up by neuronal presynaptic terminals where it is metabolised to glutamate by the mitochondrial enzyme, glutaminase (Schousboe *et al.*, 1993; Augustine, 2008).

Once, glutamate is synthesised in the presynaptic terminal, it is packaged into synaptic vesicles and can then be released in to the synaptic cleft, where it binds to its post-synaptic receptors. On the postsynaptic cell, glutamate binds to either ligand gated ionotropic

glutamate receptors (iGluRs) or G-protein coupled metabotropic glutamate receptors (mGluRs) causing postsynaptic excitation. Glutamate in the synaptic cleft is removed by high-affinity, sodium-dependent excitatory amino acid transporters (EAATs) which transport glutamate to astrocytes (Rothstein *et al.*, 1994). Here, it is converted back to glutamine by the enzyme glutamine synthase, thus completing the glutamate-glutamine cycle (Schousboe *et al.*, 1993). Transfer of glutamine from astrocytes back to neurones is mediated by glutamine transporters; system N transport (SN1) in astrocytes allow release of glutamine into the interstitial fluid, where it is then taken up by system A transport (SAT/ATA) in neurones (Bröer and Brookes, 2001). In human white matter, oligodendrocytes have also been shown to express glutamate transporters and appear to be responsible for the majority of glutamate clearance in white matter (Pitt *et al.*, 2003).

Potentially toxic effects of excess glutamate where first reported in 1957 when paraenterally administered L-glutamate was seen to damage the neuroretinal layer in new born mice (Lucas and Newhouse, 1957). In 1969, John Olney discovered that this phenomenon was not restricted to the retina, but occurred throughout the brain (Olney, 1969; Olney and Sharpe, 1969). Olney demonstrated that glutamate mediated injury was restricted to the postsynaptic cells, whilst sparing the presynaptic terminal, and that antagonists at glutamate receptors ameliorated glutamate mediated cell damage (Olney, 1971; Olney *et al.*, 1971). Olney coined the term "excitotoxicity", postulating that the mechanisms leading to injury where produced by prolonged activation of postsynaptic receptors.

Alterations in normal extracellular concentrations of glutamate have since been reported to play a role in a number of neurodegenerative diseases, including stroke (Arundine and Tymianski, 2004), schizophrenia (Egerton *et al.*, 2012; Ota *et al.*, 2012), Parkinson's disease

(Caudle and Zhang, 2009) and amyotrophic lateral sclerosis (Shaw and Ince, 1997). Neuronal excitotoxicity usually refers to the injury and death of neurons arising from prolonged exposure to glutamate and the associated excessive influx of ions into the cell. Excessive activation of glutamate receptors by excitatory amino acids leads to a number of deleterious consequences, including impaired calcium buffering, formation of free radicals, activation of the mitochondrial permeability transition and subsequent secondary excitotoxicity (Dong *et al.*, 2009).

Evidence supporting the excitotoxicity hypothesis in MS includes the presence of elevated plasma glutamate levels in RRMS (Pampliega *et al.*, 2008) as well as elevated glutamate within the CSF of RRMS patients with active lesions (Stover *et al.*, 1997; Gurwitz and Kloog, 1998). Interestingly, CSF glutamate levels are similar in controls and RRMS patients with silent lesions, which seems to suggest that dysregulation of glutamate homeostasis occurs during the active inflammatory phase of the disease. This is supported by the observation that microglia and macrophages within MS lesions show decreased expression of glutamine synthase and glutamate dehydrogenase, the enzymes that convert glutamate back to glutamine (Werner *et al.*, 2001). Activated leukocytes and microglial cells, have also been shown in vitro to produce large quantities of glutamate by upregulating the glutamate producing enzyme glutaminase (Piani *et al.*, 1991), which suggests that, infiltrating, inflammatory cells are the likely source of the glutamate causing excitotoxic damage in MS.

A clinical, magnetic resonance spectroscopy (MRS) study in MS patients found elevated glutamate concentrations in acute brain lesions (Srinivasan *et al.*, 2005). In a follow up study by the same research group, which included 382 MS patients, those with higher concentrations of glutamate quantified from normal appearing white matter (NAWM) and

grey matter using MRS showed faster rate of neurodegeneration over 12 month follow up demonstrated by greater decreases in the neuronal marker, N-acetyl-aspartate (tNAA) (Baranzini *et al.*, 2010). There was increased prevalence in those patients of a common polymorphism (rs794185) within the gene sulphatase modifying factor 1 (SUMF1) which may indirectly regulate extracellular glutamate by altering the activity of steroid sulphatases (Baranzini *et al.*, 2010).

Whether or not, increased glutamate in MS is clinically relevant, however, remains to be established. Some supportive evidence comes from animal studies, where suppression of disease activity and reduction of axonal damage were seen in experimental autoimmune encephalitis (EAE) mice, treated with the AMPA/kainate antagonist, NBQX (Pitt *et al.*, 2000). In a small double-blinded, placebo controlled treatment trial, a reduction in relapse rate was seen in MS patients treated with amantadine, a weak NMDA receptor antagonist, though no difference in disability progression between the treated and placebo groups was seen (Plaut, 1987). However, a small, open label, pilot study of 16 patients with PPMS treated with Riluzole (Kalkers *et al.*, 2002), a licensed therapy for ALS, which ameliorates EAE (Gilgun-Sherki *et al.*, 2003) and is thought to reduce extracellular glutamate by reducing release of glutamate from pre-synaptic terminals (Killestein *et al.*, 2005) and up-regulating the major astrocyte glutamate transporter, GLT-1 (Carbone *et al.*, 2012), did not report clinical outcomes. Instead, the study showed a non-significant reduction in the rate of cervical cord atrophy, and development of new hypointense lesions on T1 weighted MRI. The study was small, uncontrolled and unblinded but the results showed some promise and there are currently on-going trials of riluzole in patients with clinically isolated syndromes (CIS) and MS to establish efficacy as a neuroprotective agent.

1.5.3 Mitochondrial dysfunction and axonal damage

Mitochondrial injury with subsequent energy deficiency seems to be an important factor in the induction of axonal injury in MS lesions (Trapp and Stys, 2009). Mitochondria are the site of aerobic respiration and ATP synthesis within cells; they meet the axons energy demands, hence, are crucial to their survival. In MS, reduced production of ATP as a consequence of mitochondrial dysfunction, occurs concurrently with increased energy demand which contributes to axonal loss (van Horssen *et al.*, 2012). Several mechanisms are thought to contribute to mitochondrial dysfunction and lead to axonal injury. Firstly, during MS lesion formation, activated mononuclear cells produce reactive oxygen species (ROS) such as nitric oxide (NO) and inducible nitric oxide synthase (iNOS) is up-regulated, leading to further production of inducible nitric oxide. ROS inhibit mitochondrial respiration and ATP synthesis (Cross *et al.*, 1997; Vladimirova *et al.*, 1998; Brown and Borutaite, 2001). Secondly, elevated glutamate levels and activation of post-synaptic glutamate receptors, leads to an increase in intracellular calcium which activates phospholipases, endonucleases, and proteases, which damage mitochondrial DNA, disrupt the cytoskeleton, and alter membrane lipids within mitochondria (Su *et al.*, 2009). Thirdly, the glutamate mediated pathway and NO mediated pathway converge onto a common pathway causing mitochondrial dysfunction; both mechanisms affect the electron transport chain, ATP synthesis, ionic homeostasis, and release of pro-apoptotic factors and it is thought that this convergence is present during inflammatory and progressive phases of the disease (Su *et al.*, 2009).

1.5.4 Sodium and axonal damage

Demyelinated axons in MS are not as efficient at conducting electrical impulses due to interruption of normal salutatory conduction. This results in increased expression of voltage-gated sodium channels in order to maintain conduction. The Nav1.6 subtype, which is

normally confined to the nodes of Ranvier, is redistributed along the demyelinated axon, where it is co-expressed with the Nav1.2 subtype (Craner *et al.*, 2004b; Bouafia *et al.*, 2014). What ensues is improved conduction but at the cost of a rising intra-axonal sodium (Smith, 2007). Excess sodium would normally be cleared by the energy dependent Na+/K+ ATPase. However, in the energy deficient axon, following mitochondrial injury, not all sodium can be cleared by the energy dependent transporter and consequently, there is a reversal of the Na+/Ca2+ exchanger to clear excess sodium (Andrews *et al.*, 2005). The resultant rise in intra-cellular calcium leads to multiple injurious pathways that involve calpain and other degrading enzymes (Stys and Jiang, 2002). Sodium channel blockade has therefore been proposed as a potential neuroprotective strategy in MS and has shown promise in animal studies (Lo *et al.*, 2002; Bechtold *et al.*, 2006; Black and Waxman, 2008) but, to date, human trials have not shown any clear benefit (Kapoor *et al.*, 2010).

1.6 Mechanisms of adaptation and repair

Axonal degeneration leads to permanent, non-remitting, clinical deficits, but following an acute inflammatory event, repair mechanisms can lead to clinical improvement in approximately up to two-thirds of cases (Ciccarelli *et al.*, 2010a). Resolution of inflammation, remyelination, electrophysiological adaptation and restoration of mitochondrial function may lead to tissue repair and may underlie clinical recovery (Craner *et al.*, 2004a; Black *et al.*, 2007; Ciccarelli *et al.*, 2014; Hartley *et al.*, 2014; Olsen and Akirav, 2014).

1.6.1 Remyelination

Within inflammatory MS lesions, alongside the inflammatory changes, demyelination and axonal degeneration, there is often evidence of remyelination. Remyelination of axons enables normal salutatory conduction to resume which is both more efficient and saves energy (Keough and Yong, 2013). For remyelination to occur, adult oligodendrocyte progenitor cells (OPCs) must migrate and differentiate into oligodendrocytes that re-envelope the demyelinated axon with new myelin (Franklin and Ffrench-Constant, 2008; Franklin *et al.*, 2012). Cells from the subependymal zone can also contribute remyelinating cells to areas of injury (Menn *et al.*, 2006; Franklin *et al.*, 2012). The efficiency of remyelination in MS declines with increasing age (Franklin *et al.*, 2012) which may explain why disease progression in MS appears to be so age-dependent (Confavreux and Vukusic, 2006a). Evidence from animal models suggests that remyelination slows down with ageing as a result of impaired recruitment of oligodendrocyte progenitors and subsequent differentiation into remyelinating oligodendrocytes (Sim *et al.*, 2002).

1.6.2 Electrophysiological adaptation

As discussed in *Section 1.5.4*, following demyelination of an axon, the cell increases expression of voltage-gated sodium channels, of the Nav1.6 subtype to demyelinated segments of the axolemma, in order to maintain conduction (Craner *et al.*, 2004b). What ensues is improved conduction but at the cost of a rising intra-axonal sodium (Smith, 2007). The effects of rising intra-cellular sodium are discussed in *Section 1.5.4*

1.6.3 Restoration of mitochondrial function

Data from post-mortem and MR spectroscopy studies suggests that in MS lesions, upregulation of mitochondria occurs to meet increased energy demands and is associated with clinical recovery. Mitochondrial density in axons and astrocytes is increased in active demyelinating lesions (Mahad *et al.*, 2008), and protective anti-oxidant enzymes and mitochondrial heat shock protein 70 (mtHSP70) are up-regulated, in particular in astrocytes and axons (Witte *et al.*, 2009; Nijland *et al.*, 2014) suggesting axons respond to the increased energy requirements through mitochondrial upregulation.

Although, there is no method for directly measuring mitochondrial function in vivo, tNAA concentrations estimated with ^{1}H-MRS, reflects neuronal number and is believed to have a bioenergetic role in neuronal mitochondria, thereby representing a unique marker for neuronal structure and neuronal (mitochondrial) metabolism in the CNS (Ciccarelli *et al.*, 2014). MRS studies have demonstrated reversible decreases in tNAA during recovery from acute MS brain lesions (Davie *et al.*, 1994; De Stefano *et al.*, 1995b; Mader *et al.*, 2000; Tiberio *et al.*, 2006), and acute MS spinal lesions (Ciccarelli *et al.*, 2010a; Ciccarelli *et al.*, 2010b). This reversal of tNAA decreases in the brain (De Stefano *et al.*, 1998) and spinal cord (Ciccarelli *et al.*, 2010a; Ciccarelli *et al.*, 2010b) were also associated with clinical recovery, suggesting that reversal of mitochondria dysfunction, reflected by tNAA changes is a clinically important biological process.

1.7 Clinical Course and Diagnosis of Multiple Sclerosis

1.7.1 Presentation: Relapse Onset MS

Approximately 85% of patients with MS will present with acute or sub-acute onset neurological symptoms characteristic of CNS demyelination. This initial presentation is termed a 'clinically isolated syndrome' or 'CIS' (Confavreux and Vukusic, 2006b). To be termed CIS, the episode should last for at least 24 h and occur in the absence of fever or infection, with no clinical features of encephalopathy (Miller *et al.*, 2008). By definition, CIS is isolated in time and clinically, it is often isolated in space (Miller *et al.*, 2012). The commonest presentations include long tract symptoms and signs (46%), optic neuritis (21%), and brainstem syndromes (10%), with 23% presenting with multifocal abnormalities (Confavreux *et al.*, 2000). Typically, first presentation of CIS in patients who go on to develop MS occurs in the third and fourth decades of life, with a median age of onset of 29 - 31 years (Confavreux *et al.*, 1980; Weinshenker *et al.*, 1989).

1.7.2 Conversion from CIS to MS

Conversion to RRMS depends on further clinical relapses disseminated in time and space. Approximately 63% of patients will convert to clinically definite MS within 20 years (Fisniku *et al.*, 2008). Baseline MRI data can be helpful in risk stratifying patients at initial presentation. Studies following up cohorts of patients with CIS have revealed that subsequent further clinical relapses leading to a diagnosis of clinically definite MS (Poser *et al.*, 1983) occur in 70–80% of patients with abnormal scans and in 20–25% with normal imaging (Fisniku *et al.*, 2008; Group, 2008).

1.7.3 Clinical Course: Relapse Onset MS

In the initial phase of RRMS, the disease is characterised by periods of clinical relapse, causing neurological symptoms, followed by partial or complete recovery and remission. As the disease progresses, relapse rates are seen to decrease (Weinshenker, 1994) and disability increases. In the majority of untreated patients, neurological and functional deficits will accumulate with each relapse. Early natural history studies, prior to the advent of disease modifying therapies estimate that 50% of patients with RRMS will go on to develop gradual progression in disability, independent of relapses after 10 years and approximately 90% will develop progressive disease after 25 years (Weinshenker *et al.*, 1989). This progressive phase of the disease is known as 'secondary progressive MS' or 'SPMS' (Lublin and Reingold, 1996). During this phase, relapses may continue on a background of progressive clinical decline.

A proportion of patients will have relapses followed by complete recovery for most of their disease course and are said to have 'benign MS'. Several definitions for benign MS exist, based on (Expanded) Disability Status Scale score at 10 or 15 years; arguably the most common definition is an EDSS score ≤ 3 at 10 years from onset (Sayao *et al.*, 2007). The precise prevalence is unknown and there have been widely varying estimates ranging from five to forty percent (Hawkins and McDonnell, 1999). Several studies have confirmed that following a benign disease course for 15 years only a small percentage will later develop more rapid disability progression (Runmarker and Andersen, 1993; Pittock *et al.*, 2004).

1.7.4 Prognosis: Relapse Onset MS

From the Ontario cohort data, the median time to reach a Disability Status Scale (DSS) score of 6 (assistance required for walking) from onset of relapsing onset MS was 14.97 +/- 0.31 years (Weinshenker *et al.*, 1989) and disability was distributed bimodally, with peaks at DSS 1 (no disability) and DSS 6. However rate of progression is highly variable from patient to patient. The ability to predict an individual patients clinical course at time of diagnosis, based on the initial presentation and early features, would be invaluable and several clinical and radiological characteristics have been demonstrated to be of prognostic significance (**Table 1.1**) but no disease biomarker is yet available to accurately predict future prognosis on an individual basis.

Factors associated with good prognosis	Factors associated with bad prognosis
Young age at onset	Older age at onset
Female	Male
Onset with optic neuritis or isolated sensory symptoms	Multifocal onset
Full clinical recovery from attacks	Motor or cerebellar symptoms
Long interval between 1st and 2nd attack	High relapse rate in first 5 years
No disability after 5 years	Substantial disability after 5 years
Normal MRI or lower lesion load	Abnormal MRI with large lesion load
No posterior fossa lesions	Posterior fossa lesions

Table 1.1: Table summarising prognostic indicators in MS (Miller *et al.*, 2005)

1.7.5 Presentation: Progressive onset MS

Approximately 10-15% of patients with multiple sclerosis present with progressive neurological dysfunction from onset without an initial period of clinical relapses with remissions (Thompson *et al.*, 1997). This disease pattern is called primary progressive MS (PPMS). Patients presenting with initial symptoms of PPMS, are likely to be older than those with RRMS, with a mean age of onset of 38.5 years compared with 28.6 years, respectively, in the Ontario study (Cottrell *et al.*, 1999). MS with onset after the age of 40 years is progressive in over 60 percent of patients (Weinshenker, 1994). The incidence in males and females is similar, with a male to female ratio of 1:1.3 from the Ontario cohort. In general, women will develop PPMS at a later age (40-45years) than men (30-35years) (Ebers, 2004), such that in PPMS with onset over the age of 50 years, the male to female sex ratio approaches 1: 2 (Noseworthy *et al.*, 1983). The most common presentation is of progressive myelopathy, usually with spastic paraparesis (39%) or sensory impairment (33%), followed by cerebellar symptoms (16%) and brainstem syndromes (5%), whilst presentation with optic neuritis is rare (Thompson *et al.*, 1997; Cottrell *et al.*, 1999).

1.7.6 Clinical Course and Prognosis: Progressive onset MS

PPMS is characterised by a progressive disease course from onset without an initial period of relapses (Stevenson *et al.*, 1999). The rate at which disability is accrued varies but generally disability accumulates more rapidly in PPMS than RRMS from disease onset with a median time to DSS 6 of 8 years (compared to 15 years in RRMS) and median time to DSS 8 of 18 years (Cottrell *et al.*, 1999). Sex, age of onset and symptoms at presentation don't seem to affect prognosis, but those with 3 or more systems involved progress more rapidly (Cottrell *et al.*, 1999).

1.8 Measuring disability in MS

1.8.1 The expanded disability status scale (EDSS)

The expanded disability status scale (EDSS) is a widely used and validated clinical scale for grading disability in persons with MS (**Table 1.5**) (Kurtzke, 1983). The score increases in 0.5 point increments from 0 to10 depending on disease severity. The EDSS score is determined by the degree of dysfunction in eight functional systems (FS) which are assessed during the neurological examination (pyramidal, cerebellar, brainstem, sensory, bowel and bladder, visual, cerebral or mental, and other), with 0 indicating a normal neurological examination and 10 indicating death from MS (**Table1.2**).

Advantages of the EDSS include that it is widely known, understood and is easy to apply. However, the EDSS does have some major disadvantages; it is not a linear scale, so each increment is not equivalent to the next, with some increments representing such significant clinical deterioration that it makes the scale insensitive to small clinical improvements or deterioration. This can be seen in clinical trial results, where the EDSS tends to generate a bimodal distribution of scores (Sharrack and Hughes, 1996). Another criticism of the EDSS has been that it is heavily weighted towards ambulation, with increasing disability in other domains poorly reflected in the score, once walking is limited. At lower levels of the scale, some studies have reported poor inter-rater agreement which may limit its reliability (Noseworthy *et al.*, 1990).

1.8.2 Towards more sensitive clinical scales

There is a need to incorporate more sensitive and objective clinical measures in clinical studies in MS. With respect to spinal cord studies, clinical scales which are more sensitive to changes in clinical functions mediated by spinal pathways than conventional clinical tests, such as the EDSS, need to be incorporated. Measures such as postural stability, vibration perception thresholds (VPT) and dynamometry are more responsive to small clinical changes due to damage in the spinal cord than the EDSS, and have been shown to be more strongly associated with MRI abnormalities in the spinal cord (Zackowski *et al.*, 2009; Oh *et al.*, 2013b).

Vibration perception threshold

Vibration perception threshold (VPT) is a form of quantitative sensory testing used for quantifying impairment in vibratory perception. A number of instruments exist for making these measurements including the Bio-Thesiometer (Biothesiometer USA), Vibrameter (SPM Instrument AB, Strängnäs, Sweden), Vibratron (Physitemp Instruments, Inc., Clifton, New Jersey, USA) and Neurothesiometer (Algeo Limited, Liverpool, UK). They all generally work on a similar principle; the vibrator is applied to a bony prominence such as the hallux or medial malleolus and a fixed frequency stimulus is generated. The voltage is then manually graduated by the clinician until the patient/test subject is able to perceive the vibration. VPT is defined as the lowest voltage at which vibration can be detected at least 50% of the time (Garrow and Boulton, 2006).

Measures of postural stability

Several tests of functional performance exist for the assessment of balance; they include the Berg Balance Scale (BBS), Timed Up and Go (TUG), Balance Screening Tool (BST), and Fullerton Advanced Balance (FAB) scale. Although these assessments correlate with clinical symptoms, the inter-rater reliability can introduce unwanted bias (Ozinga and Alberts, 2014). Objective assessments of postural stability, that are independent of subject or rater bias can be more reliable but require significant investment in equipment, space and time and are therefore not always readily available. Force plate posturography, in which test subjects stand on a platform equipped with pressure sensitive sensors, allows measurement of vertical forces, typically at three separate sites on the platform. Force plate analysis quantifies centre of pressure displacement, which represents a weighted average of all the pressures over the plate, which when analysed in the time domain provides a quantifiable measure of stability (Ozinga and Alberts, 2014).

An alternative to the force plate method is the use of body worn accelerometers and gyroscopes to obtain kinematic values. Accelerometers are used to quantify truncal motion in two planes; the *Roll* or medial–lateral plane and the *Pitch* or anterior–posterior plane, during stance (Ozinga and Alberts, 2014). This accuracy of this method is comparable to force plate analysis (Moe-Nilssen, 1998) but it also has the advantage of reduced costs, smaller space requirement and is mobile which allows measurements in multiple locations. For these reasons, this is the method chosen for use in this thesis.

Score	Description
0.0	Normal neurological examination
1.0	No disability, minimal signs in one FS
1.5	No disability, minimal signs in more than one FS
2.0	Minimal disability in one FS
2.5	Mild disability in one FS or minimal disability in two FS
3.0	Moderate disability in one FS, or mild disability in three or four FS. No impairment to walking
3.5	Moderate disability in one FS and more than minimal disability in several others. No impairment to walking
4.0	Significant disability but self-sufficient and up and about some 12 hours a day. Able to walk without aid or rest for 500m
4.5	Significant disability but up and about much of the day, able to work a full day, may otherwise have some limitation of full activity or require minimal assistance. Able to walk without aid or rest for 300m
5.0	Disability severe enough to impair full daily activities and ability to work a full day without special provisions. Able to walk without aid or rest for 200m
5.5	Disability severe enough to preclude full daily activities. Able to walk without aid or rest for 100m
6.0	Requires a unilateral walking aid to walk about 100m with or without resting
6.5	Requires bilateral walking aids to walk about 20m without resting
7.0	Unable to walk beyond approximately 5m even with aid. Essentially restricted to wheelchair; though wheels self in standard wheelchair and transfers alone. Up and about in wheelchair some 12 hours a day
7.5	Unable to take more than a few steps. Restricted to wheelchair and may need aid in transferring. Can wheel self but cannot carry on in standard wheelchair for a full day and may require a motorised wheelchair
8.0	Essentially restricted to bed or chair or pushed in wheelchair. May be out of bed itself much of the day. Retains many self-care functions. Generally has effective use of arms
8.5	Essentially restricted to bed much of day. Has some effective use of arms retains some self-care functions
9.0	Confined to bed. Can still communicate and eat
9.5	Confined to bed and totally dependent. Unable to communicate effectively or eat/swallow
10.0	Death due to MS

Table 1.2: The expanded disability status scale

Chapter Two

Principles of magnetic resonance imaging

2.1 Introduction

Magnetic resonance imaging (MRI), is a non-invasive medical imaging technique with multiple possible configurations and applications, able to provide structural, microstructural and functional information relating to healthy and pathological animal tissues *in vivo*. To provide a complete review of the fundamentals of MRI, would require an introduction to quantum physics which is beyond the scope of this thesis. Instead, this chapter will focus on introducing basic principles relating to MRI, with a more in-depth review of techniques relevant to this thesis.

2.2 Nuclear Magnetic Resonance

Nuclear magnetic resonance (NMR) is a physical phenomenon which describes the absorption and emission of electromagnetic radiation by magnetic nuclei within a magnetic field. The first successful NMR experiments were performed by Felix Bloch and Edward Purcell in 1946. Independently of each other, they observed that the magnetic moments of nuclei in solid matter will, under a constant magnetic field, polarize and that the application of a radiofrequency field at right angles to the constant field causes a forced precession at the Larmor frequency and that they re-emitted this energy when the nuclei transferred to their original state (Bloch, 1946; Purcell *et al.*, 1946).

2.3 Basic Principles

Within all atoms, the nucleic particles, neutrons and protons, spin about their axis. Pairs of protons and neutrons spin in opposite directions at the same rate. Therefore in atoms with an even atomic mass, the nucleus has a net spin of zero. In nuclei with unpaired nucleons, the spin directions are not equal and opposite so the nucleus has a net spin, and is said to exhibit nuclear magnetism. These nuclei are sometimes referred to as MRI active nuclei.

As the protons within the nucleus spin, they induce a magnetic field (Faraday's law of electromagnetic induction) and behave as magnetic dipoles. Magnetic fields have both size and direction which are denoted as a magnetic moment (μ). The magnetic moment of a nucleus is the vector sum of the individual magnetic moments of nuclear protons. Therefore, nuclei which have larger numbers of protons generally have lower magnetic moments because of differences in alignment of nucleic protons. The hydrogen nucleus (^{1}H), is made up of a single proton, which is positively charged giving ^{1}H a relatively large magnetic moment which makes ^{1}H particularly suitable for NMR experiments. ^{1}H is the most abundant MRI active nuclei in the human body (in the form of water, fats and proteins etc) which also makes it the most relevant for human *in-vivo* imaging studies.

Under normal conditions, the magnetic moments of protons in tissues are randomly orientated. Once the protons are placed in a strong external magnetic field (B_0), their respective magnetic moments either align parallel to B_0, in a low energy state or anti-parallel to B_0 in a high energy state. Proportionally more protons will align parallel to B_0 as this is the lower energy state giving a net longitudinal magnetisation (M) in the direction of B_0 (**Figure 2.1**).

Figure 2.1: Alignment of spins after application of an external magnetic field. There is a net longitudinal magnetisation in the direction of B_0.
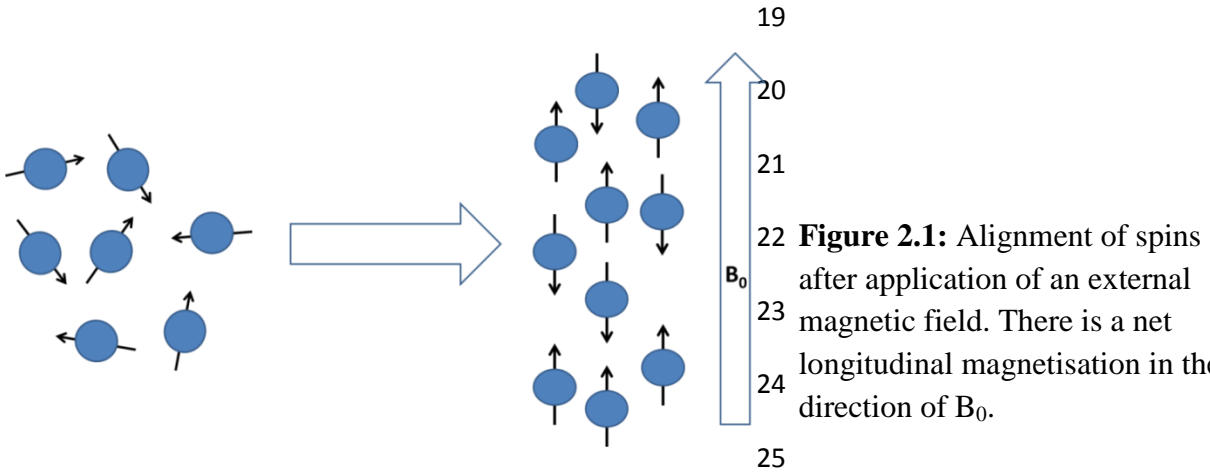
1 **2.4 Precession**

2 Protons aligned in the magnetic field gyrate around their own axis in a motion known as

3 precession (**Figure 2.2**). The rate of precession, known as the precession frequency depends

4 on the strength of the magnetic field and can be calculated using the Lamor equation:

$$\omega 0 = \gamma B0$$

5 Where $\omega 0$ is the precession frequency given in Hz, γ is the gyromagnetic ratio and B_0 is the

6 strength of the magnetic field in Tesla.

7

8

9

10

11

12
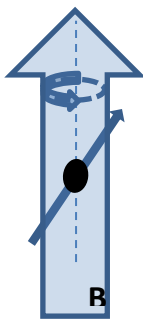
Figure 2.2: Precession of a spin under the influence of B_0. The large arrow represents the external field and the small

13 The gyromagnetic ratio is the ratio between the magnetic dipole moment to the angular

14 momentum of each MR active nucleus. It is unique for each MR active nucleus and expressed

15 in units of MHz/T (**Table 2.1**). It therefore follows that the stronger the magnetic field

16 strength, the higher the precession frequency.

17

18

19

Nucleus	Precession frequency $(MHzT^{-1})$
Proton (^1H)	42.576
Phosphorus (^{31}P)	17.235
Sodium (^{23}Na)	11.262
Carbon (^{13}C)	10.705

20

21

22 **Table 2.1:** Precession (Lamor) frequencies of common MR active

23 nuclei

24

2.5 Excitation

Applying energy in the form of a brief, radiofrequency (RF) pulse which oscillates at the Lamor frequency of ^{1}H, results in a number of measurable effects; i) it causes a transfer of energy to the hydrogen spins causing them to resonate. Other MR active nuclei aligned with B_0 do not resonate as their precessional frequencies are different to that of hydrogen. ii) By adding energy into the system, it brings the spins out of equilibrium so that some low energy spins, originally aligned parallel to B_0 gain sufficient energy to re-align, anti-parallel to B_0 which has the effect of reducing the net longitudinal magnetisation. iii) The RF pulse also brings precessing spins, which were previously out of phase, into phase (phase coherence) which generates a net transverse magnetisation.

Exciting spins by applying an RF pulse will therefore affect the net magnetisation vector. The amplitude and duration of the RF pulse will determine the flip angle, which is the angle at which the net magnetisation deviates from B_0. The subsequent movement of the magnetic field towards the transverse plane induces a voltage in the MR receiver coil which is the basis of the MR signal.

2.6 Relaxation

Once the RF pulse is turned off, spins release energy to their surroundings (lattice) in a process known as, relaxation. Upon releasing their energy, spins fall back under the influence of B_0 and return to the equilibrium position, in alignment with B_0 (spin-lattice relaxation). At the same time, by turning off the RF pulse, phase coherence is lost and spins de-phase. The dephasing of spins depends on the neighbouring spins (spin-spin relaxation). The net effects of relaxation are therefore; i) recovery of longitudinal magnetisation and ii) decay in transverse magnetisation. As the transverse magnetisation decays, so does the voltage

induced in the MR receiver coil and this reducing signal is known as free induction decay (FID).

2.6.1 T1 Recovery (Spin-Lattice relaxation)

Recovery of longitudinal magnetisation depends on spins losing energy gained from the RF pulse. Once the RF pulse is turned off, this recovery occurs exponentially (**Figure 2.3**) but the rate of recovery depends on tissue properties and varies between tissue types. The time constant, T1 can be viewed as the time required for the z-component of net longitudinal magnetisation to reach $(1 - 1/e)$ or 63% of its maximum value (**Figure 2.3**).
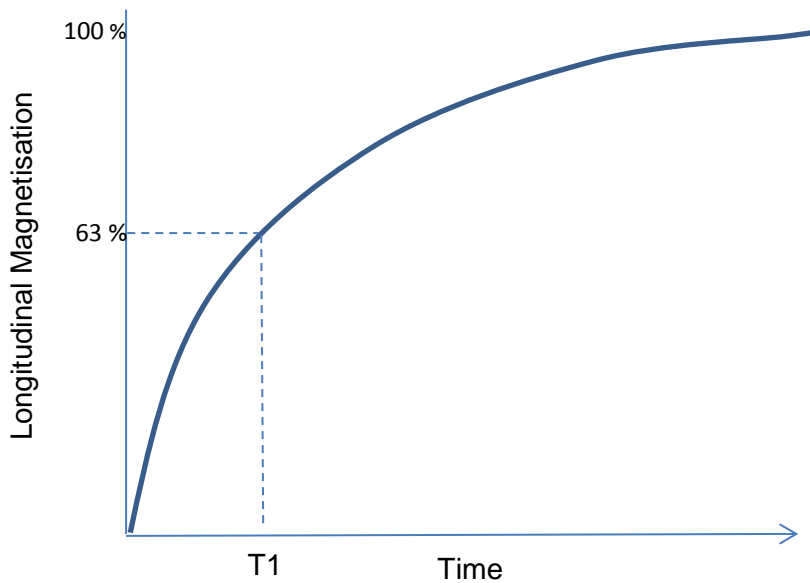
Figure 2.3 Showing the exponential T1 recovery curve: T1 relaxation time refers to the time taken for 63% of the longitudinal magnetisation to recover within the tissue

2.6.2 T2 Decay (spin-spin relaxation)

On turning off the RF pulse, the spins are able to exchange energy with neighbouring spins. As one spin comes into proximity with another, it will have a slightly lower or higher magnetic field to its neighbour leading to small differences in their precessional frequencies and causing them to dephase. As spins come out of phase, the transverse magnetisation decays exponentially. This interaction is termed spin-spin relaxation and can be denoted using the T2 time constant which represents the time taken for 63% of the transverse magnetisation to be lost (**Figure 2.4**).
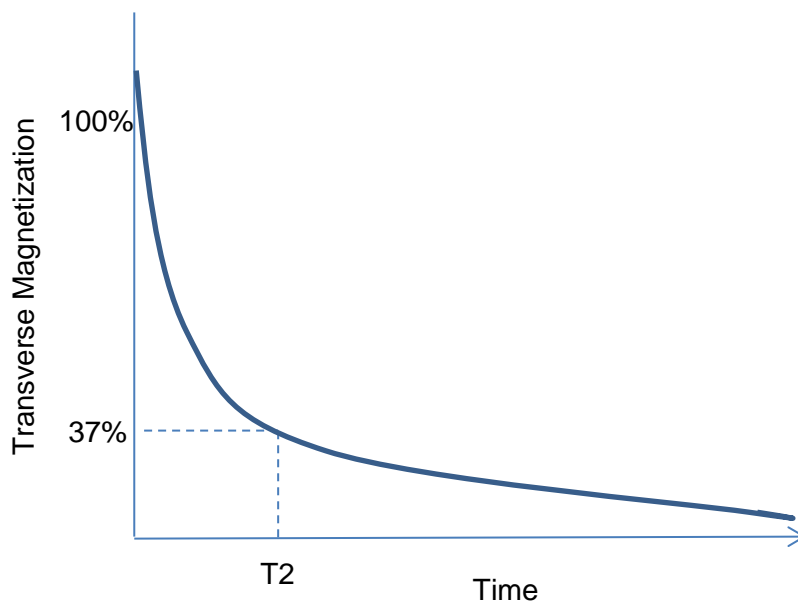
Figure 2.4: Showing the exponential T2 relaxation curve: T2 relaxation time refers to the time taken for the transverse magnetisation to decay to 37%

2.6.3 T2* Decay

When the RF pulse is removed, a phenomenon known as T2* decay also occurs, which is rapid dephasing of spins, which occurs faster than T2 decay. T2* decay is the result of T2 decay itself and dephasing of spins due to magnetic field inhomogeneity. As the precession

1 frequency of spins is affected by the magnetic field strength, inhomogeneity within the field

2 results in spins precessing at differing frequencies causing loss of phase coherence, and

3 therefore transverse magnetisation producing an FID signal. This resultant rapid loss of signal

4 occurs before most tissues have had sufficient time to reach their T1 and T2 relaxation times.

5 Therefore to measure relaxation times accurately, which is needed to produce good image

6 contrast, a second re-phasing pulse is required and this will be discussed further in the section

7 on pulse sequences.

8

9

10 **2.7 Signal Location and Image Formation**

11

12 **2.7.1 Spatial encoding**

13 The receiver coil detects voltage from spins when they are in phase, in the transverse plane.

14 Before an image can be formed, signals need to be located spatially in three dimensions.

15 Spatial encoding is used to encode the NMR signal with spatial information. The process uses

16 linear magnetic gradients in three planes (x,y,z). A frequency encoding gradient plus two

17 orthogonally aligned phase encoding gradients are required. The frequency encoding gradient

18 by convention is applied along the long axis of the anatomy and the phase encoding gradients

19 along the short axes.

20

21 **2.7.2 Slice selection gradient**

22 Slice selection requires the application of a slice selection gradient (G_{slice}, G_z), a linear

23 gradient which is orientated orthogonally to the plane the images are acquired in. The field

24 strength is non-uniform across the gradient, and is highest at the top end and lowest at the

lower end. This has the effect of increasing the precession frequency of spins at the top end of the gradients and reducing the precession frequency of spins at the lower end of the gradient. An RF pulse can then be applied at the precession frequency of selected sections of the gradient to selectively excite spins in a pre-selected slice.

Slice thickness is determined by thickness in space of the spins excited by the RF pulse. The angle at which the slice selection gradient is applied will determine the differences in precessional frequencies of spins between a given distance. Steeper gradients produce larger differences in precessional frequencies, whilst shallow gradients produce smaller differences. The RF pulse which is applied needs to contain a range of frequencies (the bandwidth) to excite spins within two defined points. Therefore by varying the slope of the gradient and bandwidth it is possible to alter the slice thickness.

2.7.3 Frequency encoding gradient

Once a slice has been selected, a frequency encoding gradient (G_{read}, G_x) along the long axis of the anatomy is applied. When the frequency encoding gradient is turned on, the magnetic field along the axis of the gradient and precessional frequencies are altered in a linear manner. The signal can then be located along the length of the gradient by its frequency.

2.7.4 Phase encoding

A phase encoding gradient (G_{phase}, G_y) is applied perpendicular to the frequency encoding gradient and is needed to locate signal along the short axes. The gradient produced by the

phase encoding gradient, causes spins to precess at different frequencies such that phase coherence is lost along the gradient. The phase of the spins now depends on their position along the short axis and can be used to locate them. For this to be done accurately, this step needs to be repeated several times with increasing amplitudes, so that spins with a particular position can be identified by their combinations of phases.

2.7.5 K-Space

The signals detected by the receiver coil are made up of amplitudes, frequency shifts and phase shifts. Once this data is digitised, it is written to a data acquisition matrix called k-space, which acts as a temporary memory of the spatial frequency information. K-space comprises a horizontal (frequency) axis and a vertical (phase) axis.

One line of k-space is filled with each repetition time (TR). TR is discussed later. The phase gradient is altered with each TR, allowing a new line to be filled. There are, therefore as many lines to the k-space matrix as there are phase encoding steps. The slope of the gradient selects which line will be filled; steep gradients, select peripheral lines, while shallow gradients select the central lines.

2.7.6 Fourier Transformation

The data acquisition matrix contains raw data which needs to be converted to an image before it can be viewed. Each voxel is assigned a colour on the greyscale which corresponds to amplitudes of frequencies coming from that spatial location. Frequency amplitudes are in the

1   time domain and therefore need to undergo a mathematical conversion, known as a Fourier

2   transformation to convert them to the frequency domain.

3

4   **2.8 Pulse Sequences**

5   MRI pulse sequences are composed of a set of pre-defined RF pulses, rephasing pulses and

6   gradient pulses. Pulse sequence diagrams are usually used to illustrate the application of

7   pulses and gradients. A simplified pulse sequence diagram is represented in **Figure 2.5**,

8   where the horizontal axis represents time and vertical axis represents amplitude and illustrates

9   the timing parameters common to all pulse sequences.

10

11
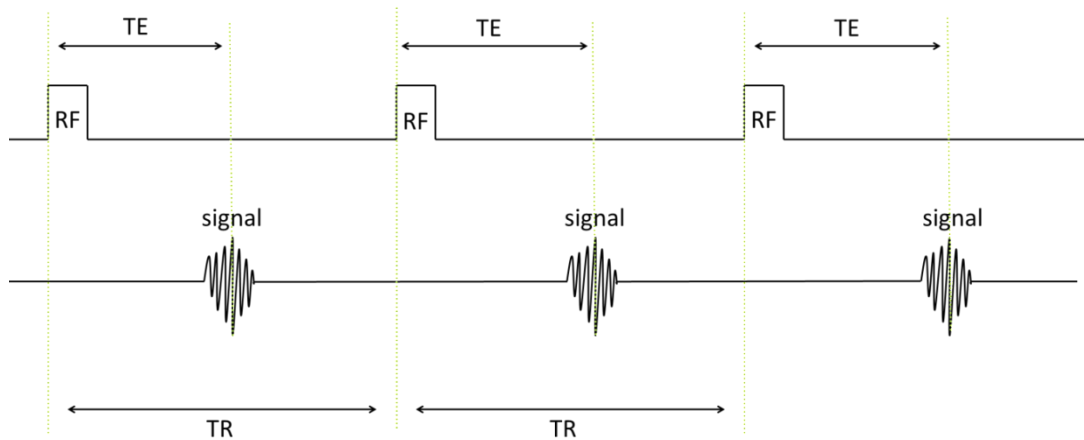
12

13   **Figure 2.5:** Simplified pulse sequence diagram: Illustrating the timing parameters used in
14   more sophisticated sequences; the Echo time (TE) is the interval between the application of
     the RF pulse to peak signal in the receiver coil and repetition time (TR) is the interval
15   between RF pulses.

16

17

2.8.1 Spin Echo

The spin echo effect was first described by Hahn (Hahn, 1950) and further developed by Carr and Purcell (Carr and Purcell, 1954). The sequence (**Figure 2.6**) delivers an initial 90 degree RF pulse which causes loss of longitudinal magnetisation and maximises transverse magnetisation, whilst placing the spins into phase. Once the RF pulse is turned off, longitudinal magnetisation recovers (T1 recovery) and spin-spin interactions cause the spins to dephase (T2 decay). To limit the effects of field inhomogeneity on spins (T2* decay), an 180° rephasing pulse is applied at time, **t,** which flips the spins through 180°, inverting the magnetisation vector. This has the effect of inverting the spins such that slower spins lead the main moment and the faster spins trail behind. As the spins continue to precess at a similar rate as prior to the 180° pulse, the faster spins catch up, refocusing the spins and bringing them momentarily back into phase. At this moment there is maximal transverse magnetisation which induces a voltage within the receiver coil at time 2**t**. This signal is the spin echo which contains both T1 and T2 information, having eliminated the effect of T2*.
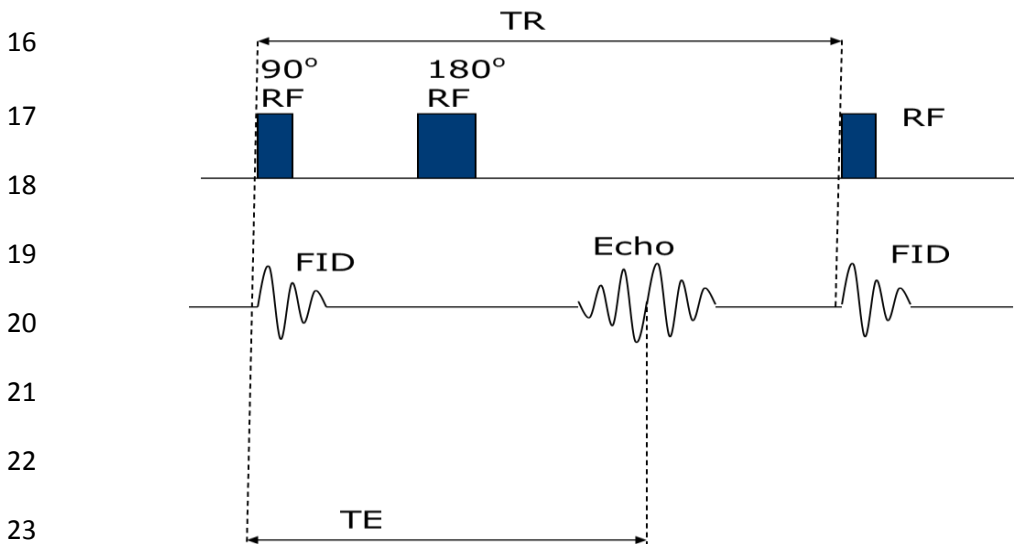
Figure 2.6: Pulse sequence diagram for a spin echo sequence. An 180° pulse is applied at time t and an echo is detected at time 2t.

2.8.2 Dual Echo

The dual echo sequence relies on similar principle to the spin echo, but utilises two 180° RF pulses after the initial 90° pulse to produce two echoes, allowing two images to be acquired with each TR. Most commonly, one image is acquired with a short TE, to produce a proton density image, and a second longer TE, provides a T2 weighted image. At shorter TE's, little T2 decay has occurred, but with longer TE, more complete T2 decay has occurred, highlighting differences in T2 times between tissues.

2.8.3 Fast Spin Echo

The fast spin echo sequence is a spin echo pulse sequence that allows much shorter scan times than the conventional spin echo sequence. After the original 90° RF pulse, multiple 180° pulses are applied, generating multiple spin echoes and generating an echo train. The number of pulses applied during each TR is called the Echo Train Length (ETL).

However, were as in conventional spin echo only one phase encoding step is applied per TR on each slice, the fast spin echo sequence reduces scan time by performing more than one phase encoding step, filling multiple lines of k-space per TR. At each 180° rephasing pulse, an echo is produced and a different phase encoding step is performed.

2.8.4 Gradient Echo

The gradient echo sequence differs from the spin echo in that the initial RF pulse typically produces a flip angle lower than 90°, which results in a reduction to the magnetisation in the transverse plane. An FID signal is produced once the RF pulse is withdrawn and longitudinal

1 magnetisation recovers. Smaller flip angles result in more complete recovery of longitudinal

2 magnetisation for a given T1 and TR, whilst the opposite is true of larger flip angles.

3

4 Once the RF pulse is turned off, spins within the transverse plane also begin to dephase due

5 to T2* effects and therefore need to be re-phased. This is achieved using gradients. First, a

6 negative, dephasing gradient is applied which has the effect of speeding up fast spins and

7 slowing down slow spins. Secondly, a positive gradient is applied (**Figure 2.7**) which speeds

8 up slow spins and decelerates fast spins, rephasing the spins and producing a voltage in the

9 receiver coil.

10

11 The main benefit of using smaller flip angles is that longitudinal magnetisation is able to

12 recover faster, allowing shorter echo times and therefore repetition times and permitting

13 shorter scan times. However, applying gradients for re-phasing, is not as effective as using an

14 180° RF pulse and doesn't rephase all the spins. There is also larger field inhomogeneity

15 when gradients are used leading to greater T2* effects.

16
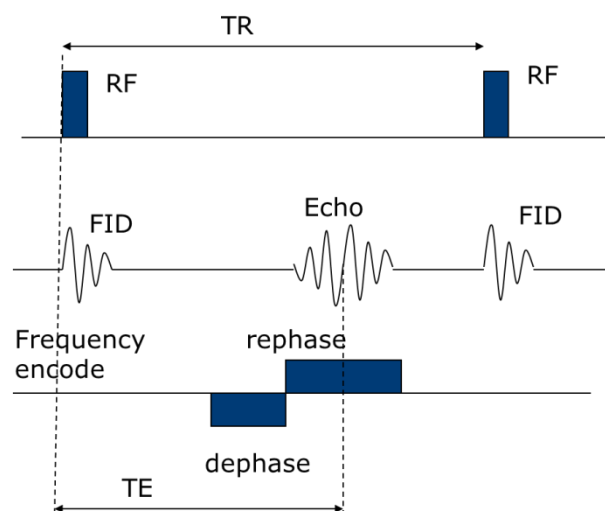
Figure 2.7: Pulse sequence diagram for a gradient echo sequence. An RF pulse producing a flip angle $<90^{o}$ is applied followed by a dephasing and rephasing gradients to produce the echo.

2.8.5 Echo Planar Imaging (EPI)

Echo planar imaging (EPI) (Mansfield and Pykett, 1978) allows rapid image acquisition by using highly efficient filling of k space. EPI can acquire the data necessary to fill all lines of k space within a single TR from a single echo train (single shot EPI) or multiple TR's (multi-shot EPI). However, the EPI sequences have the disadvantage of image artefacts and image distortions that occur as a result of T2* decay and fat/water chemical shifts and the long readout time necessary to generate the echo train.

Single-shot EPI sequences are often used for diffusion weighted imaging (*Section 2.10*) but high resolution images are difficult to achieve. A number of reduced field of view (FOV) EPI methods have been proposed to improve in plane resolution on spinal cord axial acquisitions (Wheeler-Kingshott *et al.*, 2002; Wilm *et al.*, 2007; Saritas *et al.*, 2008). They also have the advantage of reducing susceptibility artefacts caused by differences between the spinal cord and surrounding bony structures and soft tissues.

2.9 Magnetic Resonance Spectroscopy

Unlike conventional MRI used for structural imaging, which relies on excitation of protons and signal localisation, Magnetic Resonance Spectroscopy (MRS) sacrifices signal localisation in order to quantify the number of protons from molecules of interest within a tissue sample.

MRS detects magnetic resonance signals produced by atomic nuclei located within molecules in tissue. Quantification of the MRS signal amplitude can provide a means of estimating the tissue concentration of the signal generating molecules (Alger, 2010). The molecules that are

most readily detected by MRS *in vivo* are involved in metabolic pathways therefore making MRS a useful method of studying metabolic changes in tissues. *In vivo* biomedical applications of MRS largely focus on detection and quantification of proton (^{1}H), phosphorus (^{31}P) and carbon (^{13}C) isotopes. The remainder of this section will therefore focus on ^{1}H MRS and will introduce the technique of MRS, cover basic physics principles, and technical considerations.

2.9.1 Chemical Shift

As discussed earlier in this chapter, precession frequencies of spins are determined by the applied magnetic field (B_0) and magnetic field gradients. However, nuclei are also susceptible to changes within their local environment. Neighbouring electrons and nuclei are able to exert a small, yet significant effect on the local net magnetic field. Electrons moving around adjacent nuclei create a small local field able to shield ^{1}H spins from B_0. This will in turn affect the precession frequency of local spins as determined by the Larmor equation and shielding electrons are therefore said to produce a chemical shift in the resonant frequency of the spins. It is based on this principle that MRS experiments work, as they try to separate and quantify metabolites of interest based on variations of precessional frequencies of nuclei within compounds. The x-axis of MR spectra (**Figure 2.8**) are displayed in parts per million (ppm) which refers to the frequency of resonance of spins in metabolites of interest relative to the resonant frequency of a reference chemical. Historically, 0.1% of tetramethylsilane (TMS) is used as a reference for calibrating the chemical shifts of spins belonging to metabolites of interest. The resonant frequency of spins in TMS lies at 0 ppm.
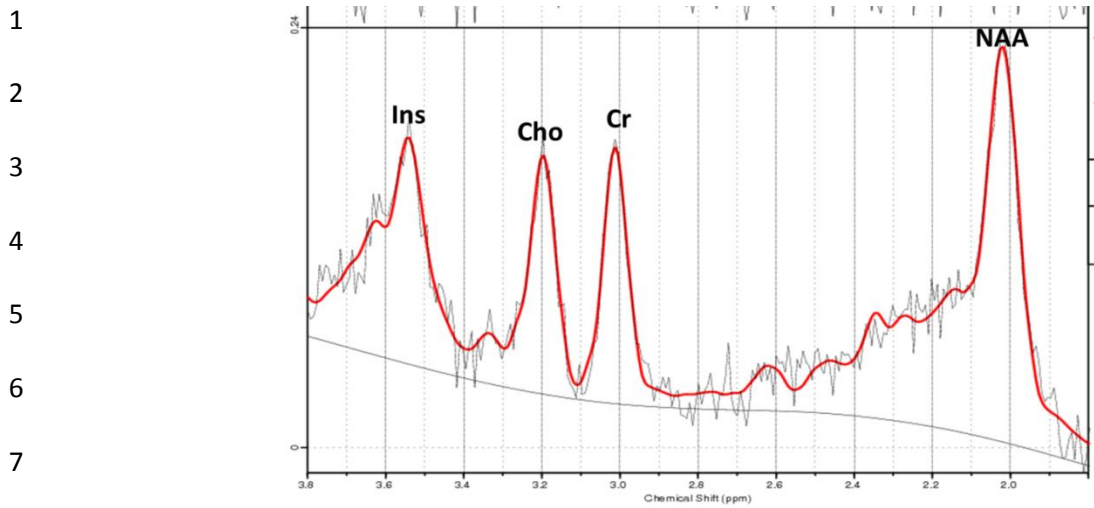
Figure 2.8: A typical post-processed spectrum from a healthy spinal cord. Chemical shift in ppm is plotted along the x-axis, with signal intensity on the y-axis.

2.9.2 Spin-Spin Coupling (J-coupling)

MR spectra can sometimes contain doublet, triplet of multiplet peaks which occur as a consequence of splitting of a peak representing signal from a common hydrogen environment. The phenomenon arises from spin-spin coupling, also known as J-coupling. This occurs because adjacent spins will align either parallel or anti-parallel to B_0 and subsequently effect the local field of the spin of interest. A good example is that of glutamate, which contains two methylene (CH_2) groups and a methine (^2CH) group which produce a resonance. The signal from the methine group appears as a doublet of doublets at 3.75ppm and signal from the four protons belonging to the methylene groups appears as multiplets between 2.04 and 2.35 ppm.

Each methylene group contains two protons, which can align parallel or anti-parallel to B_0, giving four possible orientations of the spins (**Figure 2.9**). If spins are paired and aligned with B_0, this has the effect of increasing the field experienced by neighbouring spins in the

second methylene group resulting in a decrease in chemical shift. When spins are paired and

opposed to B_0, they will reduce the field experienced by neighbouring spins resulting in a

slight increase in chemical shift. When the two spins are aligned in opposite directions they

exert no net effect on the field of neighbouring spins. It is these relatively small effects of the

spin-spin coupling that produces the multiplet peaks. The spacing between these peaks has a

fixed frequency value (Hz), called the J-coupling constant.
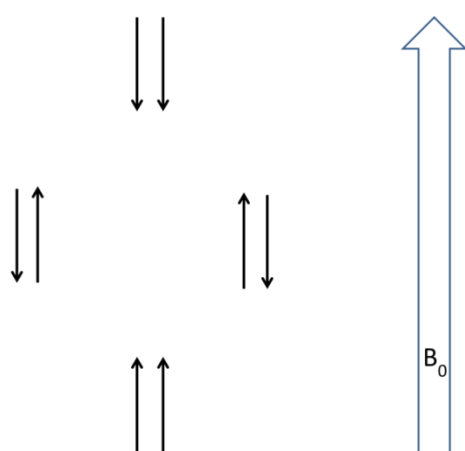
Figure 2.9: The four possible orientations of methylene protons (represented by the black arrows) once an external magnetic field is applied. Spins can be both parallel, both anti-parallel, 1st parallel and 2nd anti-parallel, or 1st anti-parallel and 2nd parallel

2.9.3 Localisation

In order for useful data to be acquired, it is necessary for the MR signal to be localised to a

pre-defined volume of interest (VOI), most often, a cuboid voxel. Localisation techniques are

used to excite predefined voxels which are prescribed by the operator in single-voxel MRS.

Single-voxel spectra are usually acquired using either the **ST**imulated **E**cho **A**cquisition

Mode (STEAM) (Frahm *et al.*, 1989) or **P**oint **RES**olved **S**pectroscopy (PRESS) (Bottomley,

1987) methods. In unlocalised spectra, often large signals from surrounding tissues cause

contamination such that metabolites of interest can no longer be seen. Furthermore B_0

magnetic field is inherently harder to optimise over larger areas, resulting in broader

resonances and a reduction spectral resolution. Upon spatial localisation, large signals eg. from lipids can be minimised which improves spectral quality.

2.9.3.1 PRESS (**P**oint **RES**olved **S**pectroscopy)

The PRESS localisation sequence is a multi-echo sequence. After an initial 90^0 RF pulse, two 180^0 pulses are applied. Each pulse is accompanied with a slice selective gradient in each of the three axes so that only spins within the voxel experience all three RF pulses. Historically, longer sequence preparation times meant that PRESS was better suited to acquisitions with longer echo times, which allowed good visualisation of metabolites with longer relaxation times. More recently short echo times have also been used allowing quantification of metabolites not seen on long TE (Marliani *et al.*, 2007; Ciccarelli *et al.*, 2010a; Marliani *et al.*, 2010). PRESS has an advantage over STEAM of superior SNR by a factor of two when similar voxel volumes, TR,TE, and number of averages are used (Barker, 2010) .

2.9.3.2 STEAM (**ST**imulated **E**cho **A**cquisition **M**ode)

The stimulated echo acquisition mode (STEAM) is also a multi-echo sequence and is similar to PRESS except a 90-90-90 pulse sequence is used instead of 90-180-180. The "stimulated echo" is collected whilst all the spin echoes are dephased by a large crusher gradient (Barker, 2010). The STEAM sequence suffers from lower SNR because the final stimulated echo yields only a fraction of the possible signal from the voxel. However it is more suited to short TE acquisition and on an MR system with strong field gradients, it has been demonstrated that highly resolved ^{1}H spectra with metabolite linewidths of between 8-10 Hz can be obtained with a TE of 1ms (Tkac *et al.*, 1999). Additionally STEAM is thought to have

slightly superior water suppression factors to PRESS because water suppression pulses can be

added during the mixing time period which does not occur in PRESS (Barker, 2010).

2.9.4 Voxel Positioning

In spinal cord spectroscopy, the spectroscopic voxel is prescribed by the user (Figure 2.10) using coronal and sagittal structural imaging as a reference. The voxel size is limited by the small diameter of the cord. The spinal cord is surrounded by CSF, therefore careful positioning of the voxel within the spinal cord, avoiding CSF is necessary to reduce partial volume effects in order to provide more accurate tissue characterisation.
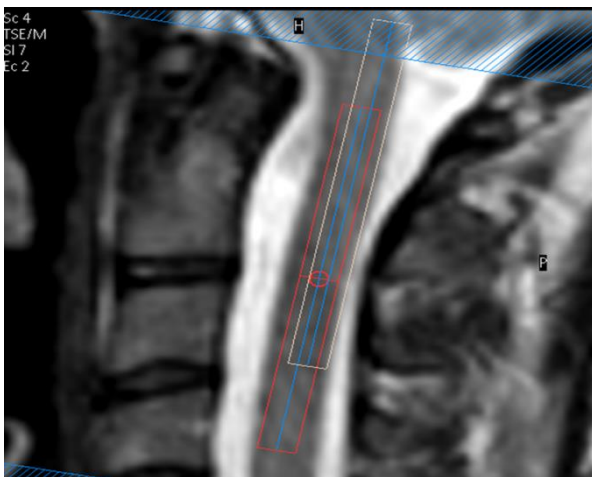
Figure 2.10: Positioning of spinal spectroscopy voxel. Sagittal T2 weighted spinal cord image showing spectroscopy voxel (red) and shifted water voxel (orange) positioning within the upper cervical cord, avoiding the surrounding CSF to minimise partial volume effects

2.9.5 Shimming

Shimming refers to the processes used for achieving magnetic field homogeneity over the volume of interest. Inherently, there will be some minor inhomogeneity in the magnetic field, which is exacerbated by placing a patient into the magnet due to magnetic susceptibility variations. The spinal cord is surrounded by CSF and vertebral bodies which cause distortions of the magnetic field along the spinal cord (Cooke *et al.*, 2004). Shimming is achieved by

making subtle alterations to the field gradients prior to data acquisition. Homogeneity can be assessed by calculating the linewidth of the water resonance in Hz or ppm. Good shimming usually produces a narrow linewidth, whilst poor shimming broadens the linewidth.

Accurate shimming is important as a poor shim, will result in a rapid T2* decay, resulting in broad spectral lines. In contrast, with good shimming, the signal in the time domain is present for a longer time, producing spectra with higher peaks and smaller linewidths. A poor shim will therefore not produce adequate signal to noise ratio for metabolite quantification.

2.9.6 Water Suppression

The concentration of water in the brain and spinal cord is several orders higher than the concentration of other metabolites. The large signal produced by water during an MRS experiment may disturb signals of the remaining resonances with lower intensities. In order to reliably quantify metabolites with lower intensities, it is therefore necessary to supress the water signal during in vivo MRS experiments. Several water suppression methods exist and selecting the correct method depends on the localisation sequence used and this will be discussed further in *Chapter 3*.

2.9.7 Additional Technical Considerations for Spinal Cord Spectroscopy

Each cardiac cycle produces a pulsation within the CSF and oscillation of the cervical cord in the craniocaudal direction (Mikulis *et al.*, 1994; Loth *et al.*, 2001) which can affect water suppression and reduce spectral quality. Pulse triggering has been suggested as method to reduce the effects of normal physiological motion (Cooke *et al.*, 2004), though this will usually necessitate an increase in acquisition times.

Subject motion is possibly the largest limitation to producing good quality spinal cord spectra. Once the voxel has been prescribed, the subject needs to remain in the same position during the acquisition which can be difficult. Yiannakas *et al* recently reported reduction in motion artefacts in a long spinal cord imaging protocol by using an MR compatible cervical collar (Yiannakas *et al.*, 2012) which could also have applications in MRS experiments.

2.9.8 Signal to Noise Ratio and Signal Averaging

Detection of a signal during an MRS experiment depends on both the signal amplitude and the degree of noise (the signal to noise ratio). The noise in the spectrum arises from the random thermal motion of electrons in the radiofrequency coil used to detect the signal and the subject being scanned. Since noise is random, signal averaging also enables a reduction in noise, relative to the signal.

2.9.9 Choice of Echo Time (TE)

The choice of echo time is important in spectroscopy experiments and will effect which resonances will be detected depending on their T2 relaxation properties. At long echo times (TE 136 to 288ms), three major resonances are detectable within the CNS; i) N-Acetyl-aspartate (NAA), ii) Choline containing compounds (tCho), and iii) Creatine (Cr). At shorter echo times (TE 20–30 ms), metabolites with both short and long T2 relaxation times are observed, therefore allowing a larger numbers of metabolites to be quantified, and typically, glutamate (Glu) and myo-inositol (Ins) are seen in addition to NAA, tCho and Cr at short TE.

2.9.10 The Principal Metabolites: tNAA, tCho, tCr, Glu, Gln, Ins

The resonance found at 2.02 parts per million (ppm) is produced by the N-acetyl group of NAA and to a lesser extent, of N-acetyl aspartyl glutamate (NAAG) (Aggarwal and Nicholson, 2002). NAA is a non-essential amino acid and, in health, produces the largest metabolite signal in the CNS. NAA is produced by the mitochondria from L-aspartate and acetyl-CoA and is dependent on normal mitochondrial metabolism (Clarke *et al.*, 1975; Patel and Clark, 1979; Truckenmiller *et al.*, 1985). However, despite the abundance of NAA in the CNS, its precise biological function remains unknown. It has been proposed that it might provide a source of acetyl groups for lipid synthesis, participate in osmotic regulation or regulate protein synthesis (Clarke *et al.*, 1975; Birken and Oldendorf, 1989; Lee *et al.*, 1994). In MRS experiments, NAA is generally regarded as a "neuronal marker" as it is thought to be found exclusively in the CNS, and is predominantly localised to neurones, axons and dendrites (Simmons *et al.*, 1991). More recently, quantification of NAA using MRS has also been suggested as a surrogate marker of mitochondrial function in a study of multiple sclerosis (Ciccarelli *et al.*, 2010a). Decreases in NAA have therefore been interpreted to indicate underlying axonal loss or injury, impaired neuronal mitochondrial metabolism or both.

In acute MS lesions a drop in NAA is typically seen, with several studies reporting partial recovery months later (Arnold *et al.*, 1994; De Stefano *et al.*, 1995a; Ciccarelli *et al.*, 2010a). Given that axonal regrowth seems an implausible explanation for the recovery in NAA, the two most likely explanations include dilution of NAA due to tissue oedema at the time of relapse followed by resolution of oedema and subsequent rise in NAA concentration after recovery, or recovery of mitochondrial function following resolution of inflammation. A recent study examining changes in water content and NAA concentrations in new MS lesions

over six months found that water content changes were insufficient to account for all of the recovery of NAA after relapse (Vavasour *et al.*, 2011). This would suggest at least some of the recovery was due to recovery of mitochondrial function as demonstrated by Cicceralli *et al* (Ciccarelli *et al.*, 2010a) or due to alterations in NAA relaxation time as a consequence of alterations to tissue chemistry or proliferation of oligodendrocyte progenitor cells (which contain NAA) to enhance remyelination (Davie *et al.*, 1994).

The methyl and methylene portions of creatine (Cr) and phosphocreatine (PCr) produce the second largest resonance in the CNS and form a composite peak at 3.03 ppm. Cr and PCr are important intermediaries of energy metabolism and are involved in the creatine kinase reaction to generate ATP. Creatine concentrations in the brain are thought to remain fairly constant with aging (Saunders *et al.*, 1999) and are unaffected in many diseases. For this reason creatine is sometimes used as an internal reference standard to normalise the intensity of other resonances. However caution is needed when using creatine as an internal reference when studying patients with MS, as brain creatine concentrations were shown to be higher in RRMS (Inglese *et al.*, 2003).

In vitro, glial cells contain two to four times higher concentrations of creatine than neurons (Urenjak *et al.*, 1993). Elevated Cr in MRS experiments has therefore often been interpreted to represent increased gliosis and possibly remyelination (Inglese *et al.*, 2003).

A resonance from the methyl protons of choline containing compounds is seen at 3.2 ppm. The resonance for total choline (tCho) is contributed to by glycerophosphorylcholine and phosphorylcholine and possibly betaine and taurine (Brenner *et al.*, 1993). Choline containing compounds are normal constituents of myelin and membrane phospholipids and changes in the resonance intensity of choline has been suggested to reflect increases in the steady state

levels of membrane phospholipids released during myelin breakdown, for example in active demyelinating disease (Davie *et al.*, 1993; Tartaglia *et al.*, 2002; Gonzalez-Toledo *et al.*, 2006), acute stroke (Dani *et al.*, 2012) and neoplasms (Horska and Barker, 2010). In MS, cerebral Cho is elevated in NAWM (Inglese *et al.*, 2003) and Cho/Cr ratio rises have been reported in areas of NAWM which later develop into focal lesions (Tartaglia *et al.*, 2002) and thought to return to normal with resolution of inflammation and onset of remyelination (Degaonkar *et al.*, 2002).

The resonance, split into a doublet of doublets centred at 3.52 ppm comes from the ^{1}CH and ^{3}CH protons of Ins, a cyclic sugar alcohol, which can be made in cells from glucose. It is a ubiquitous sugar and can be found in cells in most organ systems. In the CNS it has been proposed as a glial marker (Chard *et al.*, 2002) and in multiple sclerosis, elevated Ins has been seen in early disease (Chard *et al.*, 2002) and clinically isolated syndromes (Fernando *et al.*, 2004), with the highest levels seen in acute lesions (Srinivasan *et al.*, 2005) suggesting that, in the brain, glial proliferation plays a role in early disease as well as during the active disease phase.

Glutamate (Glu) is the most abundant amino acid in the CNS, and as discussed in *Chapter 1*, is the major excitatory neurotransmitter in the mammalian nervous system and is the precursor for the major inhibitory transmitter GABA. Glu has two methylene groups and a methine group that are strongly coupled which gives Glu a complex spectrum, with the proton from the methine group appearing as a doublet of doublets at 3.75 ppm and the signal from the other four protons appearing as multiplets between 2.04 ppm and 2.35 ppm. Glutamine (Gln) is structurally similar to Glu and also has one methine and two methylene groups and therefore has similar coupling interactions to Glu. The four protons from the

methylene groups produce a resonance that appears as multiplets between 2.12 and 2.46 ppm whilst the methine group produces a triplet at 3.76 ppm. Gln also has two further resonances at 6.82 and 7.73 ppm which are rarely used for quantification in vivo.

Due to the similarities in their spectra, Glu and Gln are virtually indistinguishable at lower magnetic field strengths, and using conventional localisation sequences they have previously only been separated at field strengths of 7T or higher (Tkac *et al.*, 2001). Being able to separate the metabolites allows much more accurate quantification of Glu which is thought to be involved in the pathogenesis of many diseases. Most MRS studies of neurological diseases to date have focused on quantifying glutamate + glutamine (Glx) complex (Hattori *et al.*, 2002). More recently, a modified PRESS localisation sequence was described that could separate Glu and Gln at 2.35 ppm at 3T (Hurd *et al.*, 2004). Subsequently, these modified protocols have been used to demonstrate elevated Glu levels in acute MS brain lesions (Srinivasan *et al.*, 2005).

2.9.11 Spectral Fitting

The spectrum (**Figure 2.8**) is a plot of signal intensity on the Y-axis, which approximates metabolite concentration against chemical shift on the x-axis, which is usually denoted in parts per million (ppm). *In vivo* NMR signal processing can now be performed using several line fitting algorithms that incorporate prior knowledge of metabolites used, such as LC model (Provencher, 1993), jMRUI (Naressi *et al.*, 2001a; Naressi *et al.*, 2001b) and others. Recent advances have made it easier to quantify metabolites from a predefined area within the spinal cord using simulated basis sets and LCmodel (Provencher, 2001).

The reliability of spectral fitting in LCModel is dependent on adequate SNR, which increases with voxel size and acquisition time. Optimising field homogeneity using shimming will also reduce width of peaks and therefore their resolution from adjacent signals. Within the output file produced by LCModel, some data is provided to help the user assess the reliability of the fit; i) FWHM (full width at half-maximum) provides an estimate of the line width of the spectrum, ii) signal to noise ratio (S/N), estimated standard deviations (Cramér-Rao lower bounds) expressed in percent of the estimated concentrations.

2.10 Diffusion Imaging

2.10.1 Introduction

Molecular diffusion or Brownian motion refers to the random movement of molecules in solution. The process is thermally driven and can be described by the diffusion co-efficient (D), which is dependent on temperature, viscosity of the solution and the molecular weight of the diffusing particle. Diffusion which occurs when mixing two liquids or gases will occur along a concentration gradient from areas of relatively high concentration, to regions of lower concentration, whilst diffusion of water molecules in biological tissues, is thermally agitated and is described as self-diffusion (Wheeler-Kingshott *et al.*, 2003). In either case, the random movement of molecules can be described statistically using the displacement distribution which describes the proportion of molecules travelling over a particular distance in a given direction. The displacement distribution for unrestricted water molecules is a Gaussian function whereas water diffusing within highly ordered and organised structures may be non-Gaussian.

Studying water diffusion is a useful method for studying integrity of white matter tracts. During health, white matter tracts consist of closely packed, myelinated axons connecting two regions within the CNS, which are therefore orientated in a similar direction. Diffusion of water molecules within axons and in the extracellular space between fibres preferentially occurs parallel to fibres, rather than perpendicular to them due to microstructures and cell membranes acting as barriers (Wheeler-Kingshott *et al.*, 2003). This ordered, directional diffusion is known as anisotropic diffusion. Anisotropy is reduced when there is disruption to the microstructural integrity of white matter tracts, which allows water molecules to diffuse more freely in directions other than the main orientation of the tract.

2.10.2 Diffusion Weighted Imaging

Diffusion weighted imaging (DWI) is performed by spatially labelling spins (from water molecules) at two time points, between which, the displacement of spins is measured. This time interval is known as the diffusion time (Δ) and the net displacement of water molecules is called the *apparent diffusion coefficient* (ADC). The pulsed gradient spin echo sequence (PGSE) developed by Stejskal and Tanner (Stejskal and Tanner, 1965) is one of the earliest methods for measuring diffusion and consists of a spin echo sequence, with two equal and opposite magnetic field gradients applied either side of the 180° pulse. Addition of the gradients, as discussed earlier will mean that precession speed of spins will be dependent on their spatial location along the direction of the gradient. Spins will also acquire different phase shifts dependent on their location. The stronger the field gradient, the more marked the phase changes will be across the subject, causing an increased sensitivity to diffusion. The '*b*-value' which is proportional to the square of the gradient strength is used to describe the

diffusion weighting of a sequence. In the PGSE sequence the *b*-value has units of mm^2/sec
and is given by:

$$b = \gamma^2 G^2 \delta^2 (\Delta - \delta/3)$$

Where G is the gradient amplitude, δ is the duration the gradient is applied and Δ is the
diffusion time.

The 180° RF pulse between the two gradient pulses reverses the phase changes caused by the
first gradient. Hence, once the second gradient is applied, spins which stayed in their original
position will experience no net change in phase, whilst those that diffuse will see their phase
altered dependent on the distance over which diffusion has occurred over. Therefore due to
the individual spins being out of phase, the signal produced is attenuated, provided that
sufficient diffusion weighting is applied. The degree of signal attenuation will therefore
depend on diffusion properties of the tissue as well as sequence parameters determining the
size of the gradient and the diffusion time. The greater the degree of motion the more signal
attenuation occurs ie. lower signal is detected.

2.10.3 Diffusion Tensor Model

The Diffusion tensor model is a better mathematical model of water diffusion within white
matter tracts. It is superior to the simple ADC as it provides information about direction of
diffusion, and whereas the ADC is dependent on the direction in which it is measured, the
diffusion tensor can characterise multi directional diffusion. The tensor model is represented
mathematically by a 3 x 3 matrix with nine elements as below, with the diagonal elements of
the matrix (Dxx, Dyy and Dzz) corresponding to diffusivity in three orthogonal planes, and

off-diagonal elements showing information regarding the correlation between displacements in the three orthogonal planes. For example the Dyz correlates diffusion along the y and z axes.

$$\mathbf{D} = \begin{bmatrix} D_{xx} & D_{xy} & D_{xz} \\ D_{xy} & D_{yy} & D_{yz} \\ D_{xz} & D_{yz} & D_{zz} \end{bmatrix}$$

2.10.4 The Eigensystem and Measuring Anisotropy

The orientation of the three orthogonal axes, are denoted by the three eigenvectors; ε_1, ε_2, and ε_3. The diffusivities along each of the three orthogonal axes are denoted by the eigenvalues; λ_1, λ_2, and λ_3. The eigenvector associated with the largest eigenvalue is taken to be the principal eigenvector ε_1, and as such the tensor is orientated parallel to this (Jones, 2009). The corresponding diffusivity, λ_1, is known as the longitudinal diffusivity or the axial diffusivity (AD). The radial diffusivity (RD) is calculated by calculating the mean of the diffusivities along the two minor axes (λ_2, and λ_3), whilst the mean diffusivity (MD) is calculated by averaging, the three eigenvalues. The most commonly used anisotropy index is the fractional anisotropy (FA) which measures the fraction of diffusion within a given voxel can be ascribed to anisotropic diffusion (Basser and Pierpaoli, 1996).

2.10.5 Relevance of Anisotropy Indices and Application in Spinal Cord Studies

FA, which is derived by the DTI, reflects the underlying tissue microstructure within spinal white matter tracts (Gulani *et al.*, 2001), whilst animal studies have shown that demyelination often leads to an increase in RD, and axonal loss leads to a rise in AD (Song *et al.*, 2002). It is difficult to extrapolate the findings from these animal studies to patient studies, so findings on axial and radial diffusivities in patient studies must be interpreted with caution. However, the spinal cord DTI-derived parameters have the potential to be used as biomarkers of both myelin and axonal integrity, and have been demonstrated to significantly change over time after an acute injury, such as an acute demyelinating lesion (Freund *et al.*, 2010).

MD is very sensitive to general change in tissue microstructure that allows water molecules to move less or more freely; for example, a reduction of the MD has been detected following acute neurological insults, but in chronic neurological disease, or where cellular necrosis leads to increased membrane permeability, a relative increase in the MD value can be seen (Gass *et al.*, 2001).

FA, RD, AD, and MD can all be measured within the spinal cord using regions-of-interest, which can be drawn on the basis of the user's anatomical knowledge. Additionally, they can be measured within tracts, which are reconstructed using fibre tracking (FT) algorithms. Probabilistic tractography algorithms allow the user to obtain an estimate of white matter connectivity within the spinal cord tracts, which may change with pathology.

2.10.6 Practical Considerations

Spinal cord DTI studies in patients have been performed with the assumption that DTI measures do not change across spinal cord levels. Wheeler-Kingshott *et al.* (Wheeler-Kingshott *et al.*, 2002) confirmed a uniform MD along the cervical spinal cord, but found a higher FA in the mid and lower section of the cervical cord compared with the upper cervical cord. Regional differences in DTI metrics of the cervical cord have also been reported by Mamata *et al* who found higher mean FA and ADC in the upper segments of the cervical cord (C2- C3) than in lower segments (C4- C7) in healthy volunteers (Mamata *et al.*, 2005). These findings suggest that regional DTI measures should be compared between patients and controls whenever possible, since averaging values of DTI measures may dilute the effect of focal pathology.

2.10.7 Technical Considerations

Although the DTI model has proven a valuable tool for the study of numerous neurological diseases, it suffers from several technical limitations. Firstly, in brain regions where fibres might be crossing, fibres within a given voxel may not be orientated in the same direction. The effect of signal averaging across such voxels can result in inaccurate representation of true tract orientation and integrity (Tuch *et al.*, 2002). Secondly, the DTI model assumes a Gaussian distribution for the displacement distribution function which is unlikely to reflect true diffusion characteristics within neuronal tissue, which is structurally complex and risks underestimating the slow diffusion component within the intra-axonal compartment (Assaf *et al.*, 2002).

2.10.8 Q-Space Analysis

In DTI analysis, the mathematical model assumes that the displacement distribution function has a Gaussian distribution. Q-space analysis differs in that it employs a Fourier transformation of the signal attenuation curve to determine the displacement distribution without assuming a Gaussian distribution. Q-space imaging (QSI) is a model free diffusion weighted imaging (DWI) technique (Callaghan *et al.*, 1988) which employs Q-space analysis to provide displacement probability profiles of water molecules within each voxel, hence allowing the user to study water diffusion characteristics in multiple regions of interest.

When the signal attenuation curve is Fourier transformed, the user obtains the probability density distribution of the diffusion from which we are able to derive summary statistics, most commonly the full width of half maximum (FWHM) and zero displacement probability (P_0). **Figure 2.11** outlines the steps in Q-space imaging analysis. The FWHM and P_0 functions describe the width and height of the displacement distribution function. A high P_0 and low FWHM are generally indicative of restricted diffusion, whilst a wider FWHM and lower P_0 are suggestive of less restricted diffusion.
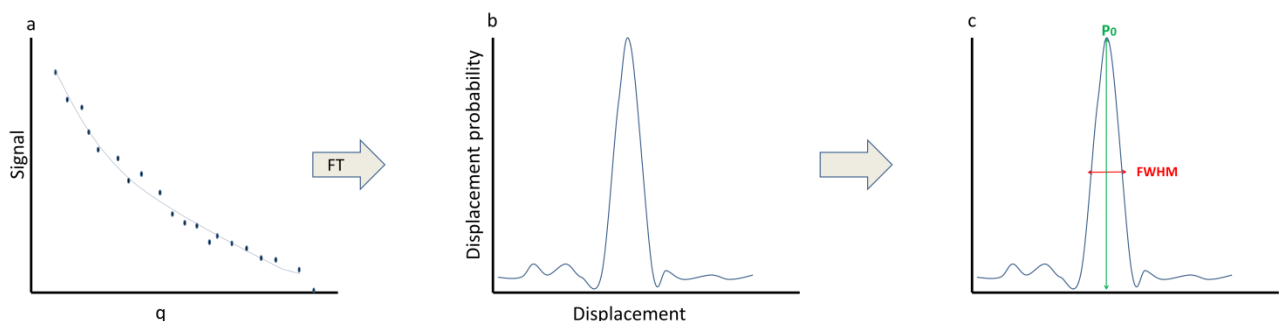
Figure 2.11: Summary of steps in Q-space imaging analysis. The signal attenuation curve (a) from the raw Q-space imaging data is Fourier transformed to give the probability density function (b) from which summary statistics can be derived (c).

In early experimental work on biological samples, Q-space analysis was successfully applied to accurately measure the dimensions of yeast cells (Cory and Garroway, 1990), by using a wide range of *b*-values and diffusion times to assess the effects on the displacement distribution function. It had therefore been predicted that similar techniques might allow measurement of mean axonal diameters, however interpretation of Q-space metrics in CNS samples for this purpose has proven difficult due to the compartmentalisation of water in the CNS by membranes of varying permeability, such that it is impossible, currently, to isolate individual compartments for study (Assaf and Cohen, 2000). However, because q-space parameters are contributed to from areas with non-Gaussian diffusion, it is a more sensitive technique for detecting restricted diffusion (Assaf and Cohen, 2000; Assaf *et al.*, 2002). Therefore, it is assumed, from Q-space theory, that compartments that show slower diffusion, such as intra-axonal fluid might contribute more to Q-space metrics than DTI metrics (Schneider and Wheeler-Kingshott, 2014).

The spinal cord makes an ideal model for Q-space imaging because myelinated axons in the spinal cord are organised in tightly packed tracts, predominantly orientated in a single direction which allows diffusion weighting gradients to be oriented parallel and perpendicular to ascending and descending tracts, which would be more difficult to achieve in the brain to the complexity of its white matter architecture.

2.10.9 Technical Considerations

Q-space imaging requires much higher diffusion weighting (*b*-value) than DTI which can be difficult to achieve on clinical scanners. Large gradients and short gradient pulses needed to

perform true Q-space imaging (which requires $\delta \ll \Delta$) cannot be achieved due to hardware limitations of currently available systems, but several studies have attempted to compensate for this by using smaller gradients and longer gradient pulses which has the effect of narrowing the PDF produced by Q-space analysis (Assaf *et al.*, 2002; Nossin-Manor *et al.*, 2005) which leads to longer scan times and can underestimate the FWHM. It has therefore been proposed that these should be considered as "apparent values" (Assaf *et al.*, 2005; Farrell *et al.*, 2008). Additionally the use of heavy diffusion weighting has the effect of reducing SNR.

Chapter Three

Spinal cord imaging in MS

3.1 The Spinal Cord

The spinal cord extends from the cranial border of the atlas to the lower level of the L1 lumbar vertebrae. Superiorly, it is continuous with the medulla and inferiorly the spinal cord terminates at the conus medullaris. Once adulthood is reached, the average length of the human spinal cord is 45cm in the male and 42 cm in the female. The corresponding average length of the spinal column is approximately 70cm (Williams and Warwick).

3.1.1 Cross Sectional Anatomy of the Spinal Cord

In cross-section (**Figure 3.1**), the spinal cord contains central grey matter, in a modified "H" shape, surrounded by white matter tracts. The grey matter is organised as two lateral columns, each having a dorsal horn, lying dorsolaterally and a ventral horn lying ventrolaterally. The central canal runs through the centre of the grey commissure and the grey matter dorsal to the central canal is referred to as the dorsal grey commissure and the grey matter lying ventral to the canal is the ventral grey commissure.

The white matter tracts surrounding the grey matter are separated into three columns in each half of the cord by the grey matter and the intramedullary portions of the spinal roots as follows: i) the posterior column lies between the posterolateral sulcus and the posterior median sulcus, ii) the anterior column between the anterior median fissure and the most lateral of the anterior nerve roots and iii) the lateral column between the dorsolateral and ventrolateral sulci.

The columns compartmentalise the major ascending and descending tracts of the spinal cord. The ascending, afferent tracts carry sensory input to the brain whilst descending motor tracts

exert their effects on motor neurons. Afferent sensory input enters the spinal cord via the dorsal roots where fibres bifurcate within the zone of Lissauer. The axons of second order neurons decussate over several spinal segments through the ventral white commissure to the anterolateral cord, where they ascend as the lateral spinothalamic tract in the lateral column, conveying pain and temperature sensation. Fibres carrying information regarding light touch ascend in the ventral spinothalamic tract after decussating. Discriminative senses such as joint position sense, vibration sense and weight perception are conveyed in the posterior column. Other ascending tracts include the anterior and posterior spinocerebellar tracts and the cuneocerebellar and rostrocerebellar tracts which carry unconscious proprioceptive information from the lower part and upper part of the body respectively.
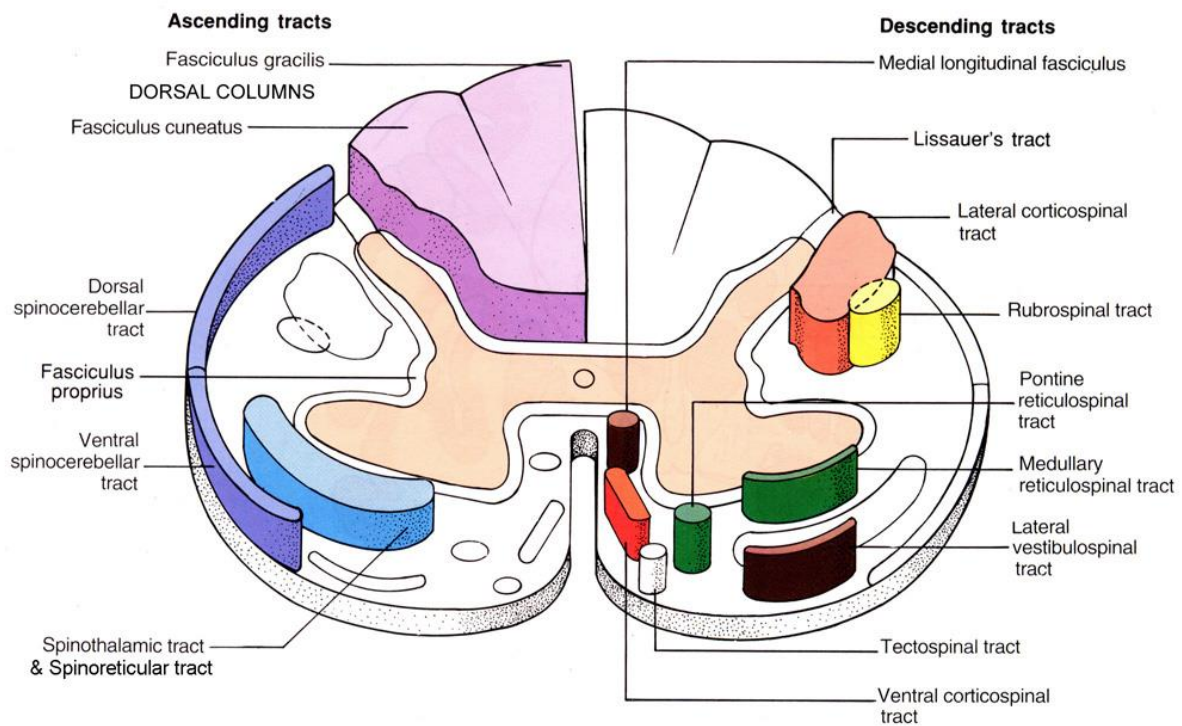
Figure 3.1: Cross sectional anatomy of the spinal cord showing main spinal cord tracts (Image from www.acbrown.com).

There are five descending tracts within the spinal cord; i) the corticospinal tract, ii) the corticorubrospinal tract, iii) the lateral reticulospinal tract, iv) the medial reticulospinal tract and v) the vestibulospinal tract. The corticospinal tract arises from fibres from the primary motor cortex, lateral premotor cortex and the supplementary motor cortex of the contralateral hemisphere. The fibres descend through the corona radiata to the posterior limb of the internal capsule and pons, to reach the ventral medulla where they form two large pyramids. When the fibres reach the caudal medulla, approximately 90% will decussate to form the lateral corticospinal tract, which runs in the lateral column. The remaining 10% of fibres descend in the ipsilateral anterior column in the anterior corticospinal tract. The axons of the upper motor neuron connect via interneurons and rarely, direct synapses with the lower motor neurones within the ventral horn of the spinal cord.

The corticorubrospinal tract is formed from cells in the primary motor cortex which project to the ipsilateral red nucleus, before decussating in the brainstem and descending through the brainstem tegmentum and the lateral column of the spinal cord. The lateral reticulospinal tract is an extrapyramidal motor tract which descends from the reticular formation within the medulla down the ipsilateral lateral column. The medial reticulospinal tract arises from pontine and medullary reticular formation and descends in the ipsilateral anterior column. The vestibulospinal tract fibres originate in the lateral vestibular nucleus and run anteriorly, in the lateral column where they produce corrective motions of the head, body and limbs in response to afferent input from the eighth cranial nerve.

3.1.2 Blood Supply and Venous Drainage of the Spinal Cord

The anterior two thirds of the spinal cord receives its blood supply from the anterior spinal artery which arises from the radiculomedullary arteries and runs along the mid-line of the anterior surface of the spinal cord. The posterior spinal arteries are smaller, paired branches of the intracranial vertebral arteries and provide the blood supply to the posterior column and posterior horn. Anastomotic radicular arteries, mainly branching from the aorta also feed the posterior and anterior arterial systems at various levels.

Venous drainage of the spinal cord follows the arterial system ie. the posterior and anterior segments have dedicated drainage systems. The anterior spinal vein runs in the anterior sulcus, adjacent to the anterior spinal artery and the posterior spinal veins are run parallel to the posterior spinal arteries and drain the posterior column.

3.1.3 Spinal Cord Physiology

The spinal cord is bathed in the cerebrospinal fluid (CSF) produced by the choroid plexus in lateral, III, and IV ventricles in the brain. From the fourth ventricle, CSF flows down through the foramen of Lusha into the pontine cisterns and cisterna magna to reach the upper cervical cord. The CSF is contained within the subarachnoid space between the pia and arachnoid mater. CSF enters the spinal cord through the Virchow-Robbins spaces that surround blood vessels penetrating the cord. It then diffuses to the spinal canal where it is taken up, flows back, upwards towards the brain. Secretory mechanisms in the choroid plexus transport water soluble micronutrients, including vitamin C, folates, deoxyribonucleosides, vitamin B6 and certain trace elements into the CSF for eventual delivery to the brain and spinal cord (Johanson, 2008).

3.2 Application of spinal MRI to multiple sclerosis

3.2.1 Spinal Cord MRI in MS

Spinal cord imaging comes with specific technical challenges. As discussed in chapter two, the spinal cord is a small region of interest and motion artefact is caused by oscillation of the cervical cord in the craniocaudal direction after each cardiac systole (Mikulis *et al.*, 1994). Truncation (Gibbs) artefacts which occur at the interface between high and low signal as a consequence of under-sampling of data in the phase direction can cause misrepresentation of the CSF/spinal cord interface within the image and appear as parallel lines adjacent to cerebrospinal fluid interfaces, within the spinal cord and canal, degrading image quality (Bronskill *et al.*, 1988; Levy *et al.*, 1988). It is, however possible to reduce most of the motion artefacts during spinal cord imaging, using cardiac triggering and saturation bands and the development of phased-array receiver coils and fast imaging techniques has led to more reliable imaging of the spinal cord and has improved the quality of quantitative data (Filippi and Rocca, 2011). Technical improvements in spinal cord imaging have led to an increase in clinical studies focusing on the spinal cord in MS which has led to the inclusion of spinal imaging in the MS diagnostic criteria since 2005 (Polman *et al.*, 2005; Polman *et al.*, 2011).

3.2.2 Imaging Spinal Cord Lesions

Spinal cord imaging sequence selection in MS depends on the purpose of the scan. The dual fast spin-echo (FSE) sequence remains the reference standard for imaging the spinal cord in MS (Hittmair *et al.*, 1996). Both short and long echo times can be used to detect focal lesions

(Lycklama a Nijeholt *et al.*, 1997), but diffuse lesions are usually only seen with short echo times (Hittmair *et al.*, 1996). The short inversion time inversion-recovery (STIR) sequence shows good lesion to cord contrast and has particularly good sensitivity for detecting diffuse spinal cord pathology (Hittmair *et al.*, 1996). However STIR is more susceptible to flow-related artefacts and reduced image quality than conventional sequences and cannot therefore be used as substitute for other sequences, rather it should be used to supplement imaging protocols (Hittmair *et al.*, 1996). The phase sensitive inversion recovery (PSIR) sequence is a T1-weighted inversion prepared 3D gradient echo (turbo field echo) sequence which provides good contrast between grey matter and white matter in the spinal cord and can improve detection of lesions when used in combination with FSE sequences (Poonawalla *et al.*, 2008). Although PSIR has been used successfully in the brain to detect pure grey matter lesions (Sethi *et al.*, 2012), a recent PSIR study failed to detect pure grey matter lesions in the spinal cord (Kearney *et al.*, 2013a). The double inversion recovery (DIR) sequence has recently been demonstrated to improve detection of small spinal cord lesions in MS (Riederer *et al.*, 2014). Fluid attenuated inversion recovery (FLAIR) sequences which are commonly used for brain imaging in MS have low sensitivity for detecting spinal cord lesions, with only $6 - 73\%$ of spinal lesions seen on T2 weighted FSE sequences detected using FLAIR sequences (Keiper *et al.*, 1997; Stevenson *et al.*, 1997).

3.2.3 Characteristics of MRI detectable Spinal Cord Lesions in Multiple Sclerosis

MRI-detectable spinal cord MS plaques (**Figure 3.2**) are seen in up to 82% of newly diagnosed MS patients (Bot *et al.*, 2004) and up to 90% of patients with more established disease (Lycklama *et al.*, 2003). Spinal cord involvement in the absence of brain lesions is rare but has been reported in up to 10% of cases (Honig and Sheremata, 1989; Bot *et al.*, 2002). Interestingly, spinal cord lesions occur independently from brain lesions (Bot *et al.*,

2004) which suggests that the mechanisms behind the development of spinal cord lesions and brain lesions may be different.

Lesions are most often located in the cervical cord and are characteristically peripherally located, most frequently affecting the posterior columns, are typically less than two vertebral segments in length, and occupy less than half the cross-sectional area of the cord (Kearney *et al.*, 2013a; Riederer *et al.*, 2014). Acute spinal cord lesions and those occupying greater than 50% of the cross sectional area can be associated with vasogenic oedema, seen as cord swelling (Tartaglino *et al.*, 1995; Thielen and Miller, 1996). In contrast, chronic lesions rarely alter cord morphology but can sometimes be associated with local volume loss (Tartaglino *et al.*, 1995).

Unlike the brain, T1 "black holes" at the site of tissue loss are rarely seen in the spinal cord, but T1 relaxation time is longer in the cervical cord of MS patients compared to healthy controls and signal intensity from the cervical cord on T1-weighted MRI correlates with cord atrophy and disability in PPMS patients (Nijeholt *et al.*, 1998). In RRMS and SPMS patients T1 relaxation also correlates well with EDSS (Vaithianathar *et al.*, 2003).

Focal lesions within the spinal cord are thought to be similar in number between MS sub-types but in progressive forms of MS, more confluent lesions are seen (Thorpe *et al.*, 1996). The spinal cord is a particularly important region to study in PPMS as patients have prominent spinal cord symptoms and relatively fewer T2-weighted brain lesions than in other MS subtypes (Thompson *et al.*, 1990). The majority of lesions affect the white matter columns and extend to involve grey matter (Tartaglino *et al.*, 1995; Thielen and Miller, 1996) which is supported by findings from histological studies (Gilmore *et al.*, 2006).

3.2.4 Gadolinium Enhancement

Contrast methods using gadolinium-diethylenetriamine pentaacetic acid (DTPA) are able to define areas of active blood-brain barrier breakdown thought to represent areas of acute inflammation. A longer delay following gadolinium injection, giving time for adequate circulation and using larger doses of contrast agent can improve detection rates (Tartaglino *et al.*, 1995). Spinal cord enhancement in one study was found to accompany enhancement within the brain suggestive of global disease activity (Silver *et al.*, 2001) but more commonly, spinal cord lesions enhance (**Figure 3.2**) in conjunction with the onset of spinal cord relapse (Thorpe *et al.*, 1996). In a study of 25 MS patients presenting with acute spinal cord relapse, 13 patients (52%) had a total of 15 enhancing spinal cord lesions at relapse onset, of which 72% had resolved by 2 month follow up (Trop *et al.*, 1998).

Figure 3.2: Sagittal PD-weighted image of the spinal cord showing expansile MS lesion at C2/3 (left) and GAD enhanced T1-weighted sequence in the same patient showing enhancement of lesion at onset of a relapse (right)

3.2.5 The clinico-radiological paradox

As the most visually evident imaging abnormality in MS, focal T2 lesions might be expected to be the predominant substrate of disability but spinal cord lesion load does not correlate well with disability (Kidd *et al.*, 1993), even when disability is determined using a clinical measure such as the EDSS which is heavily weighted towards spinal cord functions such as ambulation. In fact, spinal cord T2 lesions are often clinically silent. Asymptomatic spinal cord lesions have been reported in about 50% of patients with CIS and early MS (O'Riordan *et al.*, 1998; Lycklama a Nijeholt *et al.*, 2000).

This clinico-radiological paradox might partly be explained by difficulties in accurately quantifying neurological dysfunction (Barkhof, 2002), but it is more likely to be explained by the lack of sensitivity and specificity of conventional MRI techniques for detecting microscopic histopathological change. Axonal loss, which is the principle substrate for chronic, irreversible disability in MS (Tallantyre *et al.*, 2010), occurs largely independently of T2 weighted lesions (Bergers *et al.*, 2002). The development of new quantitative MRI techniques which are more sensitive to change in underlying tissue microstructure and metabolism within the spinal cord show much better correlation with disability (Ciccarelli *et al.*, 2007; Benedetti *et al.*, 2010; Freund *et al.*, 2010) and can more accurately discriminate between patients with similar T2 lesion load on the basis of disability (Benedetti *et al.*, 2010).

3.2.6 Spinal Cord Atrophy in Multiple Sclerosis

Axonal loss has been noted in both NAWM and lesions within the spinal cord (Lin *et al.*, 2004). Additionally, histopathology studies demonstrated that spinal cord atrophy in MS occurs predominantly in the white matter, with similar grey matter volumes between patients and controls (Gilmore *et al.*, 2005). It is therefore thought that spinal cord atrophy in MS

predominantly reflects underlying axonal loss in the spinal cord as a consequence of destructive pathological changes within lesions and in the NAWM.

Spinal cord atrophy can be an early feature of MS and progresses with time. In patients presenting with CIS suggestive of MS, evidence of cord atrophy can be seen even in the absence of spinal cord symptoms (Brex *et al.*, 2001). However, spinal cord volume loss is most marked in progressive forms of MS and greatest in SPMS (Losseff *et al.*, 1996). In clinical studies of MS of long disease duration, spinal cord atrophy remains significantly associated with disability (Bonati *et al.*, 2011; Cohen *et al.*, 2012; Kearney *et al.*, 2014a). In the largest of these MS cohort studies, Kearney *et al* found that cervical cord atrophy in patients with $\geq$ 20 years disease duration was independently associated with EDSS and was more closely associated with disability than measures of brain atrophy (Kearney *et al.*, 2014a). Interestingly, the rate of spinal cord atrophy in PPMS does not correlate with rate of brain atrophy which further supports the presence of two independent disease processes causing injury to the brain and spinal cord (Ingle *et al.*, 2003).

Spinal cord atrophy measured using MRI is reproducible and has been demonstrated to correlate strongly with EDSS in cross-sectional studies; ($r = -0.7$, $P < 0.001$) (Losseff *et al.*, 1996); ($r = -0.52$, $p = 0.005$) (Stevenson *et al.*, 1998), making it a potentially useful tool for measuring disease progression and as an endpoint in clinical trials of neuroprotective agents. To date two MS clinical trials have included cord cross sectional area as an exploratory endpoint (Kalkers *et al.*, 2002; Lin *et al.*, 2003), and as an outcome measure, shows promise for use in future clinical trials.

3.2.7 Spinal Cord Spectroscopy in MS

Over the past decade, developments in imaging acquisition and post-processing, have made it possible to use MRS in clinical studies of spinal cord pathology, giving insights into pathogenesis. Reliable quantification of metabolites from the spinal cord using 1.5 tesla (T) scanners had been limited to a few metabolites (Gomez-Anson *et al.*, 2000; Kendi *et al.*, 2004). High (3T) field strength scanners should in theory allow increased separation of metabolite peaks, and allow the study of metabolites of relevance to the pathogenesis of MS, such as Glu and Ins.

3.2.8 Insights from Spinal Cord MRS Studies in MS

As discussed in *Chapter 2*, N-acetylaspartate (NAA) is synthesised by neuronal mitochondria (Patel and Clark, 1979), and commonly used as a marker of axonal integrity in neuroimaging studies. All cross sectional, spinal cord MRS studies in MS published to date (**Table 3.1**) have reported a reduction in NAA compared to healthy controls, which is thought to reflect axonal loss (Kendi *et al.*, 2004; Blamire *et al.*, 2007; Ciccarelli *et al.*, 2007; Marliani *et al.*, 2007; Henning *et al.*, 2008). In one study, cervical cord NAA was shown to correlate with clinical disability (Ciccarelli *et al.*, 2007), but most of the early exploratory studies have not reported clinical findings.

More recently, a study modelling NAA concentration in the spinal cord with other markers of axonal integrity, such as cross sectional cord area, demonstrated that mathematically derived estimates of mitochondrial function can be made from spectroscopic data (Ciccarelli *et al.*, 2010a). Development of such imaging biomarkers of mitochondrial function has implications for studying mitochondrial dysfunction in MS. Ciccarelli *et al*. demonstrated that following cervical cord relapse, NAA levels are low, compared to controls but, as patients recover from

their relapse, the NAA concentration can recover. Using a model that uses cord area as a surrogate marker of axonal density, they demonstrated that changes in NAA were not entirely due to axonal loss but also reflected mitochondrial dysfunction and concluded that recovery in NAA following relapse was partially explained by recovering mitochondrial function.

An increase in the spectral peak for choline-containing compounds (Cho), in patients with MS is considered to reflect breakdown of cell membranes. In a study of patients with chronic spinal cord lesions, cervical cord Cho/Cr ratio was elevated (Marliani *et al.*, 2010) which may reflect ongoing remyelination within plaques, though this finding has not been reproduced in other cohort studies. Unlike the brain where elevated Cr has been reported, Cr has not been shown to change in the spinal cord (**Table 3.1**).

Myo-Inositol (Ins) is the best available in-vivo glia-specific marker (Brand *et al.*, 1993). Elevated m-Ins is seen in the brain of patients with CIS who convert to MS, suggesting that gliosis may be a process of pathogenic importance in MS (Fernando *et al.*, 2004). In the cervical cord, m-Ins is marginally increased in patients with MS at the onset of a spinal cord relapse and was shown to correlate with disability in one study (Ciccarelli *et al.*, 2007). Another study showed a reduced Ins concentration in the spinal cord of a single MS patient (Henning *et al.*, 2008).

Study	Cohort size	Patient group	Field strength	TE (ms)	Calibration method	tNAA	tCho	tCr	Ins	Glx
Kendi et al 2004	9 MS 12HC	Normal appearing cervical SC	1.5 T	35	Quantification Not reported	↓	↔	↔	↔	?
Ciccarelli et al 2007	14 MS 13 HC	Acute cervical SC lesion	1.5 T	30	External phantom	↓	↔	↔	↔	?
Blamire et al 2007	5RR, 6SP, 11HC	Not specified	2 T	30	Unsuppressed water	↓	↔	↔	↔	?
Henning et al 2008	1MS 11HC	Active C6/7 lesion	3 T	42	Ratio Cr and Cho	↓	↑	?	↓	?
Marliani et al 2010	15MS 10HC	Chronic cervical lesions	3 T	35	Ratio Cr	↓	↑	?	↑	?

Table 3.1: Findings from cross sectional spinal cord spectroscopy studies in MS. Comparison between studies must be made with caution and allow for differences in calibration methods, patient group, field strength and acquisition parameters.

3.2.9 Q-space Imaging Studies of Relevance to the Study of MS

Early, pre-clinical Q-space imaging studies examining diffusion in ex-vivo rat spinal cord of varying stages of maturation and myelination demonstrated the technique was highly sensitive to the myelination status of rat spinal axons (Assaf *et al.*, 2000). In the mature spinal cord, very good white matter/grey matter contrast can be achieved owing to differences in diffusion characteristics. Mature, intact myelinated spinal cord, was associated with slower diffusion and exchange of water. Similarly, increased perpendicular diffusion was seen in the white matter of myelin deficient rats (Biton *et al.*, 2006). This sensitivity to myelin status makes Q-space a potentially useful tool for the study of demyelinating diseases such as MS (Assaf *et al.*, 2000).

Although the large gradients and short gradient pulses required to perform true Q-space imaging are unachievable on clinical scanners, due to hardware limitations, Q-space metrics have still been successfully derived from experiments on clinical systems by increasing gradient pulses to compensate for the low gradients (Assaf *et al.*, 2002; Assaf *et al.*, 2005; Latt *et al.*, 2007b). However, patient studies on clinical scanners have so far been limited. The earliest attempt to apply Q-space analysis to brain DWI to study a cohort of MS patients found that the slow diffusion component of water is diminished in NAWM compared to white matter from healthy controls (seen as a decrease in the amplitude and broadening of the displacement distribution profile) and is lost in lesional white matter. Interestingly, some of the diffusion abnormalities detected in NAWM were not detected on conventional DTI and it has been suggested that Q-space might therefore be able to give a better indication of disease load than conventional DTI, though clinical relevance of these findings were not assessed (Assaf *et al.*, 2002). The modifications to gradients and gradient pulse length necessary to enable the use of clinical scanners has the advantage of exaggerating the contribution of slow diffusing water to Q-space metrics (Assaf *et al.*, 2002) which may also make it more sensitive to axonal damage than conventional DTI (Assaf *et al.*, 2002; Assaf *et al.*, 2005). More recently, Assaf *et al,* using Q-space analysis have also reported decreased anisotropy of white matter tracts affected by MS lesions and in the peri-lesional white matter and demonstrated that Q-space indices were also correlated with NAA/Cr quantified using ^{1}H MRS across multiple brain regions (Assaf *et al.*, 2005).

A single clinical study using Q-space analysis to study spinal cord pathology in four MS patients has demonstrated the feasibility of such a study in the spinal cord (Farrell *et al.*, 2008). The study demonstrated the sensitivity of Q-space metrics to white matter damage in

the spinal cord. In keeping with findings from animal studies (Assaf and Cohen, 2000; Assaf *et al.*, 2000) and studies of MS brain (Assaf *et al.*, 2005), a decrease in anisotropy was seen in areas of demyelination. Schneider *et al* from UCL have recently demonstrated good reproducibility of Q-space metrics for studying diffusion parallel and perpendicular to the major ascending and descending tracts in healthy spinal cord (Schneider *et al.*, 2011) which now shows promise as a technique for the study of spinal cord pathology in MS.

Chapter Four

Optimising a spinal cord spectroscopy protocol

The role of spinal cord spectroscopy in studying MS pathophysiology has been discussed in *Chapter 3*. One major limitation of spinal spectroscopy studies in MS to date has been that glutamate, a potential mediator of axonal loss has not been quantified. In order for us to improve our understanding of the role of glutamate in axonal degeneration in MS, there is a need for new spinal spectroscopy protocols to be optimised for the detection of glutamate.

Within this chapter I will describe experiments performed to optimise a novel spinal spectroscopy protocol for detection of glutamate-glutamine (Glx) from the spinal cord (*Section 4.1*), investigate whether or not age and gender are associated with spinal metabolite concentrations (*Section 4.2*), and finally I have indirectly investigated differences in metabolite concentrations between the spinal grey and white matter by examining the associations between metabolite concentrations and the spinal grey matter volume fraction, which reflects the ratio of grey matter : white matter (*Section 4.3*).

4.1 Optimisation of a Spinal Cord Proton Spectroscopy Protocol for Quantification of Glutamate-Glutamine.

4.1.1 Introduction

Glutamate (Glu) is the major excitatory neurotransmitter in the central nervous system (CNS). As discussed in *Chapter 1*, excess extracellular Glu has been shown to cause damage to neurons and oligodendrocytes through activation of neurotoxic cascades and has been implicated in neuronal injury in several neurodegenerative diseases (Rothstein *et al.*, 1992; Hugon *et al.*, 1996; Arundine and Tymianski, 2004), including MS (Srinivasan *et al.*, 2005; Pampliega *et al.*, 2008).

In the brains of patients with early PPMS, glutamate-glutamine (Glx) is reduced in the cortical grey matter but not the normal appearing white matter (NAWM) (Sastre-Garriga et al., 2005). In SPMS, measurements from NAWM showed mean annualised declines of −4.2% (Glu), −7.3% (Gln), and −5.2% (Glx) which suggests that as disease progresses, Glu makes up proportionally more of the Glx signal (MacMillan *et al.*, 2015). In contrast, in early RRMS there is no change in brain Glx concentrations (Tiberio et al., 2006). But in acute brain lesions, Glu is elevated (Srinivasan et al., 2005) and higher brain Glu concentrations are predictive of accelerated axonal loss (Baranzini et al., 2010). However, it is not known if Glu-mediated excitotoxicity is also an important mechanism of neurodegeneration in the spinal cord. To answer this question, it is necessary to develop a [1]H-magnetic resonance spectroscopy (MRS) protocol that can accurately measure changes in Glu concentration *in vivo* using standard commercial scanners.

As discussed in *Chapter 2*, measurement of Glu using [1]H-magnetic resonance spectroscopy (MRS) is challenging at lower field strengths. Resolving Glu from the glutamine (Gln) peak at 3T in the brain has been the focus of a number of studies (Hurd *et al.*, 2004; Mayer and Spielman, 2005; Hancu, 2009). Strategies such as 2D J spectra and spectral editing techniques that exploit the scalar coupling of Glu have been shown from spectral simulations and *in vivo* investigations to be selective for Glu. However, these methods also result in the reduction of absolute signal amplitude, which compounds the inherently low signal-to-noise ratio (SNR) of Glu and could potentially result in the loss of other valuable metabolic information including, N-acetylaspartate (tNAA), total creatine (tCr), total choline (tCho) and myo-inositol (Ins).

In 2009, Hancu simulated 11 different sequences for detection of non-edited Glu and showed that Carr-Purcell point resolved spectroscopy (CPRESS) with a minimal echo time (TE) and short-TE (TE = 35 ms) point resolved spectroscopy (PRESS) give the most reproducible measurements, while JPRESS, an MRS technique to detect J-coupled metabolites, showed better accuracy when tested *in vivo* (Hancu, 2009). To date, little progress has been made on protocols capable of quantifying Glu or Glx from the spinal cord. A single spinal cord study in patients with spinal cord tumours reported Glu concentrations using a simulated echo acquisition mode sequence (STEAM TE = 30 ms, 1.5 T), reporting a considerable rise in Glu and drop in tNAA at the tumour site (Kim *et al.*, 2004).

Glx detection in the cervical cord is more challenging because, a) the spinal cord is less homogeneous than the brain, due to the proximity of multiple tissue types and b) CSF and physiological movement artefacts are more pronounced. Additionally, the majority of spinal

cord spectroscopy studies have used smaller volume voxels ($\leq$ 2 ml) (Cooke *et al.*, 2004; Marliani *et al.*, 2007), exacerbating the low SNR associated with Glx. This study therefore aims to optimise a spinal cord spectroscopy protocol for the quantification of Glx in the upper spinal cord by i) using a longer spectroscopy voxel to optimise SNR, ii) optimising RF coil and water suppression settings, iii) evaluating the sensitivity of two commercially available MRS sequences (PRESS and STEAM) for measurement of Glx in the healthy upper cervical spinal cord and iv) assessing the reproducibility of these sequences.

4.1.2 Methods

4.1.2.1 Study Participants

Nine healthy participants with mean age 31(SD $\pm$ 7) years (six male, three female) were prospectively recruited. Of the nine subjects, four (mean age 28 $\pm$ 2 years, 3 males) took part in the RF coil comparison and water suppression optimisation studies. The other five subjects (mean age 32 $\pm$ 3 years, 3 males) were scanned in the PRESS vs STEAM experiment and three of the five were re-scanned in the reproducibility experiment. All subjects provided written, informed consent prior to taking part in the research which was approved by the local research ethics committee.

4.1.2.2 Scanner

All scans were performed using a 3T Achieva system (Philips Medical Systems, Best, Netherlands). To reduce motion artefacts during scanning, an MR compatible cervical collar (Bodymedics Range, TalarMade™ Ltd, Chesterfield, UK) was worn by all volunteers as this

has been shown to reduce motion artefacts (Yiannakas *et al.*, 2012) and to lengthen the straight section of the cord allowing easier voxel placement.

4.1.2.3 MRI and MRS Protocol

All subjects underwent conventional structural imaging of the upper cervical cord with: (a) Spin-echo T2w sequence, with TR = 4000 ms; TE = 100ms; echo train length = 24 echoes; FOV= 160 x 250 mm^2; voxel size = 0.6 x 0.6 x 3.0 mm^3;number of excitations (NEX) = 2; 13 contiguous coronal slices, and (b) Dual-echo PD/T2w sequence with TR = 4000 ms; TE = 15/80ms; FOV= 256 x 160 mm^2; voxel size = 1.0 x 1.0 x 3.0 mm^3; NEX = 2; 12 contiguous sagittal slices.

Using the structural images to guide voxel placement, single voxel MRS data was then acquired by positioning a 2.1 ml (5 x 7.8 x 55mm^3) cuboid spectroscopy voxel within the cervical cord at the C1-C3 spinal level, centred at the C2/3 intervertebral disc (**Figure 4.1**). The tNAA voxel was chosen as the plan metabolite voxel instead of Glu because the position of the entire spectrum used for analysis could be covered using the lower tNAA chemical shift of 2.01 ppm and water. Both the tNAA voxel and the shifted water voxel were visible when planning the spectroscopy scan; they were positioned such that both voxels lay within tissue without CSF contamination.
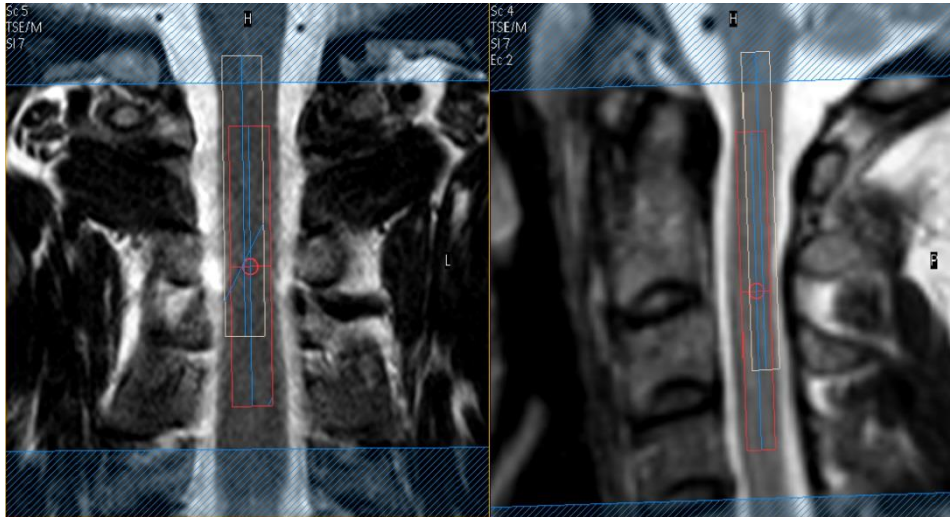
Figure 4.1: Spectroscopy voxel placement. Coronal (left) and sagittal (right) views of the cervical cord, showing voxel placement. The tNAA voxel (red) is centred on the C2/3 intervertabral disc, avoiding surrounding CSF. The white voxel illustrates the chemical shift displacement of water. Keeping both the red voxel (on resonance, 2ppm) and white voxel (4.7ppm) within the cord, ensures that metabolites between 2 and 4.7ppm (tNAA, Cr, tCho, Glx, Ins) also arise from within the spinal cord and chemical shift displacement of each metabolite need not be an issue.

Four outer volume suppression (OVS) slabs were orientated in the anterior-posterior (AP) and rostro-caudal (RC) directions. All scans were cardiac triggered following every third heartbeat with a 350-ms delay using a peripheral pulse unit (PPU) device that resulted in a TR of approximately 3000ms. Shimming was performed on the water signal from the voxel of interest itself.

4.1.2.4 RF Coil Comparison

Optimisation was performed on four healthy controls with a mean age of 28 (SD ±2) years (3 males, 1 female). We compared two multi-element head coils; the manufacturer's 32-channel head coil and the manufacturer's 16-channel neurovascular coil using only the 4 neck

1   elements. Each volunteer was scanned once with each coil (sequence parameters are shown in

2   **Table 4.1**). The SNR of the tNAA peak derived from LCModel was used to compare coils.

Experiment	Sequence	Voxel size (mm)	Water suppression	TR/TE/TM (ms)	NSA	Coil	OVS slabs
Coil Comparison	PRESS	5 x 7.8 x 50	MOIST	3RR/36	192	32Ch	RC-AP
	PRESS	5 x 7.8 x 50	MOIST	3RR/36	192	NVn	RC-AP
Water Suppression	PRESS	5 x 7.8 x 50	Inversion	3RR/36	8	NVn	RC-AP
	PRESS	5 x 7.8 x 50	Excitation	3RR/36	8	NVn	RC-AP
	PRESS	5 x 7.8 x 50	VAPOR	3RR/36	8	NVn	Circular
	PRESS	5 x 7.8 x 50	CHESS	3RR/36	8	NVn	RC-AP
	PRESS	5 x 7.8 x 50	MOIST	3RR/36	8	NVn	RC-AP
PRESS v STEAM	PRESS	5 x 7.8 x 55	MOIST	3RR/36	376	NVn	RC-AP
	STEAM	5 x 7.8 x 55	MOIST	3RR/11/17	376	NVn	RC-AP

3   NSA = number of signal averages, OVS = Outer volume suppression

4   **Table 4.1**: Sequence parameters for the optimisation scans and PRESS vs STEAM sequence
5   comparison

6

7   **4.1.2.5 Water Suppression Optimisation**

8   The same four volunteers were re-scanned using each of the five available water suppression

9   options on the Philips system; frequency selective excitation (Morris and Freeman, 1978) and

10   inversion (Patt and Sykes, 1972), chemical shift selective suppression (CHESS) (Haase *et al.*,

11   1985), multiply optimised insensitive suppression train (MOIST) and variable pulse power

12   and optimised relaxation delays (VAPOR) (Tkac *et al.*, 1999) were tested once on each of the

13   four volunteers. In addition, an unsuppressed reference scan was acquired. Using the

14   suppressed and unsuppressed scans, the residual water peak as a percentage was calculated

15   and used to determine the optimal water suppression module. **Table 4.1** shows the parameters

16   for each of the scans.

17

4.1.2.6 PRESS Vs STEAM

Five of the nine recruited volunteers (mean age 32 ±3 years, 3 males, and 2 females) were scanned with PRESS and STEAM sequences acquired on two separate occasions. Sequence parameters are shown in **Table 4.1**. Both sequences were acquired with 376 averages in a similar scan time of approximately 20 minutes. An additional unsuppressed water scan was also collected for quantification. The unsuppressed water was collected from the plan metabolite voxel; in this case, the position of the tNAA voxel. To assess intra-subject variability, the PRESS sequence was performed twice in 3 of the 5 volunteers. Using screenshots of the voxel placement taken during the first scan, the voxel was placed in the same region in the second scan.

4.1.2.7 Post-Processing

Metabolite concentrations were quantified using the user-independent LCModel (version 6.3) package (Provencher, 1993). PRESS data were analysed using a basis set created using the GAMMA simulation package (Smith *et al.*, 1994). For the STEAM sequence, twenty-four metabolites were simulated in MATLAB R2012a (The MathWorks, Inc. Natick, MA). Data was analysed with water scaling to get concentrations in mmol/l. The SNR reported by LCModel for each spectrum was used an indicator of overall spectral quality and Cramér–Rao lower bounds (CRLB) values provided by LCModel were used as a measure of reliability of the Glx and tNAA fit. Spectral quality and fit were assessed using the quality indicators provided by LCModel; spectra were excluded when SNR was < 3 and FWHM >

0.13 and metabolite concentrations were considered reliable only when CRLB $\leq$ 20% (Provencher, 2014).

4.1.2.8 Statistical Analysis

All statistical analyses were performed using IBM SPSS statistical package version 22.0 (IBM Corporation, Armonk, NY, USA) and a P-value < 0.05 was considered significant. To assess differences in spectral quality obtained using the 2 RF coils, a paired t-test was used to assess differences in SNR obtained with each coil. A paired t-test was also used to assess differences in % residual water using each of the water suppression modules.

To assess differences in the reliability of metabolite fitting between the PRESS and STEAM protocols, differences in CRLB's between STEAM and PRESS sequences were assessed using a non-parametric bias-corrected bootstrap method (Carpenter and Bithell, 2000). Scan, re-scan reproducibility was assessed by calculating the mean percentage change following each subject's second scan.

4.1.3 Results

Example of post-processed spectra obtained using the neurovascular and 32-Channel coils are shown in **Figure 4.2**. The mean ratio of SNR_{NV}: SNR_{32-Ch} was 1.4 (SD ± 0.7). Although the difference was not statistically significant (P = 0.13), given the small number of subjects, the results were sufficiently encouraging to select the neurovascular coil for use in the later optimisation experiments.
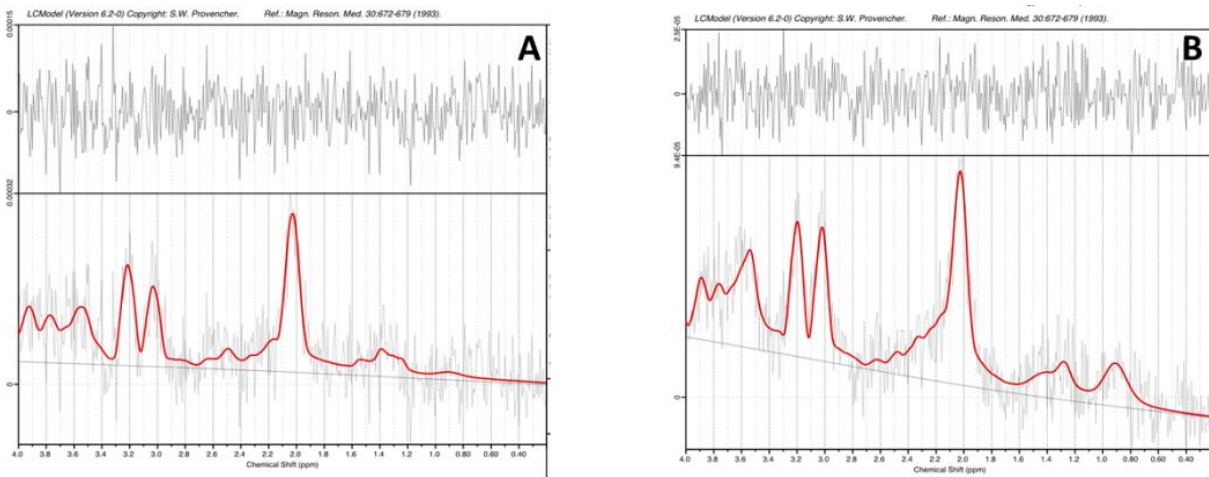
Figure 4.2: Representative spectra obtained from a single volunteer using (a) the 32 channel coil and (b) the neurovascular coil.

Table 4.2 shows the residual water peak as a percentage for each water suppression module in all 4 subjects and **Figure 4.3** illustrates differences in water signal in a single volunteer. The module with the lowest % residual water peak was MOIST. Residual water peaks obtained using the MOIST module were significantly smaller than those using the inversion and VAPOR modules (P <0.05) but there was no statistical difference between the MOIST, CHESS and excitation modules.

Subject	CHESS	Excitation	Inversion	MOIST	VAPOR
Subject 1	2.7	0.91	22.92	0.77	1.19
Subject 2	0.35	0.80	7.23	0.23	1.50
Subject 3	2.94	0.89	16.5	0.37	1.10
Subject 4	0.90	0.91	6.98	0.96	1.70
Mean (SD)	1.73 (1.29)	0.87 (0.05)	13.4 (7.73)	0.58 (0.34)	1.37 (0.28)

1

2 **Table 4.2:** Percentage residual water for each of the four subjects scanned using each of the 5

3 water suppression modules. The module with lowest mean residual water was MOIST.

4

5
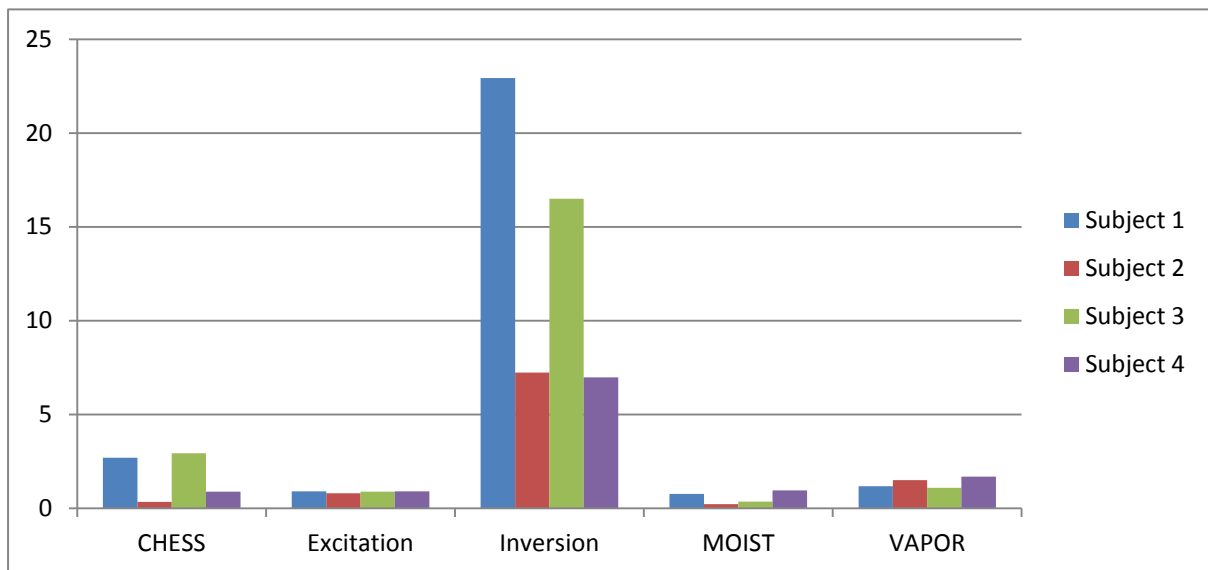
6

Figure 4.3: Water suppression optimisation. Residual water heights as a percentage of reference water signal for each subject shown for CHESS, Excitation, Inversion, MOIST and VAPOR water suppression techniques.

1   Typical spectra obtained using the PRESS and STEAM protocols are shown in **Figure 4.4**

2   and CRLB values for Glu, Glx and tNAA using PRESS and STEAM sequences for each of

3   the five healthy controls are detailed in **Table 4.3**. Data acquired with the PRESS sequence

4   showed a reliable fit (CRLB $\leq$ 20%) for Glx and tNAA, but not Glu in all 5 subjects. In

5   contrast, Glx quantification with STEAM did not meet these reliability criteria. The

6   improvement in metabolite quantification using the PRESS sequence was significant (P <

7   0.01). SNR was also higher using PRESS; STEAM averaged 34.6% lower than PRESS (P <

8   0.01).
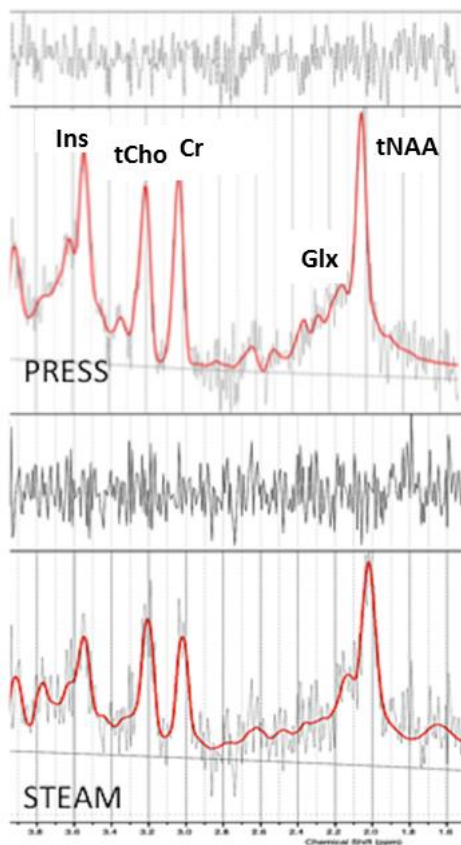
Figure 4.4: PRESS vs STEAM

Typical spectra obtained from a single volunteer using the PRESS sequence (above) and the STEAM sequence (below).

9

10   Results from the reproducibility study are shown in Table 4.4. Intra-subject variability in

11   tNAA concentration was 8.1 % and for Glx concentration was 19.9%. These values however

12   are potentially biased by the relatively poor spectral quality of the second spectrum obtained

13   from subject 4.

	CRLB % (PRESS)				CRLB % (STEAM)			
	Glu	**Glx**	**tNAA**	**SNR**	**Glu**	**Glx**	**tNAA**	**SNR**
Subject 1	30	20	7	5	48	48	13	3
Subject 2	30	16	9	5	59	59	20	4
Subject 3	25	16	7	7	NA	33	11	3
Subject 4	25	15	11	3	59	59	15	3
Subject 5	21	19	6	6	89	48	10	4
Mean (SD)	26.2 (1.6)	17.2 (0.8)	8.0 (.08)	5.2 (0.6)	63.8 (7.1)*	49.4 (4.4)*	13.8 (1.6)*	3.4 (0.2)*
CV (%)	6	5	10	11	11	9	12	6

1 **Table 4.3:** Reliability of metabolite fit. Table shows CRLB values for water-scaled
2 metabolite concentrations; PRESS vs STEAM. Significant differences between reliability of
3 fit are marked. * $P < 0.01$

4

Subject	Scan	tNAA mmol/l	Glx mmol/l	tCho mmol/l	tCr mmol/l
Subject 3	1	6.26	5.84	1.28	3.59
	2	5.47	5.53	1.01	3.88
Subject 4	1	6.82	7.10	0.98	3.46
	2	2.85	3.17	0.98	3.06
Subject 5	1	4.86	4.86	1.29	4.41
	2	4.41	5.31	1.34	4.61
Mean % difference		8.1%	19.9%	5.4%	12.1%

5

6 **Table 4.4:** Scan/re-scan reproducibility. Subjects 3-5 were scanned and re-scanned using the
7 PRESS sequence. Metabolite quantification from both scans and mean percentage change in
8 metabolite concentration is shown. Scan 2 from subject 4 is highlighted and was of poor
9 quality (low SNR and linewidth broadening) and therefore the concentrations should be
10 treated cautiously.

11

12

4.1.4 Discussion

The results from these experiments demonstrate the feasibility of Glx detection in healthy human spinal cord, *in vivo,* using a short-TE PRESS localisation sequence on a clinical scanner, within acceptable (approximately 25 minutes) scan times. However, the fit of Glu itself did not satisfy the requirement of a $\leq 20\%$ CRLB threshold. These findings represent a step forward in the development of routine Glx detection in spinal cord.

Protocol Optimisation

The C1-C3 segment of the spinal cord was chosen as the region of interest in this study as this has previously been demonstrated to be the optimum spinal level for spectroscopy experiments since this region of the cord lies in the most homogenous part of the B_0 field (Henning *et al.*, 2008). The C1-3 level is also the most commonly affected by spinal cord pathology in MS as discussed in *Chapter 3*. Cardiac triggering was used for all scans to further improve spectral quality (Cooke *et al.*, 2004). The triggered iterative shimming process, which utilises the gradient coils in the X, Y and Z directions to optimise field homogeneity by iteratively running through different combinations of gradients in the X, Y and Z directions, achieved consistently good results using a voxel of this size (range of 14-22 Hz for FWHM of water resonance).

Although the difference in SNR achieved between the neurovascular coil and 32 channel coil did not reach statistical significance, the neurovascular coil did appear to perform better *in vivo* than the 32 channel coil. The close-fitting shape and selection of the 4 neck elements results in a reduction of noise accumulation from elements of the coil distant from the

selected voxel which would explain the relatively higher SNR seen with the neurovascular coil. When comparing the water suppression modules, MOIST gave consistently good water suppression. This could have reflected relative insensitivity to differences in T1 characteristics of different tissues within the region of interest, when compared to other water suppression modules. Alternatively, or additionally, the timing of the triggering of the PRESS sequence (see *Chapter 2*), relative to the monitored cardiac waveform may be important. Triggering was set at the beginning of water suppression rather than the beginning of PRESS excitation. The length of the water suppression pulse may therefore be important. The MOIST module was ~ 190 ms, which is similar to the second best performing module; the excitation module (~150 ms). The poorer performing inversion, CHESS and VAPOR profiles had different delays, with the short inversion module being just 36 ms long, whilst CHESS and seven-pulse VAPOR were longer (~ 230 and 745 ms long respectively). This would suggest that the timing of the water suppression module in PRESS sequences is an important determinant of the effectiveness of water suppression and subsequent spectral quality.

PRESS vs. STEAM Sequence Comparison

In the comparison between the STEAM and PRESS sequences, the PRESS sequence was able to reliably fit Glx (CRLB $\leq$ 20%) in all five volunteers whilst the STEAM did not meet the reliability criteria in any of the volunteers. By using each subject as their own control and performing a paired-difference analysis; a statistically significant difference in reliability between PRESS and STEAM was shown ($P < 0.01$). Spectra obtained using the STEAM sequence also had lower SNR compared to PRESS ($P < 0.01$). As discussed in *Chapter 2*, the STEAM sequence suffers from lower SNR because the final stimulated echo yields only a

fraction of the possible signal from the voxel. This intrinsic loss in signal associated with the STEAM sequence could not be recovered through shorter TE and extra averaging.

Voxel definition could also have been different in PRESS, since two of the 90º pulses used for STEAM localisation were replaced with 180º pulses for refocusing. The differing extent of chemical shift displacements gives rise to slightly different volumes per metabolite, contributing to the spectrum for each sequence. However, as much as possible, this was anticipated and remedied whilst positioning the spectroscopy voxels before the scan by ensuring that the chemically shifted tNAA and water voxels were both fully within the cord and similar shim values were attained.

It is interesting, that in contrast to previously reported findings by Kim et al, the STEAM sequence here was unsuitable for detection of Glx (Kim *et al.*, 2004). These investigators reported a rise in Glu in spinal meningiomas using a STEAM sequence (TE = 30ms) on a 1.5 T GE system using a surface coil (Kim *et al.*, 2004). It is certainly known from spectroscopy studies in the brain, that cerebral tumours can be associated with very significant rises in Glu and Glx (Rijpkema *et al.*, 2003; McKnight, 2004). It is therefore possible that similar very large rises in Glu occur in spinal tumours which might make it easier to detect in that patient group. The differences in RF coil used between this study and that of Kim *et al* may also be an explanation for the apparent improved detection in that study. However, a potential limitation of the Kim *et al* study was that the authors did not report the Cramér–Rao lower bound (CRLB) of the metabolites quantified nor was any other indication given for reliability of fit.

Overall, the findings in this study are in agreement with those of Hancu, who concluded that a short-TE PRESS sequence was optimal for Glu detection in the brain (Hancu, 2009). In this

study, a slightly shorter TE was used (TE = 30ms as opposed to 35ms used in the Hancu report), to minimise T2 relaxation but whether this improved spectral quality or not was not specifically examined.

Scan, Re-scan Reproducibility

The reproducibility study involving volunteers 3, 4 and 5 (**Table 4.4**) shows that there was a reliable fit and good reproducibility between initial and follow up scans for subjects 3 and 5. Subject 4, however, had a poorly resolved spectrum with significant line-broadening which may have been due to subject motion or higher susceptibility.

Limitations

A potential limitation of the study is that T1 and T2 corrections were not performed. Although T1 and T2 for water protons have been reported in the spinal grey and white matter, the corresponding T1 and T2's for metabolites have not yet been determined (Smith *et al.*, 2008). A spinal MRSI study has previously used the values found in brain as an approximation (Edden *et al.*, 2007) but for this to have been applied correctly in the current study, it would have been necessary to segment the grey and white matter within the spectroscopy voxel which would be technically challenging.

The LCModel derived CRLB for Glu was 26%, which may be sufficiently reliable for detecting changes in Glu of about 40%, as are seen in some pathologies (Provencher, 2014), however reliability would need to improved significantly to detect more subtle changes. Although spectral quality could potentially be improved by prescribing shorter voxels (Cooke *et al.*, 2004; Edden *et al.*, 2007), this would be at the cost of SNR and may deleteriously

impact on Glx quantification. A further key limitation of the study was the small cohort size, and for the reproducibility studies, only 2 scans were acquired.

Future Directions

Although Glx detection using our protocol can be performed reliably within scan times that should be acceptable to patients with MS and other neurodegenerative diseases, future work should focus on developing faster and more specific sequences to detect Glu in the cervical cord and to increase reliability and reproducibility. Alternative Glu-specific sequences need to be assessed for use in the cervical cord. Hurd *et al.* reported low inter-subject variation (7-9%) for Glu in the brain, with good visual separation of Glu using a TE-averaged PRESS sequence (Hurd *et al.*, 2004). However, to apply a similar sequence to the spinal cord would not be straight forward; the voxel volume used by Hurd *et al.* was four times larger than the voxel used in this study and reducing the voxel size to fit within the spinal cord would result in a loss of signal.

The B_0 inhomogeneity of the spinal cord region together with the smaller voxels required for spinal cord MRS may also limit the use of more sophisticated sequences proposed for Glu and Gln detection (Hurd *et al.*, 2004; Hancu, 2009; O'Gorman *et al.*, 2011). By combining the optimised protocol presented here with a J-edited PRESS sequence, which combines PRESS localisation with two frequency-selective editing pulses to filter out J-coupled metabolites such as Glu, on the basis of their specific coherence evolution, it could be possible to directly measure Glu with no Gln overlap. This would allow more accurate evaluation of disruption to glutamatergic pathways in MS and other neurodegenerative diseases.

1

2

4.2 Effect of Age and Gender on Spinal Metabolite Concentrations

4

4.2.1 Introduction

Normative spinal cord metabolite concentrations have previously been reported in earlier studies (Cooke *et al.*, 2004; Marliani *et al.*, 2007), but it has not yet been reported whether there is any variation in spinal metabolite concentrations with ageing or gender as has been shown to occur in the brain (Batra *et al.*, 2008; Haga *et al.*, 2009; Zahr *et al.*, 2013). It might be expected that healthy ageing is associated with changes in spinal cord metabolites as many of the changes in physical performance associated with normal ageing such as, decline in motor agility (Murray *et al.*, 1969; Wolfson *et al.*, 1990), impairment of sensory perception (Deneeling *et al.*, 1994; Robbins *et al.*, 1995) and increased bowel, bladder and erectile dysfunction (Marcio *et al.*, 1993; Kaiser, 1999; Siroky, 2004; Aversa *et al.*, 2010), could possibly be explained by age-related neurodegeneration of the spinal cord. There is evidence for age-related degeneration of the spinal cord from studies of humans and rodents which have shown that advancing age is associated with aberrations of spinal myelin, proliferation of astrocytes and reduced axonal number and diameter within spinal sensory and motor tracts (Burek *et al.*, 1976; Cruz-Sanchez *et al.*, 1998; Nonaka *et al.*, 2008). In fact, diffusion MRI has shown that diffusion anisotropy in the upper cervical cord declines with normal ageing, with loss of fibre coherence beginning from the age of ten (Agosta *et al.*, 2007). Understanding whether commonly quantified spinal metabolites also change with age is potentially important if serial MRS investigations are performed in patients with neurodegenerative diseases to monitor disease progression and/or response to treatments as

periodic imaging is potentially vulnerable to temporal changes in metabolite concentrations associated with healthy ageing, rather than disease progression. It is therefore important to understand how spinal metabolites change with age to inform interpretation of interval changes.

In the brain, differences in metabolite concentrations have also been reported between men and women. More specifically, gender differences are seen in the concentrations of Glu and GABA (Sailasuta *et al.*, 2008; O'Gorman *et al.*, 2011). It has been proposed that hormonal differences between men and women may contribute to the observed variance. This is supported by observations of varying Glu/Cr ratios in women during the different stages of the menstrual cycle (Batra *et al.*, 2008). It is therefore feasible that similar changes could be present in the spinal cord and knowledge of such differences would be important when planning spinal cord spectroscopy studies. This study therefore aims to apply the MRS protocol that was developed and optimised in *Section 4.1* to (i) investigate whether, in healthy adults, age is associated with changes in concentrations of commonly quantified metabolites and (ii) explore the effect of gender on metabolite concentrations.

4.2.2 Methods

4.2.2.1 Study Participants

Healthy volunteers were prospectively recruited from amongst university staff and respondents to adverts within the university and neurology outpatient clinic. A minimum of two subjects per decade of life (between the ages of 20 and 65) were recruited in order to achieve a good spread of ages. Participants found to have severe spondylitic changes (Thorpe *et al.*, 1993), compression of the cord or an intrinsic cord lesion were excluded from the

study. All subjects provided written, informed consent prior to taking part in the research, which was approved by our local research ethics committee.

4.2.2.2 MRI Protocol

All scans were performed using a 3T Achieva system (Philips Medical Systems, Best, Netherlands), with the manufacturer's 16-channel neurovascular coil. An MR compatible cervical collar was worn by all volunteers (Yiannakas *et al.*, 2012). All subjects initially underwent conventional structural imaging of the upper cervical cord with: (a) Spin-echo T2w sequence, with TR = 4000 ms; TE = 100ms; echo train length = 24 echoes; FOV= 160 x 250 mm^2; voxel size = 0.6 x 0.6 x 3.0 mm^3;number of excitations (NEX) = 2; 13 contiguous coronal slices, and (b) Dual-echo PD/T2w sequence with TR = 4000 ms; TE = 15/80ms; FOV= 256 x 160 mm^2; voxel size = 1.0 x 1.0 x 3.0 mm^3; NEX = 2; 12 contiguous sagittal slices.

Single voxel MRS data was then acquired using the MRS protocol optimised in section 4.1. Cuboid volumes of interest (VOI) with dimensions of approximately 5.4 x 7.76 x 55mm^3 (2.3 ml) were prescribed and centred on the C2/3 intervertebral disc (**Figure 4.1**) using the previously acquired coronal and sagittal T2w and PD/T2w reference scans. The dimensions of the VOI were adjusted in the anterior-posterior (AP) dimension dependent on the size of each subjects spinal cord (mean VOI 2.02 ml; SD ±0.22ml). MRS data was acquired using a point resolved spectroscopy (PRESS) localisation sequence, with triggered iterative shimming, MOIST water suppression, 4 outer volume suppression (OVS) slabs in the AP and rostrocaudal directions and cardiac gating (TR = 3 R-R intervals ≈ 3000 ms) using a peripheral pulse unit (350ms delay from R-wave peak), TE = 30 ms, number of averages = 376.

1

4.2.2.3 Post processing

Structural scans were assessed by Dr Khaled Abdel-Aziz for the presence of intrinsic cord lesions, spondylitic changes or disc protrusions that may have affected the measurements, and subsequently the interpretation of the MRS data.

Metabolite concentrations were quantified using the LCModel (version 6.3) package (Provencher, 1993) and a set of basis spectra simulated using GAMMA (Smith *et al.*, 1994), comprising seventeen metabolites including NAA, N-acetylaspartyl glutamate (NAAG), gamma-Aminobutyric acid (GABA), Ins, tCr, Cho, Glu, Gln, lactate, alanine and aspartate. Quantification of metabolites was performed by using the unsuppressed water signal obtained from the same voxel (Gasparovic *et al.*, 2006). NAA + NAAG (hereafter, tNAA), tCho, tCr, Ins and Glx concentrations formed the focus of our analysis. SNR and full width of half maximum (FWHM) of the tNAA peak provided by LCModel were used to assess spectral quality and Cramér–Rao Lower Bounds (CRLB) values $< 20\%$ for each metabolite were used to assess the reliability of the spectral fit. Poor quality spectra were excluded from the analysis. Criteria for exclusion were poor water suppression or FWHM > 0.13 with SNR <3.

4.2.2.4 Statistical Analysis

All statistical analyses were performed using IBM SPSS statistical package version 22.0 (IBM Corporation, Armonk, NY, USA). Associations between metabolites and age were examined using linear regression of the metabolite as response variable on age, with gender, FWHM and voxel volume covariates; a quadratic term in age was also entered to examine evidence of non-linearity and removed if $p > 0.1$. Gender differences reported from these

1   models are adjusted for age, FWHM and voxel volume. *P* values of < 0.05 were taken to be

2   statistically significant.

4.2.3 Results

4   Twenty-five healthy participants were prospectively recruited and scanned. Assessment of

5   the structural spinal cord imaging excluded any significant spondylitic change/cord

6   compression or intrinsic cord lesions which could have affected metabolite quantification in

7   all subjects. Four participants were excluded from the analysis due to poor spectral quality.

8   Therefore, twenty-two healthy participants (15 females) with a mean age of 40.5 years,

9   standard deviation (SD) 13.1, range 23-65 were included in the final analysis.

10

11   **Figure 4.5** shows examples of spectra which were excluded from the analysis and **Figure 4.6**

12   shows typical examples of post-processed spectra included in the final analysis. The FWHM

13   and SNR estimated by LCModel (reported as mean $\pm$ SD) were 0.11 ± 0.02 ppm and $5.05 \pm$

14   1.75 respectively. Cramér–Rao lower bounds (CRLBs) indicated a reliable fit for tNAA,

15   tCho, and tCr. A reliable fit was achieved for Glx in 19 out of 22 spectra and for Ins in 20

16   out of 22 spectra (Provencher, 2014). Mean CRLBs for each metabolites were; tNAA (7%),

17   tCr (11%), tCho (10%), Ins (11%) and Glx (17%).
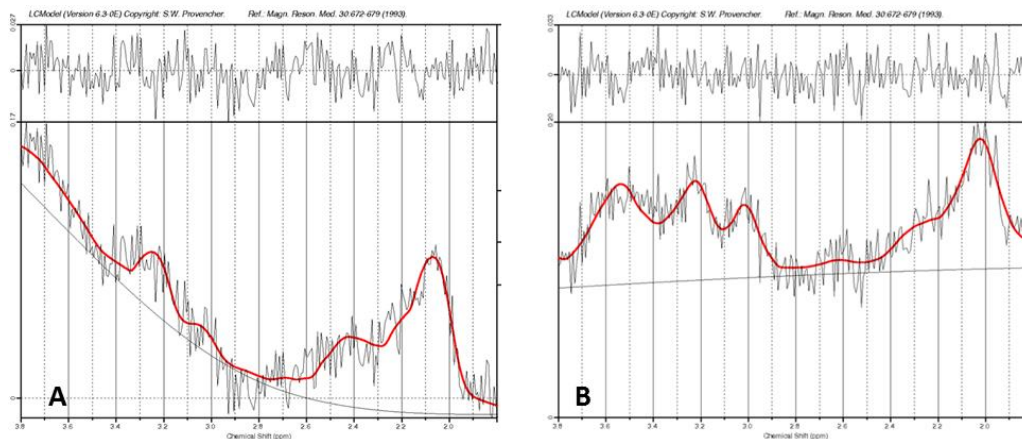
1

2
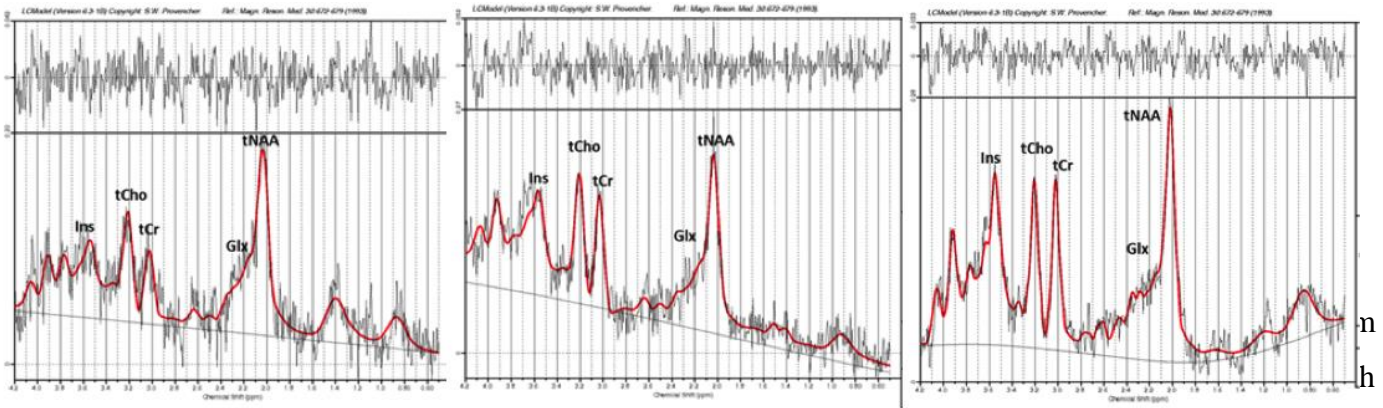
Figure 4.6 Representative spectra obtained using LCModel from (right) a 23 year old healthy female, (centre) a 32 year old healthy male and (left) a 54 year old healthy female.

3 broadening likely due to subject motion during the scan

4

5

6   There was no statistical evidence of a non-linear relationship between metabolite

7   concentrations and age. Older age predicted lower spinal tNAA concentration (0.049 mmol/L

8   lower per additional year of age, p = 0.010) and lower Glx concentration (0.054mmol/L

9   lower per additional year of age, p = 0.002) (Table 4.5). Age was not significantly associated

10   with the other metabolites (**Figure 4.7**).
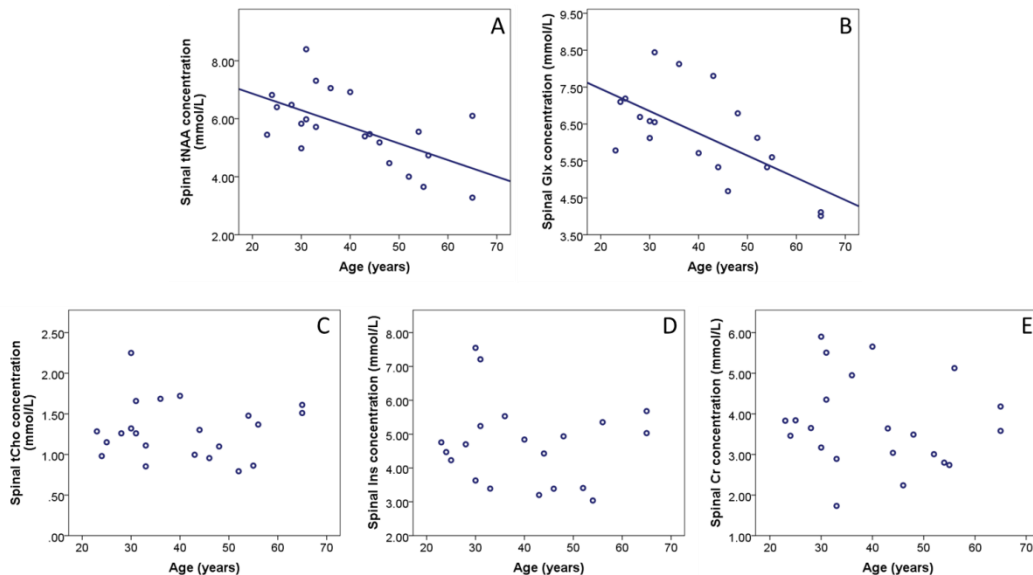
Glx concentration was significantly higher in men, mean (SD) 7.27 (0.97) mmol/L, than females, mean (SD) 5.73 (1.05) mmol/L (p = 0.010, adjusting for age, FWHM and voxel volume), but no gender differences were seen with other metabolites (**Table 4.6**).

Association between age and metabolite concentrations

	Regression coefficient	Standardised regression coefficient	95% CI for regression coefficient	p-value
tNAA	-0.049	-0.522	-0.085, -0.013	0.010
Glx	-0.054	-0.579	-0.085, -0.022	0.002
tCho	0.001	0.026	-0.014, 0.015	0.920
Ins	-0.006	-0.067	-0.055, 0.043	0.791
tCr	-0.004		-0.046, 0.039	0.867

Figure 4.7: Scatter plots of relationship between age and (A) tNAA, (B) Glx, (C) tCho, (D) Ins and (E) tCr concentrations from the upper cervical cord. Regression lines are shown where there was a significant association (A, B). No significant association was seen between age and tCho, Ins or tCr (C - E).

Table 4.5: Associations between age (predictor) and metabolite concentrations (response variable). Unstandardised and standardised regression coefficients calculated from the multivariate model are reported with 95% confidence intervals and p-values. The regression models adjusted for gender, FWHM and voxel volume.

Metabolite concentrations (mmol/L) by gender

	All subjects (*n=22*)	Male (*n=7*)	Female (*n=15*)
tNAA	5.69 (1.24)	6.05 (1.37)	5.52 (1.18)
Glx	6.21 (1.24)	7.27 (0.97)	5.73 (1.05)*
tCho	1.30 (0.35)	1.36 (0.53)	1.27 (0.25)
Ins	4.70 (1.23)	5.36 (1.83)	4.42 (0.79)
tCr	3.76 (1.11)	4.15 (1.47)	3.60 (0.90)

Table 4.6: Mean (SD) water scaled metabolite concentrations derived with LCModel for all subjects and by gender. *Significant difference in Glx concentration between male and female (p = 0.010, after adjusting for age, linewidth and voxel volume)

1

2

4.2.4 Discussion

MRS studies of the brain have previously shown that cerebral metabolite concentrations change are affected by age (Moreno-Torres *et al.*, 2005; Zahr *et al.*, 2008; Haga *et al.*, 2009) and gender (Sailasuta *et al.*, 2008; O'Gorman *et al.*, 2011). The aim of this study was therefore to evaluate whether, or not age and gender had a similar effect on metabolite concentrations of the upper cervical cord. The results suggest that older age was strongly associated with lower concentrations of tNAA (R^2 = 0.285) and Glx (R^2 = 0.45) and that there were significantly lower Glx concentrations in female subjects compared to males.

By employing the MRS protocol optimised in *Section 4.1*, it was possible to achieve sufficiently high SNR to reliably quantify spinal Glx. After elimination of the poor spectra, other spectral quality indicators, such as FWHM and CRLB, were comparable to those published by other groups (Marliani *et al.*, 2007; Henning *et al.*, 2008).

Age-related Changes in Metabolite Concentrations

As previously discussed in *Chapter 2*, axonal numbers closely correlate with NAA levels quantified by immunoassay (Bjartmar *et al.*, 2000), and NAA levels decrease in the presence of inhibitors of complexes I, III, IV and V of the mitochondrial respiratory chain (Bates *et al.*, 1996). Therefore, in MRS studies, concentrations of tNAA are commonly interpreted as reflecting neuroaxonal integrity and/or mitochondrial energy production (Moffett *et al.*, 2007). In the current study, there was a linear decrease in tNAA concentration in the upper cervical cord with ageing, which may reflect age-related neuroaxonal loss and mitochondrial dysfunction. In fact, mitochondrial DNA (MtDNA) deletions and point mutations accumulate

during normal CNS ageing (Lin *et al.*, 2002; Beal, 2005) and, together with increased production of reactive oxygen species (Gupta *et al.*, 1991; Keller and Mattson, 1998; Butler and Bahr, 2006), are thought to be responsible for age-related neuroaxonal degeneration.

Healthy brain ageing is associated with reductions in tNAA in grey matter regions (Charles *et al.*, 1994; Lim and Spielman, 1997; Brooks *et al.*, 2001; Moreno-Torres *et al.*, 2005), but rarely seen in the white matter (Charles *et al.*, 1994; Chang *et al.*, 1996; Saunders *et al.*, 1999; Moreno-Torres *et al.*, 2005). This may, at least in part, be explained by a slower rate of ageing-related white matter volume loss in the brain when compared with grey matter (Ge *et al.*, 2002). Studies including older subjects have demonstrated that cerebral white matter volume loss does accelerate from the age of 70 (Raz *et al.*, 2005), it is therefore possible that tNAA decline might be more apparent in that age group. In the study by Kadota *et al*, the tNAA/Cho ratio increased rapidly in the cerebral white matter during the first decade of life before peaking in the second or early third decade. This was followed by a steady decline starting in the latter half of the third decade of life, whilst in the grey matter, the tNAA/Cho ratio enters a steady decline from childhood (Kadota *et al.*, 2001). Although this study did not assess whether the age-related decline in tNAA in the spinal cord is also tissue dependent, it is certainly possible that tNAA concentration declines faster in spinal grey matter than white matter and this warrants future research.

Glutamate (Glu), plays a major role in the coordination of basic propulsive movement synergy for locomotion at the spinal level (Grillner *et al.*, 2008) and processing and transmitting sensory information in the spinal cord (Todd, 2010). As discussed in section 4.1, Glu, as opposed to Glx, is difficult to measure in the spinal cord. However, between 75 - 86% of the Glx signal is thought to come from Glu (Baker *et al.*, 2008), with the rest coming from

coupled Gln. The results demonstrate an age-related decline in spinal Glx which could be explained by ageing-related neuroaxonal degeneration. Glu in the extracellular compartment and glial cells is present in very low concentration and therefore contributes very little to the spectroscopy signal (Rothstein *et al.*, 1992; Kaiser *et al.*, 2005). The majority of Glu is present in neurones at synaptic terminals and it would therefore be expected that Glu (and therefore Glx) will decrease where there is neuronal loss. In fact within our cohort of healthy adults, there was a significant correlation between Glx and tNAA concentrations (r = 0.534, p = 0.027), suggesting that Glx, in part, reflects neuronal density.

The observed association between age and Glx in the spinal cord is in keeping with previous MRS investigations in the brain which have consistently shown declining concentrations of Glu with older age in multiple brain regions including the frontal white matter, parietal grey matter, motor cortex, anterior cingulate cortex, hippocampus, basal ganglia and striatum (Schubert *et al.*, 2004; Kaiser *et al.*, 2005; Choi *et al.*, 2006; Zahr *et al.*, 2008; Chang *et al.*, 2009).

In the present study, no evidence of association was seen between tCho, tCr and Ins concentrations in the spinal cord and age. Although changes have been reported in these metabolites in the brain with ageing and have been interpreted as reflecting changes in glial proliferation, those changes are not thought to occur uniformly in the brain, with regional variation commonly reported. tCho concentrations have been reported to be higher in the corpus callosum, parietal lobe, frontal grey matter and pons in older people (Chang *et al.*, 1996; Soher *et al.*, 1996; Moreno-Torres *et al.*, 2005; Haga *et al.*, 2009), but remain stable in the frontal, occipital and temporal lobes and the basal ganglia in other studies (Christiansen *et*

al., 1993; Brooks *et al.*, 2001) and decline in the midbrain (Moreno-Torres *et al.*, 2005). Similarly, tCr was seen to increase in the parietal, frontal grey and white matter (Chang *et al.*, 1996; Schuff *et al.*, 2001; Haga *et al.*, 2009), but other studies found no change in tCr with ageing (Christiansen *et al.*, 1993; Brooks *et al.*, 2001). Fewer brain studies have assessed Ins levels with ageing; a single study found an increase in the frontal grey matter (Chang *et al.*, 1996), whilst another study reported that Ins/Cr ratios decreased in the frontal grey matter, basal ganglia, and occipital grey matter (Fan *et al.*, 2003). A recent meta-analysis of 18 spectroscopy studies assessing regional metabolite changes in healthy brain ageing found that there were significant increases in parietal tCho and tCr; although fewer studies assessing changes in Ins had been carried out, levels were not seen to change significantly in the brain with age (Haga *et al.*, 2009). Methodological differences in studies addressing the change of these metabolites in the brain with ageing means conclusions about changes in tCho, tCr and Ins with age cannot yet reliably be made

Effect of Gender on Metabolite Concentrations

An interesting observation in the current study was that of higher concentrations of Glx in men than women. MRS studies in the brain measuring Glx and Glu concentrations have been inconclusive on whether gender differences exist. Higher levels have been reported in men compared to women in the parietal grey matter and dorsolateral prefrontal cortex (Sailasuta *et al.*, 2008; O'Gorman *et al.*, 2011), whilst other studies have reported higher concentrations in women in the cerebellum and striatum (Zahr *et al.*, 2013). Kaiser *et al*. however found no differences in Glu and Gln concentrations between men and women in the corona radiata and mesial motor cortex (Kaiser *et al.*, 2005). Hormonal factors may be responsible for some of the observed gender differences in our study. An examination of the medial prefrontal cortex

during the follicular phase and the luteal phase of the menstrual cycle found that Glu/Cr ratios were significantly lower during the luteal phase compared with the follicular phase (Batra *et al.*, 2008). Additionally, blood Glu levels vary during the menstrual cycle such that blood Glu levels are inversely correlated to levels of plasma oestrogen and progesterone (Zlotnik *et al.*, 2011), but interestingly in the work by Zlontik *et al*, Glu levels were significantly higher in men than women at any stage of the menstrual cycle. Unfortunately the current study was not designed or adequately powered to assess whether or not the stage of menstruation in female subjects effects Glx quantification. It will need to be determined whether higher concentrations of spinal Glx are detectable during the follicular phase as is seen in some brain regions.

Limitations

A limitation of the study is that the sample age range only starts at 23 years. It has therefore not been possible to ascertain whether or not age-related changes in the spinal cord occur before the early twenties. Within the sample age range of 23 - 65, we did not find a quadratic association between age and the concentrations of tNAA and Glx, which suggests the decline in these metabolites with age, within the studied age range, is linear. However it is also possible that subjects older than 65 could show accelerated decline of tNAA which would not have been identified by restricting the age limit for the study to 65.

Future Directions

Future longitudinal studies will be required to determine the rate of change in metabolites over time in healthy ageing and whether metabolite concentrations decline at differing rates

in spinal grey matter and white matter. Furthermore, studies of brain ageing have previously shown that age-related metabolite changes are not uniform and can vary between brain regions, and it is possible that metabolite changes during ageing occur at dissimilar rates at different spinal levels which will also require further investigation. Finally, future studies should also include older participants to assess whether or not the trajectory of metabolite decline changes at the extremes of age.

4.3 Study of Effect of Grey Matter Volume Fraction on Metabolite Ratios.

4.3.1 Introduction

As discussed earlier within this chapter, when planning spectroscopy voxel placement in spinal MRS, a compromise must be reached between maximising SNR and minimising partial volume effects from surrounding CSF. All *in vivo* spinal cord MRS studies published so far in human subjects, spectroscopy voxels have taken up most of the cross-sectional area of the spinal cord and incorporate both grey matter (GM) and white matter (WM). However, this approach is potentially problematic as it is not known whether or not metabolite concentrations vary between GM and WM in the spinal cord as they do in the brain (Kreis *et al.*, 1993; Saunders *et al.*, 1999; Degaonkar *et al.*, 2005; Choi *et al.*, 2006; Baker *et al.*, 2008).

Recent imaging advances have demonstrated that WM and GM segmentation in the spinal cord is feasible (Yiannakas *et al.*, 2012). This segmentation enables calculation of the spinal cord GM volume relative to the total spinal cord volume (i.e., GM volume fraction). Understanding the relationship between spinal cord GM volume fraction (GMVF) and metabolite levels is important, as significant inter-subject variability in GMVF has been shown to exist between healthy subjects in imaging and post-mortem studies (Bjartmar *et al.*, 2000; Yiannakas *et al.*, 2012). This variability in turn, may influence quantification of metabolite concentrations. If a link between GMVF and spinal cord metabolites were to exist, it would be important to routinely calculate GMVF in clinical studies of neurodegenerative diseases, where spinal cord atrophy predominantly occurs in one tissue compartment. For example, in amyotrophic lateral sclerosis (ALS), there is MRI evidence at very high field for predominant GM atrophy, which may reflect anterior horn cell degeneration (Cohen-Adad *et al.*, 2013). As discussed in *Chapter 1*, in patients with MS, post-mortem analysis has

suggested that WM volume loss accounts for the majority of spinal cord atrophy (Gilmore *et al.*, 2005). This study therefore aims to assess the degree of variance in GMVF between healthy subjects and whether there is a relationship between GMVF and relative metabolite concentrations at 3 T.

4.3.2 Methods

4.3.2.1 Study Participants

Fifteen healthy participants, mean age 38.7 years (SD $\pm$ 12.4) (10 females) were prospectively recruited for the study. All subjects provided written, informed consent prior to taking part in the research which was approved by our local research ethics committee.

4.3.2.2 MRI Protocol

All scans were performed using a 3T Achieva system (Philips Medical Systems, Best, Netherlands), with the manufacturer's 16-channel neurovascular coil. To reduce motion artefacts during scanning, an MR compatible cervical collar was worn by all volunteers (Yiannakas *et al.*, 2012).

Single voxel MRS data was acquired using the protocol described in *Section 4.2.2.2*. VOIs with dimensions of approximately 5.4 x 7.76 x 55mm^3 (2.3 ml) were prescribed using the reference images and centred on the C2/3 intervertebral disc (**Figure 4.8A**). The dimensions of the VOI were adjusted in the AP direction dependent on the size of each individual's spinal cord (mean VOI 2.08 ml; SD 0.19).

For volumetric measurements, the cervical cord was imaged in the axial plane, perpendicular to the axis of the cord with the imaging volume centred on the C2/3 intervertebral disc, using a fat-suppressed 3D slab selective fast field echo (FFE) sequence with TR = 23 ms; TE = 5ms; flip angle α = 7°; FOV= 240 x 180 mm^2; voxel size = 0.5 x 0.5 x 5 mm^3; NEX = 8; 11 axial contiguous slices. In order to match the position and orientation of the volumetric scan to the spectroscopy voxel, the prescription values used for the MRS acquisition were copied and manually entered by the operator when setting up the 3D FFE scan (**Figure 4.8B**).
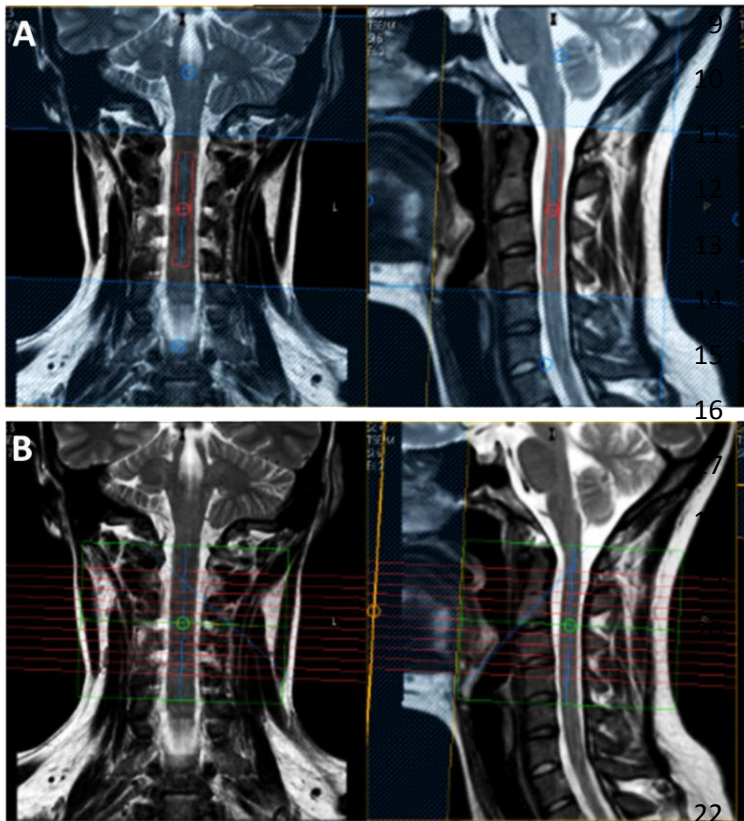
Figure 4.8: Planning of spectroscopy and volumetric scans. Sagittal and coronal T2w images of the upper cervical cord in a healthy subject showing a) Placement of PRESS VOI (5.4 x 7.76 x 55 mm^3) centred on the C2/3 intervertebral disc and b) Planning of the 3D FFE imaging volume to match the angulation and orientation of the spectroscopy VOI.

4.3.2.3 Post Processing

Image segmentation and volumetric measurements were performed using the 3D-FFE dataset in Jim 6.0 Software (Xinapse systems, Northants, England, www.xinapse.com). The spinal

1 cord was segmented (**Figure 4.9A**) using the active surface model method (Horsfield *et al.*,

2 2010). The total cord volume (TCV) for the 55mm section of cervical cord studied was

3 calculated by multiplying total cord area (TCA) by slice thickness. Spinal cord GM was then

4 segmented using a combination of the fuzzy connector algorithm and manual editing within

5 Jim 6.0 as recently described (Yiannakas *et al.*, 2012) (**Figure 4.9B**). The total grey matter

6 volume (TGMV) was calculated by multiplying total grey matter area (TGMA) by slice

7 thickness. GMVF was then derived, such that GMVF = (TGMV/TCV) x100%. Since the

8 TCV has been assumed to consist of only total GM and WM volumes for practical purposes,

9 we have not specifically reported, in this paper, associations between WM volume fraction

10 and metabolite ratios, as the associations will be equal, but opposite, to the those of GMVF.
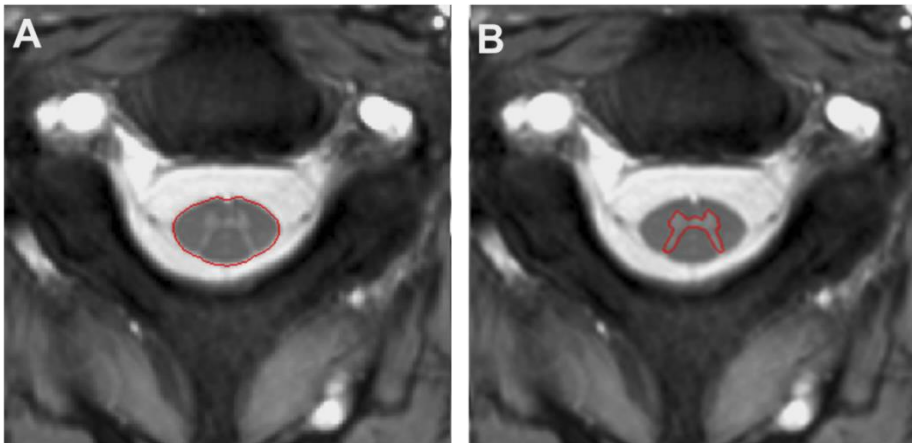
11

12 **Figure 4.9**: Axial 3D-FFE images (resolution 0.5 x 0.5 x 5mm^3) through the C2/3

13 intervertebral disc showing a) segmentation of the spinal cord using the active surface model

14 to calculate total cord volume (TCV) and b) segmentation of the spinal cord grey matter to

15 calculate total grey matter volume (TGMV).

16

17 Metabolite concentrations were quantified using the user independent LCModel package

18 (Provencher, 1993) and a set of basis spectra simulated using GAMMA (Smith *et al.*, 1994)

as described in *Section 4.2.2.3*. Total creatine (tCr) concentration was used as an internal reference and tNAA/tCr, Cho/tCr, Ins/tCr and Glx/tCr ratios were the focus of our analysis. Overall spectral quality was assessed using the SNR and FWHM values provided by LCModel. Cramér-Rao lower bounds (CRLBs), for each metabolite were used to assess the reliability of the metabolite fit. CRLBs of $< 20\%$ were taken to represent a reliable fit (Provencher, 2014).

4.3.2.4 Statistical analysis

All statistical analyses were performed using IBM SPSS statistical package version 22.0 (IBM Corporation, Armonk, NY, USA). Gender differences in GMVF were tested using an unpaired t-test. Multiple linear regressions were used to explore the relationship between the metabolite ratios (response variables) and the GMVF (predictor) with age, gender, FWHM and voxel volume as additional covariates. A P value of < 0.05 was taken to be significant.

4.3.3 Results

Spectral Quality

The FWHM and SNR estimated by LCModel (reported as mean ± SD) were $0.11 ± 0.02$ ppm and $5.3 ± 1.9$ respectively. Cramér–Rao lower bounds (CRLBs) indicated a reliable fit for tNAA/tCr, tCho/tCr and Ins/tCr. A reliable fit was achieved for Glx/tCr in 14 out of 15 spectra (Provencher, 2014). Mean CRLBs for metabolite ratios were; tNAA/tCr (6.6%), tCho/tCr (9.2%), Ins/tCr (10.5%) and Glx/tCr (16.4%).

Normative values for GMVF

Visual inspection of the scans did not show any evident motion; there was good GM/WM contrast on the axial FFE images for GM segmentation. GMVF in our healthy participants ranged between 16.1% and 24.8% (mean 19.8 ± 2.4%). The distribution of GMVF by gender is shown in **Figure 4.9**. There were no gender differences in GMVF, nor did it vary with age.
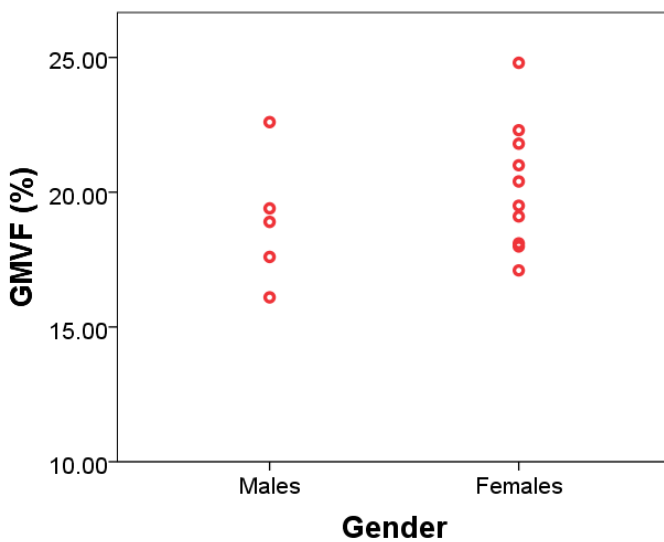
Figure 4.9: Distribution of grey matter volume fraction (GMVF) by gender. Range (all subjects) was 16.1 to 24.8%. No significant gender differences were seen.

Associations between GMVF and metabolite ratios

There was a significant positive association between GMVF and tNAA/tCr and Glx/tCr. A one percentage point increase in GMVF significantly predicts a tNAA/tCr increase of 0.12 (95% confidence interval (CI) 0.04, 0.19, $p = 0.006$) and a Glx/tCr increase of 0.15 (95% CI 0.07, 0.23, $p = 0.004$) independently of voxel volume, FWHM, age and gender. However, there was no association between GMVF and Ins/tCr or Cho/tCr ratios (**Figure 4.10 and Table 4.7**). **Table 4.8** summarises predicted metabolite ratios based on variation of GMVF.

Metabolite	Regression coefficient	Standardised regression coefficient	p-value	95% CI for regression coefficient
tNAA/tCr	0.12	0.93	0.006	0.04 to 0.19
Cho/tCr	-0.002	-0.12	0.701	-0.02 to 0.01
Ins/tCr	-0.03	-0.20	0.546	-0.12 to 0.07
Glx/tCr	0.15	0.91	0.004	0.07 to 0.23

1

2 **Table 4.7:** Associations between GMVF (predictor) and metabolite ratios (response
3 variable). Unstandardised and standardised regression coefficients for GMVF are reported
4 with 95% confidence intervals and p-values. The regression models adjusted for age, gender
5 and voxel volume.

6

7

	GMVF (%)										
	15	**16**	**17**	**18**	**19**	**20**	**21**	**22**	**23**	**24**	**25**
tNAA/Cr	0.918	1.038	1.158	1.278	1.398	1.518	1.638	1.758	1.878	1.998	2.118
tCho/Cr	0.352	0.350	0.348	0.346	0.344	0.342	0.340	0.338	0.336	0.334	0.332
Glx/Cr	0.797	0.947	1.097	1.247	1.397	1.547	1.697	1.847	1.997	2.147	2.297
Ins/Cr	1.398	1.368	1.338	1.308	1.278	1.248	1.218	1.188	1.158	1.128	1.098

8

9 **Table 4.8:** Predicted metabolite ratios with variation of GMVF after adjusting for age, gender
10 and voxel volume.

1
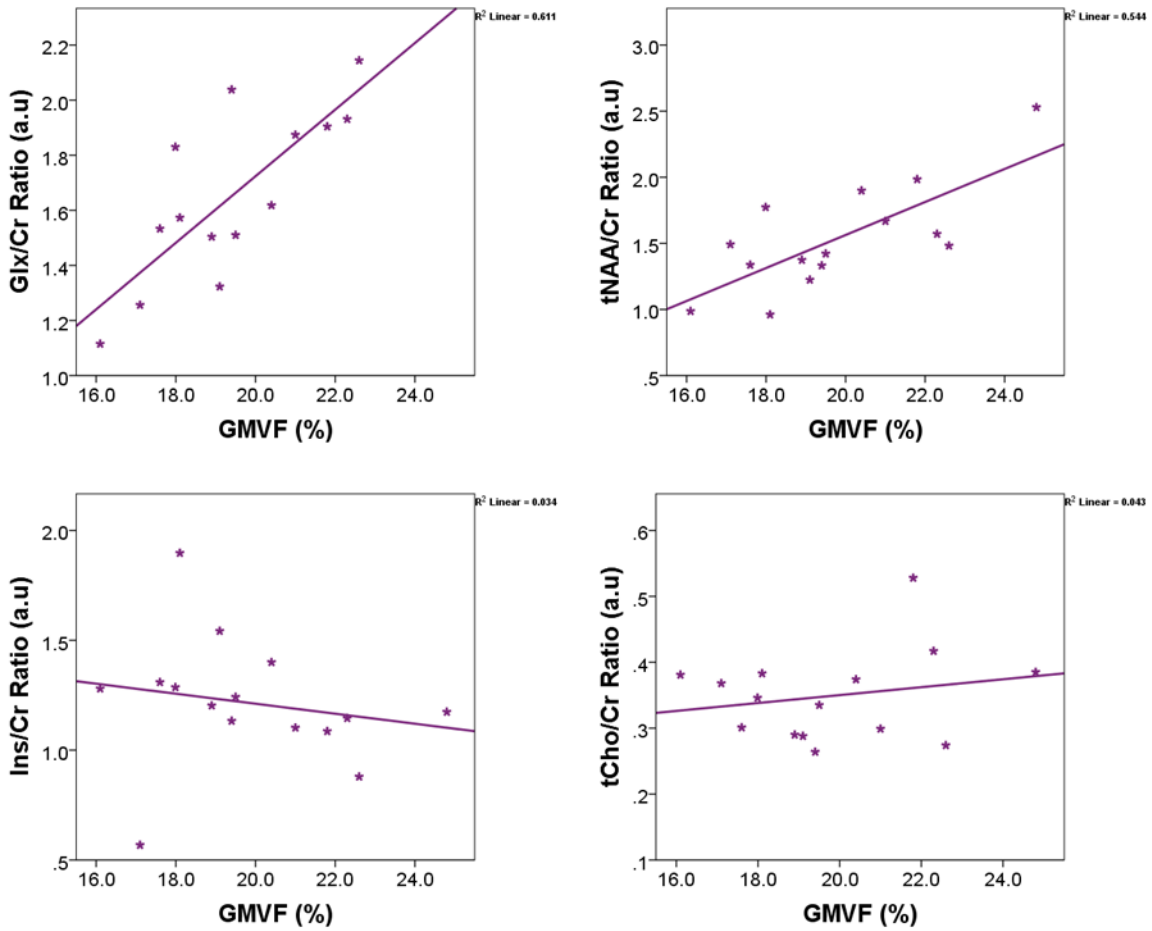
Figure 4.10: Graphs showing correlations between grey matter volume fraction (GMVF) and metabolite ratios. Regression lines and R^2 values denoting the strength of association are marked. GMVF was significantly associated with tNAA/tCr and Glx/tCr but not other metabolite ratios.

4.3.4 Discussion

This study examined the relationship between normative metabolite ratios in the spinal cord and GMVF. A positive association was found between GMVF and both tNAA/tCr and Glx/tCr ratios, suggesting that GMVF should be calculated and corrected for when estimating these metabolite ratios in the spinal cord, since changes between groups in metabolite ratios could be secondary to differences in GMVF. The impact of such a correction is likely to be most significant in studies of neurodegenerative spinal cord diseases where tissue loss occurs predominantly in either white matter or grey matter because in both instances the GMVF will be abnormal.

At present, MRS of separate GM and WM compartments in the human spinal cord is not feasible *in vivo,* using currently available techniques. This study demonstrated that higher GMVF predicts higher tNAA/tCr ratios which could reflect higher concentrations of tNAA in the spinal cord GM than WM. Numbers of mitochondria (where NAA is synthesised), are highest in areas with high demands for ATP, such as presynaptic and postsynaptic terminals, active growth cones and nodes of Ranvier (Ruthel and Hollenbeck, 2003). However, distribution of NAA within neurones will depend upon its biological function, which remains uncertain. Immunohistochemical studies have demonstrated that NAA concentrations are substantially higher in cerebral GM than in WM (Moffett *et al.*, 2007). Previous MRS studies reporting GM/WM differences in tNAA in the brain have described conflicting results, with some studies reporting higher tNAA in the WM than GM (Pouwels and Frahm, 1998), whilst the majority report modestly increased tNAA in the GM (Michaelis *et al.*, 1993; Chard *et al.*, 2002; Kaiser *et al.*, 2005).

In their 1D MRSI study in the spinal cord, Edden *et al* demonstrated an upward trend in tCr concentration and downward trend in tNAA concentration between the C1 segment and C2/3 segment of the cervical spine (Edden *et al.*, 2007). This might be explained by the changing cross-sectional morphology from the upper to mid-cervical cord; specifically highest GMVF at the C1 level with a gradient reduction in GMVF into mid-cervical cord (Williams and Warwick).

With regard to Glx levels, a relative increase in Glx in GM could be assumed as Glu and Gln would be expected to co-localise in close proximity to synapses where they serve their physiological function of synaptic neurotransmission; greater Glx levels in the GM than WM have been detected in the brain (Pan *et al.*, 1996; Pouwels and Frahm, 1998; Choi *et al.*, 2006; Baker *et al.*, 2008). Overall, MRS studies of the brain have reported smaller differences in tNAA than Glx between WM and GM (Michaelis *et al.*, 1993; Pan *et al.*, 1996; Chard *et al.*, 2002; Choi *et al.*, 2006; Baker *et al.*, 2008). Similarly, in this study we found an increase in GMVF produced a much larger rise in Glx/tCr ratio (regression coefficient = 0.15) than tNAA/tCr ratio (regression coefficient = 0.12), suggesting that the difference in Glx concentration between the GM and WM is higher than for tNAA.

In the cerebrum, tCr concentration decreases by approximately 15% in the WM and increases by approximately 12% in the GM from the anterior to the posterior pole (Baker *et al.*, 2008). Consequently there is higher tCr concentration in the WM in the frontal lobes and higher concentration in the GM in the occipital lobe. In this study there was a positive linear association between GMVF and both tNAA/tCr and Glx/tCr ratios. As already postulated, this is likely to reflect higher tNAA and Glx concentrations in the spinal GM. However, it is

also possible, if tCr concentration in the cervical cord is higher in WM than GM that this may be driving the relationship seen between GMVF and tNAA/tCr and Glx/tCr.

In the brain, tCho is consistently reported as higher in the WM than GM (Kreis *et al.*, 1993; Michaelis *et al.*, 1993; Soher *et al.*, 1996; Baker *et al.*, 2008). In contrast, in this study there was no association between GMVF and tCho/tCr in the spinal cord. Neither was there a significant association between GMVF and Ins/tCr ratio suggesting that there is no significant difference in Ins concentration between GM and WM in the spinal cord, unlike the brain where Ins concentration is thought to be higher in the GM (Pouwels and Frahm, 1998; Baker *et al.*, 2008).

GMVF was calculated using the methods recently published by Yiannakas *et al* (Yiannakas *et al.*, 2012) which highlighted considerable variation in GMVF between healthy controls. The mean recorded GMVF of 19.8% (SD ±2.4) is slightly higher than those reported in previous work by Yiannakas *et al*, who noted a mean GMVF of 17% (SD ±1) (Yiannakas *et al.*, 2012). However, a larger number of subjects was studied (15 vs 10) and a longer segment of the cervical cord was imaged (55mm vs 15mm) in the current study which may account for some of the difference. Measurements from a post-mortem study of lower cervical cord (C4 – 8) samples from 6 adults not known to have suffered with a neurological illness showed that spinal cord GM makes up 22.4% (SD ±1.3) of the cross-sectional area of the cervical cord at that level (Bjartmar *et al.*, 2000). GMVF would be expected to vary with spinal cord level and reflects changing cross sectional morphology of the cord in the rostrocaudal direction; it is therefore important to measure the GMVF at the same level as the VOI when performing an analysis which combines volumetric data with MRS data.

Spinal cord volume loss (or atrophy) occurs in many common neurological diseases and correlates with disability in amyotrophic lateral sclerosis (ALS) (Cohen-Adad *et al.*, 2013), multiple sclerosis (MS)(Losseff *et al.*, 1996; Stevenson *et al.*, 1998; Liu *et al.*, 1999) and spinocerebellar ataxias (Chevis *et al.*, 2013). However, volume loss is not always uniform across GM and WM compartments. In post-mortem spinal cord samples from MS patients, atrophy is largely due to WM volume loss (Gilmore *et al.*, 2005), whereas in ALS, segmental GM volume loss, as measured with MRI at very high field, is thought to occur and explains the level of motor deficits (Cohen-Adad *et al.*, 2013). Spinal cord MRS studies in patients with MS have detected decreases in tNAA levels of between 21 and 39% compared to healthy controls (Blamire *et al.*, 2007; Ciccarelli *et al.*, 2007; Marliani *et al.*, 2010). Lower tNAA/tCr ratios have also been reported in the cervical cord of patients with cervical spondylitic myelopathy (Holly *et al.*, 2009) and ALS (Carew *et al.*, 2011). These observed changes in tNAA are often interpreted as reflecting both neuroaxonal injury and impaired metabolic mitochondrial energy production (Moffett *et al.*, 2007). However, it is unclear from those studies, whether (and to what extent) these changes depend on tissue specific volume loss. Our study results indicate that measuring GMVF may be an important methodological consideration when planning similar MRS studies of spinal cord diseases in future.

Limitations and Future Directions

Although no significant difference in GMVF was seen between men and women in this group. However, it is possible this may be due to the small sample size; this work should therefore be repeated in the future with a larger sample size to investigate gender differences further. This study was also limited due to GM fraction not being determined within the VOI; instead we used GMVF of the cord to look at associations with metabolite ratios. We

1 considered using the spatial information of the VOI contained within the headers of the MRS

2 data files to create a binarised mask of the VOI, which can be multiplied by a binarised mask

3 of the spinal cord GM to give the GMVF within the VOI. However, due to the small size of

4 the spinal cord, any subject motion during the 58 minutes of scanning could affect results and

5 could not be corrected for. We therefore opted to use the more objective cord GMVF to look

6 for associations. Visual inspection of the scans did not show any evident motion.

7

8

9

10

11

12

13

14

Chapter Five

Measuring early spinal neuronal loss in PPMS

In this chapter I have used the spinal cord MRS protocol optimised in *Chapter 4* along with a high b-value Q-space imaging (QSI) protocol optimised for the spinal cord (discussed in *Chapter 2*) to assess the degree of early spinal injury in PPMS. I have then assessed how closely these new measures reflect clinical disability.

5.1 INTRODUCTION

As discussed in *Chapter 1*, the clinical phenotype of primary progressive multiple sclerosis (PPMS) is characterised by sustained disability progression from disease onset and is typically associated with severe locomotor disability (Thompson *et al.*, 2000a), with a median time to DSS 6 (walking with a cane) of between 6 to 8.5 years (Runmarker and Andersen, 1993; Cottrell *et al.*, 1999; Confavreux *et al.*, 2000). The rate of disability progression is highly variable, but occurs more quickly early in the disease course and reflects, in part, neuroaxonal loss and neuronal dysfunction in the spinal cord (Bjartmar *et al.*, 2000). There would be great value in applying the imaging markers of neurodegenerative processes discussed in earlier chapters to the spinal cord in early PPMS in order to improve our understanding of the early pathological events that occur in the injury pathway responsible for clinical disability. This step is considered to be crucial in the translational pathway that aims to validate biomarkers that predict clinical outcomes and treatment response in clinical trials in PPMS (Fox *et al.*, 2012).

Advanced quantitative MRI (qMRI) has already been applied in the brain in early PPMS and has improved our understanding of the mechanisms leading to tissue damage, beyond that associated with macroscopic T2 lesions (Wheeler-Kingshott *et al.*, 2014). Measures provided by diffusion tensor imaging (DTI) and ^{1}H-MR spectroscopy (^{1}H-MRS), have been shown to correlate with disability (Sastre-Garriga *et al.*, 2005; Ramio-Torrenta *et al.*, 2006; Bodini *et al.*, 2013), and to predict progression (Khaleeli *et al.*, 2007; Khaleeli *et al.*, 2008). Applying similar techniques to the spinal cord has been technically challenging (Wheeler-Kingshott *et al.*, 2014). However, as discussed in *Chapter 3*, recent developments have led to applications of advanced qMRI in the spinal cord in relapsing-remitting multiple sclerosis (RRMS) and

have provided insights into underlying spinal tissue pathology (Ciccarelli *et al.*, 2007; Farrell *et al.*, 2008; Marliani *et al.*, 2010; Ciccarelli *et al.*, 2013; Kearney *et al.*, 2014b).

Two promising qMRI techniques are high b-value Q-space imaging (QSI) and ^{1}H magnetic resonance spectroscopy (MRS) (see *Chapter 2*). A small pilot study in relapse-onset MS demonstrated the feasibility of using high b-value QSI in the spinal cord with improved detection of abnormal diffusion compared with the conventional DWI acquisition and analysis (Farrell *et al.*, 2008). Spinal cord MRS studies in patients with RRMS and neuromyelitis optica (NMO), have consistently shown neuronal loss and metabolic dysfunction, as reflected by reduced concentration in tNAA in the cervical cord of patients compared to controls (Ciccarelli *et al.*, 2007; Marliani *et al.*, 2007; Ciccarelli *et al.*, 2013), however to date neither of these spinal cord imaging techniques have been applied to patients with PPMS.

Besides the need to utilise more pathologically specific *in vivo* spinal cord imaging techniques in PPMS, there is also a need to incorporate objective clinical measures, which are more sensitive to changes in clinical functions mediated by spinal pathways than conventional clinical tests, such as the Expanded Disability Severity Scale (EDSS) (Kurtzke, 1983). Measures such as postural stability, vibration perception thresholds (VPT) and dynamometry are more responsive to small clinical changes due to damage in the spinal cord than the EDSS, and have been shown to increase the sensitivity for detecting correlations between MRI abnormalities in the spinal cord and disability (Zackowski *et al.*, 2009; Oh *et al.*, 2013a).

In this chapter, I will apply the new MRS protocol (described in *Chapter 4*) in combination with a spinal cord QSI protocol to investigate changes in the cervical cord which underlie disability in patients with early PPMS, to test two hypotheses; i) MRS and QSI demonstrate early pathological changes in the upper cervical cord in patients with PPMS before the occurrence of spinal cord atrophy; ii) in patients, there is a relationship between MRS and QSI measures and disability, as reflected by newer spinal-cord specific clinical scores, alongside standard MS clinical scales, suggesting that early spinal cord neurodegeneration is linked with clinical impairment in PPMS.

5.2 MATERIALS AND METHODS

5.2.1 Study participants

I prospectively recruited patients with an established diagnosis of PPMS (Polman *et al.*, 2005), aged between 18 – 65 years, within 6 years from disease onset, along with, age and gender matched healthy controls. On the day of the MRI, patients were clinically assessed. All subjects provided written, informed consent prior to taking part in the study which was approved by our local research ethics committee.

5.2.2 Clinical Assessments

All patients were assessed using conventional clinical scales, including the EDSS (Kurtzke, 1983), 9-Hole Peg Test (HPT) (Goodkin *et al.*, 1988) and Timed 25-foot Walk Test (TWT) (Cutter *et al.*, 1999). For the purpose of statistical analysis, the average of two trials of the TWT and the average of four trials of the HPT (averaged as reciprocals of the mean times from two trials for each hand) (Fischer *et al.*, 1999) were calculated. We also used the

Multiple Sclerosis Walking Scale-12 (MSWS-12) (Hobart *et al.*, 2003), and the Modified Ashworth Scale (MAS) (Bohannon and Smith, 1987). The MAS values from 16 muscle groups in the upper and lower limbs were converted from a 0–4 scale (which includes a value of 1+ between scores of 1 and 2) to a 0 –5 scale; the resulting values were summated to obtain an overall score ranging from 0 to 80 (Stein *et al.*, 2007).

Clinical scales that are expected to be more sensitive to spinal cord pathways injury than conventional scores were used, including the mean grip strength from both upper limbs, using the Jamar hydraulic dynamometer (Sammons Preston Incorporated, Bolingbrook, IL, USA) (Svens and Lee, 2005), and the vibration perception thresholds (VPTs), which were measured from all 4 limbs at the lateral malleoli and ulna styloid processes using the biosthesiometer (Bio-Medical Instrument Company, Newbury, Ohio). Mean VPTs were calculated and used in the analysis. Finally, postural stability was assessed using a modified version of a recently described protocol for quantifying stance instability (Bunn *et al.*, 2013). Subjects were asked to stand relaxed and still, facing a blank wall at a distance of 1 metre, in a well-lit room, for 40 second-long trials. Three trials under each of the four conditions were recorded, consisting of 2 stance widths (inter-malleolar distance of 32 cm and 4 cm) under 2 visual conditions (eyes either open or closed). Body sway was measured using a 3-D orientation sensor (MTx: Xsens, Enschede, NL), which was fixed to the skin, just below the C7 spinous process. The device measured the instantaneous angular position of the trunk in the anteroposterior (pitch) and mediolateral (roll) planes and was sampled at 100Hz. Summary measures were made on these signals using custom scripts written in Matlab (The Mathworks, Natick, MA USA). The raw data were low-pass filtered at 10Hz using a zero-phase, 5th order Butterworth filter. The amount of angular motion was then calculated separately for the roll and pitch body sway

data and from the combined motion given by square root (pitch-motion^2 + roll-motion^2), termed total sway. All three signals were summarised by summing the sample-to-sample absolute change in signal and then dividing by the duration of the trial to yield average angular speeds of body sway reported in degrees/second. The mean of the three trials per condition were used for statistical analysis. An index of exacerbation of sway on eye closure was obtained from the Romberg quotient calculated as sway eyes closed/sway eyes open at both stance widths.

5.2.3 MRI Protocol

All scans were performed using a 3T Achieva system (Philips Medical Systems, Best, Netherlands) and all participants wore a cervical collar as described earlier.

Using the manufacturer's 16-channel neurovascular coil (Phillips Healthcare Systems), single voxel MRS was acquired as described in *Section 4.2.2.2*.

For cord mean cross-sectional area (CSA) measurements, the cervical cord was imaged in the axial plane, perpendicular to the longitudinal axis of the cord using a fat-suppressed 3D slab-selective fast field echo (FFE) sequence as described in section *4.3.2.2*. In order to match the position and orientation of the volumetric scan to the spectroscopy voxel, the prescription values used for the MRS acquisition were copied and manually entered by the operator when setting up the 3D-FFE scan (**Figure 4.8**).

Using the manufacturer's 32-channel receive coil (Philips Medical Systems, Best, Netherlands), each subject underwent a cardiac gated DWI acquisition [parameters: voxel size=1×1×5 mm^3 (interpolated in k-space to a 0.5 x 0.5mm^2 in-plane resolution) FOV = 64 × 64mm^2; TR = 9RR, TE = 129ms] performed with the volume centred on the C2/C3 disc to ensure similar coverage as the spectroscopy voxel (**Figure 5.1**). A ZOOM sequence was used with outer-volume suppression to minimise artefacts (Wilm *et al.*, 2007). Thirty DWI volumes with equally spaced **q**-values (Schneider and Wheeler-Kingshott, 2014) and two non-diffusion weighted (b0) volumes were acquired with diffusion weighting in two perpendicular (x and y) and one parallel (z) direction to the main axis of the spinal cord [parameters: diffusion pulse duration δ=11.4 ms, diffusion time Δ=75ms, gradient strength G linearly increased in 31 steps from 0 to 87.5mT/m in x and y direction and 62mT/m in z direction].

To achieve the maximum possible gradient strength on the scanner, we exploited the combination of parallel gradient amplifiers in the scanner, which each generate a maximum diffusion gradient strength of 62mT/m along the major axis of the scanner bore. Assuming axial symmetry of the axons along the long axis of the spinal cord, we applied gradient amplifiers in two orthogonal directions that maximise gradient strength perpendicular to axis of the spinal cord (**Figure 5.2**). This allowed us to generate a guaranteed maximum gradient strength of √2*62mT/m in the xy direction. In the z direction we use a maximum gradient of 62 mT/m. q-value were the same in xy and z direction, but the increase in gradient strength allowed us to use a smaller gradient pulse duration of 11.4ms in xy direction (16ms in z), which has been shown in experimental models (Latt *et al.*, 2007a; Latt *et al.*, 2007b), to provide more accurate estimations of displacement.
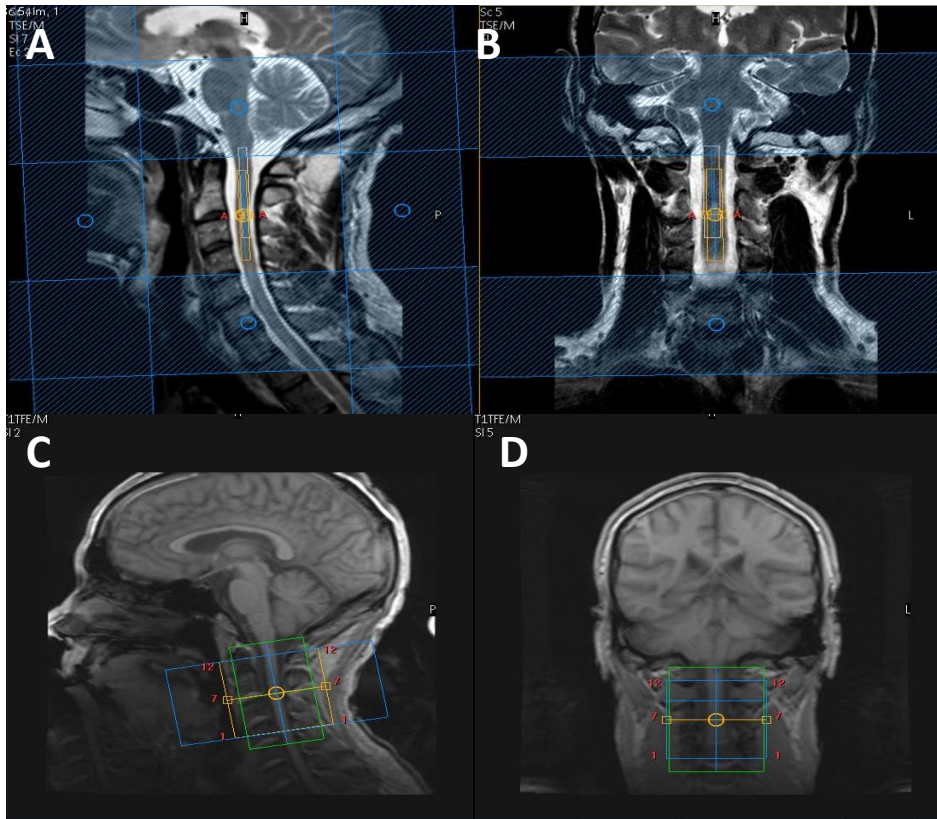
Figure 5.1: Planning of spectroscopy voxel and DWI volume. Above: sagittal (A) and coronal (B) T2w images of the cervical cord with spectroscopy voxel centred on C2/3 intervertebral disc. Below: sagittal (C) and coronal (D) T1w image of the cervical cord showing DWI volume coverage centred on the C2/3 disc.
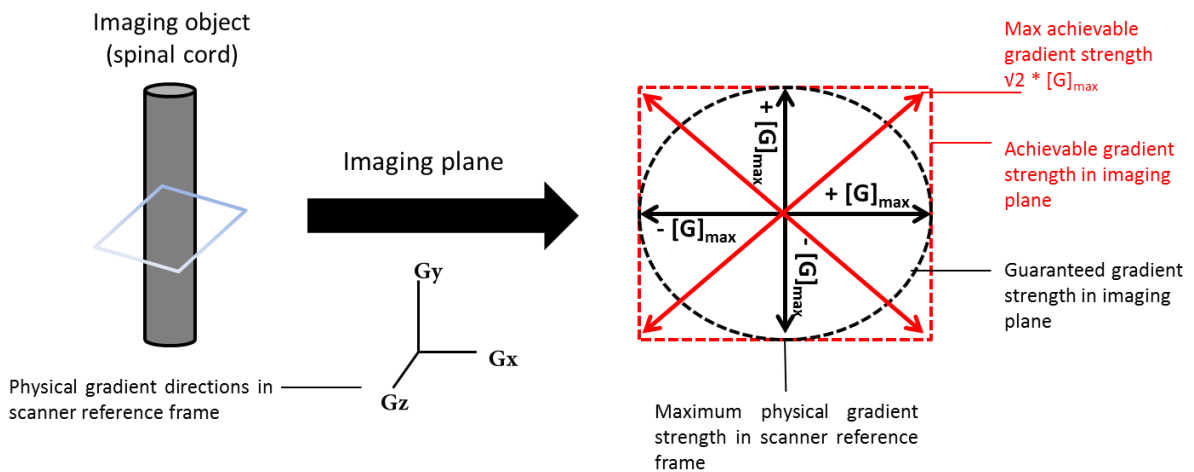
Figure 5.2: Illustration of gradient direction scheme used for x and y QSI encoding. The QSI gradient directions are chosen to maximise the diffusion encoding gradient strength in the perpendicular plane to the spinal cord (red arrows). *Figure reproduced with permission from Dr Torben Schneider*

For calculation of brain T2 lesion volumes, PD/T2 weighted images were acquired using a dual-echo TSE sequence [parameters: TR = 3500 ms; TE = 15/85 ms; flip angle α = 90°; FOV= 240 x 180 mm^2; voxel size = 1 x 1 x 3 mm^3; NEX = 1; 50 axial contiguous slices]. For calculation of brain tissue volumes a 3D T1-weighted magnetisation-prepared gradient-echo sequence was used [TR = 6.9 ms; TE = 3.1 ms; TI = 824 ms; flip angle α = 8°; FOV= 256 x 256 mm^2; voxel size = 1 x 1 x 1 mm^3; NEX = 1; 180 sagittal contiguous slices].

5.2.4 Post processing

Spinal cord metabolite quantification:

Metabolite concentrations were quantified using the user-independent LCModel (version 6.3) package (Provencher, 1993) and a set of basis spectra simulated using GAMMA (Smith *et al.*, 1994) as previously described (*Section 4.2.2.3*). tNAA, tCho, tCr, Ins and Glx concentrations were quantified using the unsuppressed water signal obtained from the same voxel as a reference (Gasparovic *et al.*, 2006) and formed the focus of our analysis. The signal-to-noise ratio (SNR) and full width of half maximum (FWHM) of the tNAA peak provided by LCModel were used to assess spectral quality and Cramér–Rao Lower Bounds (CRLB) values of <20% for tNAA, tCr, tCho and Ins and <30% for Glx were used to confirm the reliability of the spectral fit (Provencher, 2014). Poor quality spectra were excluded from the analysis. Criteria for exclusion were poor water suppression or FWHM > 0.13 with SNR < 3.

Spinal cord area measurement:

Image segmentation and CSA measurements were performed using the 3D-FFE dataset in Jim 6.0 Software (Xinapse systems, Northants, England). Three contiguous 5mm axial slices, centred on the C2/3 disc were segmented using the active surface model method (Horsfield *et al.*, 2010). The mean cross-sectional area of these three slices was then calculated.

Post processing of DWI and ROI analysis:

The two perpendicular diffusion directions were averaged (xy) to increase the signal-to-noise ratio. The diffusion dPDF was computed using inverse Fast Fourier Transformation. To increase the resolution of the dPDF, the signal was extrapolated in Q-space to a maximum $q=200\text{mm}^{-1}$ by fitting a bi-exponential decay curve to the DWI data (Farrell *et al.*, 2008).

Data was corrected for motion using reg_aladin from the NiftyReg toolkit (Ourselin *et al.*, 2000). Registration was performed between the interleaved b=0 acquisitions of the xy and z protocol using the first b=0 of the xy protocol as reference. The estimated registration was then applied to the intermediate DWI images. The quality of the motion correction was assessed in each subject and mis-registered slices/subjects were excluded from the study.

Voxel-wise maps of the full width at half maximum (FWHM); which represents the width of the displacement distribution function and the zero displacement probability (P0); representing the height of the displacement distribution function, were derived from the dPDF for xy and z. Conventional Apparent diffusion coefficient (ADC) maps were also

derived from the low b-value part of the decay curve ($b < 1100s/mm^2$) for both xy and z directions using a constrained non-linear least squares fitting algorithm.

To assess region specific differences in QSI metrics, the whole 60mm length of cervical spinal cord was first extracted from CSF and other tissue types, and four regions of interest (ROIs) were created using the ROI tool in JIM 6.0 and drawn on the b0 images for each axial slice. ADC and QSI indices were measured from ROIs in the anterior, right lateral, left lateral and posterior columns, as well as whole cord (**Figure 5.3**). No statistical differences were found between Q-space indices from the right and left lateral columns; therefore for ease of analysis a mean value from both columns was calculated for each of the Q-space indices.
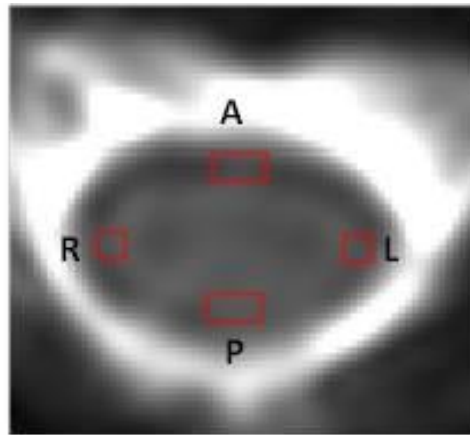
Figure 5.3 Axial b0 image of the cervical spinal cord showing the location of regions of interest (ROIs) placed in the anterior (A), right lateral (R), left lateral (L) and posterior (P) columns. After ROI's were drawn on the b0 images, they were overlaid onto the QSI and ADC maps.

Brain grey matter and white matter volumes:

To avoid segmentation errors due to white matter (WM) lesions, an automated lesion-filling technique was employed (Chard *et al.*, 2010). Lesion masks were created based on 3D-T1 weighted sequences. The lesion-filled images were segmented into WM, grey matter (GM) and cerebrospinal fluid (CSF), using the 'new segment' option in SPM8 (statistical parametric mapping; Wellcome Trust Centre for Neuroimaging, University College London (UCL) Institute of Neurology, London). Segmentations were reviewed to exclude errors. WM and GM fractional (WMF and GMF) volumes, relative to total intracranial volume (the sum of GM, WM and CSF volumes), were calculated.

Brain T2 Lesion Volumes:

Brain T2-lesion volume (T2LV) was calculated by outlining lesions on T2-weighted MRI scans using a semi-automated edge finding tool (JIM v. 6.0). Total lesion volume was recorded in mLs for each subject.

5.2.5 Statistical analysis

Analyses were performed in Stata 13.1 (Stata Corporation, College Station, Texas, USA). Adjusted differences between patients and controls were obtained by multiple regression of the relevant measure on a subject type indicator with age, gender and CSA as covariates (except for the difference in mean cord area itself, which just controlled for age and gender). This analysis was then repeated to evaluate the adjusted difference between controls and patients with and without spinal cord lesions within the C1-3 region of interest.

In patients, univariable associations between metabolites and whole cord QSI metrics were examined with Pearson correlations. Associations between spinal cord measures and EDSS, Summated MAS, peg test and vibration perception were examined with multiple regression of the clinical variable on the spinal cord measure as predictor, with the following potential confounders as covariates: age, gender, mean cord area, brain T2 lesion volume, GM fraction and WM fraction; because of the large number of covariates, these were entered singly into the model, and the unadjusted association is only reported where it was not materially affected by entering any of these covariates. Where regression residuals showed signs of non-normality (e.g. for EDSS), the non-parametric bias corrected and accelerated bootstrap was used (1000 - 5000 replicates, depending on the p-value resolution required), and then, if more precise determination was too computer intensive, the P-value was reported as a range.

For associations between spinal cord measures and measures of postural stability, multivariate regression was used because of the highly related nature of the clinical measures: by performing joint tests of association, the danger of spurious significant results was minimised by reporting associations only where the joint test was significant; where the joint test is not significant, there is no global evidence for any of the individual associations tested, in which case these are not reported as significant even when individually $P<0.05$. The multivariate associations were carried out with potential confounders entered as described above.

5.3 RESULTS

5.3.1 Participant demographics and characteristics

Twenty-three patients with early PPMS and 26 healthy controls were recruited. One patient was unable to tolerate the scan and was excluded; a second patient's scans were excluded from final analysis due to severe motion-related image degradation. Two control subjects were excluded from the study due to unexpected abnormalities on structural imaging. Therefore data from 21 patients and 24 healthy controls were included in the final analysis. Patients had short disease duration and mild to moderate levels of disability. Conventional MRI of the cervical cord identified lesions in 18 out of 21 patients. Of the 18 patients with cervical cord lesions, 12 patients had lesions within the C1 to C3 segments covered by the MRS and QSI volumes. Patient characteristics, disability and conventional MRI findings are summarised in **table 5.1.** Spinal cord imaging findings and disability scores presented patient-by-patient are summarised in **table 5.2**.

1

	Healthy Controls (n = 24)	PPMS Patients (n = 21)
Mean age (SD)	42.1 (11.5) years	48 (7.9) years
Gender	19F: 5M	12F: 9M
Mean CSA (SD)	81.8 (8.1) mm^2	77.5 (9.6) mm^2
Mean GMVF (SD)	0.48 (0.01)	0.47 (0.01)
Mean WMVF (SD)	0.34 (0.01)	0.33 (0.01)
Mean brain parenchymal fraction (SD)	0.82 (0.02)	0.80 (0.02)
Mean T2 lesion volume (SD)		11.6 (9.4) ml
Mean disease duration (SD)		3.9 (1.5) years
Median EDSS (range)		5.0 (3.0 - 6.5)
Mean TWT (SD)		8.1 (5.9) seconds
Mean MSWS-12 (SD)		44.4 (11.4)
Mean summated MAS (SD)		7.2 (9.3)
Mean HPT (SD)		30.0 (13.3) seconds
Mean grip strength (SD)		50.2 (26.4) lbs force
Mean vibration perception threshold (SD)		10.7 (10.6)
Mean sway, 32cm, EO (SD)		0.87 (0.37) deg/s
Mean sway, 32cm, EC (SD)		1.07 (0.46) deg/s
Mean sway, 4cm, EO (SD)		0.98 (0.38) deg/s
Mean sway, 4cm, EC (SD)		1.28 (0.58) deg/s

2 Abbreviations: GMVF = brain grey matter volume fraction, WMVF = brain white matter volume fraction.

3   **Table 5.1**: Demographic and clinical characteristics of patients and volunteers

4

5

6

Patient	Gender	Age (years)	Disease duration (years)	MRI findings cervical cord
1	F	39	4	Single lesion anterior cord at level of C3/4 disc
2	F	42	5	Normal appearing cervical cord
3	F	52	2	Patchy signal change C2 – C5
4	F	46	3	Posterior lesion at C2 and anterior lesion at C4
5	F	57	2	Posterior lesion C3/4 and C6
6	F	38	2.5	Patchy change at C3-4 and a posterior lesion at T3
7	M	44	5	Diffuse signal change C2-6
8	F	50	3	Patchy signal change C6-7 anteriorly
9	M	45	6	Anterior lesions at C3, C4 and C6
10	F	57	2.5	Normal appearing cervical cord
11	M	54	3	Small anterior lesion at C3/4 and a posterior lesion at C6/7
12	F	44	2	Posterior lesion at C6
13	M	57	4	Central lesion C2 and posterior lesions C5 and C6
14	M	55	5	Anterior lesion at C6/7
15	M	50	3	Anterior lesion C5/6
16	M	36	6	Small posterior lesion at C2 and diffuse change C2-C7
17	F	63	6	Anterior lesion C2/3 posterior lesion C3/4
18	M	35	6.5	Anterior lesion T1
19	F	56	5	Patchy lesion at C2/3 and focal anterior lesions at C4 and C7
20	M	42	3	Anterior lesion at C1 and patchy signal change C3-C5
21	F	45	3	Lesion at C1 and C7 with patchy signal abnormality C3-4.

Table 5.2: Patients' demographic data and MRI findings

5.3.2 Differences in qMRI measures between patients and controls

After adjusting for age and gender there was no significant difference in CSA between patients and controls (P = 0.092). Patients had lower spinal tNAA (mean 5.31 vs 4.01 mmol/L, P = 0.02) and Glx (mean 5.93 vs 4.65 mmol/L, P = 0.04) concentrations than healthy controls, after correction for age, gender and CSA, and this was most marked in patients with spinal cord lesions within the spectroscopic volume (**Table 5.3 and Figure 5.4**). Ins concentrations were borderline significantly higher in patients than healthy controls (mean 4.49 vs 5.55 mmol/L, P = 0.08), but were significantly elevated in patients with a C1-C3 lesion (**Table 5.3**).

Tables 5.3 and 5.4 summarise mean values for QSI indices and gives P-values for the adjusted comparisons between patients and controls. Patients had significantly higher perpendicular diffusivity than controls, as reflected in both ADCxy and QSI metrics (FWHMxy and P0xy) in the whole cord and white matter tracts, and a significant increase in parallel diffusivity confined to the posterior columns compared to controls, when adjusting for age, gender and CSA (**Table 5.4 and Figure 5.4**). Perpendicular diffusivity derived from QSI indices (FWHMxy and P0xy), but not ADCxy was also significantly higher in patients with normal appearing spinal tissue compared with healthy controls (**Table 5.3**).

Cord Measure	Healthy Controls (n = 24)	Patients without C1-3 lesion (n = 9)	Patients with C1-3 lesion (n= 12)	All Patients (n = 21)
tNAA	5.31 (1.47)	4.23 (0.86)	3.89 (1.31)	**4.01 (1.16)**
(mmol/L)		P=0.206	P=0.102	**P=0.020**
tCho	1.31 (0.41)	1.12 (0.22)	1.33 (0.38)	1.26 (0.34)
(mmol/L)		P=0.241	P=0.852	P=0.610
tCr	3.76 (1.13)	3.04 (0.35)	4.22 (1.73)	3.79 (1.48)
(mmol/L)		P=0.099	P=0.908	P=0.963
Ins	4.49 (1.23)	4.25 (1.17)	**6.26 (1.84)**	5.55 (1.88)
(mmol/L)		P=0.287	**P=0.006**	P=0.081
Glx	5.93 (1.66)	5.01 (1.90)	**4.50 (0.71)**	**4.65 (1.11)**
(mmol/L)		P=0.170	**P=0.047**	**P=0.043**
ADCxy (μm^2/ms)	0.390 (0.09)	0.421 (0.05)	**0.481 (0.10)**	**0.454 (0.08)**
		P=0.151	**P=0.002**	**P=0.006**
ADCz (μm^2/ms)	1.783 (0.10)	0.183 (0.01)	0.183 (0.02)	1.834 (0.14)
		P=0.123	P=0.119	P=0.123
FWHMxy ($\mu m \times 10^2$)	0.236 (0.02)	**0.251 (0.01)**	**0.276 (0.04)**	**0.265 (0.03)**
		P=0.020	**P<0.001**	**P=0.001**
FWHMz ($\mu m \times 10^2$)	0.550 (0.03)	0.553 (0.03)	**0.560 (0.03)**	0.557 (0.03)
		P=0.427	**0.019**	P=0.120
P0xy (a.u)	0.202 (0.02)	**0.188 (0.01)**	**0.174 (0.03)**	**0.180 (0.02)**
		P=0.025	**0.001**	**P=0.001**
P0z (a.u)	0.113 (0.004)	0.112 (0.003)	0.113 (0.004)	0.113 (0.004)
		P=0.278	P=0.481	P=0.470

1

2 **Table 5.3**: Summary of mean (SD) metabolite concentrations and QSI indices from the cervical

3 cord of patients and controls and P-values for adjusted group comparisons after correcting for

4 age, gender and mean cord cross-sectional area.
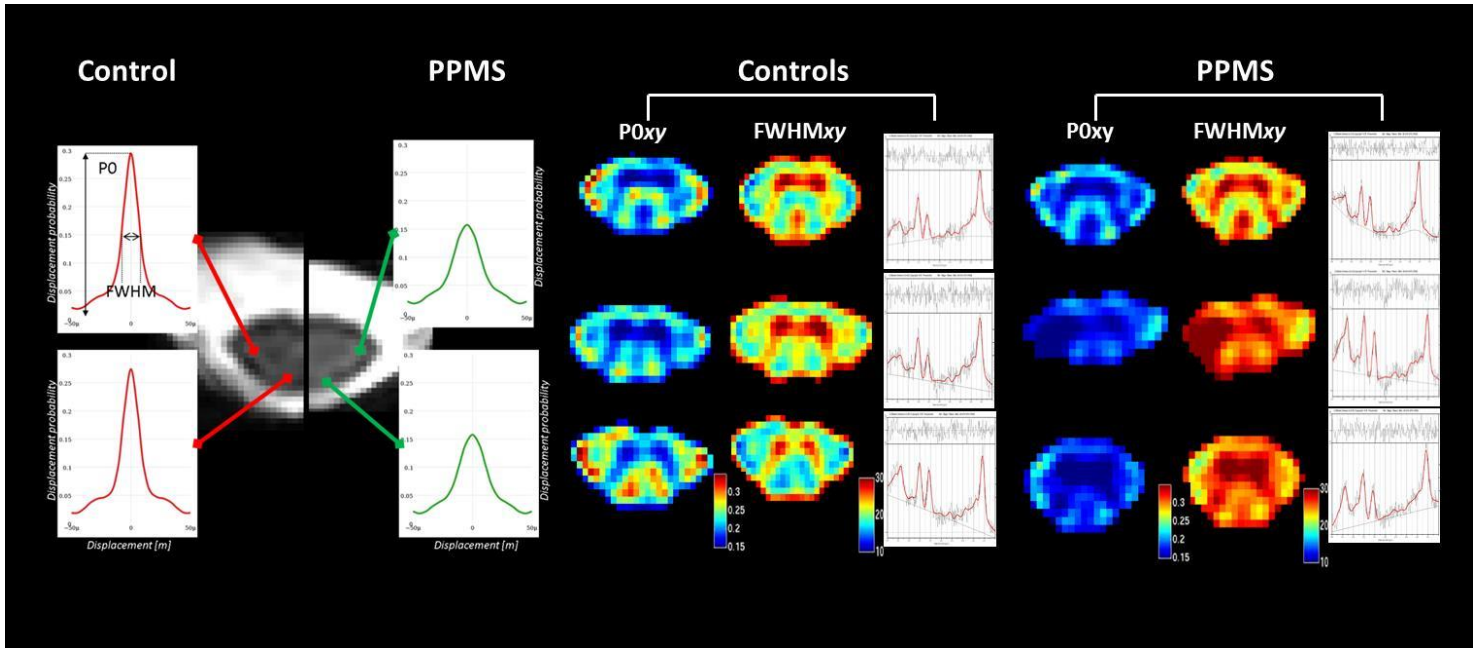
Figure 5.4: PDF, QSI maps and post-processed spectra from patients and controls. Differences in height and width of the dPDF from the posterior and lateral columns between a healthy control and patient are shown on the far left. Grouped P0xy maps, FWHMxy maps and post-processed spectra from 3 controls (central) and 3 patients (far right) demonstrate lower probability of zero net displacement (P0xy) and increased diffusion distribution (FWHMxy) in the patients. The spectra show reduced tNAA and Glx levels in the patients compared to the controls

1

Region of interest	Diffusion measure		PPMS Patients (n=21)	Healthy Controls (n=24)	P-value
Anterior *Column*	ADCxy	(μm^2/ms)	0.497 (0.15)	0.388 (0.12)	**0.028**
	ADCz	(μm^2/ms)	1.921 (0.20)	1.867 (0.17)	0.331
	FWHMxy	(μm x 10^2)	0.266 (0.04)	0.229 (0.02)	**0.001**
	FWHMz	(μm x 10^2)	0.562 (0.03)	0.600 (0.04)	0.159
	P0xy	(a.u)	0.180 (0.03)	0.210 (0.02)	**0.002**
	P0z	(a.u)	0.111 (0.004)	0.111 (0.01)	0.411
Posterior *Column*	ADCxy	(μm^2/ms)	0.458 (0.16)	0.368 (0.10)	**0.017**
	ADCz	(μm^2/ms)	2.181 (0.26)	2.092 (0.14)	**0.050**
	FWHMxy	(μm x 10^2)	0.261 (0.06)	0.229 (0.03)	**0.029**
	FWHMz	(μm x 10^2)	0.610 (0.04)	0.602 (0.04)	0.122
	P0xy	(a.u)	0.185 (0.03)	0.208 (0.03)	**0.018**
	P0z	(a.u)	0.102 (0.004)	0.103 (0.004)	**0.045**
Mean *Lateral* *Columns*	ADCxy	(μm^2/ms)	0.416 (0.11)	0.319 (0.10)	**0.001**
	ADCz	(μm^2/ms)	1.989 (0.26)	1.979 (0.12)	0.581
	FWHMxy	(μm x 10^2)	0.254 (0.04)	0.214 (0.02)	**< 0.001**
	FWHMz	(μm x 10^2)	0.579 (0.02)	0.579 (0.03)	0.318
	P0xy	(a.u)	0.189 (0.03)	0.224 (0.03)	**< 0.001**
	P0z	(a.u)	0.108 (0.007)	0.106 (0.004)	0.757

2

Table 5.4: Summary of mean (SD) Q-space imaging (QSI) indices and apparent diffusion coefficients (ADC) from the major white matter tracts of patients and controls. P-values given for adjusted group comparisons after correcting for age, gender and CSA.

5.3.3 Univariable analysis of spinal cord metabolite concentrations and QSI metrics in patients

In patients, spinal cord tNAA concentration was negatively correlated with whole cord ADCxy (r = - 0.581, p = 0.011) and FWHMxy (r = - 0.636, p = 0.005) and positively correlated with whole cord P0xy (r = 0.646, p = 0.004) (**Figure 5.5**). Other spinal metabolite concentrations did not correlate significantly with each other, or with cord QSI indices.
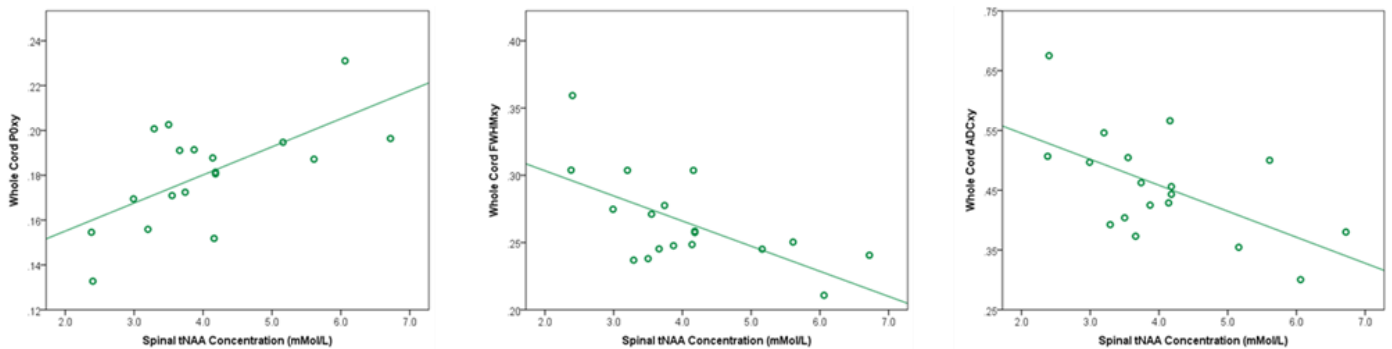
Figure 5.5: Scatter graphs showing correlation between spinal tNAA concentration and whole cord P0xy (left), FWHMxy (centre) and ADCxy (right)

5.3.4 Associations between whole cord qMRI measures and clinical disability

Associations between whole cord qMRI measures and EDSS, summated MAS scores, 1/HPT, grip strength and vibration perception threshold are summarised in **table 5.5** and associations with truncal stability measures are shown in **table 5.6**. A significant association was seen between lower spinal tNAA concentrations and increased physical disability, increased spasticity, and worsening vibration sensory function and postural stability (as reflected by higher EDSS, summated MAS scores, vibration perception threshold and postural sway respectively) (**tables 5.5 and 5.6**). Lower spinal Glx and higher Ins were both independently

associated with increased postural instability. Higher tCho concentrations were independently associated with impairment in upper limb function as reflected by 9HPT. Increased perpendicular diffusivity, indicating increased movement of water in the direction perpendicular to the main axis of the cord, was associated with higher summated MAS scores, higher vibration perception threshold and increased postural instability. There was also a borderline association between lower P0xy, which reflects an increase in perpendicular diffusivity and reduced grip strength.

Clinical Score	Spinal Cord Measure	Regression Coefficient	95 % Confidence Interval	P-value
EDSS	tNAA	-0.41	-1.06, 0.34	0.01 < P < 0.05 *
Summated MAS	tNAA	-3.78	-16.49, 2.16	0.01 < P < 0.05 *
	P0xy	-283.72	-444.26, -123.19	0.002
	FWHMxy	191.30	86.36, 269.24	0.001
	ADCxy	63.64	18.89, 103.39	0.008
1/HPT	tCho	-0.013	-0.03, 0.00	0.05 *
Mean grip	P0xy	435.96	-61.67, 933.59	0.081
Vibration perception threshold	tNAA	-4.37	-8.08, -0.66	0.021
	P0xy	-344.27	-512.61, -175.93	0.001
	FWHMxy	226.49	115.73, 337.26	0.001
	ADCxy	88.06	49.02, 127.10	< 0.001

Table 5.5: Associations between whole cord measures (predictors) and clinical scores (response variables). Unstandardised regression coefficients for imaging measures are reported with 95% confidence intervals and p-values. The regression models were adjusted for age, gender and mean cord area. * Bootstrap P-values.

	Sway Coefficient (95% CI; P-value)	Pitch Coefficient (95% CI; P-value)	Roll Coefficient (95% CI; P-value)	Romberg Quotient Coefficient (95% CI; P-value)
tNAA	**P < 0.001**	**P < 0.0001**	**P = 0.005**	**P = 0.003**
	4EO: -0.057 (-0.188, 0.074; P = 0.393)	4EO: -0.036 (-0.144, 0.073; P = 0.517)	4EO: -0.039 (-0.111, 0.033; P = 0.286)	4cm: -0.112 (-0.191,-0.033; P = 0.006)
	4EC: -0.192 (-0.416, 0.033; P = 0.094)	4EC: -0.137 (-0.277, 0.003; P = 0.056)	4EC: -0.103 (-0.256, 0.049; P = 0.184)	32cm: -0.191 (-0.123, 0.085; P = 0.718)
	32EO: -0.072 (-0.118,-0.022; P = 0.004)	32EO: -0.047 (-0.099, 0.006; P = 0.082)	32EO: -0.044 (-0.069,-0.018; P = 0.001)	
	32EC: -0.086 (-0.221, 0.048; P = 0.208)	32EC: -0.063 (-0.192, 0.066; P = 0.338)	32EC: -0.046 (-0.083,-0.009; P = 0.014)	
Glx	**P = 0.017**	**P < 0.001**	**P = 0.012**	**P < 0.0001**
	4EO: -0.171 (-0.301, -0.042; P = 0.010)	4EO: -0.110 (-0.227, 0.007; P = 0.065)	4EO: -0.108 (-0.171, -0.046; P = 0.001)	4cm: -0.134 (-0.236,-0.032; P = 0.010)
	4EC: -0.320 (-0.564, -0.076; P = 0.010)	4EC: -0.204 (-0.360, -0.049; P = 0.010)	4EC: -0.207 (-0.367, -0.046; P = 0.012)	32cm: -0.140 (0.232,-0.048; P = 0.003)
	32EO: -0.057 (-0.127, 0.014; P = 0.114)	32EO: -0.033 (-0.103, 0.038; P = 0.366)	32EO: -0.039 (-0.076,-0.002; P = 0.039)	
	32EC: -0.163 (-0.310,-0.015; P = 0.031)	32EC: -0.134 (-0.279, 0.010; P = 0.069)	32EC: -0.062 (-0.104, 0.020; P = 0.004)	
Ins	**P < 0.0001**	**P = 0.014**	**P = 0.440**	**P = 0.046**
	4EO: 0.062 (-0.061, 0.185; P = 0.324)	4EO: 0.068 (-0.324, 0.170; P = 0.184)		4cm: 0.031 (-0.052, 0.113; P = 0.467)
	4EC: 0.100 (-0.102, 0.303; P = 0.332)	4EC: 0.062 (-0.078, 0.201; P = 0.388)		32cm: 0.086 (-0.019, 0.153; P = 0.012)
	32EO: 0.019 (-0.065, 0.103; P = 0.660)	32EO: 0.026 (-0.045, 0.097; P = 0.477)		
	32EC: 0.090 (-0.010, 0.191; P = 0.078)	32EC: 0.093 (0.004, 0.183; P = 0.040)		
tCho	**P = 0.545**	**P = 0.144**	**P = 0.979**	**P = 0.113**
tCr	**P = 0.306**	**P = 0.237**	**P = 0.821**	**P = 0.363**
ADCxy		4EC: 2.48 (0.44, 4.51; P = 0.017)	32EO: 0.93 (0.34, 1.52; P = 0.002)	4cm: 1.41 (0.24, 2.59; P = 0.023)
			32EC: 1.24 (0.28, 2.21; P = 0.011)	
FWHMxy		4EC: 5.57 (0.02, 11.12; P = 0.049)	32EO: 2.25 (0.56, 3.94; P = 0.009)	
P0xy			32EO: -3.80 (-6.14, -1.46; P = 0.001)	
			32EC: -5.01 (-8.84,-1.18; P = 0.010)	

EC = eyes closed; EO = eues open.

Table 5.6: Associations between whole cord imaging measures and truncal stability. A multivariate analysis was used to assess associations between metabolite predictors and the multiple stability scores as response variables. P-values for the joint test of the metabolite predictor are shown in **bold**. Metabolite regression coefficients, 95% confidence intervals and p-values are shown for the individual stability variables, and these are only shown where the joint test was significant. The regression models adjusted for age, gender and mean cord area.

5.3.5 Associations between column-specific QSI metrics and clinical disability

When examining the results of the ROI-specific analysis, significant associations between QSI and clinical disability were found in all columns, although some columns showed preference for specific clinical tests. Increased spasticity was predicted by lower P0xy in the anterior, lateral and posterior columns; increased FWHMxy in the anterior and lateral columns and increased ADCxy in the lateral columns. Reduced vibration sensation was predicted by increased perpendicular diffusivity (reduced P0xy and increased FWHMxy and ADCxy) in the anterior, lateral and posterior columns. Instability in the roll plane was predicted by reduced P0xy (increased perpendicular diffusivity) in the posterior column, while instability in the pitch plane was predicted by increased ADCxy (increased perpendicular diffusivity) in the anterior column. A summary of associations is presented in **table 5.7**.

Clinical Score	Region of interest	Diffusion Measure	Regression Coefficient	95 % Confidence Interval	P-value
	Lateral Column	P0xy	-205.16	-322.34, -87.97	0.002
		FWHMxy	171.80	91.34, 252.27	< 0.001
		ADCxy	50.66	16.50, 84.83	0.006
	Anterior Column	P0xy	-185.96	-316.30, -55.62	0.008
Summated MAS		FWHMxy	157.38	64.03, 250.72	0.002
	Posterior Column	P0xy	-136.56	-267.09, -6.03	0.04
		P0xy	-268.54	-421.03, -116.05	0.002
		FWHMxy	223.44	125.91, 320.90	< 0.001
	Lateral Column	ADCxy	67.20	28.07, 106.33	0.002
		P0xy	-239.01	-384.52, -93.50	0.003
Vibration		FWHMxy	200.74	106.07,295.41	0.001
	Anterior Column	ADCxy	40.73	7.82, 73.64	0.02
		P0xy	-219.76	-353.71, -85.80	0.003
		FWHMxy	101.77	32.47, 171.08	0.007
	Posterior Column	ADCxy	46.29	22.24, 70.34	0.001
32EO Sway	Anterior Column	ADCxy	0.81	0.12, 1.50	0.021
32EO Roll	Posterior Column	P0xy	-2.16	-4.07, -0.26	0.026
32EO Pitch	Anterior Column	ADCxy	0.69	0.15, 1.23	0.013
32EC Roll	Posterior Column	P0xy	-3.85	-6.58, -1.12	0.006
32EC Pitch	Anterior Column	ADCxy	1.04	0.12, 1.94	0.026
4EO Pitch	Anterior Column	ADCxy	1.02	0.13, 1.91	0.025
4EC Pitch	Anterior Column	ADCxy	1.54	0.47, 2.63	0.005
4cm Romberg	Lateral Column	ADCxy	1.18	0.20, 2.16	0.023

Table 5.7: Associations between tract-specific diffusion indices (predictors) and clinical scores (response variable). Unstandardised regression coefficients for imaging measures are reported with 95% confidence intervals and p-values. The regression models were adjusted for age, gender and mean cord area

5.4 Discussion

By applying novel spinal qMRI techniques this study has demonstrated that there is lower tNAA and Glx, and increased QSI-derived perpendicular diffusivity (seen as an increase in FWHMxy and a decrease in P0xy) in the cervical cords of patients with early PPMS compared to controls. These findings suggest that neuronal loss, metabolic dysfunction and changes in the glutamatergic pathway, occur in the spinal cord in the early stages of the disease. Significant associations between spinal cord tNAA, Glx and QSI-derived perpendicular diffusivity and newer measures of clinical disability, such as postural stability and VPT, suggest that these imaging measures reflect the abnormalities that contribute to clinical impairment.

These results could suggest that neurodegeneration occurs early in the spinal cord, in the absence of extensive spinal cord atrophy. These qMRI abnormalities correlated with clinical impairment and could provide insights into the pathological events that occur in PPMS. This study provides justification for further developing these qMRI measures and for their validation as useful biomarkers of disease progression and treatment response in clinical trials.

Differences in qMRI between patients and controls

The lower tNAA concentrations in the spinal cord of PPMS patients when compared with healthy controls are consistent with metabolite abnormalities in the brain, where tNAA is lower in cortical grey matter and NAWM early in PPMS (Sastre-Garriga *et al.*, 2005). In

addition, findings from this study are qualitatively similar to those seen in acute (Ciccarelli *et al.*, 2007; Henning *et al.*, 2008; Ciccarelli *et al.*, 2010a) and chronic (Marliani *et al.*, 2010; Ciccarelli *et al.*, 2013) spinal cord lesions in RRMS. The majority of the early PPMS patients included in the present study (N=12) had a lesion (or part of a lesion) within the spectroscopic voxel and in these patients, spinal tNAA concentrations were lower than patients without a lesion. There were too few subjects in the study to detect a statistically significant difference in tNAA concentrations between patients with and without spinal lesions within the spectroscopic voxel: we estimated that the sample size required to detect a difference between those two groups with 80% power (alpha 0.05) using the spectroscopy protocol described in this study would be 168 subjects per group; this finding suggests that tNAA concentration is lowest in the lesional tissue of the spinal cord, but reduced less dramatically, in the normal-appearing white matter when compared with the healthy tissue, which is similar to what has been previously been demonstrated in the brain (Caramanos *et al.*, 2005).

Glx, which represents the sum of Glu and its precursor Gln, was also significantly lower in patients than controls. These changes were most significant in patients with spinal cord lesions within the spectroscopic voxel and likely reflect changes in the spinal glutamatergic pathways. As discussed previously, because Glu, which is predominantly found in the synaptic terminals makes up the majority of the Glx signal, it is possible that lower spinal Glx in this patient group could, in part, be explained by neuro-axonal degeneration. In the brains of patients with early PPMS, similar findings have been reported; Glx is reduced in the cortical grey matter, but not the NAWM (Sastre-Garriga *et al.*, 2005). Similarly, in patients with clinically stable RRMS, Glu and Glx are both reduced in grey matter regions (Muhlert *et*

al., 2014). Together these results would suggest that the reductions in Glx reflect reduced synaptic density in the grey matter secondary to neuronal loss. In contrast to the control group (see section 4.2), in patients, we found that Glx did not correlate well with tNAA, which suggests that impairment of glutamatergic metabolism as well as neuroaxonal loss may occur in early PPMS, and these metabolites reflect different aspects of the underlying tissue changes.

QSI-derived diffusivity was measured parallel and perpendicular to the long axis of the spinal cord which showed significantly increased perpendicular diffusivity in patients compared with controls. Data from animal studies suggests that increased perpendicular diffusivity using QSI is not specific to demyelination (Farrell *et al.*, 2010), as has been reported with DTI (Song *et al.*, 2002). Instead, the changes in the dPDF shape in this patient group are likely to reflect a breakdown in myelin and axonal membranes which both act as microstructural barriers to perpendicular diffusion (Beaulieu, 2002) and corresponds to what would be expected based on findings from murine and canine models of aberrant myelination and axonal loss (Biton *et al.*, 2006; Farrell *et al.*, 2010; Wu *et al.*, 2011; Anaby *et al.*, 2013), as well as to what has previously been reported in patients with relapse-onset MS (Assaf *et al.*, 2002; Farrell *et al.*, 2008).

The differences in QSI measures between patients and controls are in agreement with the tNAA and Glx changes and provide corroborating evidence for early neuroaxonal injury in the cervical cord. Importantly, in patients with normal appearing spinal tissue within the diffusion imaging volume, FWHMxy and P0xy remained significantly different to controls,

whereas ADCxy did not, suggesting that QSI indices are more sensitive to microstructural injury than conventional ADC measures.

Interestingly, spinal CSA, a measure of tissue loss, which is often used as an imaging surrogate of axonal loss (Kearney *et al.*, 2013b) was not significantly different between patients and controls despite earlier studies with larger sample sizes (Bieniek *et al.*, 2006) and those which included patients with longer disease duration (Losseff *et al.*, 1996), demonstrating significant cord atrophy in PPMS. It is therefore likely the reason we did not detect significant differences in CSA between patients and controls in the current study was that the sample size was small and patients were selected on the basis of short disease duration. Based on CSA measures from our cohort of patients and controls, we estimate that the sample size required to detect significant differences in CSA in early PPMS, using the method described in this study with 80% power (alpha = 0.05), is 68 subjects per group. Using measurements obtained from another study of cord atrophy in PPMS (Ruggieri *et al.*, 2015), 41 subjects per group would be required to detect significant group differences. Our study comprises early duration PPMS, in whom mean cord area differed from controls by only 4.3mm^2, compared to a difference of 7.0 mm^2 in the study by Ruggieri et al, in which disease duration of the patient group is not reported although patients had similar disability on EDSS, TWT and HPT as our patient group.

This would suggest that much smaller sample sizes are required to detect group differences early in the disease course with newer qMRI measures that reflect neurodegenerative processes other than atrophy alone. We cannot exclude that alternative image segmentation methods, such as the edge detection and partial volume correction method proposed by Tench

et al (Tench *et al.*, 2005) may have enabled detection of significant cord atrophy in this patient group and this merits further study in future. In order to validate these new measures for clinical trials, it is important to test whether or not these qMRI measures and metabolite concentrations are sensitive to changes occurring over time and predict clinical outcome at follow-up.

In addition to the differences in tNAA, Glx and QSI-derived perpendicular diffusivity between groups, we found that patients had higher spinal Ins levels than controls but this finding did not reach statistical significance. We calculated that for Ins, to have 80% power to detect a patient vs control difference of the size observed (which is about two thirds of a standard deviation) at 5% significance, 40 subjects per group would be necessary. Patients with a spinal cord lesion within the spectroscopic voxel did have significantly elevated Ins concentrations, which is likely to reflect astrocytic proliferation and activation (or gliosis) occurs in spinal cord lesions in early PPMS. Previous studies have suggested that gliosis is an early pathological process in MS, and gliosis may be an important mechanism of disease progression (Ciccarelli *et al.*, 2014). Our results suggest this process is more active in lesional than non-lesional tissue. With regard to tCho, which is a marker of inflammation and membrane turnover (Henning *et al.*, 2008; Marliani *et al.*, 2010), since the observed differences between groups is less than 15% of the SD, it would take hundreds of subjects per arm to detect such a small difference, suggesting that this metabolite is unlikely to be useful for distinguishing patients from healthy controls in future studies.

Association between spinal cord metabolites and diffusion indices

The modifications to gradients and pulse lengths necessary to perform QSI on clinical scanners have the effect of exaggerating the contribution of slow diffusing water to QSI metrics (Assaf *et al.*, 2002), consequently, diffusion of intra-axonal water is highly represented (Assaf and Cohen, 2000; Assaf *et al.*, 2000; Assaf *et al.*, 2005) and it has therefore been suggested that QSI metrics make useful markers of axonal integrity. Interestingly, in our study, spinal tNAA concentration which reflects axonal integrity correlated more strongly with QSI derived indices of perpendicular diffusivity than ADC suggesting these indices are more indicative of axonal integrity.

Associations between whole cord qMRI measurements and clinical disability

When applying new clinical scales, there is a significant association between increased clinical disability and lower spinal tNAA and Glx and higher spinal tCho and Ins concentrations (**tables 5.5 and 5.6**). Lower Glx and tNAA may be a reflection of neuroaxonal loss, which is known to be an important substrate for clinical disability in MS (Bjartmar *et al.*, 2000; Tallantyre *et al.*, 2010). In RRMS, low spinal tNAA has also been shown to correlate with increased disability scores (Blamire *et al.*, 2007; Ciccarelli *et al.*, 2007) but to the best of my knowledge, this is the first time spinal Glx concentrations have been reported in MS.

Although tCho concentrations were not significantly different between patients and controls in this cohort, higher tCho in patients did correlate with disability. This is in contrast to

findings in patients with RRMS, where higher spinal tCho concentrations have been reported (Henning *et al.*, 2008; Marliani *et al.*, 2010). In RRMS, spinal tCho has been shown to correlate with higher EDSS scores (Ciccarelli *et al.*, 2007) and it has previously been proposed that elevated tCho levels reflect breakdown of membranes and ongoing remyelination within spinal plaques (Marliani *et al.*, 2010).

Increased perpendicular diffusivity reflects breakdown of myelin and axonal microstructure which are important determinants of disability. In their feasibility study, Farrell *et al* demonstrated that there was an increase in the width and a decrease in the height of the dPDF in spinal lesions but did not report on correlations with clinical scores (Farrell *et al.*, 2008). Increased whole cord perpendicular diffusivity in our study, was independently associated with increased spasticity, vibration perception thresholds and postural instability which suggests that whole cord QSI may be a potentially useful imaging biomarker of disease progression. Although it is can be assumed that QSI metrics coming from lesional spinal cord tissue reflect in part tissue damage at the site of lesions, the contribution of tissue changes secondary to tract-mediated Wallerian degeneration in axons that traverse lesions at a distant site, either in the brain or spinal cord (Evangelou *et al.*, 2005) could not reliably be quantified.

Associations between column-specific diffusion indices and disability

There were several significant associations which were expected based on *a priori* knowledge of spinal WM tract function. Namely, increased perpendicular diffusivity within the anterior

1   and lateral corticospinal tracts independently predicted spasticity, whilst instability in the roll

2   plane and vibration perception threshold was predicted by increased perpendicular diffusivity

3   in the posterior columns. It is interesting that the effect emerges with the feet wider apart

4   when the body is normally more stable. It has previously been suggested that part of this

5   increased stability with increasing stance width arises from hip proprioceptors being

6   increasingly able to signal lateral sway because of the mechanical linkage between hips and

7   ankles (Day *et al.*, 1993) which may be degraded when there is posterior column pathology.

8   Higher ADCxy in the anterior column predicted instability in the pitch plane which suggests

9   that pitch plane abnormalities are predominantly due to problems of motor organisation or

10 coordination. The coordination of joints is probably more demanding in the sagittal (pitch)

11 plane since there are more degrees of freedom due to independent action of leg joints. In

12 contrast, in the frontal (roll) plane the knees cannot contribute much to instability while the

13 ankle and hips are no longer independent (Day *et al.*, 1993).

14

15

16 **Limitations**

17 There are a number of limitations of the current study which should be noted. Firstly, there is

18 a subtle age and gender mismatch between the patient and control groups despite best efforts

19 to match the groups. The age difference between the groups was not statistically significant

20 and when assessing group differences in MRI measures, I used a regression analysis

21 correcting for age and gender which will have corrected for these small differences.

22

Secondly, although the MRS protocol reliably quantified Glx (Glu + Gln) in the spinal cord for the first time in an MS patient group, separate information about Glu and Gln could not be derived. Strategies for separating Glu and Gln at 3T have already been discussed in *Chapter 4;* future technical developments should aim to allow direct measurement of Glu with no Gln overlap in order to allow a more specific evaluation of the role of Glu in MS pathophysiology.

Thirdly, although we acknowledge there is always a risk of spuriously significant results at 5%, with Type 1 error, we have not corrected for multiple comparisons within this study. Corrections for multiple comparisons are typically appropriate when there is a single null hypothesis which is tested using a number of comparisons, and where the significance of any one of these comparisons is sufficient to reject the single hypothesis or when multiple tests are individually reported or highlighted not because of their relevance to prior individual hypotheses of interest, but because of being statistically significant (Rothman, 1990; Perneger, 1998). In the current study we were not examining a single null hypotheses, but several; we are reporting significant and non-significant results, and highlighting the former in relation to prior and plausible hypotheses. Where similar tests were used (eg. in the case of the postural stability measures), a multivariate statistical approach was used to reduce the risk of Type 1 errors. It should also be noted that methods employed for multiple comparison corrections such as the Bonferroni test do not completely eliminate the risk of Type 1 error and could potentially eliminate genuinely significant results as spurious and in the context of scientifically exploratory, hypothesis-generating context, the consequences of Type 2 error can be at least as important as Type 1 error (Rothman, 1990; Perneger, 1998). We therefore prefer to consider any borderline significant results as hypothesis-generating which can form the basis for future research.

Finally, although a state-of-the-art spinal cord QSI sequence was used in this study, the smaller gradients and longer gradient pulses needed to perform QSI on a clinical scanner have the effect of narrowing the PDF produced by Q-space analysis, leading to an under-estimate of the FWHM. As discussed in earlier chapters, it has therefore been proposed that these should be considered as, apparent values (Assaf *et al.*, 2005; Farrell *et al.*, 2008). Therefore direct comparison with previously published studies should be made with care, and only after taking into account differences in gradient settings.

Future directions

A future longitudinal extension of the current study should investigate whether QSI and MRS measures are predictive of future disability and cord atrophy. Further work is still needed to assess how closely longitudinal changes in imaging measures reflect clinical change in order to validate the use of these advanced spinal cord imaging protocols as potential imaging biomarkers of the future.

1

2

Chapter Six

Mechanisms of spinal neurodegeneration and repair in RRMS

As discussed in *Chapter 1,* data from earlier pathological, imaging and animal studies have identified a number of viable disease mechanisms to explain the neurodegenerative and repair pathways in multiple sclerosis which are responsible for clinical outcomes. Within Chapter 6, by utilising the imaging measures used in *Chapter 5,* within a longitudinal study design, I will aim to determine the contribution of spinal neuroaxonal loss and dysfunction, glutamate-mediated excitotoxicity, gliosis and repair mechanisms to clinical outcomes following spinal cord relapse in RRMS.

6.1 Introduction

Relapsing remitting multiple sclerosis (RRMS) is characterised by episodic clinical relapses, associated with inflammatory plaque formation within the central nervous system. Inflammatory demyelination, axonal transection and oedema associated with acute lesions cause transient interruption to normal salutatory conduction, giving rise to clinical symptoms. With time, clinical recovery can occur but may be incomplete or even absent, depending upon a complex interaction between neurodegenerative and repair mechanisms(Compston and Coles, 2002).

In early RRMS, clinical relapses are often followed by complete recovery, whereas in later disease, there is increased chance disability will persist and even, evolve to secondary, disability progression (Confavreux *et al.*, 2000; Lublin *et al.*, 2003; Confavreux and Vukusic, 2006b). Imaging and pathology studies suggest neuroaxonal loss is the substrate for disability progression (De Stefano *et al.*, 1998; Bjartmar *et al.*, 2000; Frischer *et al.*, 2009; Tallantyre *et al.*, 2010). In contrast, resolution of inflammation, remyelination, and electrophysiological adaptation may underlie clinical recovery (Craner *et al.*, 2004a; Black *et al.*, 2007; Hartley *et al.*, 2014; Olsen and Akirav, 2014). Understanding the mechanisms of neurodegeneration and repair following clinical relapses is critically important as they may represent modifiable biological processes which can be targeted by novel therapies.

Inflammatory demyelination is thought to account for a proportion of axonal damage (Trapp *et al.*, 1998; Reynolds *et al.*, 2011) and in early disease, there is some evidence that

aggressive immunomodulation may slow the neurodegeneration underlying disability progression (Coles *et al.*, 2008). However, as discussed in *Chapter 1*, evidence from epidemiological, imaging and laboratory studies suggest that non-inflammatory mechanisms also play an important role.

Measurements obtained using high b-value Q-space imaging (QSI) and ^{1}H-MR spectroscopy (^{1}H-MRS), as discussed earlier (**Chapter 2**), reflect biological processes which may be important in spinal neurodegeneration and repair following acute attacks. In the current study, I will therefore employ a combination of spinal MRS and QSI to investigate four important biological mechanisms and their effect on disability following acute spinal cord relapse; specifically:

1. The effect of spinal tNAA and perpendicular diffusivity, which reflect neuronal density, mitochondrial function and myelination on acute disability following spinal cord relapse and disability progression over 6 months.

2. The effect of spinal glutamate-glutamine (assessed using MRS) on disability following spinal cord relapse and disability progression over 6 months.

3. The effect of spinal inositol, an imaging marker of gliosis (assessed using MRS) on disability following spinal cord relapse and disability progression over 6 months.

4. The relationship between temporal QSI changes which may reflect underlying remyelination and repair on clinical recovery following spinal cord relapse.

6.2 MATERIALS AND METHODS

6.2.1 Study participants

Patients with an established diagnosis of RRMS (Polman *et al.*, 2011), aged between $18 - 65$ years, within 4 weeks of developing symptoms consistent with cervical cord relapse were prospectively recruited, along with, age and gender matched healthy controls. All subjects provided written, informed consent prior to taking part in the study.

6.2.2 Clinical Assessments

Patients were clinically assessed at baseline, 1,3 and 6 months as described in chapter 5 with the EDSS (Kurtzke, 1983), 9-Hole Peg Test (HPT) (Goodkin *et al.*, 1988), Timed 25-foot Walk Test (TWT) (Cutter *et al.*, 1999), Multiple Sclerosis Walking Scale-12 (MSWS-12) (Hobart *et al.*, 2003), Modified Ashworth Scale (MAS) (Bohannon and Smith, 1987), mean grip strength using the Jamar hydraulic dynamometer (Sammons Preston Incorporated, Bolingbrook, IL, USA) (Svens and Lee, 2005), VPTs using the biosthesiometer (Bio-Medical Instrument Company, Newbury, Ohio) and postural instability (Bunn *et al.*, 2013).

6.2.3 MRI Protocol

Patients and controls were scanned at baseline, 1, 3 and 6 months using a 3T Achieva system (Philips Medical Systems, Best, Netherlands), whilst wearing a cervical collar as described in earlier chapters.

At each of the 4 time points, patients and controls were scanned with the following protocol:

1.   Single voxel spinal MRS protocol (**Section 4.2.2.2**).

2.   Fat-suppressed 3D slab-selective fast field echo (FFE) spinal cord sequence (**Section 4.3.2.2**).

3.   Spinal cord QSI (**Section 5.2.3**).

4.   Pre-contrast brain PD/T2 weighted dual-echo TSE sequence (**Section 5.2.3**).

5.   Pre-contrast brain 3D T1-weighted magnetisation-prepared gradient-echo sequence (**Section 5.2.3**).

In patients only, post-gadolinium scans of the brain and cervical spine (**Figure 6.1**) were acquired at baseline, five minutes after administration of 0.2ml per kg Dotarem (Guerbet, France). The purpose of the post-contrast images was to confirm that relapse symptoms were due to a new inflammatory lesion within the cervical spinal cord. Post-contrast images of the spinal cord were acquired using a sagittal T1-weighted TSE sequence [parameters: TR = 502 ms; TE = 8 ms; flip angle α = 90°; FOV= 259 x 160 mm^2; voxel size = 0.8 x 1 x 3 mm^3; NEX = 3; 14 axial contiguous slices]. Post contrast brain images were acquired using an axial oblique T1-weighted spin echo sequence [parameters: TR = 625 ms; TE = 10 ms; flip angle α = 90°; FOV= 240 x 180 mm^2; voxel size = 1 x 1 x 3 mm^3; NEX = 1; 50 axial contiguous slices].
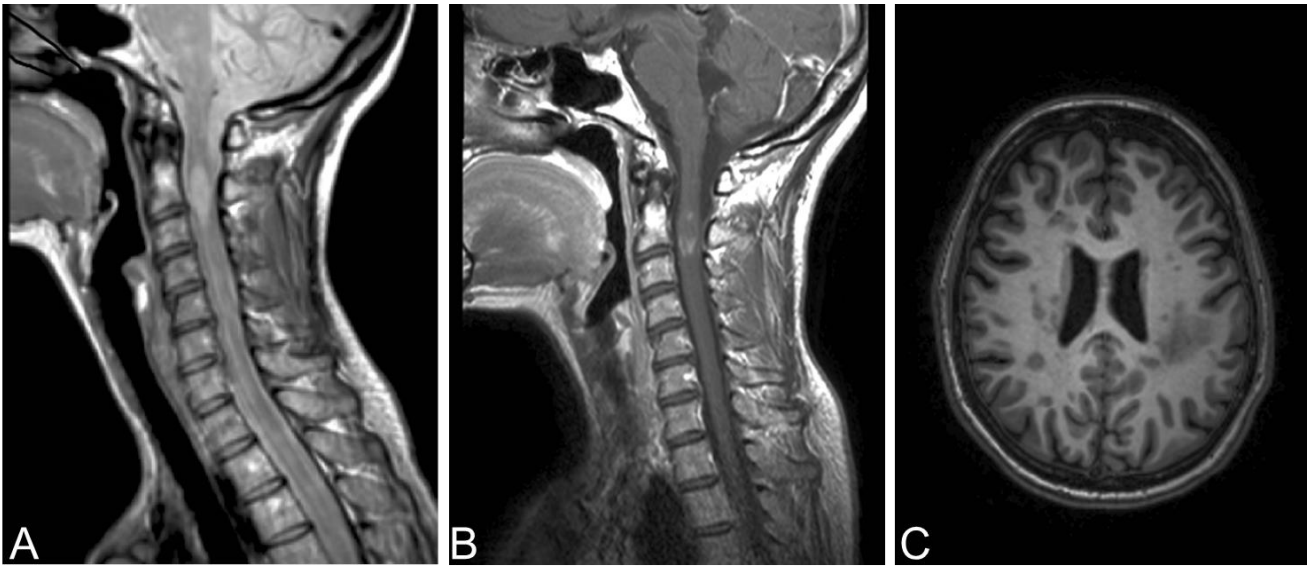
Figure 6.1 Pre and post-contrast spinal and brain images from a patient participating in the study. A) Shows a sagittal proton density scan showing spinal cord lesion at the level of C2/3 with associated swelling. B) Shows sagittal T1w post-contrast scan showing patchy contrast enhancement. C) Shows a single axial slice from the T1w post –contrast brain scan which confirms the absence of any active inflammatory lesions but the presence of hypointense lesions, in agreement with a diagnosis of MS.

6.2.4 Post processing

Spinal cord metabolite quantification:

Metabolite concentrations were quantified using the user-independent LCModel (version 6.3) package (Provencher, 1993) and a set of basis spectra simulated using GAMMA (Smith *et al.*, 1994) as previously described (**Section 4.2.2.3**). tNAA, tCho, Cr, Ins and Glx concentrations were quantified using the unsuppressed water signal obtained from the same voxel as a reference (Gasparovic *et al.*, 2006) and formed the focus of our analysis. Overall spectral quality was assessed as described in chapter 5 (**Section 5.2.4**).

Spinal cord area measurement:

Image segmentation and CSA measurements were performed as described in **Section 5.2.4**. The mean cross-sectional area of three slices was then calculated.

Post processing of DWI and ROI analysis:

Post-processing of DWI data is fully described in **Section 5.2.4**. Voxel-wise maps of the full width at half maximum (FWHM), zero displacement probability (P0), and apparent diffusion coefficient (ADC) were derived for both xy and z directions using a constrained non-linear least squares fitting algorithm.

To assess region specific differences in QSI metrics, the whole 60mm length of cervical spinal cord was first extracted from CSF and other tissue types, and four regions of interest (ROIs) were created using the ROI tool in JIM 6.0 and drawn on the b0 images for each axial slice. ADC and QSI indices were measured from ROIs in the anterior, right lateral, left lateral and posterior columns, as well as whole cord. No statistical differences were found between Q-space indices from the right and left lateral columns; therefore for ease of analysis a mean value from both columns was calculated for each of the Q-space indices.

Brain grey matter and white matter volumes:

WM and GM fractional (WMF and GMF) volumes, relative to total intracranial volume (the sum of GM, WM and CSF volumes), were calculated as described in **Section 5.2.4**.

Brain T2 Lesion Volumes:

Brain T2-lesion volume (T2LV) was calculated as described in **Section 5.2.4**.

6.2.5 Statistical analysis

Cross-sectional adjusted differences in spinal cord imaging measures between patients and controls at the four time points were estimated from linear mixed models over all four time points with random coefficients for subject id intercept and time: the variable compared was regressed on categorical time point indicators, a group indicator, a group X time interaction term, and age and gender, from which differences at each time points were estimated. The advantage of such models, compared to separate models at each time point, is that all available data points contribute to estimation, and adjustment for age and gender is better estimated when all time points are simultaneously modelled.

Associations between baseline spinal cord imaging measures and acute disability at baseline were examined with multiple regression of the clinical variables on the spinal cord imaging measure as predictor, with the following potential confounders as covariates: age, gender, mean cord area, brain T2 lesion volume, GMF and WMF; because of the large number of covariates, these were entered singly into the model. Where significant univariate associations were not materially affected by entering confounders into the model as described, the unadjusted association is reported. Where entering any of the covariates resulted in confounding of the association, the association is regarded as non-significant and has not been reported.

In order to examine temporal changes in imaging measures associated with repair, patients were classed as "improvers" (EDSS change of ≤ -0.5 over 6 months), or "non-improvers" (no improvement on EDSS). Adjusted differences between improvers and controls, as well as, non-improvers and controls were obtained by multiple regression of the relevant imaging measure on a subject type indicator, with age, gender and CSA as covariates. A similar analysis was then repeated but instead of patients being divided based on EDSS change, they were categorised based on imaging findings, as either, "radiologically confirmed relapse" (includes patients with acute spinal cord swelling or enhancement at baseline, or those in whom C1-3 lesions had resolved by 6 month follow up) or "radiologically ambiguous cases" (static spinal MRI appearances during 6 month follow up).

Associations between baseline spinal cord imaging measures and changes in clinical scores examined using linear mixed models as above, but with the clinical score as response variable and, as predictors, time point indicators, the centred baseline imaging variable, and the interaction terms between the baseline imaging variable and time points. The following potential confounders were added separately to the models as covariates: age, gender, CSA, brain T2 lesion volume, GMF and WMF. In such models the time point coefficients estimate the change in clinical score over the relevant time period in subjects with average levels of the baseline imaging variable (because the centred imaging variable has the mean value subtracted so that it takes the value zero at its average); and the interaction terms represent the association between the baseline imaging variable and the clinical change over the relevant time period.

Associations between extent of change in imaging measures and the extent of change in clinical scores was examined using linear mixed models identical to the above except that instead of the centred baseline imaging predictor, the centred baseline to six-month change in the imaging predictor was used. In such models the time point coefficients estimate the change in clinical score over the relevant time period in subjects with average six-month change in the imaging variable; and the interaction terms represent the association between six-month change in imaging variable and the clinical score change over the relevant time period. The same potential confounders as above were added separately to models.

6.3 Results

6.3.1 Participant demographics and characteristics

Twenty patients with RRMS and 24 healthy controls were recruited. Two healthy control subjects were excluded from the study due to incidental spinal pathology identified on structural imaging. Therefore data from 20 patients and 22 healthy controls were included in the final analysis (**Table 6.1**). Due to participant drop out/ non-availability for follow-up, 18, 16 and 15 patients were scanned at 1 month, 3 months and 6 months respectively and 19, 21 and 20 controls were scanned at 1 month (mean 33, SD 7 days), 3 months (mean 95, SD 10 days) and 6 months (mean 184, SD 10 days) respectively.

Patients had a wide range of disease duration (1 to 27 years) and mild to moderate levels of disability; further details on patient characteristics, disability and conventional brain MRI are summarised in **Table 6.1**. Relapse symptoms, relapse history and disease modifying therapy

at baseline, presented patient-by-patient are summarised in **table 6.2**. Nineteen out of 20 patients were treated with three days pulsed IV Methylprednisolone prior to scanning and one patient (Patient 12, **table 6.2**), with predominantly sensory symptoms was managed conservatively.

Conventional MRI of the cervical cord identified lesions between the level of C1-3 in all patients. At baseline, cord swelling was seen in four patients and gadolinium enhancement of spinal lesions was seen in three out of 19 patients receiving contrast (**Table 6.3**). During the 6 month follow up period, five patients had a further relapse (Patients 1,2,5,9 and 15). Changes in conventional spinal MRI between baseline and 6 months in patients who completed the study are summarised in **table 6.3**.

	Healthy Controls (n = 22)	RRMS Patients (n = 20)
Mean age (SD)	43.7 (11.5) years	40.8 (9.6) years
Gender	17F: 5M	14F: 6M
Mean CSA (SD)	82.0 (8.3) mm^2	75.0 (9.4) mm^2
Mean GMF (SD)	0.48 (0.01)	0.48 (0.02)
Mean WMF (SD)	0.34 (0.01)	0.33 (0.01)
Mean T2 lesion volume (SD)		7.1 (7.0) ml
Mean brain parenchymal fraction (SD)		0.80 (0.02)
Mean disease duration (SD)		8.3 (7.5) years
Median EDSS (range)		4.5 (2.5 - 6.5)
Mean TWT (SD)		7.2 (3.4) seconds
Mean MSWS-12 (SD)		46.5 (12.3)
Mean summated MAS (SD)		7.9 (8.7)
Mean HPT (SD)		25.8 (9.5) seconds
Mean grip strength (SD)		40.1 (24.3) lbs force
Mean vibration perception threshold (SD)		14.5 (14.1)
Mean sway, 32cm, EO (SD)		1.30 (1.01) deg/s
Mean sway, 32cm, EC (SD)		2.41 (2.92) deg/s
Mean sway, 4cm, EO (SD)		2.62 (3.49) deg/s
Mean sway, 4cm, EC (SD)		4.90 (9.64) deg/s

2

3 **Table 6.1**: Demographics and clinical characteristics of patients and controls at baseline.

Patient	Age	Disease duration (years)	Relapses in past 2 years	Current DMT	Relapse symptoms	Time between symptom onset and baseline scan (days)
1	41	7	0	Glatiramer acetate	Deteriorating mobility, pain, limb weakness, falls.	29
2	37	2	3	Interferon beta-1a	Paraesthesia in all limbs, urinary urgency	30
3	30	3	2	Nil	Decreased sensation in limbs, incoordination, risk of falls.	13
4	37	3	3	Nil	Numbness below costal margin, hands, and slowed walking	19
5	57	27	0	Interferon beta-1a	Stiffness both legs and decreased dexterity hands	47
6	42	11	0	Glatiramer acetate	Bilateral leg heaviness and paraesthesia in hands	19
7	48	12	2	Interferon beta-1a	Bilateral arm and leg heaviness and pains	21
8	38	11	2	Nil	Altered sensation in legs, intermittent arm/finger shaking	16
9	46	17	5	Nil	L'hermitte, Right arm and leg weakness	14
10	63	23	2	Interferon beta-1a44mcg	Bilateral leg weakness and spasms, left hand weakness.	23
11	43	10	2	Nil	Cervical Brown-Sequard syndrome	15
12	30	1	2	Nil	Sensory symptoms below chest, l'hermitte	9
13	32	2	2	Nil	Weakness in legs and increased numbness/decreased dexterity in hands	20
14	35	3	5	Interferon beta-1a44mcg	Weakness both arms and legs – falls	8
15	45	2	3	Interferon beta-1a	Weakness right hand and bilateral leg weakness, decreased mobility	22
16	47	14	3	Glatiramer acetate	Reduced balance with leg spasms. Weak, numb hands	24
17	25	2.5	4	Glatiramer acetate	L'hermittes sign, left arm and leg numbness	27
18	28	4	0	Nil	Bilateral arm and leg weakness, decreased balance	14
19	42	1.5	4	Interferon beta-1a	Bilateral upper and lower limb sensory impairment and pain	9
20	49	9	0	Nil	L'hermittes sign, mild bilateral leg weakness	22

Table 6.2: Description of relapse symptoms, relapse history and current disease modifying therapy of individual patients at baseline.

Patient	Baseline spinal imaging	Baseline spine + GAD	Baseline brain + GAD	6 month spinal imaging
1	Cord atrophied. Large lesion at C3/4 and small lesion at C1 posteriorly. Patchy signal change at C2 anteriorly.	No enhancement	No enhancement	Didn't complete study
2	Anterior C3/4 lesion with local swelling and patchy signal change at C4-6.	No enhancement	No enhancement	Patchy signal change C4-6
3	Posterior C1/2 lesion and patchy C3-5 change	No enhancement	No enhancement	Incomplete resolution of C1/2 lesion. Patchy signal unchanged
4	Posterior C3 and C4 lesions with mild swelling. Patchy change at C5-6 posteriorly.	Enhancing C3 lesion	No enhancement	Posterior C3-4 lesions, confluent signal change C3-5
5	Predominantly posterior lesion at C2. Patchy signal change at C3/4.	No enhancement	No enhancement	Unchanged
6	Posterior C3 and C6 lesions and anterior C3/4 lesion.	No enhancement	Enhancing lesion supraventricular WM (left).	Didn't complete study
7	C2 lesion, patchy C3-4 signal change.	Enhancing C2 lesion.	No enhancement	Some regression of C2 lesion, otherwise unchanged.
8	Posterior C2/3 lesion	No enhancement	No enhancement	Radiological resolution
9	Lesions C2 and C3 anteriorly.	No enhancement	No enhancement	Patchy signal C2-3 with remnant of C2 and C3 lesions.
10				
11	Large flame lesion C2/3, swollen cord.	Enhancing C2/3 lesion	Enhancing lesion in left centrum semi-ovale	Small residual signal abnormality at C2.
12	Posterior C3 lesion	No enhancement	No enhancement	Unchanged
13	Posterior lesion at C1 with patchy signal change C2-4.	No enhancement	No enhancement	Patchy signal C2-4, partial resolution of C1 lesion.
14	Lesion at C1/2.	No enhancement	No enhancement	Unchanged
15	Anterior C2 lesion	No enhancement	No enhancement	Unchanged
16	Posterior C2, C4 lesions	No enhancement	No enhancement	Unchanged
17	Large posterior lesion C2-3.	No enhancement	No enhancement	Didn't complete study
18	Posterior lesions at C3, C4/5 and C5/6.	No enhancement	No enhancement	Didn't complete study
19	Posterior C2 lesion	No enhancement	No enhancement	Unchanged
20	Anterior C3 and posterior C2 lesions	Contrast not given (patient withheld consent)		Didn't complete study

Table 6.3: Summary of conventional brain and cervical cord imaging in all patients at baseline and 6 months.

6.3.2 Differences in spinal cord measures between patients and controls over the six month follow-up period

Reported differences in spinal cord measures between groups are corrected for age, gender and CSA at all 4 time points. Differences in CSA were corrected for age and gender only.

Patients had lower CSA at baseline and showed a significant decrease in CSA over 6 months (**Table 6.4**). Patients had lower spinal tNAA at baseline, 1 month and 6 months (but not 3 months) compared to controls (**Figure 6.2 and Table 6.5**). Patients had significantly higher spinal Glx concentrations than controls at baseline, but concentrations begin to normalise by 1 month (**Table 6.5**). On the diffusion measures, patients had significantly higher perpendicular diffusivity (reflected by increased ADCxy and FWHMxy and reduced P0xy) in the whole cord and the anterior, posterior and lateral columns, compared with controls at baseline. Perpendicular diffusivity remained higher in patients at each time point, reaching statistical significance in the whole cord and anterior column at 1 month, anterior, posterior and lateral columns at 3 months and all regions of interest at 6 months (**Tables 6.6, 6.7, 6.8 and 6.9**).

Time Point (months)	Healthy Controls	RRMS Patients	Adjusted difference (95% CI)	P-value
0	82.02 (8.30)	75.01 (9.40)	-7.0087 (-12.36, -1.65)	**0.010**
1	82.14 (8.35)	75.51 (9.45)	-7.3110 (-12.62, -2.01)	**0.007**
3	81.94 (8.42)	75.53 (8.42)	-7.5467 (-12.79, -2.31)	**0.005**
6	81.97 (8.73)	75.18 (7.41)	-9.0139 (-14.20, -3.83)	**0.001**

Table 6.4: Summary of mean (SD) mean cord cross sectional area (mm^2) from the cervical cord of patients and controls over 6 months and P-values for adjusted group comparisons after correcting for age and gender.

Metabolite	Time Point (months)	Healthy Controls	RRMS Patients	Adjusted difference (95% CI)	P-value
tNAA	0	4.96 (1.62)	3.32 (1.90)	-1.3033 (-2.21, -0.40)	**0.005**
	1	5.22 (1.47)	4.09 (0.91)	-1.2075 (-2.20, -0.21)	**0.017**
	3	4.87 (1.01)	4.01 (1.88)	-0.6802 (-1.68, 0.32)	0.181
	6	5.74 (1.56)	4.00 (1.03)	-1.8037 (-2.77, -0.83)	**<0.001**
tCho	0	1.25 (0.46)	1.21 (0.34)	-0.0604 (-0.33, 0.21)	0.664
	1	1.33 (0.32)	1.13 (0.37)	-0.1771 (-0.46, 0.10)	0.213
	3	1.14 (0.28)	1.53 (0.55)	0.3226 (0.06, 0.59)	**0.017**
	6	1.33 (0.27)	1.09 (0.18)	-0.2254 (-0.45, 0.00)	0.054
tCr	0	3.70 (1.23)	3.43 (0.94)	-0.3177 (-1.03, 0.40)	0.384
	1	3.69 (1.25)	3.41 (0.69)	-0.1314 (-0.94, 0.68)	0.751
	3	3.42 (1.12)	3.86 (1.57)	0.5941 (-0.26, 1.45)	0.174
	6	4.28 (1.00)	3.24 (1.19)	-1.0770 (-1.94, -0.21)	**0.014**
Ins	0	4.63 (1.64)	4.97 (1.72)	0.2872 (-1.15, 1.73)	0.696
	1	4.48 (1.64)	5.00 (1.94)	0.5282 (-1.14, 2.19)	0.534
	3	5.12 (2.41)	6.87 (3.65)	2.3203 (0.70, 3.94)	**0.005**
	6	5.42 (1.19)	5.93 (2.13)	0.4520 (-1.16, 2.07)	0.583
Glx	0	5.10 (2.18)	7.60 (3.71)	2.534 (0.04, 5.03)	**0.047**
	1	6.50 (1.96)	8.10 (3.58)	1.8812 (-0.68, 4.44)	0.149
	3	6.46 (2.58)	6.58 (3.23)	-0.0232 (-2.18, 2.14)	0.983
	6	7.05 (2.62)	6.94 (3.08)	-0.1202 (-2.32, 2.08)	0.915

Table 6.5: Summary of mean (SD) metabolite concentrations (mmol/L) from the cervical cord of patients and controls over the 6 month follow up and p-values for adjusted group comparisons after correcting for age, gender and mean cord area.
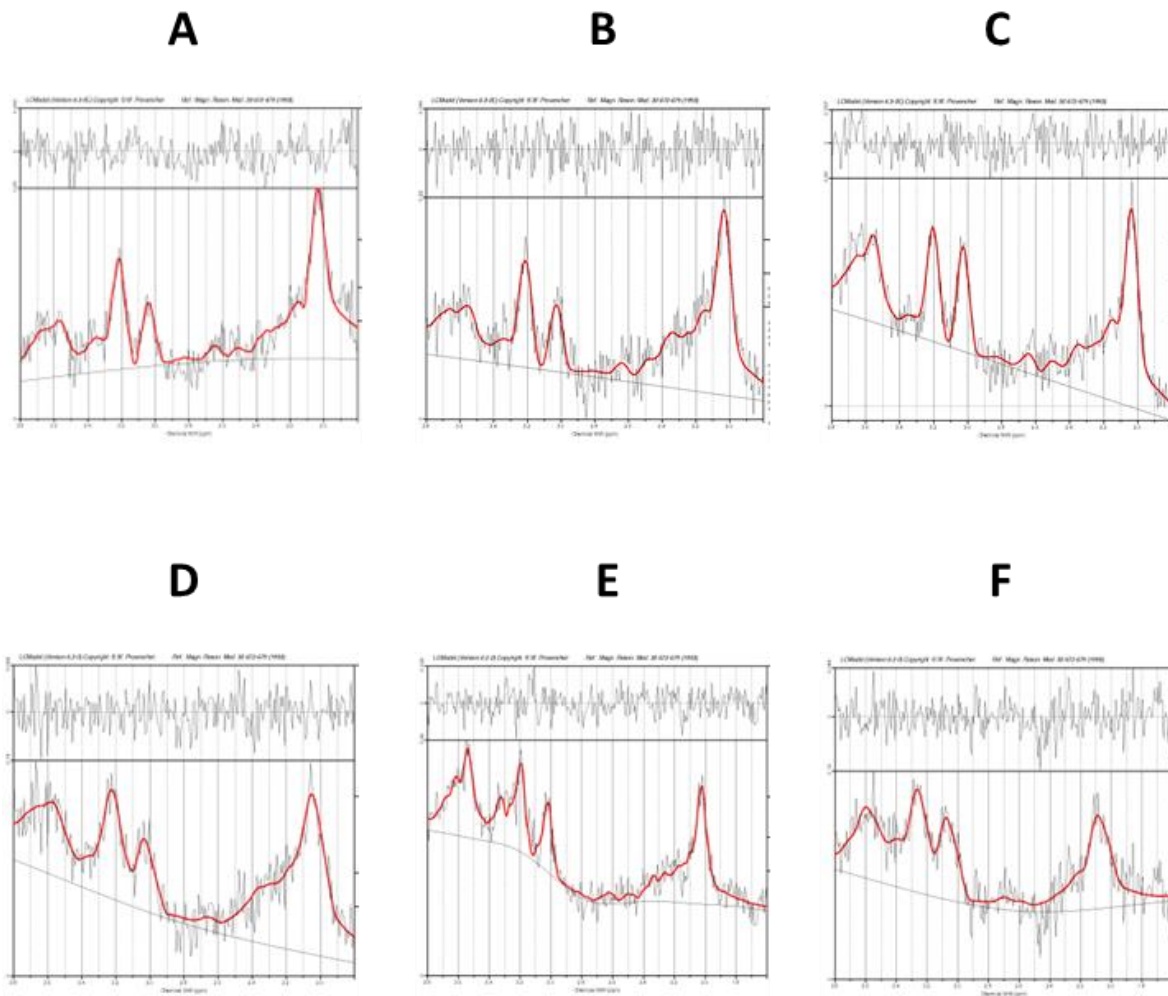
Figure 6.2: Exemplary post-processed spectra from three healthy controls (A-C) and three patients (D-F) acquired at baseline showing reduced tNAA in patients compared to controls.

Changes in whole cord QSI indices over 6 months

QSI Index	Time Point (months)	Healthy Controls	RRMS Patients	Adjusted difference (95% CI)	P-value
ADCxy	0	0.373 (0.05)	0.532 (0.22)	0.1615 (0.08, 0.24)	**<0.001**
	1	0.397 (0.09)	0.435 (0.09)	0.0305 (-0.05, 0.11)	0.462
	3	0.398 (0.11)	0.456 (0.12)	0.0357 (-0.05, 0.12)	0.424
	6	0.388 (0.08)	0.500 (0.20)	0.0998 (0.01, 0.19)	**0.026**
FWHMxy	0	0.235 (0.02)	0.275 (0.03)	0.0409 (0.02, 0.06)	**<0.001**
	1	0.240 (0.02)	0.261 (0.03)	0.01922 (0.00, 0.04)	**0.030**
	3	0.242 (0.03)	0.263 (0.03)	0.0172 (-0.00, 0.04)	0.071
	6	0.237 (0.02)	0.270 (0.04)	0.0327 (0.014, 0.05)	**<0.001**
P0xy	0	0.204 (0.02)	0.173 (0.02)	-0.0308 (-0.04, -0.02)	**<0.001**
	1	0.200 (0.02)	0.184 (0.02)	-0.0135 (-0.03, -0.00)	**0.049**
	3	0.199 (0.03)	0.183 (0.02)	-0.0133 (-0.03, -0.00)	0.070
	6	0.202 (0.02)	0.178 (0.03)	-0.0238 (-0.04, -0.01)	**0.002**
ADCz	0	1.761 (0.08)	1.773 (0.11)	0.0079 (-0.06, 0.07)	0.811
	1	1.760 (0.08)	1.773 (0.11)	-0.0801 (-0.15, -0.01)	**0.030**
	3	1.749 (0.09)	1.751 (0.08)	-0.0090 (-0.10, 0.08)	0.842
	6	1.743 (0.07)	1.827 (0.32)	0.0830 (-0.04, 0.20)	0.173
FWHMz	0	0.547 (0.03)	0.548 (0.02)	0.0020 (-0.01, 0.02)	0.806
	1	0.556 (0.03)	0.547 (0.04)	-0.0084 (-0.03, 0.01)	0.349
	3	0.546 (0.02)	0.549 (0.04)	0.0026 (-0.02, 0.23)	0.802
	6	0.544 (0.03)	0.564 (0.06)	0.0241(-0.00, 0.05)	0.062
P0z	0	0.114 (0.003)	0.115 (0.01)	0.0008 (-0.00, 0.00)	0.602
	1	0.113 (0.01)	0.115(0.01)	0.0017 (-0.00, 0.01)	0.281
	3	0.114 (0.004)	0.114 (0.004)	0.0000 (-0.00, 0.00)	0.995
	6	0.115 (0.004)	0.114(0.01)	-0.0010 (-0.01, 0.00)	0.597

Table 6.6: Summary of mean (SD) diffusivity from the cervical cord of patients and controls over the 6 month follow up period and P-values for adjusted group comparisons after correcting for age and gender.

Changes in anterior column QSI indices over 6 months

QSI Index	Time Point (months)	Healthy Controls	RRMS Patients	Adjusted difference (95% CI)	P-value
ADCxy	0	0.364 (0.11)	0.620 (0.25)	0.2681 (0.17, 0.37)	**<0.001**
	1	0.452 (0.11)	0.581 (0.18)	0.1354 (0.03, 0.24)	**0.010**
	3	0.444 (0.12)	0.486 (0.15)	0.0468 (-0.06, 0.15)	0.392
	6	0.445 (0.11)	0.605 (0.24)	0.1736 (0.07, 0.27)	**0.001**
FWHMxy	0	0.227 (0.02)	0.281 (0.03)	0.0558 (0.04, 0.07)	**<0.001**
	1	0.241 (0.02)	0.272 (0.04)	0.0320 (0.01, 0.05)	**0.001**
	3	0.240 (0.03)	0.262 (0.03)	0.0226 (0.00, 0.04)	**0.024**
	6	0.238 (0.02)	0.276 (0.04)	0.0435 (0.02, 0.06)	**<0.001**
P0xy	0	0.211 (0.02)	0.167 (0.02)	-0.0454 (-0.06, -0.03)	**<0.001**
	1	0.197 (0.02)	0.176 (0.03)	-0.0234 (-0.04, -0.01)	**0.003**
	3	0.201 (0.03)	0.185 (0.03)	-0.0180 (-0.04, -0.00)	**0.037**
	6	0.202 (0.02)	0.171 (0.03)	-0.0360 (-0.05, -0.02)	**<0.001**
ADCz	0	1.820 (0.14)	1.866 (0.21)	0.0468 (-.076, 0.17)	0.457
	1	1.793 (0.12)	1.939 (0.23)	-0.0209 (-0.15, 0.10)	0.741
	3	1.960 (0.13)	1.885 (0.12)	-0.0806 (-0.21, 0.05)	0.215
	6	1.979 (0.12)	2.107 (0.37)	0.1196 (-0.02, 0.26)	0.096
FWHMz	0	0.553 (0.04)	0.547 (0.03)	-0.0043 (-0.02, 0.18)	0.699
	1	0.575 (0.03)	0.557 (0.05)	-0.0166 (-0.04, 0.01)	0.159
	3	0.565 (0.03)	0.561 (0.05)	-0.0033 (-0.03, 0.02)	0.797
	6	0.568 (0.04)	0.582 (0.07)	0.0177 (-0.01, 0.05)	0.267
P0z	0	0.113 (0.01)	0.114 (0.01)	0.0013 (-0.00, 0.01)	0.514
	1	0.109 (0.01)	0.111 (0.01)	0.0018 (-0.00, 0.01)	0.396
	3	0.110 (0.004)	0.112 (0.01)	0.0024 (-0.00, 0.01)	0.267
	6	0.109 (0.003)	0.109 (0.01)	-0.0009 (-0.00, 0.00)	0.635

Table 6.7: Summary of mean (SD) diffusivity from the anterior column of patients and controls over the 6 month follow up period and P-values for adjusted group comparisons after correcting for age and gender.

Changes in posterior column QSI indices over 6 months

QSI Index	Time Point (months)	Healthy Controls	RRMS Patients	Adjusted difference (95% CI)	P-value
ADCxy	0	0.361 (0.08)	0.528 (0.24)	0.1722 (0.09, 0.26)	**<0.001**
	1	0.388 (0.10)	0.439 (0.12)	0.0480 (-0.04, 0.14)	0.288
	3	0.400 (0.11)	0.466 (0.15)	0.0475 (-0.04, 0.14)	0.314
	6	0.397 (0.10)	0.488 (0.19)	0.0771 (-0.01, 0.17)	0.091
FWHMxy	0	0.228 (0.03)	0.278 (0.05)	0.0474 (0.02, 0.07)	**<0.001**
	1	0.235 (0.03)	0.260 (0.04)	0.0209 (-0.00, 0.05)	0.103
	3	0.235 (0.03)	0.264 (0.04)	0.0218 (-0.00, 0.04)	0.092
	6	0.230 (0.03)	0.266 (0.05)	0.0299 (0.01, 0.05)	**0.016**
P0xy	0	0.208 (0.02)	0.176 (0.04)	-0.0301 (-0.05, -0.01)	**0.001**
	1	0.202 (0.02)	0.186 (0.03)	-0.0110 (-0.03, 0.01)	0.258
	3	0.202 (0.03)	0.183 (0.03)	-0.0133 (-0.03, 0.01)	**0.019**
	6	0.206 (0.03)	0.182 (0.03)	-0.0200 (-0.04, 0.00)	**0.054**
ADCz	0	2.076 (0.13)	2.039 (0.16)	-0.0472 (-0.13, 0.05)	0.372
	1	2.112 (0.15)	2.041 (0.16)	-0.0708 (-0.17, 0.03)	0.177
	3	2.051 (0.11)	2.020 (0.11)	-0.0406 (-0.17, 0.09)	0.584
	6	2.048 (0.09)	2.120 (0.50)	0.0775 (-0.11, 0.27)	0.418
FWHMz	0	0.601 (0.04)	0.602 (0.03)	0.0010 (-0.02, 0.02)	0.923
	1	0.609 (0.03)	0.599 (0.05)	0.0080 (-0.03, 0.02)	0.506
	3	0.596 (0.03)	0.589 (0.06)	-0.0099 (-0.04, 0.02)	0.487
	6	0.593 (0.04)	0.612 (0.08)	0.0218 (-0.01, 0.06)	0.203
P0z	0	0.104 (0.004)	0.105 (0.01)	0.0018 (-0.00, 0.00)	0.235
	1	0.103 (0.01)	0.105 (0.01)	0.0013 (-0.00, 0.00)	0.409
	3	0.103 (0.003)	0.106 (0.01)	0.0021 (-0.00, 0.01)	0.242
	6	0.105 (0.003)	0.105 (0.01)	0.0003 (-0.00, 0.00)	0.869

Table 6.8: Summary of mean (SD) diffusivity from the posterior column of patients and controls over the 6 month follow up period with P-values for adjusted group comparisons after correcting for age and gender.

Changes in lateral column QSI indices over 6 months

QSI Index	Time Point (months)	Healthy Controls	RRMS Patients	Adjusted difference (95% CI)	P-value
ADCxy	0	0.317 (0.06)	0.502 (0.23)	0.1872 (0.11, 0.27)	**<0.001**
	1	0.328 (0.10)	0.395 (0.09)	0.0589 (-0.02, 0.14)	0.161
	3	0.350 (0.11)	0.424 (0.12)	0.0497 (-0.04, 0.13)	0.261
	6	0.324 (0.08)	0.440 (0.17)	0.1066 (0.02, 0.19)	**0.013**
FWHMxy	0	0.215 (0.02)	0.265 (0.04)	0.0509 (0.03, 0.07)	**<0.001**
	1	0.218 (0.02)	0.245 (0.03)	0.0251 (0.004, 0.05)	**0.018**
	3	0.222 (0.03)	0.249 (0.04)	0.0230 (-0.001,0.05)	**0.056**
	6	0.203 (0.05)	0.255 (0.04)	0.0529 (0.03, 0.08)	**<0.001**
P0xy	0	0.221 (0.02)	0.180 (0.03)	-0.0413 (-0.06, -0.02)	**<0.001**
	1	0.214 (0.04)	0.196 (0.03)	-0.0165 (-0.03, 0.00)	0.069
	3	0.216 (0.03)	0.193 (0.03)	-0.0195 (-0.04, -0.00)	**0.045**
	6	0.223 (0.02)	0.190 (0.03)	-0.0331 (-0.05, -0.01)	**0.001**
ADCz	0	1.948 (0.11)	1.817 (0.45)	-0.1344 (-0.31, 0.04)	0.127
	1	2.012 (0.13)	1.772 (0.47)	-0.2409 (-0.42, -0.06)	**0.009**
	3	1.941 (0.08)	1.921 (0.13)	-0.0375 (-0.23, 0.15)	0.695
	6	1.975 (0.10)	2.012 (0.38)	0.0884 (-0.14, 0.21)	0.690
FWHMz	0	0.571 (0.03)	0.541 (0.13)	-1.344 (-0.31, 0.04)	0.127
	1	0.587 (0.03)	0.541 (0.15)	-0.2409 (-0.42, -0.06)	**0.009**
	3	0.574 (0.03)	0.572 (0.05)	-0.0375 (-0.23, 0.15)	0.695
	6	0.577 (0.04)	0.598 (0.08)	0.03524 (-0.14, 0.21)	0.690
P0z	0	0.107 (0.00)	0.104 (0.03)	-0.0031 (-0.01, 0.01)	0.511
	1	0.106 (0.00)	0.102 (0.03)	-0.0039 (-0.01,0.01)	0.416
	3	0.107 (0.00)	0.108 (0.01)	0.0003 (-0.01, 0.01)	0.935
	6	0.106 (0.00)	0.108 (0.01)	0.0011 (-0.01, 0.01)	0.782

Table 6.9: Summary of mean (SD) diffusivity from the lateral columns of patients and controls over the 6 month follow up period and P-values for adjusted group comparisons after correcting for age and gender.

6.3.3 Assessment of acute disability with spinal QSI and MRS

The regression models used in this section were all adjusted for age, gender, CSA, brain T2 lesion volume, GMF and WMF.

6.3.3.1 Associations between whole cord imaging measures and disability at baseline

In patients, higher tCr and Glx concentrations were independently associated with increased disability at baseline. Higher spinal Glx concentrations were associated with increased postural instability, and higher spinal tCr were associated with increased EDSS and slower completion of the timed walk test (**Table 6.10**).

Clinical Score	Spinal Cord Measure	Regression Coefficient	95 % Confidence Interval	P-value
EDSS	tCr	0.83	0.16, 1.50	**P = 0.019**
1/TWT	tCr	-0.05	-0.08, -0.02	**P = 0.006**
Sway 4EO	Glx	0.40	0.23, 0.57	**P = 0.003**
Sway 32EO	Glx	0.21	0.14, 0.29	**P = 0.002**
Sway 32EC	Glx	0.32	0.13, 0.52	**P = 0.010**
Pitch 4EO	Glx	0.40	0.23, 0.57	**P = 0.003**
Pitch 4EC	Glx	0.30	0.11, 0.50	**P = 0.010**
Pitch 32 EO	Glx	0.17	0.11, 0.24	**P = 0.002**
Pitch 32EC	Glx	0.25	0.13, 0.37	**P = 0.005**
Roll 4EO	Glx	0.21	0.11, 0.30	**P = 0.005**

Table 6.10: Associations between whole cord measures (predictors) and clinical scores (response variables). Unstandardised regression coefficients for imaging measures are reported with 95% confidence intervals and p-values. The regression models were adjusted for age, gender, CSA, brain T2 lesion volume, GMF and WMF.

6.3.3.2 Associations between column-specific QSI indices and disability at baseline

Increased perpendicular and parallel diffusivity within the anterior and posterior spinal columns was associated with increased disability. Specifically, increased parallel diffusivity (increased FWHMz and ADCz) in the anterior column was independently associated with higher EDSS, MSWS and TWT. Increased perpendicular diffusivity (higher FWHMxy and lower P0xy) in the anterior column was associated with higher MSWS. Increased parallel diffusivity (increased ADCz and FWHMz) in the posterior column predicted longer timed walk. A summary of these associations is presented in **Table 6.11**.

Region of interest	QSI index	EDSS (Coefficient; CI)	1/TWT (Coefficient; CI)	MSWS (Coefficient; CI)
Anterior Column	**FWHMxy**			**P = 0.026** 189.38 (25.34, 353.42)
	P0xy			**P = 0.023** -269.82 (-497.22, -42.41)
	ADCz	**P < 0.001** 4.95 (2.78, 7.12)	**P = 0.011** -0.19 (-0.33, -0.05)	**P = 0.018** 32.70 (6.23, 59.18)
	FWHMz	**P = 0.024** 20.88 (3.15, 38.60)	**P = 0.001** -1.44 (-2.20, -0.68)	**P = 0.006** 234.29 (80.87, 387.59)
	P0z			**P = 0.016** -784.73 (-1394.92,-174.53)
Posterior Column	**ADCz**		**P = 0.022** -0.23 (-0.41, -0.04)	
	FWHMz		**P = 0.035** -1.27 (-2.44, -0.10)	

Table 6.11: Associations between column-specific measures (predictors) and clinical scores (response variables). Unstandardised regression coefficients for imaging measures are reported with 95% confidence intervals and p-values. The regression models were adjusted for age, gender, CSA, brain T2 lesion volume, GMF and WMF.

6.3.4 Assessing mechanisms of spinal neurodegeneration and repair

6.3.4.1 Evolution of imaging changes in improvers on EDSS versus non-improvers

After correcting for age and gender, spinal tNAA concentrations were significantly lower in improvers and borderline significantly lower in non-improvers when compared with controls at baseline. By 6 months, tNAA had normalised in improvers but remains low in non-improvers. In non-improvers, spinal Glx concentrations are elevated at baseline compared to controls, then normalise by 1 month, whereas no significant difference in Glx concentration between improvers and controls was observed (**Table 6.12 and Figure 6.3**). A significant rise in tCho was observed in non-improvers at 3 months and a significant fall in tCr was seen in improvers at 6 months (**Table 6.12**).

After correcting for age and gender, perpendicular diffusivity was significantly higher than controls in both improvers and non-improvers at baseline. By month 1, QSI indices of perpendicular diffusivity, normalise in improvers and remain normal at 6 months, however in non-improvers, perpendicular diffusivity remains higher than controls at 6 months (**Table 6.13 and Figures 6.4 and 6.5**). When examining changes in parallel diffusivity in the two groups, parallel diffusivity remains normal in improvers and non-improvers between baseline and 3 months but by 6 months, there is a significant increase in FWHMz and borderline significant (P=0.086) decrease in P0z in non-improvers compared to controls (**Table 6.13 and Figures 6.4 and 6.6**).

Metabolite	Time Point	Healthy Controls	Improvers	P-value	Non-improvers	P-value
tNAA	0	4.96 (1.62)	3.23 (1.02)	**0.024**	3.39 (1.42)	0.089
	1	5.22 (1.47)	3.91 (0.97)	**0.046**	4.32 (0.84)	0.239
	3	4.87 (1.01)	4.34 (2.63)	0.535	3.73 (1.06)	**0.028**
	6	5.74 (1.56)	4.38 (2.63)	0.090	3.76 (0.95)	**0.003**
tCho	0	1.25 (0.46)	1.18 (0.29)	0.759	1.24 (0.40)	0.953
	1	1.33 (0.32)	1.04 (0.28)	0.063	1.29 (0.46)	0.973
	3	1.14 (0.28)	1.58 (0.88)	0.080	1.51 (0.44)	**0.026**
	6	1.33 (0.27)	1.05 (0.22)	0.077	1.12 (0.16)	0.081
tCr	0	3.70 (1.23)	3.23 (0.97)	0.350	3.65 (0.90)	0.991
	1	3.69 (1.25)	3.38 (0.40)	0.302	3.46 (0.98)	0.814
	3	3.42 (1.12)	3.27 (2.27)	0.946	4.21 (1.06)	0.137
	6	4.28 (1.00)	2.73 (0.99)	**0.011**	3.67 (1.26)	0.257
Ins	0	4.63 (1.64)	4.61 (1.07)	0.764	5.32 (2.22)	0.359
	1	4.48 (1.64)	5.41 (2.32)	0.322	4.50 (1.46)	0.869
	3	5.12 (2.41)	7.16 (5.57)	0.181	6.66 (1.90)	0.141
	6	5.42 (1.19)	5.66 (1.71)	0.735	6.12 (2.51)	0.382
Glx	0	5.10 (2.18)	5.68 (1.59)	0.650	10.47 (4.34)	**0.005**
	1	6.50 (1.96)	8.28 (4.05)	0.267	7.88 (3.49)	0.445
	3	6.46 (2.58)	7.59 (2.29)	0.438	6.24 (3.61)	0.845
	6	7.05 (2.62)	8.01 (3.92)	0.582	5.61 (0.72)	0.278

Table 6.12: Summary of mean (SD) metabolite concentrations (mmol/l) from controls, 'improvers' and 'non-improvers' over the follow up period with P-values for adjusted group comparisons after correcting for age and gender.
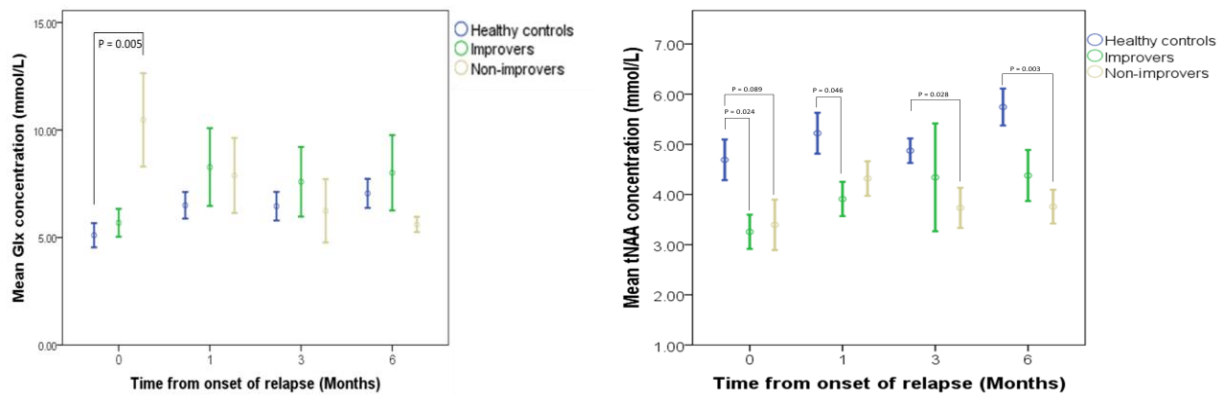
Figure 6.3: Graphs showing evolution of spinal Glx (left) and tNAA concentrations (right) over 6 months in 'improvers' (EDSS change over 6 months of $\leq$ -0.5) and 'non-improvers' (EDSS change over 6 months $\geq$ 0) compared with controls.

QSI Index	Time Point	Healthy Controls (n = 22)	Improvers (n = 10)	P-value	Non-improvers (n = 10)	P-value
FWHMxy	0	0.235 (0.02)	0.269 (0.03)	**<0.001**	0.282 (0.04)	**<0.001**
	1	0.240 (0.02)	0.256 (0.02)	0.097	0.265 (0.03)	**0.016**
	3	0.242 (0.03)	0.256 (0.03)	0.171	0.268 (0.04)	0.071
	6	0.237 (0.02)	0.246 (0.01)	0.059	0.291 (0.05)	**<0.001**
P0xy	0	0.204 (0.02)	0.176 (0.02)	**0.001**	0.170 (0.03)	**<0.001**
	1	0.200 (0.02)	0.187 (0.02)	0.170	0.182 (0.02)	**0.047**
	3	0.199 (0.03)	0.187 (0.02)	0.158	0.180 (0.03)	0.098
	6	0.202 (0.02)	0.194 (0.01)	0.144	0.164 (0.03)	**0.001**
FWHMz	0	0.547 (0.03)	0.548 (0.03)	0.802	0549 (0.02)	0.908
	1	0.556 (0.03)	0.538 (0.04)	0.122	0.553 (0.04)	0.927
	3	0.546 (0.02)	0.552 (0.04)	0.531	0.546 (0.04)	0.207
	6	0.544 (0.03)	0.543 (0.05)	0.969	0.582 (0.07)	**0.049**
P0z	0	0.114 (0.003)	0.114 (0.004)	0.910	0.115 (0.01)	0.411
	1	0.113 (0.01)	0.115 (0.01)	0.239	0.114 (0.01)	0.712
	3	0.114 (0.004)	0.114 (0.01)	0.840	0.114 (0.003)	0.966
	6	0.115 (0.004)	0.118 (0.01)	0.225	0.110 (0.01)	0.086

Table 6.13: Summary of mean (SD) of whole cord QSI indices from controls, 'improvers' and 'non-improvers' over the follow up period with P-values for adjusted group comparisons after correcting for age and gender.
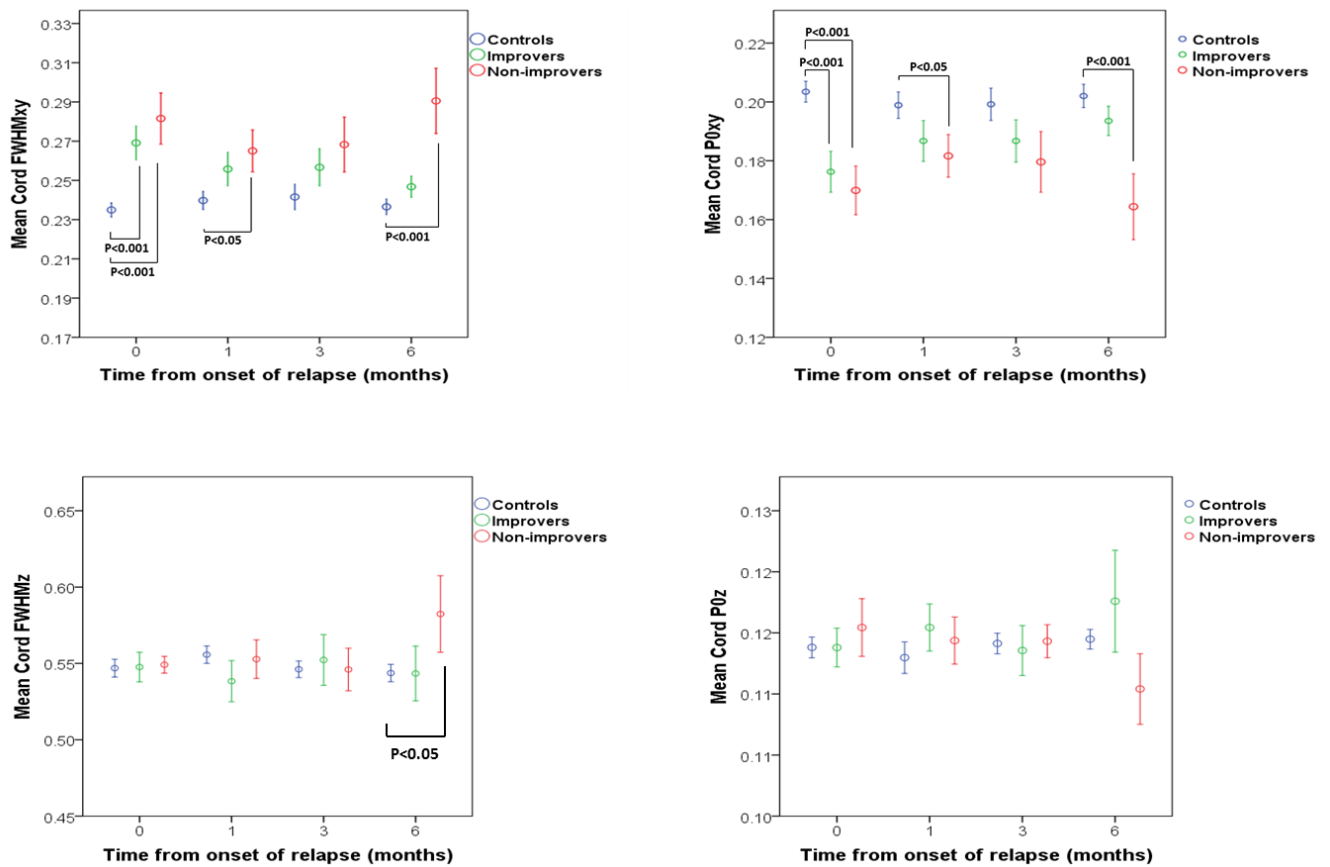
Figure 6.4: Graphs showing evolution of mean whole cord FWHMxy (top left), P0xy (top right), FWHMz (bottom left) and P0z (bottom right) over 6 months in 'improvers' (EDSS change over 6 months of ≤ -0.5) and 'non-improvers' (EDSS change over 6 months ≥ 0) compared with controls (Error bars +/- 1 SE).
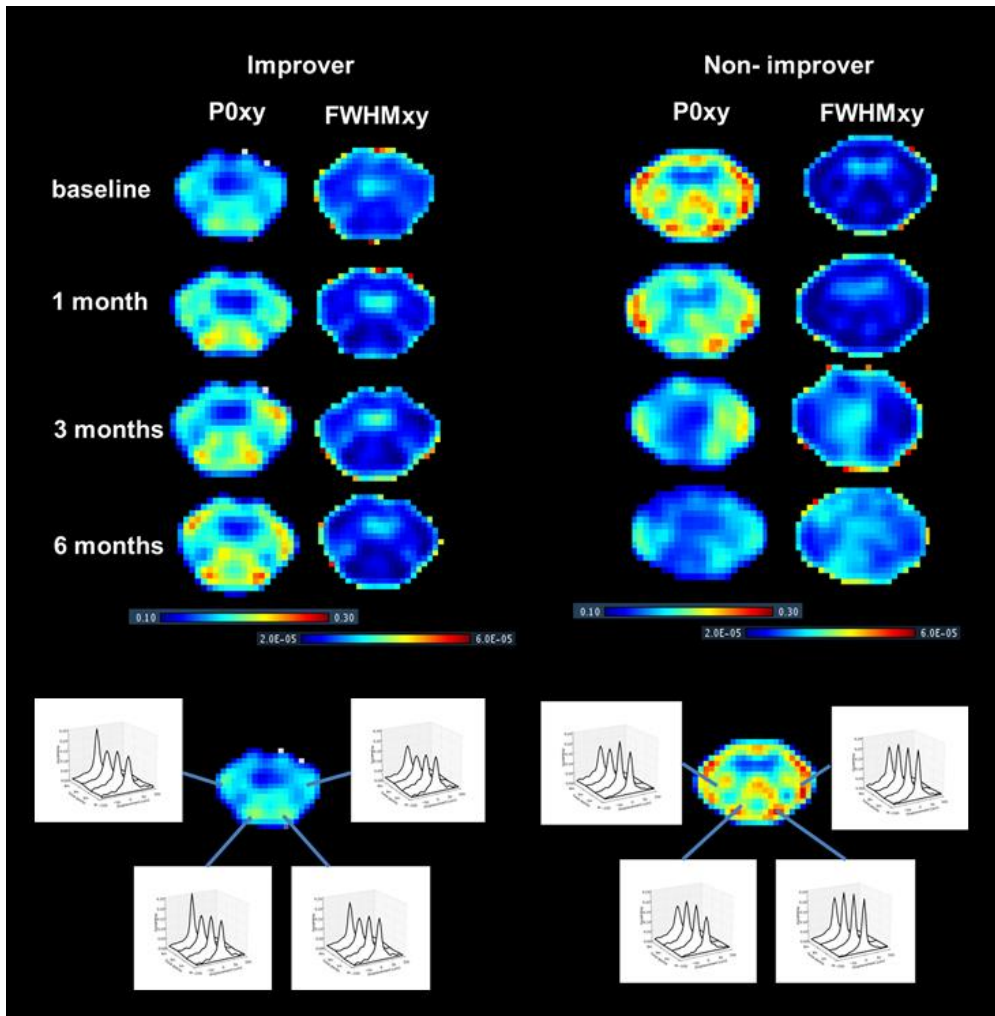
Figure 6.5: QSI maps and dPDF's showing longitudinal change in perpendicular diffusivity between an improver and non-improver. In the improver (left), perpendicular diffusivity restricts over 6 months, reflected by increasing P0xy and decreasing FWHMxy as seen in the QSI maps and dPDF. In the non-improver, there is increased perpendicular diffusion over 6 months, reflected by decreasing P0xy and increasing FWHMxy with shortening and broadening of the dPDF.
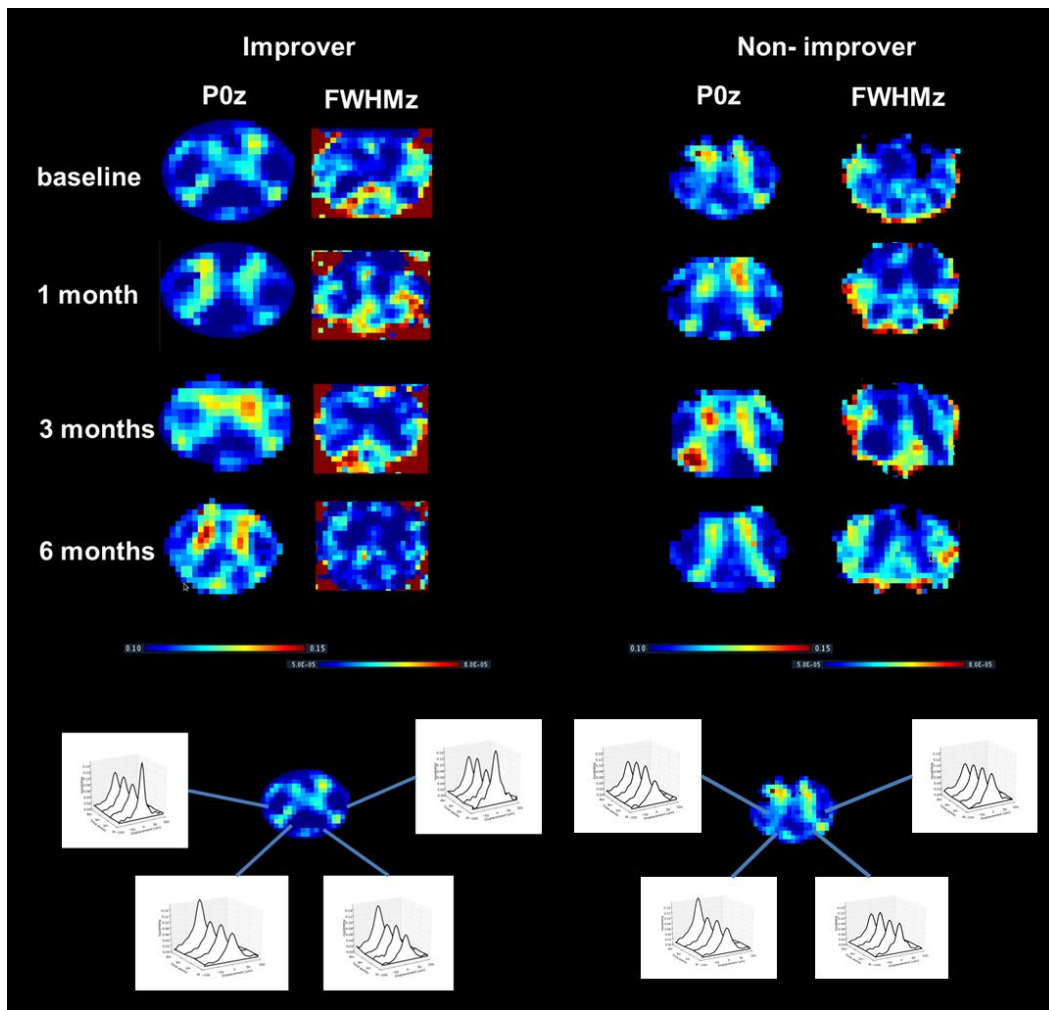
Figure 6.6: QSI maps and dPDF's showing longitudinal change in parallel diffusivity between an improver and non-improver. In the improver (left), parallel diffusivity restricts in the posterior columns over 6 months, reflected by increasing P0z and decreasing FWHMz as seen in the QSI maps and dPDF. In the non-improver, there is no restriction of diffusion over 6 months.

6.3.4.2 Evolution of imaging changes in patients with and without MRI confirmation of acute spinal cord relapse.

In patients with definite MRI evolution, consistent with spinal cord relapse, after correcting for age and gender, spinal tNAA concentrations are low throughout the follow up period and do not recover (**Table 6.14**). In this same group of patients, Glx concentrations appeared similar to controls throughout the follow up period.

In patients without clear evidence on MRI of either acute cord changes (swelling or GAD enhancement) or lesion resolution over six months, tNAA concentrations remained similar to controls despite the presence of a spinal lesion within the region of interest (**Table 6.14**). In this group Glx concentrations were higher than controls but this difference was only statistically significant at 1 month follow up.

After correcting for age and gender, perpendicular diffusivity was significantly higher in patients with definite MRI evolution throughout the follow up period but was not significantly different to controls in the group without MRI changes (**Table 6.15**).

Metabolite	Time Point	Healthy Controls (n = 22)	MRI evidence (n= 8)	P-value	No MRI evidence (n=6)	P-value
tNAA	0	4.96 (1.62)	3.06 (1.02)	0.069	4.17 (1.82)	0.725
	1	5.22 (1.47)	3.81 (0.58)	**0.014**	4.37 (0.49)	0.096
	3	4.87 (1.01)	3.17 (1.14)	**0.002**	6.05 (2.66)	0.745
	6	5.74 (1.56)	3.72 (1.16)	**0.011**	4.54 (0.70)	0.081
tCho	0	1.25 (0.46)	1.10 (0.13)	0.537	1.35 (0.66)	0.524
	1	1.33 (0.32)	1.10 (0.48)	0.346	1.19 (0.14)	0.374
	3	1.14 (0.28)	1.36 (0.44)	0.268	1.70 (0.88)	0.092
	6	1.33 (0.27)	1.10 (0.19)	0.205	1.04 (0.19)	0.128
tCr	0	3.70 (1.23)	2.89 (0.66)	0.216	3.69 (1.41)	0.888
	1	3.69 (1.25)	3.41 (0.76)	0.456	3.74 (0.94)	0.884
	3	3.42 (1.12)	3.09 (1.26)	0.602	5.56 (0.97)	0.104
	6	4.28 (1.00)	3.05 (1.01)	**0.012**	3.00 (1.29)	0.068
Ins	0	4.63 (1.64)	4.27 (1.13)	0.902	5.94 (0.26)	0.280
	1	4.48 (1.64)	5.15 (1.21)	0.199	5.59 (3.55)	0.244
	3	5.12 (2.41)	5.57 (2.70)	0.702	12.02 (5.22)	0.062
	6	5.42 (1.19)	5.70 (2.27)	0.296	6.61 (2.52)	0.176
Glx	0	5.10 (2.18)	5.63 (1.02)	0.625	9.39 (5.90)	0.060
	1	6.50 (1.96)	6.91 (3.68)	0.475	11.87 (1.07)	**0.040**
	3	6.46 (2.58)	4.80 (2.24)	0.145	10.93 (2.44)	0.424
	6	7.05 (2.62)	5.91 (2.67)	0.781	8.99 (3.24)	0.615

Table 6.14: Summary of mean (SD) metabolite concentrations (mmol/L) from controls and patients with and without MRI evidence of acute spinal relapse. P-values for adjusted group comparisons after correcting for age and gender.

QSI Index	Time Point	Healthy Controls (n = 22)	MRI evidence (n= 8)	P-value	No MRI evidence (n=6)	P-value
FWHMxy	0	0.235 (0.02)	0.283 (0.02)	**<0.001**	0.256 (0.03)	0.061
	1	0.240 (0.02)	0.267 (0.03)	**0.016**	0.241 (0.02)	0.553
	3	0.242 (0.03)	0.269 (0.03)	**0.033**	0.238 (0.02)	0.736
	6	0.237 (0.02)	0.278 (0.03)	**<0.001**	0.238 (0.02)	0.227
P0xy	0	0.204 (0.02)	0.166 (0.02)	**<0.001**	0.185 (0.02)	0.070
	1	0.200 (0.02)	0.179 (0.02)	**0.038**	0.198 (0.02)	0.657
	3	0.199 (0.03)	0.177 (0.02)	**0.030**	0.201 (0.02)	0.761
	6	0.202 (0.02)	0.171 (0.02)	**<0.001**	0.201 (0.02)	0.324
FWHMz	0	0.547 (0.03)	0.543 (0.02)	0.638	0.554 (0.02)	0.442
	1	0.556 (0.03)	0.555 (0.02)	0.857	0.544 (0.04)	0.897
	3	0.546 (0.02)	0.551 (0.04)	0.905	0.557 (0.04)	0.068
	6	0.544 (0.03)	0.556 (0.02)	0.271	0.540 (0.05)	0.773
P0z	0	0.114 (0.003)	0.114 (0.003)	0.425	0.111 (0.003)	0.271
	1	0.113 (0.01)	0.113 (0.003)	0.779	0.115 (0.01)	0.862
	3	0.114 (0.004)	0.113 (0.003)	0.787	0.112 (0.01)	0.170
	6	0.115 (0.004)	0.115 (0.01)	0.639	0.115 (0.01)	0.969

Table 6.15: Summary of mean (SD) QSI indices from controls and patients with and without MRI evidence of acute spinal relapse. P-values for adjusted group comparisons after correcting for age and gender.

6.3.4.3 Baseline imaging predictors of clinical recovery over 6 months in patients.

In patients, following adjustment for age, gender, CSA, brain T2 lesion volume, GMF and WMF, higher baseline spinal Glx concentrations predicted greater decline in postural stability over 6 months. A trend was also observed for an association between higher Glx at baseline and poorer clinical recovery on the EDSS (borderline significance P=0.075). Higher baseline Ins concentrations predicted worse postural stability at 6 months and higher tCr at baseline was associated with poor recovery on EDSS. Baseline spinal tNAA and tCho concentrations were not significant predictors of recovery over 6 months (**Table 6.16**).

Higher perpendicular diffusivity (increased P0xy and lower FWHMxy) within the whole cord, lateral columns and anterior column at baseline, predicted worse recovery in grip strength over 6 months. There was also a trend towards improvement in spasticity over 6 months in patients with lower perpendicular diffusivity in the whole cord at baseline (P =

Spinal Cord Measure	Clinical Score	Regression Coefficient	Interaction Coefficient	95 % CI	P-value
Glx	EDSS	-0.448	0.0651	-0.01, 0.14	**0.075**
	Sway 32 EO	0.193	0.2032	0.10, 0.30	**<0.001**
	Pitch 32 EO	0.141	0.1456	0.07, 0.22	**<0.001**
	Roll 32 EO	0.102	0.1138	0.06, 0.17	**<0.001**
	Sway 32 EC	0.098	0.1610	0.09, 0.24	**<0.001**
	Pitch 32 EC	0.181	0.1258	0.07, 0.18	**<0.001**
	Roll 32 EC	0.125	0.0782	0.04, 0.12	**<0.001**
Ins	Romberg 4cm	-0.281	0.309	0.07, 0.55	**0.012**
tCr	EDSS	-0.500	0.402	0.11,0.70	**0.007**
Cord FWHMxy	Grip strength	-5.100	-223.489	-393.52, -53.45	**0.010**
	MAS	-2.900	86.0149	-6.61, 178.64	**0.069**
Cord P0xy	Grip strength	-5.449	313.22	54.41, 572.04	**0.018**
Anterior FWHMxy	Grip strength	-4.658	-276.64	-456.30, -96.98	**0.003**
Anterior P0xy	Grip strength	-5.117	375.93	118.66, 633.20	**0.004**
Lateral FWHMxy	Grip strength	-5.289	-205.3352	-336.60, -74.07	**0.002**
Lateral P0xy	Grip strength	-5.741	298.79	90.37, 507.21	**0.005**

0.069) (**Table 6.16**).

Table 6.16: Associations between baseline imaging measures (predictors) and change in clinical scores over 6 months (response variables). Regression coefficients (reflecting predicted change in response variable in someone with average baseline predictor) and interaction coefficients for imaging measures, representing association between baseline imaging vs six-month clinical change are reported with 95% confidence intervals and p-

values. The regression models were adjusted separately for age, gender, CSA, brain T2 lesion volume, GMF and WMF.

6.3.4.4 Associations between temporal changes in MRI measures and clinical disability

In patients, following adjustment for age, gender, CSA, brain T2 lesion volume, GMF and WMF, a greater increase in spinal tNAA concentrations over 6 months was associated with greater clinical recovery on EDSS, TWT and Romberg's test. A greater decrease in Glx over 6 months predicted worse clinical recovery on the EDSS (**Table 6.17**).

Restriction in perpendicular diffusivity (decreasing FWHMxy and increasing P0xy) from the whole cord and anterior and lateral columns was associated with clinical improvement on the EDSS over 6 months. Similarly, restriction of perpendicular diffusivity from the posterior column was associated with clinical recovery on EDSS, MSWS, VPT and Romberg's test (**Table 6.17**).

Increasing parallel diffusivity within the whole cord (decreasing P0z and increasing FWHMz) over 6 months was associated with slower completion of the TWT, reduction in grip strength and increased spasticity. Within the anterior and posterior columns, increasing parallel diffusivity (decreasing P0z) was associated with increased spasticity scores over 6 months and increasing parallel diffusivity in the posterior columns resulted in slower completion of timed walk and loss of grip strength (**Table 6.17**).

Spinal Cord Measure	Clinical Score	Regression Coefficient	Interaction Coefficient	95 % CI	P-value
Glx	EDSS	-0.500	-0.1059	-0.18, -0.04	**0.003**
tNAA	EDSS	-0.522	-0.5216	-0.79, 0.25	**<0.001**
	1/TWT	0.012	0.0237	0.01, 0.04	**0.006**
	Romberg 32cm	-0.397	-0.7171	-1.33, -0.10	**0.022**
Cord FWHMxy	EDSS	-0.560	17.7701	8.19, 27.35	**<0.001**
Cord P0xy	EDSS	-0.564	-23.68672	-36.17, -11.20	**<0.001**
Cord FWHMz	1/TWT	0.018	-0.295	-0.53, -0.056	**0.016**
	MAS	-1.845	63.567	7.74, 119.39	**0.026**
	Grip	-5.089	-130.299	-244.29, -16.30	**0.025**
Cord P0z	MAS	-1.860	-414.027	-742.47, -85.59	**0.013**
	Grip	-3.595	1215.655	285.14, 2146.17	**0.010**
Anterior FWHMxy	EDSS	-0.575	9.1622	2.50, 15.82	**0.007**
Anterior P0xy	EDSS	-0.572	-11.4197	-20.58, -2.25	**0.015**
Anterior P0z	MAS	-1.795	-357.904	-687.80, -28.01	**0.033**
Posterior FWHMxy	MSWS	-11.850	-166.6823	-286.12, -47.25	**0.006**
	VPT	-2.068	74.9179	14.55, 135.28	**0.015**
	Romberg 32cm	-0.719	19.1002	5.43, 32.77	**0.006**
Posterior P0xy	EDSS	-0.540	-13.0379	-22.96, -3.11	**0.010**
	MSWS	-11.780	268.4052	81.78, 455.03	**0.005**
	Mean vibration	-1.634	-101.6042	-185.99, -17.21	**0.018**
	Romberg 32cm	-0.611	-23.0482	-42.78, -3.31	**0.022**
Posterior FWHMz	1/TWT	0.018	-0.255	-0.45, -0.06	**0.010**
	Grip	-5.432	-109.160	-197.70, -20.62	**0.016**
Posterior P0z	1/TWT	0.018	1.685	0.20, 3.17	**0.026**
	Grip	-4.912	960.839	167.84, 1753.84	**0.018**
Lateral FWHMxy	EDSS	-0.574	16.5759	6.71, 26.44	**0.001**
Lateral P0xy	EDSS	-0.577	-24.4868	-35.59, -13.38	**<0.001**
Lateral P0z	MAS	-2.495	-178.334	-289.20, -67.47	**0.002**

Table 6.17: Associations between rate of change in imaging measures (predictors) and rate of change in clinical scores over 6 months (response variables). Unstandardised regression coefficients (reflecting predicted change in response variable in someone with average change predictor over 6 months) and interaction coefficients for imaging measures representing association between six-month imaging change vs six-month clinical change, are reported with 95% confidence intervals and p-values. The regression models were adjusted for age, gender, CSA, brain T2 lesion volume, GMF and WMF.

6.4 Discussion

By combining spinal cord QSI and MRS techniques, this longitudinal study has provided novel insights into the mechanisms of spinal cord neurodegeneration and repair following spinal cord relapse in RRMS. Results from this study suggest that neurodegeneration with demyelination may be important substrates for persistent disability following spinal cord relapse and that glutamate excitotoxicity and axonal metabolic dysfunction may contribute to observed disability progression. Based on the findings of the study we propose restoration of normal axonal metabolism and remyelination of spinal axons may be important repair mechanisms associated with clinical recovery.

Spinal total N-acetyl aspartate (tNAA), its temporal evolution and role in spinal neurodegeneration and repair

At baseline, spinal tNAA concentrations were lower in patients than controls, reflecting axonal loss and/or axonal metabolic dysfunction. This finding is in keeping with changes seen in the PPMS cohort (**Chapter 5**) and previous MRS studies assessing acute changes associated with MS relapse (De Stefano *et al.*, 1995a; De Stefano *et al.*, 1998; Ciccarelli *et al.*, 2010a; Ciccarelli *et al.*, 2010b). Over the 6 month follow up period, tNAA concentrations were seen to rise, and normalise by month 3, in keeping with previous studies which also demonstrated reversible decreases in tNAA during recovery from acute MS brain lesions (Davie *et al.*, 1994; De Stefano *et al.*, 1995b; Mader *et al.*, 2000; Tiberio *et al.*, 2006), acute disseminated encephalomyelitis (ADEM) (Bizzi *et al.*, 2001) and acute MS spinal lesions (Ciccarelli *et al.*, 2010a; Ciccarelli *et al.*, 2010b). The current study differs from earlier studies in that tNAA concentrations fell again at month 6 (**Table 6.4**). This difference can be

understood by looking at the sub-group analysis ('improvers' versus 'non-improvers'), which confirms that the recovery in tNAA concentrations which is sustained in 'improvers' at 6 months, whereas, in 'non-improvers', tNAA concentrations remain lower than controls at 3 and 6 months (**Table 6.12, Figure 6.3**). The fall in tNAA in the 'non-improvers' is likely to reflect metabolic/structural changes occurring as a consequence of a second relapse event in that group (occurring in 5 out of 10 patients within the sub-group). Within the second sub-group analysis, tNAA concentrations were significantly lower in the group of patients with imaging changes most consistent with the clinical diagnosis of acute cervical spine relapse (acute cord swelling/GAD enhancement or resolution of C1-3 lesion on 6 month follow up), whereas changes in tNAA did not reach statistical significance in the six patients without those changes (**Table 6.14**). It might be expected that tNAA changes are greatest in patients with the greatest/ most dynamic changes on conventional imaging which might account for this difference. Alternatively, it is possible that relapse symptoms reported by patients were caused by a lesion at a site other than C1-3. In those six patients, five had new neurological symptoms in both arms and legs, which clinically is highly suggestive of cervical cord relapse. The sixth patient (patient 12) reported a new upper thoracic sensory level and L'hermitte's symptoms and it may be possible symptoms in this patients case were caused by a lesion in the upper thoracic cord.

Unlike in early PPMS (**Chapter 5**), lower spinal tNAA concentrations at onset of spinal cord relapse did not correlate with disability, nor did they predict recovery from relapse, which is in keeping with findings from previous studies of acute spinal relapse (Ciccarelli *et al.*, 2010a). However, the recovery in tNAA concentrations over 6 months was an important determinant of clinical recovery; recovery in tNAA was associated with recovery on EDSS,

TWT and postural stability (**Table 6.17, Figure 6.3**). In similarly designed studies, reversal of tNAA in the brain (De Stefano *et al.*, 1998) and spinal cord (Ciccarelli *et al.*, 2010a; Ciccarelli *et al.*, 2010b) were also associated with clinical recovery, suggesting that tNAA changes reflect a clinically important biological process.

As discussed in earlier chapters, tNAA is considered a marker of neuronal density and mitochondrial metabolism. Given that axonal regeneration seems an unlikely explanation for the recovery in tNAA, the two most plausible explanations are either; a) there is resolution of transient axonal metabolic dysfunction or b) the initially low tNAA concentrations are due to a dilutional effect, occurring as a consequence of tissue oedema and resolution of oedema results in restoration of normal concentrations. Although in the current study, it was not feasible to correct for water content directly, a similarly designed study, examining changes in water content and tNAA concentrations in new MS brain lesions over six months found that water content changes were insufficient to account for all of the recovery of tNAA following relapses (Vavasour *et al.*, 2011). In the current study, we corrected for the effect of oedema on metabolite quantification, indirectly, by co-varying CSA in the statistical model. We observed a significant relative reduction in CSA in patients at 6 months (mean annualised rate of cord atrophy of 4.02mm^2) compared to baseline which could reflect, either, axonal loss, resolution of vasogenic oedema, or a combination of the two. The annualised rate of atrophy observed in our patient cohort is greater than those reported in early RRMS cohorts (mean -0.890mm^2 per annum) (Rashid *et al.*, 2006) and in RRMS treatment trials (mean -1.9mm^2 in interferon-beta treatment arm and -2.2mm^2 in placebo arm) (Lin *et al.*, 2003). This would suggest the reduction in CSA seen in our patient group represents a combination of axonal loss and resolution of oedema. The reduction in tNAA observed in patients at

baseline, and subsequent recovery, occurred independently of CSA, suggesting that oedema alone, if present, would not fully explain these changes.

Autopsy studies have shown that in acute MS lesions, intra-axonal mitochondrial complex IV function is impaired and correlates with the numbers of microglia and infiltrating inflammatory cells (Mahad *et al.*, 2008). This inhibitory effect is thought to be mediated through reactive oxygen species (Friese *et al.*, 2014) and in fact, in animal models of MS, exogenous anti-oxidants are able to ameliorate this observed mitochondrial dysfunction (van Horssen *et al.*, 2012). Taken together, these findings suggest axonal mitochondrial function might be impaired during an acute inflammatory episode but could be restored following resolution of inflammation. Evidence that this transient metabolic dysfunction is sufficient to cause symptoms comes from an imaging study which modelled the metabolic component of the tNAA resonance from the spinal cord following spinal cord relapse; the study found that the metabolic component of tNAA was closely associated with disability measured on the EDSS (Ciccarelli *et al.*, 2010b). Restoration of neuronal metabolism may therefore be an important process for repair and recovery. Where this recovery does not take place, it is thought it will eventually lead to axonal loss (Friese *et al.*, 2014), which would account for the persistent disability in patients whose tNAA concentrations remain low.

Other potential explanations for the recovery in tNAA concentrations could be that a change in tissue chemistry during a relapse has a reversible effect on tNAA relaxation time. However, if this were the case, it might be expected that similar temporal evolution is seen with other metabolites which was not the case. Alternatively, it has previously been proposed

that a proliferation of oligodendrocyte progenitor cells (which also contain NAA), necessary for remyelination and repair may explain the increase (Davie *et al.*, 1994).

Glutamate-glutamine (Glx), its temporal evolution and role in spinal neurodegeneration and repair

At baseline, spinal Glx concentrations were elevated compared with controls and associated with acute disability (**Table 6.10**). Similar increases in Glx (Cianfoni *et al.*, 2007) and Glu (Srinivasan *et al.*, 2005) have been reported in acute MS brain lesions but associations with acute disability have not, to our knowledge, previously been assessed. In the current study, Glx concentrations normalise by 1 month, then remain at normal levels for the remainder of the follow-up period (**Table 6.4**). From the sub-group analysis, it is evident that the rise in Glx at baseline is largely driven by patients who did not recover from their relapse; whom display a roughly 2-fold increase in spinal Glx when compared with healthy controls (**Table 6.12, Figure 6.3**). This finding mirrors earlier reports of a 2 to 3 fold increase in CSF glutamate concentrations in RRMS patients during acute relapses and normal concentrations in clinically stable patients (Stover *et al.*, 1997; Sarchielli *et al.*, 2003). The temporal evolution of Glx observed in the current study would also be in keeping with current understanding of glutamate-mediated excitotoxicity in MS (discussed in more detail in **Chapter 1**). Experimental and animal models suggest that excitotoxic injury to neurones in MS may be mediated through prolonged activation of NMDA and AMPA/kainite receptors (Piani *et al.*, 1991; Piani *et al.*, 1992), and that the source of excess glutamate is likely to be infiltrating, inflammatory cells (Piani *et al.*, 1991; Werner *et al.*, 2000; Werner *et al.*, 2001). It would therefore be expected that glutamate levels will be at their highest at the onset of a

clinical relapse when inflammation is greatest and that concentrations would decline as inflammation ebbs.

Elevated Glx at baseline was an important predictor of clinical status at 6 months; higher baseline concentrations of spinal Glx predicted a deterioration in postural stability over 6 months (**Table 6.16**) and was associated with poorer recovery on the EDSS, though this association did not reach statistical significance (P=0.075) (**Table 6.16**). Decline in Glx concentrations over 6 months was associated with a fall in EDSS score of 0.5 (in patients experiencing an average decline in Glx) (**Table 6.17**). Where there were greater falls in Glx over 6 months (indicating higher baseline Glx concentration, rather than lower concentrations at 6 month follow-up), there was significantly less recovery on EDSS (**Table 6.17**). Assuming, infiltrating, inflammatory cells are the source of excess Glx, it could be inferred that acute spinal cord inflammation is an important predictor of disability at 6 months. However, there are two important caveats to bear in mind. Firstly, natural history cohorts have shown that relapses (the clinical correlate of acute inflammation), do significantly impact on disability, but only in early disease (Confavreux *et al.*, 2003; Tremlett *et al.*, 2009), and are less relevant to disability progression in later disease (Tremlett *et al.*, 2009; Scalfari *et al.*, 2010). Within our cohort, baseline spinal Glx concentrations were higher in patients with early (< 5 years) disease (n=10) compared to later (> 5 years) disease (n=10); mean 9.4 vs 5.7 mmol/l respectively, which supports the epidemiological data and would suggest that inflammation may be an important predictor of disability in early disease, and less important in later disease. Secondly, how disability is measured is important; natural history cohorts which have assessed the relationship between relapses and disability have measured disability with the DSS or EDSS, which due to their nonlinearity, are disproportionately insensitive to

smaller clinical changes in advanced disease (**Chapter 1**). Within our study, the relationship between baseline Glx and change in EDSS over 6 months did not reach statistical significance, whereas when a more linear measure of disability, such as postural stability is employed, the predictive value of baseline Glx is much more significant.

Taken together, these results provide evidence to support one of two hypotheses; either i)glutamate-mediated excitotoxic injury occurs in some patients during the initial stage of lesion formation and subsequent axonal injury is the key determinant of clinical outcomes or ii) measured rises in Glx simply reflect inflammation and inflammatory damage to axons (Trapp *et al.*, 1998) determines clinical outcomes. These findings may have important clinical implications when planning neuroprotective trials as the administration of glutamate-receptor antagonists might only be of neuroprotective benefit in the acute phase.

Total creatine (tCr), its temporal evolution and role in spinal neurodegeneration and repair

At baseline, tCr concentrations were not significantly different to controls, but higher baseline tCr was associated with increased baseline disability measured on the EDSS and TWT (**Table 6.10**), in keeping with findings from earlier, similarly designed studies (Ciccarelli *et al.*, 2007) and worse recovery on the EDSS over 6 months (**Table 6.16**). During the follow up period, tCr concentrations fall at 6 months (**Table 6.4**); with the greatest decline in tCr occurring in patients who recover from their relapse (**Table 6.12**), suggesting that either, falling tCr is a marker of repair or persistently raised tCr reflects a neurodegenerative pathway.

The tCr resonance represents the sum of creatine (Cr) and phosphocreatine (PCr) (**Chapter 2**), which are intermediaries in the ATP-generating, creatine kinase reaction. Neuronal concentrations of Cr and PCr are thought to remain fairly stable in healthy individuals (Saunders *et al.*, 1999) but are increased in relapsing and progressive forms of MS (Inglese *et al.*, 2003; Tur *et al.*, 2014), which may reflect a neuronal metabolic response to structural tissue damage (Tur *et al.*, 2014). Glial cells can contain between two to four times the concentrations of tCr found in neurons (Urenjak *et al.*, 1993) and the variability in tCr concentrations in MS has therefore been regarded by **some** as a marker of gliosis (Inglese *et al.*, 2003). Based on the findings of the current study, two hypotheses could be generated to explain the temporal changes in tCr; one potential explanation is that higher tCr in acute lesions reflects a metabolic response to an acute tissue damage and as tissue repair occurs, the metabolic requirement decreases, and is seen as a fall in tCr (in improvers). Where repair does not occur (non-improvers), tCr remains persistently elevated. Alternatively, astrocyte proliferation seen histologically within newly formed MS plaques (Popescu *et al.*, 2013), might partly determine acute disability and predicts whether or not recovery and repair can take place. Persistent astrogliosis is one of the features of chronically demyelinated plaques in which substantial loss of axons and oligodendrocytes has occurred (Popescu and Lucchinetti, 2012; Popescu *et al.*, 2013) and it is possible that persistently elevated tCr in patients who do not recover reflects this pathological process.

Myo-inositol (Ins), its temporal evolution and role in spinal neurodegeneration and repair

In the brain, elevated Ins is seen in NAWM (Fernando *et al.*, 2004) and acute lesions (Srinivasan *et al.*, 2005). In RRMS, elevated Ins concentrations has been reported in chronic spinal cord lesions (Marliani *et al.*, 2010), but this finding has not been replicated in other studies (Kendi *et al.*, 2004; Blamire *et al.*, 2007; Ciccarelli *et al.*, 2007). In the current study, spinal Ins concentrations in patients were not significantly elevated at baseline but higher Ins was associated with deterioration of postural stability over 6 months (**Table 6.16**). This is in keeping with an earlier study, which found higher spinal Ins at onset of relapse was associated with higher EDSS scores (Ciccarelli *et al.*, 2007).

Ins is considered a marker of astrocytic activation and proliferation (Brand et al., 1993) and taken together, the observation of higher baseline Ins and tCr predicting disability at 6 months suggest that there is a relationship between gliosis and spinal neurodegeneration following spinal cord relapse. The precise role of astrogliosis in MS, however, remains poorly understood; whilst gliosis and neurodegeneration appear inter-related processes, it is unclear whether gliosis is the cause or consequence of neurodegeneration. Future work should aim to address this important question.

Total Choline (tCho), its temporal evolution and role in spinal neurodegeneration and repair

In the brain, elevated tCho concentration is almost ubiquitous in MS and elevated levels have been reported in acute T2 lesions (De Stefano *et al.*, 1995a; Srinivasan *et al.*, 2005), chronic T2 lesions (He *et al.*, 2005) , T1 hypointense lesions (He *et al.*, 2005) and NAWM (Inglese *et al.*, 2003; He *et al.*, 2005). However, in the spinal cord, only a single study has reported elevated tCho in the spine, in patients with chronic spinal lesions (Marliani *et al.*, 2010). Other studies have shown no difference in spinal tCho between patients and controls; in cohorts of patients with normal appearing spinal cords (Kendi *et al.*, 2004), acute spinal lesions (Ciccarelli *et al.*, 2007; Ciccarelli *et al.*, 2010a; Ciccarelli *et al.*, 2010b) and those with a mixture of spinal changes on MRI (Blamire *et al.*, 2007).

In the current study, spinal tCho concentrations in patients were not significantly different to controls at baseline, but during the follow up period, concentrations were significantly higher than controls at 3 months before normalising again at 6 months (**Table 6.4**). From the sub-group analysis, it is evident that the rise in tCho only reaches statistical significance in non-improvers (**Table 6.12**). This may reflect active demyelination and remyelination (Marliani *et al.*, 2010), following a second relapse event. One limitation of this interpretation is that if the group difference at 3 months reflects active demyelination in only 5 patients, why is there no significant rise in tCho observed across the cohort at baseline? Timing of the scans may be important; at baseline, patients were scanned on average 20 days after the onset of relapse symptoms by which time, myelin debris which contributes to the tCho resonance may have been partially cleared by macrophages and inflammatory cells.

QSI-derived perpendicular diffusivity, its temporal evolution and role in spinal neurodegeneration and repair

At baseline, QSI-derived perpendicular diffusivity is increased in the whole cord, as well as the anterior, posterior and lateral columns and remains elevated at 6 months (**Tables 6.6-6.9**). The changes in the dPDF shape in patients at baseline (**Figure 6.5**) are similar to those seen in the PPMS cohort (**Chapter 5**) and are likely to reflect a breakdown in myelin and axonal membranes which act as microstructural barriers to perpendicular diffusion (Beaulieu, 2002). These findings also correspond to previous reported changes in the brain and spinal cords of patients with relapse-onset MS (Assaf *et al.*, 2002; Farrell *et al.*, 2008) as well as what we known about MS pathology (**Chapter 1**).

The microstructural abnormalities accounting for the differences in perpendicular diffusivity at baseline reflect acute disability and predict recovery from clinical relapse; elevated QSI-derived perpendicular diffusivity in the anterior column at baseline was associated with impaired mobility (**Table 6.11**); and higher baseline perpendicular diffusivity in the whole cord, anterior column and lateral columns predicted a decline in grip strength over 6 months (**Table 6.16**). There was also a borderline association (P=0.069) of developing increased spasticity over 6 months in patients with higher baseline FWHMxy in the whole cord (**Table 6.16**).

Perpendicular diffusivity in the whole cord evolved differently in patients who recover from their relapse compared with those that do not. In patients who recover, perpendicular

diffusivity begins to restrict by 1 month and remains comparable to controls at 6 months, whereas, in patients who do not recover, the perpendicular diffusivity remains high at 6 months (**Table 6.13, Figures 6.4 and 6.5**), suggesting that restriction of perpendicular diffusivity following a relapse reflects a tissue repair process in MS. In fact, restriction of perpendicular diffusivity was an important predictor of clinical recovery; decreasing perpendicular diffusivity in the whole cord, anterior column and lateral columns was associated with recovery on the EDSS over 6 months (**Table 6.17**) and restriction of perpendicular diffusivity in the posterior columns was associated with clinical recovery on the EDSS, MSWS, VPT and Romberg's test at a stance width of 32cm (**Table 6.17**).

Within the second sub-group analysis, in keeping with observed changes in tNAA, perpendicular diffusivity was significantly increased in patients with imaging changes most consistent with the clinical diagnosis of acute cervical spine relapse (acute cord swelling/GAD enhancement or resolution of C1-3 lesion on 6 month follow up), whereas perpendicular diffusivity within the six patients without those imaging changes was not significantly different to controls (**Table 6.15**). Again, it might be predicted that there will be greater tissue damage and hence greatest breakdown of barriers to perpendicular diffusion in patients with the greatest/most dynamic changes on conventional imaging which might account for this difference. Alternatively, it is possible that relapse symptoms reported by patients were caused by a lesion at a site other than C1-3 as discussed earlier.

Reinstatement of a physical barrier to perpendicular diffusion in the patients who improve must account for this reparative process. Axonal regeneration is unlikely to explain these changes, and therefore the most likely explanation is that the changes in QSI indices reflect

remyelination. This is supported by existing data from animal studies, which as discussed in Chapter 3, have shown that myelin has a significant effect on the restriction of QSI-derived perpendicular diffusivity (Assaf *et al.*, 2000; Cohen and Assaf, 2002; Biton *et al.*, 2005; Biton *et al.*, 2006; Biton *et al.*, 2007; Bar-Shir *et al.*, 2009).

In patients who fail to recover from their relapse, there is an increase of perpendicular diffusivity by 6 months (**Table 6.13**), which may reflect a neurodegenerative process with or without ongoing demyelination which accounts for disability.

QSI-derived parallel diffusivity, its temporal evolution and role in spinal neurodegeneration and repair

At baseline, QSI-derived parallel diffusivity in the whole cord, and major spinal cord tracts was very similar to healthy controls but by 6 months, there was a trend (P=0.062) towards higher FWHMz (increased parallel diffusivity) in the whole cord (**Table 6.6**).When looking at the sub group analysis, at 6 months, parallel diffusivity in the whole cord is significantly higher than controls in patients with a persistent deficit, but not in those who recover (**Table 6.13**), suggesting that increasing parallel diffusivity reflects a pathological process associated with disability. In fact, increasing parallel diffusivity over 6 months in the whole cord was associated with deteriorating grip strength, walking speed and increased spasticity (**Table 6.17**) and increasing parallel diffusivity in the anterior and lateral columns was associated with increasing spasticity while in the posterior column it was associated with deterioration in walking speed and grip strength (**Table 6.17**).

It is possible that the increase in diffusion parallel to the cord seen in the current cohort reflects degenerative axonal loss and mirrors findings from a DTI study of acute optic neuritis, where axial (parallel) diffusivity is restricted at symptom onset but increases over 12 months (Naismith *et al.*, 2012). It is also possible that the increase in parallel diffusivity simply reflects resolution of inflammation, which results in decreased viscosity of the extracellular fluid, allowing increased diffusion of water parallel to the cord. Whilst these findings appear to contradict the QSI studies of axotomy in rodents discussed in *Chapter 3* (Farrell *et al.*, 2010) and DTI studies in EAE (Kim *et al.*, 2006; Budde *et al.*, 2009), which all report a correlation between restricted parallel diffusivity and axonal loss, increased axial (parallel) diffusivity has been widely reported in both MS lesions and NAWM (Bammer *et al.*, 2000; Reich *et al.*, 2010; Wood *et al.*, 2012) and is thought to reflect axonal loss following a demyelinating episode. It has been proposed that parallel diffusion can be restricted at the onset of a relapse owing to an increase in intra-axonal viscosity and axonal swelling, but as oedema resolves and macrophages and inflammatory cells clear myelin debris, there are fewer barriers to diffusion, allowing water to move more freely, parallel to the orientation of axons (Naismith *et al.*, 2012; Wood *et al.*, 2012).

In conclusion, data from this study suggest that neuroaxonal loss and metabolic dysfunction, which were assessed using tNAA concentrations and QSI indices, may be important determinants of acute disability and clinical outcome following spinal cord relapse. We have described an association between spinal Glx concentrations at baseline and clinical outcomes which suggest glutamate mediated excitotoxic injury maybe an important mechanism of disability progression. Increased inositol concentrations, which in part reflect astrocyte activation and proliferation, at the onset of spinal relapse was a poor prognostic marker and

predicted poor recovery over six months. Finally, restriction of QSI-derived perpendicular diffusivity, which reflects reinstatement of perpendicular barriers to diffusion, such as myelin was associated with clinical recovery following spinal relapses.

Study limitations

Limitations of the QSI and MRS protocols used in the current experiment and the reasons for not performing corrections for multiple comparisons have previously been discussed in *Chapter 5.4*. Additional limitations with respect to the current study were, firstly, that it was not feasible to measure metabolite abnormalities within acute lesions specifically, owing to the low spatial resolution of single voxel MRS. This would have been of interest as it would provide a much more accurate picture of the pathological changes at the onset of a relapse and identify if abnormalities persist for longer within lesions than surrounding tissue. In the future it may be possible to address this by designing spinal spectroscopy studies using MRSI which has been piloted previously (Edden *et al.*, 2007). Secondly, some patients did not complete the study but by employing a mixed effect statistical model, it was possible to include all available data points into the statistical analysis, which is an approach which has been used successfully in other longitudinal studies. Thirdly, due to the delayed presentation of some patients in the study, it is possible that hyper-acute changes (eg. raised tCho or restricted parallel diffusion), had they been present, may have been missed. Finally, it is possible that 'hyper-acute' changes associated with an acute spinal cord relapse were difficult assess in the current study for 2 reasons; firstly 19 out of 20 patients were treated with high dose steroids before their first scan and secondly, the mean time to baseline scan from onset of symptoms was 20 days.

Future directions

Data from this study suggests that spinal neurodegeneration is the key substrate for persisting disability following MS relapse and that glutamate-mediated excitotoxicity, and axonal metabolic dysfunction may be important mechanisms of neurodegeneration. Future work should therefore aim to establish the relative contribution of these pathways to axonal loss in MS, with a view to developing neuroprotective agents which will limit disability progression.

Future studies should also aim to validate the use of QSI as a biomarker of remyelination. In recent years, there has been a resurgence of interest in remyelination enhancing therapies (Keough and Yong, 2013; Munzel and Williams, 2013; Franklin and Gallo, 2014; Hartley *et al.*, 2014; Olsen and Akirav, 2014). Early phase trials of the anti-LINGO-1 antibody, BIIB033 (NCT01864148), and human monoclonal IgM antibody 22 (rHIgM22) (NCT01803867) which aim to improve remyelination in patients with MS are already underway, in spite of this lack of a robust biomarker of remyelination (Munzel and Williams, 2013). If QSI derived perpendicular diffusivity was proven to reliably reflect remyelination, it would allow for a much more accurate evaluation of these new therapies.

Chapter Seven

Conclusions and future directions

7.1 Conclusions

The spinal cord is a clinically eloquent structure, commonly affected in MS, causing significant disability. However, spinal cord pathology in MS has been relatively under-studied, using advanced MRI techniques due to the technically challenging nature of MRI within this region. The aim of this thesis was therefore to use a combination of advanced quantitative MRI techniques to investigate spinal neurodegeneration and repair in PPMS and RRMS *in vivo*.

This thesis has combined single-voxel MRS and QSI, two advanced MRI techniques which have increased pathological specificity for neurodegeneration and myelin, and allow quantification of metabolites that reflect biological mechanisms, which I hypothesised, may be involved in neurodegenerative and repair pathways. By combining these imaging techniques with new clinical measures, which reflect spinal cord functions more closely than conventional clinical tests, the relationship between spinal cord structure-metabolism and function has been evaluated in greater detail than has previously been the case.

In relation to spectroscopy, this work has built on earlier spinal cord studies in MS which have used protocols which were not optimised for quantification of Glx (Chapter 3). One limitation of earlier studies has been that they have not addressed the potential contribution of glutamate-mediated excitotoxicity in the spinal cord in MS pathology. This has largely been due to the technical challenges associated with quantifying Glu or Glx from the spinal cord. Optimisation experiments performed in Chapter 4.1 were therefore aimed at developing a novel spinal MRS protocol capable of quantifying Glx. A short-TE PRESS MRS sequence

gave the best results which is broadly in keeping with earlier work carried out by Hancu, who found that short-TE PRESS was optimal for Glx detection in the brain (Hancu, 2009). The effects of age and gender on normative metabolite concentrations obtained from the healthy spinal cord were assessed in Chapter 4.2. Important associations between advancing age and declining concentrations of tNAA and Glx were identified, which likely reflect age-related neurodegeneration and is in keeping with age-related changes reported in the brain. This association represents an important consideration in any longitudinal follow up of patients using spinal MRS and will allow differentiation between changes due to pathology and those occurring as a consequence of normal ageing. Spinal Glx concentrations were lower in female subjects than males, even after correcting for age. Similar findings have previously been observed in some, but not all brain regions, in earlier studies, and it has been suggested that hormonal factors may be responsible for gender differences in Glx (Batra *et al.*, 2008; Zlotnik *et al.*, 2011). However, it should be noted that of the 22 subjects included in the final analysis, only 7 were males and this finding will therefore need to be confirmed in future studies with larger sample sizes.

In section 4.3, differences in spinal GMVF between healthy subjects were assessed. A large degree of variability in GMVF was seen in healthy controls (range 16.1 to 24.8%). In fact, the degree of variability is much greater than that seen in the brains of the same healthy controls in Chapter 5 (range 46 to 50.5%). Increasing GMVF (or decreasing WMVF) was associated with increasing tNAA/Cr and Glx/Cr ratios which suggests that there must be higher concentrations of tNAA and Glx and/or lower concentrations of tCr in the spinal grey matter compared to the white matter. This becomes relevant when studying neurodegenerative diseases in which there is tissue-specific volume loss in the spinal cord such as MS (where

spinal cord atrophy occurs predominantly because of white matter volume loss). GMVF should therefore, when possible, be calculated in patients and corrected for in spinal MRS studies. This is difficult in MS because, when using currently available imaging protocols, there isn't sufficient contrast, on axial images, between spinal grey matter and white mater lesions to allow reliable segmentation of the grey matter. More work is therefore required to develop techniques for accurate spinal grey matter segmentation in patients with spinal cord lesions.

Chapter 5 applied the newly developed MRS protocol together with QSI of the cervical cord to patients with early PPMS. The hypotheses being tested were that these imaging techniques would be more sensitive than spinal cord cross sectional area for detecting early neurodegenerative changes and that those changes in MRS and QSI metrics would reflect disability. The results suggest that QSI and MRS are promising techniques for detecting early disease changes; there were significant differences in QSI-derived perpendicular diffusivity, spinal tNAA and spinal Glx between patients and controls, which reflect changes in neuroaxonal integrity, axonal metabolic function and glutamatergic neurotransmitter pool. These changes were detectable despite there being no significant differences in cord area between the two groups. This increased sensitivity for detection of microstructural changes earlier, is important because there is currently an unmet need for sensitive imaging biomarkers of spinal neurodegeneration in progressive forms of MS; for more accurate assessment of disease progression and as an imaging outcome measure in clinical trials of new neuroprotective agents. Patients with spinal cord lesions within the spectroscopy voxel were also observed to have significantly elevated Ins concentrations compared with controls, which reflects astrocyte activation and gliosis; which correlates with histological observation

of persistent astrogliosis in chronically demyelinated plaques (Popescu and Lucchinetti, 2012; Popescu *et al.*, 2013). Ins levels in normal appearing spinal cord were comparable to controls which raises questions about the role of gliosis in neurodegeneration; whether gliosis drives neurodegeneration or is the inevitable consequence of neurodegeneration needs to be investigated further.

Lower spinal tNAA and Glx, and higher spinal Ins were all associated with increased disability. Taken together, these findings suggest that neuroaxonal loss, axonal metabolic dysfunction, alterations in glutamatergic neurotransmitter pool and astrocyte proliferation could contribute to early clinical disability in PPMS. These hypotheses were supported by the QSI data; increased QSI-derived perpendicular diffusivity in the cord, reflecting reduced axonal integrity and/or demyelination also correlated with disability. This was also true when assessing the relationship between QSI indices in spinal white matter tracts and clinical scores which reflect the motor or sensory functions conveyed within those tracts, suggesting a strong structure-function relationship between axonal microstructure and disability.

In Chapter 6, spinal MRS and QSI were applied to a cohort of RRMS patients. The study was designed to investigate the role of neurodegeneration and repair in the spinal cord on disability following acute spinal cord relapse. The specific mechanisms under investigation were the role of a) neuroaxonal loss and dysfunction, b) glutamate-excitotoxicity, c) gliosis and d) resolution of inflammation and repair mechanisms on acute disability and recovery.

Increasing QSI-derived perpendicular and parallel diffusivity over 6 months was associated with no recovery following spinal cord relapse, suggesting that neuroaxonal degeneration following acute relapses determines clinical outcomes. Glutamate mediated excitotoxicity may also be important; higher spinal Glx at onset of relapse was significantly associated with accumulation of disability. This builds on earlier work by Baranzini *et al* which demonstrated that patients with higher brain glutamate concentrations exhibited greater declines in tNAA (reflecting axonal loss) over 1 year (Baranzini *et al.*, 2010). In the spinal cord, normalisation of Glx concentrations occurred in all patients by 1 month, irrespective of recovery, which suggests that injury caused by excess glutamate is most likely to occur during the acute phase. This finding has potential implications for future therapeutic interventions which target glutamate mediated injury in MS; as effectiveness of glutamate blocking agents may be dependent on immediate administration at the onset of relapse symptoms.

Spinal tNAA concentrations which reflect neuronal density and metabolism showed two distinct patterns of evolution in the 6 month follow up period; a) in patients whom recovered there was an initial decline in tNAA, followed by recovery and b) in patients who did not recover, tNAA concentrations remained low. The reversibility of tNAA was associated with recovery on clinical scores and is likely to reflect reversal of axonal metabolic dysfunction, without which, recovery does not occur. Myelin repair (remyelination), assessed on restriction of perpendicular diffusivity over 6 months was also significantly associated with clinical recovery, as might be expected. Enhancing these biological processes should therefore be targeted by potential future therapies.

MRS and QSI measures at baseline were predictive of clinical outcomes at 6 months; in particular baseline spinal Glx, Ins and tCr concentrations and QSI-derived perpendicular diffusivity, which suggests either individual imaging measures or muti-parametric models consisting of multiple measures, could be used in the future to stratify risk for incomplete recovery and to identify patients who would benefit from early therapeutic interventions.

In summary, spinal MRS and QSI provide a sensitive and non-invasive means to quantify metabolic and microstructural tissue changes on a longitudinal basis in the cervical cord. MRS and QSI changes occur early in PPMS, prior to the development of spinal atrophy and closely related to clinical disability and likely reflect important pathological processes. Following spinal cord relapses, disability may not be attributable to a single pathologic process; this work has generated hypotheses about disease mechanisms that require more detailed evaluation; glutamate-mediated excitotoxicity and neurodegeneration are suggested as important mechanisms of disability progression and reversal of axonal metabolic dysfunction and remyelination could, in part underlie clinical recovery. This improved accessibility to assessing tissue damage in the cervical cord together with increased pathological specificity of advanced imaging techniques means that advanced quantitative MRI of the spinal cord should be considered as a potentially valuable component of future trials looking at recovery and neuroprotection in MS.

7.2 Suggested directions for future research

There is an increasing body of evidence, which has been added to by this thesis, to support a potential role for glutamate mediated excitotoxicity in MS pathophysiology. As discussed in

Chapter 4, future work should therefore now focus on developing improved MRS protocols, capable of reproducible quantification of spinal Glu concentrations in the cervical cord to allow this potentially modifiable disease process to be studied in greater detail and on a larger scale, *in vivo*. Using a 3T system, Hurd *et al*. reported reproducible Glu quantification in the brain, with good visual separation of Glu from Gln using a TE-averaged PRESS sequence (Hurd *et al.*, 2004). However, to achieve similar results the spinal cord will require ultra-high field strengths or much longer scanning times. The latter may prevent simultaneous acquisition of other sequences within acceptable scan times. Alternatively, employing spectral editing techniques such as J-editing, which have allowed reproducible quantification of strongly coupled resonances in the brain (O'Gorman *et al.*, 2011) within acceptable scan times at 3T, may be more suited to the spinal cord.

One important methodological consideration in future spinal MRS studies in MS will be the segmentation of spinal grey matter to calculate GMVF. Spinal grey matter segmentation in MS patients might be possible when higher resolution axial imaging, which provides improved contrast between lesions and grey matter, is available in the future; again work is now needed to develop this. The double inversion recovery (DIR) and phase-sensitive inversion recovery (PSIR) sequences give improved contrast between lesions and grey matter in the brain (Sethi *et al.*, 2012) and the DIR sequence has recently been adapted for the cervical cord and shows improved detection of MS lesions (Riederer *et al.*, 2014), but further work is required to determine whether these sequences could be adapted for spinal grey matter segmentation in future.

The significance of elevated spinal Ins in PPMS needs further evaluation. Results in *Chapter 5* have shown that Ins is elevated in early PPMS but that this increase is driven by data collected from patients with lesions within the spectroscopic voxel. More work is therefore needed to decipher whether gliosis is the end-stage hallmark of chronic lesions or whether it contributes to neurodegeneration. This question would be best answered through a longitudinal extension of the study in *Chapter 5* which is currently ongoing. In the 3 year longitudinal study we will also look at the prognostic value of baseline Ins and other imaging measures on progression of disability and imaging measures of neurodegeneration such as cord atrophy, spinal tNAA concentrations and QSI metrics.

It was beyond the scope of this thesis to establish whether or not QSI indices are more sensitive to spinal microstructural changes, than the more established DTI-derived indices such as fractional anisotropy (FA), radial (RD) and axial (AD) diffusivity. Non-Gaussian models such as QSI have theoretical advantages over DTI which may mean they are better suited/more sensitive for detecting early and longitudinal pathological changes. This could have important implications for future diagnostic criteria in MS, allowing earlier evaluation of 'dissemination in space', in macroscopically normal CNS sites, as well as disease monitoring and clinical trials. Although earlier work has attempted to answer this question in the brain (Assaf *et al.*, 2002; Assaf *et al.*, 2005), future studies should look at making direct comparisons between QSI and DTI models in the spinal cord in MS.

Multi-parametric imaging models in demyelinating disorders have been used with some success recently and may provide important information about microstructural spinal cord

changes and better explain the substrates of disability (Pichiecchio *et al.*, 2011; Oh *et al.*, 2013b). Studies in the future should aim to incorporate spinal QSI and MRS along with MTR and cord atrophy to improve our understanding of the interaction between structural and metabolic abnormalities that best explains disability in MS.

The need to develop neuroprotective drugs in MS is arguably the most urgent challenge facing the MS research community. Results from *Chapter 6* support existing evidence for two particularly important and potentially modifiable mechanisms of neurodegeneration following spinal cord relapse; specifically, glutamate mediated excitotoxicity and axonal metabolic (mitochondrial) dysfunction. Results from this thesis, along with earlier studies suggest that metabolic dysfunction can be reversible and as such, should be considered an important therapeutic target for new neuroprotective agents. Similarly, the evidence for glutamate mediated damage is growing and represents a potentially modifiable disease pathway. When these findings are taken in the context of supporting data from animal studies, there is a strong case to be made for designing clinical trials which use existing drugs, with acceptable risk profiles that target the glutamatergic and mitochondrial pathways implicated in neurodegeneration, similar to trials already conducted using sodium channel blockers in MS (Kapoor *et al.*, 2010; Raftopoulos *et al.*, 2014).

Reference list

Aggarwal, A. &Nicholson, G. (2002). Detection of preclinical motor neurone loss in SOD1 mutation carriers using motor unit number estimation. *Journal of Neurology, Neurosurgery & Psychiatry* 73(2): 199-201.

Agosta, F., Lagana, M., Valsasina, P., Sala, S., Dall'Occhio, L., Sormani, M. P., Judica, E. &Filippi, M. (2007). Evidence for cervical cord tissue disorganisation with aging by diffusion tensor MRI. *Neuroimage* 36(3): 728-735.

Alger, J. R. (2010). Quantitative proton magnetic resonance spectroscopy and spectroscopic imaging of the brain: a didactic review. *Top Magn Reson Imaging* 21(2): 115-128.

Allen, I. V. &McKeown, S. R. (1979). A histological, histochemical and biochemical study of the macroscopically normal white matter in multiple sclerosis. *J Neurol Sci* 41(1): 81-91.

Anaby, D., Duncan, I. D., Smith, C. M. &Cohen, Y. (2013). q-Space diffusion MRI (QSI) of the disease progression in the spinal cords of the Long Evans shaker: diffusion time and apparent anisotropy. *NMR Biomed* 26(12): 1879-1886.

Andrews, H. E., Nichols, P. P., Bates, D. &Turnbull, D. M. (2005). Mitochondrial dysfunction plays a key role in progressive axonal loss in Multiple Sclerosis. *Med Hypotheses* 64(4): 669-677.

Arnold, D. L., Riess, G. T., Matthews, P. M., Francis, G. S., Collins, D. L., Wolfson, C. &Antel, J. P. (1994). Use of proton magnetic resonance spectroscopy for monitoring disease progression in multiple sclerosis. *Ann Neurol* 36(1): 76-82.

Arundine, M. &Tymianski, M. (2004). Molecular mechanisms of glutamate-dependent neurodegeneration in ischemia and traumatic brain injury. *Cell Mol Life Sci* 61(6): 657-668.

Ascherio, A., Munger, K. L. &Simon, K. C. (2010). Vitamin D and multiple sclerosis. *Lancet Neurol* 9(6): 599-612.

Assaf, Y., Ben-Bashat, D., Chapman, J., Peled, S., Biton, I. E., Kafri, M., Segev, Y., Hendler, T., Korczyn, A. D., Graif, M. &Cohen, Y. (2002). High b-value q-space analyzed diffusion-weighted MRI: Application to multiple sclerosis. *Magnetic Resonance in Medicine* 47(1): 115-126.

Assaf, Y., Chapman, J., Ben-Bashat, D., Hendler, T., Segev, Y., Korczyn, A. D., Graif, M. &Cohen, Y. (2005). White matter changes in multiple sclerosis: correlation of q-space diffusion MRI and 1H MRS. *Magn Reson Imaging* 23(6): 703-710.

Assaf, Y. &Cohen, Y. (2000). Assignment of the water slow-diffusing component in the central nervous system using q-space diffusion MRS: Implications for fiber tract imaging. *Magnetic Resonance in Medicine* 43(2): 191-199.

Assaf, Y., Mayk, A. &Cohen, Y. (2000). Displacement imaging of spinal cord using q-space diffusion-weighted MRI. *Magnetic Resonance in Medicine* 44(5): 713-722.

Augustine, G. J. (2008).Neurotransmitters and their receptors. . In *Neuroscience*(Ed D. Purves). Sinauer associates Inc.

Aversa, A., Bruzziches, R., Francomano, D., Natali, M., Gareri, P. &Spera, G. (2010). Endothelial dysfunction and erectile dysfunction in the aging man. *International Journal of Urology* 17(1): 38-47.

Baker, E. H., Basso, G., Barker, P. B., Smith, M. A., Bonekamp, D. &Horska, A. (2008). Regional apparent metabolite concentrations in young adult brain measured by (1)H MR spectroscopy at 3 Tesla. *J Magn Reson Imaging* 27(3): 489-499.

Bammer, R., Augustin, M., Strasser-Fuchs, S., Seifert, T., Kapeller, P., Stollberger, R., Ebner, F., Hartung, H. P. &Fazekas, F. (2000). Magnetic resonance diffusion tensor imaging for characterizing diffuse and focal white matter abnormalities in multiple sclerosis. *Magn Reson Med* 44(4): 583-591.

Bar-Shir, A., Duncan, I. D. &Cohen, Y. (2009). QSI and DTI of excised brains of the myelin-deficient rat. *Neuroimage* 48(1): 109-116.

Baranzini, S. E., Jeong, M. C., Butunoi, C., Murray, R. S., Bernard, C. C. &Oksenberg, J. R. (1999). B cell repertoire diversity and clonal expansion in multiple sclerosis brain lesions. *J Immunol* 163(9): 5133-5144.

Baranzini, S. E., Srinivasan, R., Khankhanian, P., Okuda, D. T., Nelson, S. J., Matthews, P. M., Hauser, S. L., Oksenberg, J. R. &Pelletier, D. (2010). Genetic variation influences glutamate concentrations in brains of patients with multiple sclerosis. *Brain* 133(9): 2603-2611.

Barker, P. B. (2010).Fundamentals of MR spectrpscopy. In *Clinical MR neuroimaging*, 5-20 (Eds J. H. Gillard and P. B. Barker). Cambridge: Cambridge University Press.

Barkhof, F. (2002). The clinico-radiological paradox in multiple sclerosis revisited. *Curr Opin Neurol* 15(3): 239-245.

Barnett, M. H. &Prineas, J. W. (2004). Relapsing and remitting multiple sclerosis: pathology of the newly forming lesion. *Ann Neurol* 55(4): 458-468.

Basser, P. J. &Pierpaoli, C. (1996). Microstructural and physiological features of tissues elucidated by quantitative-diffusion-tensor MRI. *J Magn Reson B* 111(3): 209-219.

Bates, T. E., Strangward, M., Keelan, J., Davey, G. P., Munro, P. M. &Clark, J. B. (1996). Inhibition of N-acetylaspartate production: implications for 1H MRS studies in vivo. *Neuroreport* 7(8): 1397-1400.

Batra, N. A., Seres-Mailo, J., Hanstock, C., Seres, P., Khudabux, J., Bellavance, F., Baker, G., Allen, P., Tibbo, P., Hui, E. &Le Melledo, J. M. (2008). Proton magnetic resonance spectroscopy measurement of brain glutamate levels in premenstrual dysphoric disorder. *Biol Psychiatry* 63(12): 1178-1184.

Beal, M. F. (2005). Mitochondria take center stage in aging and neurodegeneration. *Ann Neurol* 58(4): 495-505.

Beaulieu, C. (2002). The basis of anisotropic water diffusion in the nervous system - a technical review. *NMR Biomed* 15(7-8): 435-455.

Bechtold, D. A., Miller, S. J., Dawson, A. C., Sun, Y., Kapoor, R., Berry, D. &Smith, K. J. (2006). Axonal protection achieved in a model of multiple sclerosis using lamotrigine. *J Neurol* 253(12): 1542-1551.

Benedetti, B., Rocca, M. A., Rovaris, M., Caputo, D., Zaffaroni, M., Capra, R., Bertolotto, A., Martinelli, V., Comi, G. &Filippi, M. (2010). A diffusion tensor MRI study of cervical cord damage in benign and secondary progressive multiple sclerosis patients. *Journal of Neurology, Neurosurgery & Psychiatry* 81(1): 26-30.

Bergers, E., Bot, J. C., De Groot, C. J., Polman, C. H., Lycklama a Nijeholt, G. J., Castelijns, J. A., van der Valk, P. &Barkhof, F. (2002). Axonal damage in the spinal cord of MS patients occurs largely independent of T2 MRI lesions. *Neurology* 59(11): 1766-1771.

Bieniek, M., Altmann, D. R., Davies, G. R., Ingle, G. T., Rashid, W., Sastre-Garriga, J., Thompson, A. J. &Miller, D. H. (2006). Cord atrophy separates early primary progressive and relapsing remitting multiple sclerosis. *J Neurol Neurosurg Psychiatry* 77(9): 1036-1039.

Birken, D. L. &Oldendorf, W. H. (1989). N-acetyl-L-aspartic acid: a literature review of a compound prominent in 1H-NMR spectroscopic studies of brain. *Neurosci Biobehav Rev* 13(1): 23-31.

Biton, I. E., Duncan, I. D. &Cohen, Y. (2006). High b-value q-space diffusion MRI in myelin-deficient rat spinal cords. *Magn Reson Imaging* 24(2): 161-166.

Biton, I. E., Duncan, I. D. &Cohen, Y. (2007). q-Space diffusion of myelin-deficient spinal cords. *Magn Reson Med* 58(5): 993-1000.

Biton, I. E., Mayk, A., Kidron, D., Assaf, Y. &Cohen, Y. (2005). Improved detectability of experimental allergic encephalomyelitis in excised swine spinal cords by high b-value q-space DWI. *Exp Neurol* 195(2): 437-446.

Bitsch, A., Schuchardt, J., Bunkowski, S., Kuhlmann, T. &Bruck, W. (2000). Acute axonal injury in multiple sclerosis. Correlation with demyelination and inflammation. *Brain* 123 (Pt 6): 1174-1183.

Bizzi, A., Ulug, A. M., Crawford, T. O., Passe, T., Bugiani, M., Bryan, R. N. &Barker, P. B. (2001). Quantitative proton MR spectroscopic imaging in acute disseminated encephalomyelitis. *AJNR Am J Neuroradiol* 22(6): 1125-1130.

Bjartmar, C., Kidd, G., Mork, S., Rudick, R. &Trapp, B. D. (2000). Neurological disability correlates with spinal cord axonal loss and reduced N-acetyl aspartate in chronic multiple sclerosis patients. *Ann Neurol* 48(6): 893-901.

Black, J. A., Newcombe, J., Trapp, B. D. &Waxman, S. G. (2007). Sodium Channel Expression Within Chronic Multiple Sclerosis Plaques. *Journal of Neuropathology & Experimental Neurology* 66(9): 828-837 810.1097/nen.1090b1013e3181462841.

Black, J. A. &Waxman, S. G. (2008). Phenytoin protects central axons in experimental autoimmune encephalomyelitis. *J Neurol Sci* 274(1-2): 57-63.

Blamire, A. M., Cader, S., Lee, M., Palace, J. &Matthews, P. M. (2007). Axonal damage in the spinal cord of multiple sclerosis patients detected by magnetic resonance spectroscopy. *Magnetic Resonance in Medicine* 58(5): 880-885.

Bloch, F. (1946). Nuclear Induction. *Physical Review* 70(7-8): 460-474.

Bodini, B., Cercignani, M., Toosy, A., Stefano, N. D., Miller, D. H., Thompson, A. J. &Ciccarelli, O. (2013). A novel approach with "skeletonised MTR" measures tract-specific microstructural changes in early primary-progressive MS. *Hum Brain Mapp*.

Bohannon, R. W. &Smith, M. B. (1987). Interrater reliability of a modified Ashworth scale of muscle spasticity. *Phys Ther* 67(2): 206-207.

Bonati, U., Fisniku, L. K., Altmann, D. R., Yiannakas, M. C., Furby, J., Thompson, A. J., Miller, D. H. &Chard, D. T. (2011). Cervical cord and brain grey matter atrophy independently associate with long-term MS disability. *J Neurol Neurosurg Psychiatry* 82(4): 471-472.

Bot, J. C., Barkhof, F., Lycklama a Nijeholt, G., van Schaardenburg, D., Voskuyl, A. E., Ader, H. J., Pijnenburg, J. A., Polman, C. H., Uitdehaag, B. M., Vermeulen, E. G. &Castelijns, J. A. (2002). Differentiation of multiple sclerosis from other inflammatory disorders and cerebrovascular disease: value of spinal MR imaging. *Radiology* 223(1): 46-56.

Bot, J. C., Barkhof, F., Polman, C. H., Lycklama a Nijeholt, G. J., de Groot, V., Bergers, E., Ader, H. J. &Castelijns, J. A. (2004). Spinal cord abnormalities in recently diagnosed MS patients: added value of spinal MRI examination. *Neurology* 62(2): 226-233.

Bottomley, P. A. (1987). Spatial Localization in Nmr-Spectroscopy Invivo. *Ann N Y Acad Sci* 508: 333-348.

Bouafia, A., Golmard, J. L., Thuries, V., Sazdovitch, V., Hauw, J. J., Fontaine, B. &Seilhean, D. (2014). Axonal expression of sodium channels and neuropathology of the plaques in multiple sclerosis. *Neuropathol Appl Neurobiol* 40(5): 579-590.

Brand, A., Richter-Landsberg, C. &Leibfritz, D. (1993). Multinuclear NMR studies on the energy metabolism of glial and neuronal cells. *Dev Neurosci* 15(3-5): 289-298.

Bray, P. F., Bloomer, L. C., Salmon, V. C., Bagley, M. H. &Larsen, P. D. (1983). Epstein-Barr virus infection and antibody synthesis in patients with multiple sclerosis. *Arch Neurol* 40(7): 406-408.

Brenner, R. E., Munro, P. M., Williams, S. C., Bell, J. D., Barker, G. J., Hawkins, C. P., Landon, D. N. &McDonald, W. I. (1993). The proton NMR spectrum in acute EAE: the significance of the change in the Cho:Cr ratio. *Magn Reson Med* 29(6): 737-745.

Brex, P. A., Jenkins, R., Fox, N. C., Crum, W. R., O'Riordan, J. I., Plant, G. T. &Miller, D. H. (2000). Detection of ventricular enlargement in patients at the earliest clinical stage of MS. *Neurology* 54(8): 1689-1691.

Brex, P. A., Leary, S. M., O'Riordan, J. I., Miszkiel, K. A., Plant, G. T., Thompson, A. J. &Miller, D. H. (2001). Measurement of spinal cord area in clinically isolated syndromes suggestive of multiple sclerosis. *Journal of Neurology, Neurosurgery & Psychiatry* 70(4): 544-547.

Bröer, S. &Brookes, N. (2001). Transfer of glutamine between astrocytes and neurons. *J Neurochem* 77(3): 705-719.

Bronskill, M. J., McVeigh, E. R., Kucharczyk, W. &Henkelman, R. M. (1988). Syrinx-like artifacts on MR images of the spinal cord. *Radiology* 166(2): 485-488.

Brooks, J. C., Roberts, N., Kemp, G. J., Gosney, M. A., Lye, M. &Whitehouse, G. H. (2001). A proton magnetic resonance spectroscopy study of age-related changes in frontal lobe metabolite concentrations. *Cereb Cortex* 11(7): 598-605.

Brown, G. C. &Borutaite, V. (2001). Nitric oxide, mitochondria, and cell death. *IUBMB Life* 52(3-5): 189-195.

Budde, M. D., Xie, M., Cross, A. H. &Song, S. K. (2009). Axial diffusivity is the primary correlate of axonal injury in the experimental autoimmune encephalomyelitis spinal cord: a quantitative pixelwise analysis. *J Neurosci* 29(9): 2805-2813.

Bunn, L. M., Marsden, J. F., Giunti, P. &Day, B. L. (2013). Stance instability in spinocerebellar ataxia type 6. *Mov Disord* 28(4): 510-516.

Burek, J. D., van der Kogel, A. J. &Hollander, C. F. (1976). Degenerative myelopathy in three strains of aging rats. *Vet Pathol* 13(5): 321-331.

Butler, D. &Bahr, B. A. (2006). Oxidative stress and lysosomes: CNS-related consequences and implications for lysosomal enhancement strategies and induction of autophagy. *Antioxid Redox Signal* 8(1-2): 185-196.

Callaghan, P. T., Eccles, C. D. &Xia, Y. (1988). NMR microscopy of dynamic displacements: k-space and q-space imaging. *Journal of Physics E: Scientific Instruments* 21(8): 820.

Caramanos, Z., Narayanan, S. &Arnold, D. L. (2005). *1H-MRS quantification of tNA and tCr in patients with multiple sclerosis: a meta-analytic review.*

Carbone, M., Duty, S. &Rattray, M. (2012). Riluzole elevates GLT-1 activity and levels in striatal astrocytes. *Neurochem Int* 60(1): 31-38.

Carew, J. D., Nair, G., Andersen, P. M., Wuu, J., Gronka, S., Hu, X. &Benatar, M. (2011). Presymptomatic spinal cord neurometabolic findings in SOD1-positive people at risk for familial ALS. *Neurology* 77(14): 1370-1375.

Carpenter, J. &Bithell, J. (2000). Bootstrap confidence intervals: when, which, what? A practical guide for medical statisticians. *Stat Med* 19(9): 1141-1164.

Carr, H. Y. &Purcell, E. M. (1954). Effects of Diffusion on Free Precession in Nuclear Magnetic Resonance Experiments. *Physical Review* 94(3): 630-638.

Carton, H., Vlietinck, R., Debruyne, J., De Keyser, J., D'Hooghe, M. B., Loos, R., Medaer, R., Truyen, L., Yee, I. M. &Sadovnick, A. D. (1997). Risks of multiple sclerosis in relatives of patients in Flanders, Belgium. *J Neurol Neurosurg Psychiatry* 62(4): 329-333.

Caudle, W. M. &Zhang, J. (2009). Glutamate, excitotoxicity, and programmed cell death in Parkinson disease. *Exp Neurol* 220(2): 230-233.

Chang, L., Ernst, T., Poland, R. E. &Jenden, D. J. (1996). In vivo proton magnetic resonance spectroscopy of the normal aging human brain. *Life Sci* 58(22): 2049-2056.

Chang, L., Jiang, C. S. &Ernst, T. (2009). Effects of age and sex on brain glutamate and other metabolites. *Magn Reson Imaging* 27(1): 142-145.

Chard, D. T., Griffin, C. M., McLean, M. A., Kapeller, P., Kapoor, R., Thompson, A. J. &Miller, D. H. (2002). Brain metabolite changes in cortical grey and normal-appearing white matter in clinically early relapsing-remitting multiple sclerosis. *Brain* 125(Pt 10): 2342-2352.

Chard, D. T., Jackson, J. S., Miller, D. H. &Wheeler-Kingshott, C. A. (2010). Reducing the impact of white matter lesions on automated measures of brain gray and white matter volumes. *J Magn Reson Imaging* 32(1): 223-228.

Charles, H. C., Lazeyras, F., Krishnan, K. R., Boyko, O. B., Patterson, L. J., Doraiswamy, P. M. &McDonald, W. M. (1994). Proton spectroscopy of human brain: effects of age and sex. *Prog Neuropsychopharmacol Biol Psychiatry* 18(6): 995-1004.

Chevis, C. F., da Silva, C. B., D'Abreu, A., Lopes-Cendes, I., Cendes, F., Bergo, F. P. &Franca, M. C., Jr. (2013). Spinal Cord Atrophy Correlates with Disability in Friedreich's Ataxia. *Cerebellum* 12(1): 43-47.

Choi, C., Coupland, N. J., Bhardwaj, P. P., Kalra, S., Casault, C. A., Reid, K. &Allen, P. S. (2006). T2 measurement and quantification of glutamate in human brain in vivo. *Magn Reson Med* 56(5): 971-977.

Christiansen, P., Toft, P., Larsson, H. B., Stubgaard, M. &Henriksen, O. (1993). The concentration of N-acetyl aspartate, creatine + phosphocreatine, and choline in different parts of the brain in adulthood and senium. *Magn Reson Imaging* 11(6): 799-806.

Cianfoni, A., Niku, S. &Imbesi, S. G. (2007). Metabolite findings in tumefactive demyelinating lesions utilizing short echo time proton magnetic resonance spectroscopy. *AJNR Am J Neuroradiol* 28(2): 272-277.

Ciccarelli, O., Altmann, D. R., McLean, M. A., Wheeler-Kingshott, C. A., Wimpey, K., Miller, D. H. &Thompson, A. J. (2010a). Spinal cord repair in MS: does mitochondrial metabolism play a role? *Neurology* 74(9): 721-727.

Ciccarelli, O., Barkhof, F., Bodini, B., De Stefano, N., Golay, X., Nicolay, K., Pelletier, D., Pouwels, P. J., Smith, S. A., Wheeler-Kingshott, C. A., Stankoff, B., Yousry, T. &Miller, D. H. (2014). Pathogenesis of multiple sclerosis: insights from molecular and metabolic imaging. *Lancet Neurol* 13(8): 807-822.

Ciccarelli, O., Thomas, D., De Vita, E., Wheeler-Kingshott, C., Kachramanoglou, C., Kapoor, R., Leary, S., Matthews, L., Palace, J., Chard, D., Miller, D., Toosy, A. &Thompson, A. (2013). Low myo-inositol indicating astrocytic damage in a case series of NMO. *Ann Neurol*.

Ciccarelli, O., Toosy, A. T., De Stefano, N., Wheeler-Kingshott, C. A., Miller, D. H. &Thompson, A. J. (2010b). Assessing neuronal metabolism in vivo by modeling imaging measures. *J Neurosci* 30(45): 15030-15033.

Ciccarelli, O., Wheeler-Kingshott, C. A., McLean, M. A., Cercignani, M., Wimpey, K., Miller, D. H. &Thompson, A. J. (2007). Spinal cord spectroscopy and diffusion-based tractography to assess acute disability in multiple sclerosis. *Brain* 130(Pt 8): 2220-2231.

Clarke, D. D., Greenfield, S., Dicker, E., Tirri, L. J. &Ronan, E. J. (1975). A relationship of N-acetylaspartate biosynthesis to neuronal protein synthesis. *J Neurochem* 24(3): 479-485.

Cohen-Adad, J., Mendili, M. M., Morizot-Koutlidis, R., Lehericy, S., Meininger, V., Blancho, S., Rossignol, S., Benali, H. &Pradat, P. F. (2013). Involvement of spinal sensory pathway in ALS and specificity of cord atrophy to lower motor neuron degeneration. *Amyotroph Lateral Scler Frontotemporal Degener* 14(1): 30-38.

Cohen, A. B., Neema, M., Arora, A., Dell'oglio, E., Benedict, R. H., Tauhid, S., Goldberg-Zimring, D., Chavarro-Nieto, C., Ceccarelli, A., Klein, J. P., Stankiewicz, J. M., Houtchens, M. K., Buckle, G. J., Alsop, D. C., Guttmann, C. R. &Bakshi, R. (2012). The relationships among MRI-defined spinal cord involvement, brain involvement, and disability in multiple sclerosis. *J Neuroimaging* 22(2): 122-128.

Cohen, Y. &Assaf, Y. (2002). High b-value q-space analyzed diffusion-weighted MRS and MRI in neuronal tissues - a technical review. *NMR Biomed* 15(7-8): 516-542.

Coles, A. J., Compston, D. A., Selmaj, K. W., Lake, S. L., Moran, S., Margolin, D. H., Norris, K. &Tandon, P. K. (2008). Alemtuzumab vs. interferon beta-1a in early multiple sclerosis. *N Engl J Med* 359(17): 1786-1801.

Compston, A. &Coles, A. (2002). Multiple sclerosis. *Lancet* 359(9313): 1221-1231.

Compston, A. &Coles, A. (2008). Multiple sclerosis. *Lancet* 372(9648): 1502-1517.

Confavreux, C., Aimard, G. &Devic, M. (1980). Course and prognosis of multiple sclerosis assessed by the computerized data processing of 349 patients. *Brain* 103(2): 281-300.

Confavreux, C. &Vukusic, S. (2006a). Age at disability milestones in multiple sclerosis. *Brain* 129(Pt 3): 595-605.

Confavreux, C. &Vukusic, S. (2006b). Natural history of multiple sclerosis: a unifying concept. *Brain* 129(Pt 3): 606-616.

Confavreux, C., Vukusic, S. &Adeleine, P. (2003). Early clinical predictors and progression of irreversible disability in multiple sclerosis: an amnesic process. *Brain* 126(Pt 4): 770-782.

Confavreux, C., Vukusic, S., Moreau, T. &Adeleine, P. (2000). Relapses and progression of disability in multiple sclerosis. *N Engl J Med* 343(20): 1430-1438.

Cooke, F. J., Blamire, A. M., Manners, D. N., Styles, P. &Rajagopalan, B. (2004). Quantitative proton magnetic resonance spectroscopy of the cervical spinal cord. *Magn Reson Med* 51(6): 1122-1128.

Cory, D. G. &Garroway, A. N. (1990). Measurement of Translational Displacement Probabilities by Nmr - an Indicator of Compartmentation. *Magnetic Resonance in Medicine* 14(3): 435-444.

Cottrell, D. A., Kremenchutzky, M., Rice, G. P., Koopman, W. J., Hader, W., Baskerville, J. &Ebers, G. C. (1999). The natural history of multiple sclerosis: a geographically based study. 5. The clinical features and natural history of primary progressive multiple sclerosis. *Brain* 122 (Pt 4): 625-639.

Craner, M. J., Hains, B. C., Lo, A. C., Black, J. A. &Waxman, S. G. (2004a). Co-localization of sodium channel Nav1.6 and the sodium-calcium exchanger at sites of axonal injury in the spinal cord in EAE. *Brain* 127(Pt 2): 294-303.

Craner, M. J., Newcombe, J., Black, J. A., Hartle, C., Cuzner, M. L. &Waxman, S. G. (2004b). Molecular changes in neurons in multiple sclerosis: altered axonal expression of Nav1.2 and Nav1.6 sodium channels and Na+/Ca2+ exchanger. *Proc Natl Acad Sci U S A* 101(21): 8168-8173.

Cross, A. H., Manning, P. T., Stern, M. K. &Misko, T. P. (1997). Evidence for the production of peroxynitrite in inflammatory CNS demyelination. *J Neuroimmunol* 80(1-2): 121-130.

Cruz-Sanchez, F. F., Moral, A., Tolosa, E., de Belleroche, J. &Rossi, M. L. (1998). Evaluation of neuronal loss, astrocytosis and abnormalities of cytoskeletal components of large motor neurons in the human anterior horn in aging. *Journal of Neural Transmission* 105(6-7): 689-701.

Cutter, G. R., Baier, M. L., Rudick, R. A., Cookfair, D. L., Fischer, J. S., Petkau, J., Syndulko, K., Weinshenker, B. G., Antel, J. P., Confavreux, C., Ellison, G. W., Lublin, F., Miller, A. E., Rao, S. M., Reingold, S., Thompson, A. &Willoughby, E. (1999). Development of a multiple sclerosis functional composite as a clinical trial outcome measure. *Brain* 122 (Pt 5): 871-882.

Dani, K. A., An, L., Henning, E. C., Shen, J. &Warach, S. (2012). Multivoxel MR spectroscopy in acute ischemic stroke: comparison to the stroke protocol MRI. *Stroke* 43(11): 2962-2967.

Davie, C. A., Hawkins, C. P., Barker, G. J., Brennan, A., Tofts, P. S., Miller, D. H. &McDonald, W. I. (1993). Detection of myelin breakdown products by proton magnetic resonance spectroscopy. *Lancet* 341(8845): 630-631.

Davie, C. A., Hawkins, C. P., Barker, G. J., Brennan, A., Tofts, P. S., Miller, D. H. &McDonald, W. I. (1994). Serial proton magnetic resonance spectroscopy in acute multiple sclerosis lesions. *Brain* 117(1): 49-58.

Day, B. L., Steiger, M. J., Thompson, P. D. &Marsden, C. D. (1993). Effect of vision and stance width on human body motion when standing: implications for afferent control of lateral sway. *J Physiol* 469: 479-499.

De Stefano, N., Matthews, P. M., Antel, J. P., Preul, M., Francis, G. &Arnold, D. L. (1995a). Chemical pathology of acute demyelinating lesions and its correlation with disability. *Ann Neurol* 38(6): 901-909.

De Stefano, N., Matthews, P. M. &Arnold, D. L. (1995b). Reversible decreases in N-acetylaspartate after acute brain injury. *Magn Reson Med* 34(5): 721-727.

De Stefano, N., Matthews, P. M., Fu, L., Narayanan, S., Stanley, J., Francis, G. S., Antel, J. P. &Arnold, D. L. (1998). Axonal damage correlates with disability in patients with relapsing-remitting multiple sclerosis. Results of a longitudinal magnetic resonance spectroscopy study. *Brain* 121 (Pt 8): 1469-1477.

Degaonkar, M. N., Khubchandhani, M., Dhawan, J. K., Jayasundar, R. &Jagannathan, N. R. (2002). Sequential proton MRS study of brain metabolite changes monitored during a complete pathological cycle of demyelination and remyelination in a lysophosphatidyl choline (LPC)-induced experimental demyelinating lesion model. *NMR Biomed* 15(4): 293-300.

Degaonkar, M. N., Pomper, M. G. &Barker, P. B. (2005). Quantitative proton magnetic resonance spectroscopic imaging: regional variations in the corpus callosum and cortical gray matter. *J Magn Reson Imaging* 22(2): 175-179.

Deneeling, J. N. D., Beks, P. J., Bertelsmann, F. W., Heine, R. J. &Bouter, L. M. (1994). Sensory Thresholds in Older Adults - Reproducibility and Reference Values. *Muscle Nerve* 17(4): 454-461.

Di Pauli, F., Reindl, M., Ehling, R., Schautzer, F., Gneiss, C., Lutterotti, A., O'Reilly, E., Munger, K., Deisenhammer, F., Ascherio, A. &Berger, T. (2008). Smoking is a risk factor for early conversion to clinically definite multiple sclerosis. *Mult Scler* 14(8): 1026-1030.

Disanto, G., Chaplin, G., Morahan, J. M., Giovannoni, G., Hypponen, E., Ebers, G. C. &Ramagopalan, S. V. (2012). Month of birth, vitamin D and risk of immune mediated disease: a case control study. *BMC Med* 10(1): 69.

Dong, X. X., Wang, Y. &Qin, Z. H. (2009). Molecular mechanisms of excitotoxicity and their relevance to pathogenesis of neurodegenerative diseases. *Acta Pharmacol Sin* 30(4): 379-387.

Ebers, G. C. (2004). The natural history of primary progressive multiple sclerosis. *Mult Scler* 10: S8-15.

Ebers, G. C., Bulman, D. E., Sadovnick, A. D., Paty, D. W., Warren, S., Hader, W., Murray, T. J., Seland, T. P., Duquette, P., Grey, T. &et al. (1986). A population-based study of multiple sclerosis in twins. *N Engl J Med* 315(26): 1638-1642.

Ebers, G. C., Koopman, W. J., Hader, W., Sadovnick, A. D., Kremenchutzky, M., Mandalfino, P., Wingerchuk, D. M., Baskerville, J. &Rice, G. P. (2000). The natural history of multiple sclerosis: a geographically based study: 8: familial multiple sclerosis. *Brain* 123 Pt 3: 641-649.

Ebers, G. C., Sadovnick, A. D. &Risch, N. J. (1995). A genetic basis for familial aggregation in multiple sclerosis. Canadian Collaborative Study Group. *Nature* 377(6545): 150-151.

Edden, R. A., Bonekamp, D., Smith, M. A., Dubey, P. &Barker, P. B. (2007). Proton MR spectroscopic imaging of the medulla and cervical spinal cord. *J Magn Reson Imaging* 26(4): 1101-1105.

Egerton, A., Brugger, S., Raffin, M., Barker, G. J., Lythgoe, D. J., McGuire, P. K. &Stone, J. M. (2012). Anterior cingulate glutamate levels related to clinical status following treatment in first-episode schizophrenia. *Neuropsychopharmacology* 37(11): 2515-2521.

Emre, M. &de Decker, C. (1992). Effects of cigarette smoking on motor functions in patients with multiple sclerosis. *Arch Neurol* 49(12): 1243-1247.

Engelhardt, B. &Ransohoff, R. M. (2005). The ins and outs of T-lymphocyte trafficking to the CNS: anatomical sites and molecular mechanisms. *Trends Immunol* 26(9): 485-495.

Evangelou, N., DeLuca, G. C., Owens, T. &Esiri, M. M. (2005). Pathological study of spinal cord atrophy in multiple sclerosis suggests limited role of local lesions. *Brain* 128(Pt 1): 29-34.

Evangelou, N., Esiri, M. M., Smith, S., Palace, J. &Matthews, P. M. (2000). Quantitative pathological evidence for axonal loss in normal appearing white matter in multiple sclerosis. *Ann Neurol* 47(3): 391-395.

Evangelou, N., Konz, D., Esiri, M. M., Smith, S., Palace, J. &Matthews, P. M. (2001). Size-selective neuronal changes in the anterior optic pathways suggest a differential susceptibility to injury in multiple sclerosis. *Brain* 124(Pt 9): 1813-1820.

Fan, G., Wu, Z., Pan, S. &Guo, Q. (2003). Quantitative study of MR T1 and T2 relaxation times and 1HMRS in gray matter of normal adult brain. *Chin Med J (Engl)* 116(3): 400-404.

Farrell, J. A., Smith, S. A., Gordon-Lipkin, E. M., Reich, D. S., Calabresi, P. A. &van Zijl, P. C. (2008). High b-value q-space diffusion-weighted MRI of the human cervical spinal cord in vivo: feasibility and application to multiple sclerosis. *Magn Reson Med* 59(5): 1079-1089.

Farrell, J. A., Zhang, J., Jones, M. V., Deboy, C. A., Hoffman, P. N., Landman, B. A., Smith, S. A., Reich, D. S., Calabresi, P. A. &van Zijl, P. C. (2010). q-space and conventional diffusion imaging of axon and myelin damage in the rat spinal cord after axotomy. *Magn Reson Med* 63(5): 1323-1335.

Fernando, K. T., McLean, M. A., Chard, D. T., MacManus, D. G., Dalton, C. M., Miszkiel, K. A., Gordon, R. M., Plant, G. T., Thompson, A. J. &Miller, D. H. (2004). Elevated white matter myo-inositol in clinically isolated syndromes suggestive of multiple sclerosis. *Brain* 127(Pt 6): 1361-1369.

Filippi, M., Bozzali, M., Rovaris, M., Gonen, O., Kesavadas, C., Ghezzi, A., Martinelli, V., Grossman, R. I., Scotti, G., Comi, G. &Falini, A. (2003). Evidence for widespread axonal damage at the earliest clinical stage of multiple sclerosis. *Brain* 126(Pt 2): 433-437.

Filippi, M. &Rocca, M. A. (2011). MR imaging of multiple sclerosis. *Radiology* 259(3): 659-681.

Fischer, J. S., Rudick, R. A., Cutter, G. R. &Reingold, S. C. (1999). The Multiple Sclerosis Functional Composite Measure (MSFC): an integrated approach to MS clinical outcome assessment. National MS Society Clinical Outcomes Assessment Task Force. *Mult Scler* 5(4): 244-250.

Fisniku, L. K., Brex, P. A., Altmann, D. R., Miszkiel, K. A., Benton, C. E., Lanyon, R., Thompson, A. J. &Miller, D. H. (2008). Disability and T2 MRI lesions: a 20-year follow-up of patients with relapse onset of multiple sclerosis. *Brain* 131(Pt 3): 808-817.

Flugel, A., Berkowicz, T., Ritter, T., Labeur, M., Jenne, D. E., Li, Z., Ellwart, J. W., Willem, M., Lassmann, H. &Wekerle, H. (2001). Migratory activity and functional changes of green fluorescent effector cells before and during experimental autoimmune encephalomyelitis. *Immunity* 14(5): 547-560.

Fox, R. J., Thompson, A., Baker, D., Baneke, P., Brown, D., Browne, P., Chandraratna, D., Ciccarelli, O., Coetzee, T., Comi, G., Feinstein, A., Kapoor, R., Lee, K., Salvetti, M., Sharrock, K., Toosy, A., Zaratin, P. &Zuidwijk, K. (2012). Setting a research agenda for progressive multiple sclerosis: the International Collaborative on Progressive MS. *Mult Scler* 18(11): 1534-1540.

Frahm, J., Bruhn, H., Gyngell, M. L., Merboldt, K. D., Hanicke, W. &Sauter, R. (1989). Localized High-Resolution Proton Nmr-Spectroscopy Using Stimulated Echoes - Initial Applications to Human-Brain Invivo. *Magnetic Resonance in Medicine* 9(1): 79-93.

Franklin, R. J. &Ffrench-Constant, C. (2008). Remyelination in the CNS: from biology to therapy. *Nat Rev Neurosci* 9(11): 839-855.

Franklin, R. J., ffrench-Constant, C., Edgar, J. M. &Smith, K. J. (2012). Neuroprotection and repair in multiple sclerosis. *Nat Rev Neurol* 8(11): 624-634.

Franklin, R. J. &Gallo, V. (2014). The translational biology of remyelination: Past, present, and future. *Glia* 62(11): 1905-1915.

Freund, P., Wheeler-Kingshott, C., Jackson, J., Miller, D., Thompson, A. &Ciccarelli, O. (2010). Recovery after spinal cord relapse in multiple sclerosis is predicted by radial diffusivity. *Mult Scler* 16(10): 1193-1202.

Friese, M. A., Schattling, B. &Fugger, L. (2014). Mechanisms of neurodegeneration and axonal dysfunction in multiple sclerosis. *Nat Rev Neurol* 10(4): 225-238.

Frischer, J. M., Bramow, S., Dal-Bianco, A., Lucchinetti, C. F., Rauschka, H., Schmidbauer, M., Laursen, H., Sorensen, P. S. &Lassmann, H. (2009). *The relation between inflammation and neurodegeneration in multiple sclerosis brains.*

Fu, L., Matthews, P. M., De Stefano, N., Worsley, K. J., Narayanan, S., Francis, G. S., Antel, J. P., Wolfson, C. &Arnold, D. L. (1998). Imaging axonal damage of normal-appearing white matter in multiple sclerosis. *Brain* 121 (Pt 1): 103-113.

Fukazawa, T., Yamasaki, K., Ito, H., Kikuchi, S., Minohara, M., Horiuchi, I., Tsukishima, E., Sasaki, H., Hamada, T., Nishimura, Y., Tashiro, K. &Kira, J. (2000). Both the HLA-CPB1 and -DRB1 alleles correlate with risk for multiple sclerosis in Japanese: clinical phenotypes and gender as important factors. *Tissue Antigens* 55(3): 199-205.

Gale, C. R. &Martyn, C. N. (1995). Migrant studies in multiple sclerosis. *Prog Neurobiol* 47(4-5): 425-448.

Garrow, A. P. &Boulton, A. J. (2006). Vibration perception threshold--a valuable assessment of neural dysfunction in people with diabetes. *Diabetes Metab Res Rev* 22(5): 411-419.

Gasparovic, C., Song, T., Devier, D., Bockholt, H. J., Caprihan, A., Mullins, P. G., Posse, S., Jung, R. E. &Morrison, L. A. (2006). Use of tissue water as a concentration reference for proton spectroscopic imaging. *Magn Reson Med* 55(6): 1219-1226.

Gass, A., Niendorf, T. &Hirsch, J. G. (2001). Acute and chronic changes of the apparent diffusion coefficient in neurological disorders—biophysical mechanisms and possible underlying histopathology. *J Neurol Sci* 186, Supplement 1(0): S15-S23.

Ge, Y. L., Grossman, R. I., Babb, J. S., Rabin, M. L., Mannon, L. J. &Kolson, D. L. (2002). Age-related total gray matter and white matter changes in normal adult brain. Part I: Volumetric MR imaging analysis. *American Journal of Neuroradiology* 23(8): 1327-1333.

Gilgun-Sherki, Y., Panet, H., Melamed, E. &Offen, D. (2003). Riluzole suppresses experimental autoimmune encephalomyelitis: implications for the treatment of multiple sclerosis. *Brain Res* 989(2): 196-204.

Gilmore, C. P., Bo, L., Owens, T., Lowe, J., Esiri, M. M. &Evangelou, N. (2006). Spinal cord gray matter demyelination in multiple sclerosis-a novel pattern of residual plaque morphology. *Brain Pathol* 16(3): 202-208.

Gilmore, C. P., DeLuca, G. C., Bo, L., Owens, T., Lowe, J., Esiri, M. M. &Evangelou, N. (2005). Spinal cord atrophy in multiple sclerosis caused by white matter volume loss. *Arch Neurol* 62(12): 1859-1862.

Gomez-Anson, B., MacManus, D. G., Parker, G. J., Davie, C. A., Barker, G. J., Moseley, I. F., McDonald, W. I. &Miller, D. H. (2000). In vivo 1H-magnetic resonance spectroscopy of the spinal cord in humans. *Neuroradiology* 42(7): 515-517.

Gonzalez-Toledo, E., Kelley, R. E. &Minagar, A. (2006). Role of magnetic resonance spectroscopy in diagnosis and management of multiple sclerosis. *Neurol Res* 28(3): 280-283.

Goodkin, D. E., Hertsgaard, D. &Seminary, J. (1988). Upper extremity function in multiple sclerosis: improving assessment sensitivity with box-and-block and nine-hole peg tests. *Arch Phys Med Rehabil* 69(10): 850-854.

Granieri, E. &Casetta, I. (1997). Selected reviews common childhood and adolescent infections and multiple sclerosis. *Neurology* 49(2 Suppl 2): S42-54.

Grillner, S., Wallen, P., Saitoh, K., Kozlov, A. &Robertson, B. (2008). Neural bases of goal-directed locomotion in vertebrates - An overview. *Brain Research Reviews* 57(1): 2-12.

Group, O. N. S. (2008). Multiple sclerosis risk after optic neuritis: final optic neuritis treatment trial follow-up. *Arch Neurol* 65(6): 727-732.

Gulani, V., Webb, A. G., Duncan, I. D. &Lauterbur, P. C. (2001). Apparent diffusion tensor measurements in myelin-deficient rat spinal cords. *Magn Reson Med* 45(2): 191-195.

Guo, A. C., Jewells, V. L. &Provenzale, J. M. (2001). Analysis of Normal-Appearing White Matter in Multiple Sclerosis: Comparison of Diffusion Tensor MR Imaging and Magnetization Transfer Imaging. *American Journal of Neuroradiology* 22(10): 1893-1900.

Gupta, A., Hasan, M., Chander, R. &Kapoor, N. K. (1991). Age-related elevation of lipid peroxidation products: diminution of superoxide dismutase activity in the central nervous system of rats. *Gerontology* 37(6): 305-309.

Gurwitz, D. &Kloog, Y. (1998). Peroxynitrite generation might explain elevated glutamate and aspartate levels in multiple sclerosis cerebrospinal fluid. *Eur J Clin Invest* 28(9): 760-761.

Haase, A., Frahm, J., Hanicke, W. &Matthaei, D. (1985). 1H NMR chemical shift selective (CHESS) imaging. *Phys Med Biol* 30(4): 341-344.

Haga, K. K., Khor, Y. P., Farrall, A. &Wardlaw, J. M. (2009). A systematic review of brain metabolite changes, measured with 1H magnetic resonance spectroscopy, in healthy aging. *Neurobiol Aging* 30(3): 353-363.

Hahn, E. L. (1950). Spin Echoes. *Physical Review* 80(4): 580-594.

Hancu, I. (2009). Optimized glutamate detection at 3T. *J Magn Reson Imaging* 30(5): 1155-1162.

Hartley, M. D., Altowaijri, G. &Bourdette, D. (2014). Remyelination and multiple sclerosis: therapeutic approaches and challenges. *Curr Neurol Neurosci Rep* 14(10): 485.

Hattori, N., Abe, K., Sakoda, S. &Sawada, T. (2002). Proton MR spectroscopic study at 3 Tesla on glutamate/glutamine in Alzheimer's disease. *Neuroreport* 13(1): 183-186.

Hauser, S. L., Waubant, E., Arnold, D. L., Vollmer, T., Antel, J., Fox, R. J., Bar-Or, A., Panzara, M., Sarkar, N., Agarwal, S., Langer-Gould, A. &Smith, C. H. (2008). B-cell depletion with rituximab in relapsing-remitting multiple sclerosis. *N Engl J Med* 358(7): 676-688.

Hawkins, S. A. &McDonnell, G. V. (1999). Benign multiple sclerosis? Clinical course, long term follow up, and assessment of prognostic factors. *J Neurol Neurosurg Psychiatry* 67(2): 148-152.

He, J., Inglese, M., Li, B. S., Babb, J. S., Grossman, R. I. &Gonen, O. (2005). Relapsing-remitting multiple sclerosis: metabolic abnormality in nonenhancing lesions and normal-appearing white matter at MR imaging: initial experience. *Radiology* 234(1): 211-217.

Headley, P. M. &Grillner, S. (1990). Excitatory amino acids and synaptic transmission: the evidence for a physiological function. *Trends Pharmacol Sci* 11(5): 205-211.

Henning, A., Schar, M., Kollias, S. S., Boesiger, P. &Dydak, U. (2008). Quantitative magnetic resonance spectroscopy in the entire human cervical spinal cord and beyond at 3T. *Magn Reson Med* 59(6): 1250-1258.

Hernan, M. A., Jick, S. S., Logroscino, G., Olek, M. J., Ascherio, A. &Jick, H. (2005). Cigarette smoking and the progression of multiple sclerosis. *Brain* 128(Pt 6): 1461-1465.

Hittmair, K., Mallek, R., Prayer, D., Schindler, E. G. &Kollegger, H. (1996). Spinal cord lesions in patients with multiple sclerosis: comparison of MR pulse sequences. *AJNR Am J Neuroradiol* 17(8): 1555-1565.

Hobart, J. C., Riazi, A., Lamping, D. L., Fitzpatrick, R. &Thompson, A. J. (2003). Measuring the impact of MS on walking ability: the 12-Item MS Walking Scale (MSWS-12). *Neurology* 60(1): 31-36.

Holly, L. T., Freitas, B., McArthur, D. L. &Salamon, N. (2009). Proton magnetic resonance spectroscopy to evaluate spinal cord axonal injury in cervical spondylotic myelopathy. *J Neurosurg Spine* 10(3): 194-200.

Honig, L. S. &Sheremata, W. A. (1989). Magnetic resonance imaging of spinal cord lesions in multiple sclerosis. *J Neurol Neurosurg Psychiatry* 52(4): 459-466.

Horsfield, M. A., Sala, S., Neema, M., Absinta, M., Bakshi, A., Sormani, M. P., Rocca, M. A., Bakshi, R. &Filippi, M. (2010). Rapid semi-automatic segmentation of the spinal cord from magnetic resonance images: application in multiple sclerosis. *Neuroimage* 50(2): 446-455.

Horska, A. &Barker, P. B. (2010). Imaging of brain tumors: MR spectroscopy and metabolic imaging. *Neuroimaging Clin N Am* 20(3): 293-310.

Hugon, J., Vallat, J. M. &Dumas, M. (1996). [Role of glutamate and excitotoxicity in neurologic diseases]. *Rev Neurol (Paris)* 152(4): 239-248.

Hurd, R., Sailasuta, N., Srinivasan, R., Vigneron, D. B., Pelletier, D. &Nelson, S. J. (2004). Measurement of brain glutamate using TE-averaged PRESS at 3T. *Magn Reson Med* 51(3): 435-440.

Ikuta, F. &Zimmerman, H. M. (1976). Distribution of plaques in seventy autopsy cases of multiple sclerosis in the United States. *Neurology* 26(6 PT 2): 26-28.

Ingle, G. T., Stevenson, V. L., Miller, D. H. &Thompson, A. J. (2003). Primary progressive multiple sclerosis: a 5-year clinical and MR study. *Brain* 126(Pt 11): 2528-2536.

Inglese, M., Li, B. S., Rusinek, H., Babb, J. S., Grossman, R. I. &Gonen, O. (2003). Diffusely elevated cerebral choline and creatine in relapsing-remitting multiple sclerosis. *Magn Reson Med* 50(1): 190-195.

James, W. H. (1982). Concordance in twins and recurrence in sibships of multiple sclerosis. *Lancet* 1(8273): 690.

Johanson, C. E. (2008).Choroid plexus-cerebrospinal fluid circulatory dynamics: impact on brain growth, metabolism and repair. In *Neuroscience in Medicine*(Ed P. M. Conn). Springer Science & Business Media.

Jones, K. T. (2009).Gaussian Modeling of the Diffusion Signal. In *Diffusion MRI*, 37-54 (Eds H. Johansen-Berg and T. E. J. Behrens). London: Elsevier.

Kadota, T., Horinouchi, T. &Kuroda, C. (2001). Development and aging of the cerebrum: assessment with proton MR spectroscopy. *AJNR Am J Neuroradiol* 22(1): 128-135.

Kaiser, F. E. (1999). Erectile dysfunction in the aging man. *Medical Clinics of North America* 83(5): 1267-+.

Kaiser, L. G., Schuff, N., Cashdollar, N. &Weiner, M. W. (2005). Age-related glutamate and glutamine concentration changes in normal human brain: 1H MR spectroscopy study at 4 T. *Neurobiol Aging* 26(5): 665-672.

Kalkers, N. F., Barkhof, F., Bergers, E., van Schijndel, R. &Polman, C. H. (2002). The effect of the neuroprotective agent riluzole on MRI parameters in primary progressive multiple sclerosis: a pilot study. *Mult Scler* 8(6): 532-533.

Kanter, J. L., Narayana, S., Ho, P. P., Catz, I., Warren, K. G., Sobel, R. A., Steinman, L. &Robinson, W. H. (2006). Lipid microarrays identify key mediators of autoimmune brain inflammation. *Nat Med* 12(1): 138-143.

Kapoor, R., Furby, J., Hayton, T., Smith, K. J., Altmann, D. R., Brenner, R., Chataway, J., Hughes, R. A. &Miller, D. H. (2010). Lamotrigine for neuroprotection in secondary progressive multiple sclerosis: a randomised, double-blind, placebo-controlled, parallel-group trial. *Lancet Neurol* 9(7): 681-688.

Kearney, H., Miszkiel, K. A., Yiannakas, M. C., Ciccarelli, O. &Miller, D. H. (2013a). A pilot MRI study of white and grey matter involvement by multiple sclerosis spinal cord lesions. *Multiple Sclerosis and Related Disorders* 2(2): 103-108.

Kearney, H., Rocca, M. A., Valsasina, P., Balk, L., Sastre-Garriga, J., Reinhardt, J., Ruggieri, S., Rovira, A., Stippich, C., Kappos, L., Sprenger, T., Tortorella, P., Rovaris, M., Gasperini, C., Montalban, X., Geurts, J. J., Polman, C. H., Barkhof, F., Filippi, M., Altmann, D. R., Ciccarelli, O., Miller, D. H. &Chard, D. T. (2014a). Magnetic resonance imaging correlates of physical disability in relapse onset multiple sclerosis of long disease duration. *Mult Scler* 20(1): 72-80.

Kearney, H., Yiannakas, M. C., Abdel-Aziz, K., Wheeler-Kingshott, C. A., Altmann, D. R., Ciccarelli, O. &Miller, D. H. (2013b). Improved MRI quantification of spinal cord atrophy in multiple sclerosis. *J Magn Reson Imaging*.

Kearney, H., Yiannakas, M. C., Samson, R. S., Wheeler-Kingshott, C. A., Ciccarelli, O. &Miller, D. H. (2014b). Investigation of magnetization transfer ratio-derived pial and subpial abnormalities in the multiple sclerosis spinal cord. *Brain* 137(Pt 9): 2456-2468.

Keiper, M. D., Grossman, R. I., Brunson, J. C. &Schnall, M. D. (1997). The low sensitivity of fluid-attenuated inversion-recovery MR in the detection of multiple sclerosis of the spinal cord. *AJNR Am J Neuroradiol* 18(6): 1035-1039.

Keller, J. N. &Mattson, M. P. (1998). Roles of lipid peroxidation in modulation of cellular signaling pathways, cell dysfunction, and death in the nervous system. *Rev Neurosci* 9(2): 105-116.

Kendi, A. T., Tan, F. U., Kendi, M., Yilmaz, S., Huvaj, S. &Tellioglu, S. (2004). MR spectroscopy of cervical spinal cord in patients with multiple sclerosis. *Neuroradiology* 46(9): 764-769.

Keough, M. B. &Yong, V. W. (2013). Remyelination therapy for multiple sclerosis. *Neurotherapeutics* 10(1): 44-54.

Khaleeli, Z., Ciccarelli, O., Manfredonia, F., Barkhof, F., Brochet, B., Cercignani, M., Dousset, V., Filippi, M., Montalban, X., Polman, C., Rovaris, M., Rovira, A., Sastre-Garriga, J., Vellinga, M., Miller, D. &Thompson, A. (2008). Predicting progression in primary progressive multiple sclerosis: a 10-year multicenter study. *Ann Neurol* 63(6): 790-793.

Khaleeli, Z., Sastre-Garriga, J., Ciccarelli, O., Miller, D. H. &Thompson, A. J. (2007). Magnetisation transfer ratio in the normal appearing white matter predicts progression of disability over 1 year in early primary progressive multiple sclerosis. *J Neurol Neurosurg Psychiatry* 78(10): 1076-1082.

Kidd, D., Thorpe, J. W., Thompson, A. J., Kendall, B. E., Moseley, I. F., MacManus, D. G., McDonald, W. I. &Miller, D. H. (1993). Spinal cord MRI using multi-array coils and fast spin echo: II. Findings in multiple sclerosis. *Neurology* 43(12): 2632.

Killestein, J., Kalkers, N. F. &Polman, C. H. (2005). Glutamate inhibition in MS: The neuroprotective properties of riluzole. *J Neurol Sci* 233: 113-115.

Kim, J. H., Budde, M. D., Liang, H. F., Klein, R. S., Russell, J. H., Cross, A. H. &Song, S. K. (2006). Detecting axon damage in spinal cord from a mouse model of multiple sclerosis. *Neurobiol Dis* 21(3): 626-632.

Kim, Y. G., Choi, G. H., Kim, D. H., Kim, Y. D., Kang, Y. K. &Kim, J. K. (2004). In vivo proton magnetic resonance spectroscopy of human spinal mass lesions. *J Spinal Disord Tech* 17(5): 405-411.

Kinnunen, E., Juntunen, J., Ketonen, L., Koskimies, S., Konttinen, Y. T., Salmi, T., Koskenvuo, M. &Kaprio, J. (1988). Genetic susceptibility to multiple sclerosis. A co-twin study of a nationwide series. *Arch Neurol* 45(10): 1108-1111.

Koch, M., van Harten, A., Uyttenboogaart, M. &De Keyser, J. (2007). Cigarette smoking and progression in multiple sclerosis. *Neurology* 69(15): 1515-1520.

Komiyama, Y., Nakae, S., Matsuki, T., Nambu, A., Ishigame, H., Kakuta, S., Sudo, K. &Iwakura, Y. (2006). IL-17 plays an important role in the development of experimental autoimmune encephalomyelitis. *J Immunol* 177(1): 566-573.

Kornek, B., Storch, M. K., Weissert, R., Wallstroem, E., Stefferl, A., Olsson, T., Linington, C., Schmidbauer, M. &Lassmann, H. (2000). Multiple sclerosis and chronic autoimmune encephalomyelitis: a comparative quantitative study of axonal injury in active, inactive, and remyelinated lesions. *Am J Pathol* 157(1): 267-276.

Kreis, R., Ernst, T. &Ross, B. D. (1993). Absolute Quantitation of Water and Metabolites in the Human Brain .2. Metabolite Concentrations. *Journal of Magnetic Resonance Series B* 102(1): 9-19.

Kurtzke, J. F. (1977). Geography in multiple sclerosis. *J Neurol* 215(1): 1-26.

Kurtzke, J. F. (1983). Rating neurologic impairment in multiple sclerosis: an expanded disability status scale (EDSS). *Neurology* 33(11): 1444-1452.

Lassmann, H. (2003). Axonal injury in multiple sclerosis. *J Neurol Neurosurg Psychiatry* 74(6): 695-697.

Latt, J., Nilsson, M., Malmborg, C., Rosquist, H., Wirestam, R., Sthlberg, F., Topgaard, D. &Brockstedt, S. (2007a). Accuracy of q-Space Related Parameters in MRI: Simulations and Phantom Measurements. *Medical Imaging, IEEE Transactions on* 26(11): 1437-1447.

Latt, J., Nilsson, M., Rydhog, A., Wirestam, R., Stahlberg, F. &Brockstedt, S. (2007b). Effects of restricted diffusion in a biological phantom: a q-space diffusion MRI study of asparagus stems at a 3T clinical scanner. *Magnetic Resonance Materials in Physics Biology and Medicine* 20(4): 213-222.

Leary, S. M., Silver, N. C., Stevenson, V. L., Barker, G. J., Miller, D. H. &Thompson, A. J. (1999). Magnetisation transfer of normal appearing white matter in primary progressive multiple sclerosis. *Mult Scler* 5(5): 313-316.

Lee, J. H., Arcinue, E. &Ross, B. D. (1994). Brief report: organic osmolytes in the brain of an infant with hypernatremia. *N Engl J Med* 331(7): 439-442.

Levy, L. M., Di Chiro, G., Brooks, R. A., Dwyer, A. J., Wener, L. &Frank, J. (1988). Spinal cord artifacts from truncation errors during MR imaging. *Radiology* 166(2): 479-483.

Lim, K. O. &Spielman, D. M. (1997). Estimating NAA in cortical gray matter with applications for measuring changes due to aging. *Magn Reson Med* 37(3): 372-377.

Lin, M. T., Simon, D. K., Ahn, C. H., Kim, L. M. &Beal, M. F. (2002). High aggregate burden of somatic mtDNA point mutations in aging and Alzheimer's disease brain. *Hum Mol Genet* 11(2): 133-145.

Lin, X., Tench, C. R., Evangelou, N., Jaspan, T. &Constantinescu, C. S. (2004). Measurement of spinal cord atrophy in multiple sclerosis. *J Neuroimaging* 14(3 Suppl): 20S-26S.

Lin, X., Tench, C. R., Turner, B., Blumhardt, L. D. &Constantinescu, C. S. (2003). Spinal cord atrophy and disability in multiple sclerosis over four years: application of a reproducible automated technique in monitoring disease progression in a cohort of the interferon beta-1a (Rebif) treatment trial. *J Neurol Neurosurg Psychiatry* 74(8): 1090-1094.

Liu, C., Edwards, S., Gong, Q., Roberts, N. &Blumhardt, L. D. (1999). Three dimensional MRI estimates of brain and spinal cord atrophy in multiple sclerosis. *J Neurol Neurosurg Psychiatry* 66(3): 323-330.

Lo, A. C., Black, J. A. &Waxman, S. G. (2002). Neuroprotection of axons with phenytoin in experimental allergic encephalomyelitis. *Neuroreport* 13(15): 1909-1912.

Losseff, N. A., Webb, S. L., O'Riordan, J. I., Page, R., Wang, L., Barker, G. J., Tofts, P. S., McDonald, W. I., Miller, D. H. &Thompson, A. J. (1996). Spinal cord atrophy and disability in multiple sclerosis. A new reproducible and sensitive MRI method with potential to monitor disease progression. *Brain* 119 (Pt 3): 701-708.

Loth, F., Yardimci, M. A. &Alperin, N. (2001). Hydrodynamic modeling of cerebrospinal fluid motion within the spinal cavity. *J Biomech Eng* 123(1): 71-79.

Lublin, F. D., Baier, M. &Cutter, G. (2003). Effect of relapses on development of residual deficit in multiple sclerosis. *Neurology* 61(11): 1528-1532.

Lublin, F. D. &Reingold, S. C. (1996). Defining the clinical course of multiple sclerosis: results of an international survey. National Multiple Sclerosis Society (USA) Advisory Committee on Clinical Trials of New Agents in Multiple Sclerosis. *Neurology* 46(4): 907-911.

Lucas, D. R. &Newhouse, J. P. (1957). The toxic effect of sodium L-glutamate on the inner layers of the retina. *AMA Arch Ophthalmol* 58(2): 193-201.

Lycklama a Nijeholt, G. J., Barkhof, F., Scheltens, P., Castelijns, J. A., Ader, H., van Waesberghe, J. H., Polman, C., Jongen, S. J. &Valk, J. (1997). MR of the spinal cord in multiple sclerosis: relation to clinical subtype and disability. *AJNR Am J Neuroradiol* 18(6): 1041-1048.

Lycklama a Nijeholt, G. J., Uitdehaag, B. M., Bergers, E., Castelijns, J. A., Polman, C. H. &Barkhof, F. (2000). Spinal cord magnetic resonance imaging in suspected multiple sclerosis. *Eur Radiol* 10(2): 368-376.

Lycklama, G., Thompson, A., Filippi, M., Miller, D., Polman, C., Fazekas, F. &Barkhof, F. (2003). Spinal-cord MRI in multiple sclerosis. *Lancet Neurol* 2(9): 555-562.

Mackenzie, I. S., Morant, S. V., Bloomfield, G. A., MacDonald, T. M. &O'Riordan, J. (2014). Incidence and prevalence of multiple sclerosis in the UK 1990-2010: a descriptive study in the General Practice Research Database. *J Neurol Neurosurg Psychiatry* 85(1): 76-84.

MacMillan, E., Tam, R., Zhao, Y., Vavasour, I., Li, D., Oger, J., Freedman, M., Kolind, S. &Traboulsee, A. (2015). Progressive multiple sclerosis exhibits decreasing glutamate and glutamine over two years. *Multiple Sclerosis Journal*.

Mader, I., Roser, W., Kappos, L., Hagberg, G., Seelig, J., Radue, E. W. &Steinbrich, W. (2000). Serial proton MR spectroscopy of contrast-enhancing multiple sclerosis plaques: absolute metabolic values over 2 years during a clinical pharmacological study. *AJNR Am J Neuroradiol* 21(7): 1220-1227.

Mahad, D., Ziabreva, I., Lassmann, H. &Turnbull, D. (2008). Mitochondrial defects in acute multiple sclerosis lesions. *Brain* 131(Pt 7): 1722-1735.

Mamata, H., Jolesz, F. A. &Maier, S. E. (2005). Apparent diffusion coefficient and fractional anisotropy in spinal cord: age and cervical spondylosis-related changes. *J Magn Reson Imaging* 22(1): 38-43.

Mansfield, P. &Pykett, I. L. (1978). Biological and medical imaging by NMR. . *J Magn Reson* 29(2): 355-373.

Marcio, J., Jorge, N. &Wexner, S. D. (1993). Etiology and Management of Fecal Incontinence. *Diseases of the Colon & Rectum* 36(1): 77-97.

Marliani, A. F., Clementi, V., Albini-Riccioli, L., Agati, R. &Leonardi, M. (2007). Quantitative proton magnetic resonance spectroscopy of the human cervical spinal cord at 3 tesla. *Magnetic Resonance in Medicine* 57(1): 160-163.

Marliani, A. F., Clementi, V., Albini Riccioli, L., Agati, R., Carpenzano, M., Salvi, F. &Leonardi, M. (2010). Quantitative cervical spinal cord 3T proton MR spectroscopy in multiple sclerosis. *AJNR Am J Neuroradiol* 31(1): 180-184.

Martin, R., McFarland, H. F. &McFarlin, D. E. (1992). Immunological aspects of demyelinating diseases. *Annu Rev Immunol* 10: 153-187.

Mayer, D. &Spielman, D. M. (2005). Detection of glutamate in the human brain at 3 T using optimized constant time point resolved spectroscopy. *Magn Reson Med* 54(2): 439-442.

McCrone, P., Heslin, M., Knapp, M., Bull, P. &Thompson, A. (2008). Multiple sclerosis in the UK: service use, costs, quality of life and disability. *Pharmacoeconomics* 26(10): 847-860.

McKnight, T. R. (2004). Proton magnetic resonance spectroscopic evaluation of brain tumor metabolism. *Seminars in Oncology* 31(5): 605-617.

Menn, B., Garcia-Verdugo, J. M., Yaschine, C., Gonzalez-Perez, O., Rowitch, D. &Alvarez-Buylla, A. (2006). Origin of oligodendrocytes in the subventricular zone of the adult brain. *J Neurosci* 26(30): 7907-7918.

Mews, I., Bergmann, M., Bunkowski, S., Gullotta, F. &Bruck, W. (1998). Oligodendrocyte and axon pathology in clinically silent multiple sclerosis lesions. *Mult Scler* 4(2): 55-62.

Michaelis, T., Merboldt, K. D., Bruhn, H., Hanicke, W. &Frahm, J. (1993). Absolute concentrations of metabolites in the adult human brain in vivo: quantification of localized proton MR spectra. *Radiology* 187(1): 219-227.

Mikulis, D. J., Wood, M. L., Zerdoner, O. A. &Poncelet, B. P. (1994). Oscillatory motion of the normal cervical spinal cord. *Radiology* 192(1): 117-121.

Miller, D., Barkhof, F., Montalban, X., Thompson, A. &Filippi, M. (2005). Clinically isolated syndromes suggestive of multiple sclerosis, part I: natural history, pathogenesis, diagnosis, and prognosis. *Lancet Neurol* 4(5): 281-288.

Miller, D. H., Chard, D. T. &Ciccarelli, O. (2012). Clinically isolated syndromes. *Lancet Neurol* 11(2): 157-169.

Miller, D. H., Hammond, S. R., McLeod, J. G., Purdie, G. &Skegg, D. C. (1990). Multiple sclerosis in Australia and New Zealand: are the determinants genetic or environmental? *J Neurol Neurosurg Psychiatry* 53(10): 903-905.

Miller, D. H., Weinshenker, B. G., Filippi, M., Banwell, B. L., Cohen, J. A., Freedman, M. S., Galetta, S. L., Hutchinson, M., Johnson, R. T., Kappos, L., Kira, J., Lublin, F. D., McFarland, H. F., Montalban, X., Panitch, H., Richert, J. R., Reingold, S. C. &Polman, C. H. (2008). Differential diagnosis of suspected multiple sclerosis: a consensus approach. *Mult Scler* 14(9): 1157-1174.

Minagar, A. &Alexander, J. S. (2003). Blood-brain barrier disruption in multiple sclerosis. *Mult Scler* 9(6): 540-549.

Moe-Nilssen, R. (1998). A new method for evaluating motor control in gait under real-life environmental conditions. Part 2: Gait analysis. *Clin Biomech (Bristol, Avon)* 13(4-5): 328-335.

Moffett, J. R., Ross, B., Arun, P., Madhavarao, C. N. &Namboodiri, A. M. (2007). N-Acetylaspartate in the CNS: from neurodiagnostics to neurobiology. *Prog Neurobiol* 81(2): 89-131.

Montomoli, C., Prokopenko, I., Caria, A., Ferrai, R., Mander, A., Seaman, S., Musu, L., Piras, M. L., Ticca, A. F., Murgia, S. B. &Bernardinelli, L. (2002). Multiple sclerosis recurrence risk for siblings in an isolated population of Central Sardinia, Italy. *Genet Epidemiol* 22(3): 265-271.

Moreno-Torres, A., Pujol, J., Soriano-Mas, C., Deus, J., Iranzo, A. &Santamaria, J. (2005). Age-related metabolic changes in the upper brainstem tegmentum by MR spectroscopy. *Neurobiol Aging* 26(7): 1051-1059.

Morris, G. A. &Freeman, R. (1978). Selective excitation in Fourier transform nuclear magnetic resonance. *Journal of Magnetic Resonance (1969)* 29(3): 433-462.

Moscarello, M. A., Mastronardi, F. G. &Wood, D. D. (2007). The role of citrullinated proteins suggests a novel mechanism in the pathogenesis of multiple sclerosis. *Neurochem Res* 32(2): 251-256.

Muhlert, N., Atzori, M., De Vita, E., Thomas, D. L., Samson, R. S., Wheeler-Kingshott, C. A., Geurts, J. J., Miller, D. H., Thompson, A. J. &Ciccarelli, O. (2014). Memory in multiple sclerosis is linked to glutamate concentration in grey matter regions. *J Neurol Neurosurg Psychiatry*.

Mumford, C. J., Wood, N. W., Kellar-Wood, H., Thorpe, J. W., Miller, D. H. &Compston, D. A. (1994). The British Isles survey of multiple sclerosis in twins. *Neurology* 44(1): 11-15.

Munch, M., Riisom, K., Christensen, T., Moller-Larsen, A. &Haahr, S. (1998). The significance of Epstein-Barr virus seropositivity in multiple sclerosis patients? *Acta Neurol Scand* 97(3): 171-174.

Munzel, E. J. &Williams, A. (2013). Promoting remyelination in multiple sclerosis-recent advances. *Drugs* 73(18): 2017-2029.

Murray, M. P., Kory, R. C. &Clarkson, B. H. (1969). Walking Patterns in Healthy Old Men. *Journals of Gerontology* 24(2): 169-&.

Naismith, R. T., Xu, J., Tutlam, N. T., Lancia, S., Trinkaus, K., Song, S. K. &Cross, A. H. (2012). Diffusion tensor imaging in acute optic neuropathies: predictor of clinical outcomes. *Arch Neurol* 69(1): 65-71.

Naressi, A., Couturier, C., Castang, I., de Beer, R. &Graveron-Demilly, D. (2001a). Java-based graphical user interface for MRUI, a software package for quantitation of in vivo/medical magnetic resonance spectroscopy signals. *Comput Biol Med* 31(4): 269-286.

Naressi, A., Couturier, C., Devos, J. M., Janssen, M., Mangeat, C., de Beer, R. &Graveron-Demilly, D. (2001b). Java-based graphical user interface for the MRUI quantitation package. *MAGMA* 12(2-3): 141-152.

Nijeholt, G. J., van Walderveen, M. A., Castelijns, J. A., van Waesberghe, J. H., Polman, C., Scheltens, P., Rosier, P. F., Jongen, P. J. &Barkhof, F. (1998). Brain and spinal cord abnormalities in multiple sclerosis. Correlation between MRI parameters, clinical subtypes and symptoms. *Brain* 121 (Pt 4): 687-697.

Nijland, P. G., Witte, M. E., van Het Hof, B., van der Pol, S., Bauer, J., Lassmann, H., van der Valk, P., de Vries, H. E. &van Horssen, J. (2014). Astroglial PGC-1alpha increases mitochondrial antioxidant capacity and suppresses inflammation: implications for multiple sclerosis. *Acta Neuropathol Commun* 2(1): 170.

Nonaka, N., Goto, N., Goto, J., Shibata, M. &Nakamura, M. (2008). Morphometric evaluation of the aging process in various human nerve fibers. *Okajimas Folia Anat Jpn* 85(3): 103-106.

Noseworthy, J. H., Patty, D. W., Wonacott, T., Feasby, T. &Ebers, G. C. (1983). Multiple sclerosis after age 50. *Neurology* 33(1537-44): 1537.

Noseworthy, J. H., Vandervoort, M. K., Wong, C. J. &Ebers, G. C. (1990). Interrater variability with the Expanded Disability Status Scale (EDSS) and Functional Systems (FS) in a multiple sclerosis clinical trial. The Canadian Cooperation MS Study Group. *Neurology* 40(6): 971-975.

Nossin-Manor, R., Duvdevani, R. &Cohen, Y. (2005). Effect of experimental parameters on high b-value q-space MR images of excised rat spinal cord. *Magnetic Resonance in Medicine* 54(1): 96-104.

O'Gorman, R. L., Michels, L., Edden, R. A., Murdoch, J. B. &Martin, E. (2011). In vivo detection of GABA and glutamate with MEGA-PRESS: reproducibility and gender effects. *J Magn Reson Imaging* 33(5): 1262-1267.

O'Riordan, J. I., Losseff, N. A., Phatouros, C., Thompson, A. J., Moseley, I. F., MacManus, D. G., McDonald, W. I. &Miller, D. H. (1998). Asymptomatic spinal cord lesions in clinically isolated optic nerve, brain stem, and spinal cord syndromes suggestive of demyelination. *J Neurol Neurosurg Psychiatry* 64(3): 353-357.

Oh, J., Saidha, S., Chen, M., Smith, S. A., Prince, J., Jones, C., Diener-West, M., van Zijl, P. C., Reich, D. S. &Calabresi, P. A. (2013a). Spinal cord quantitative MRI discriminates between disability levels in multiple sclerosis. *Neurology* 80(6): 540-547.

Oh, J., Zackowski, K., Chen, M., Newsome, S., Saidha, S., Smith, S. A., Diener-West, M., Prince, J., Jones, C. K., Van Zijl, P. C., Calabresi, P. A. &Reich, D. S. (2013b). Multiparametric MRI correlates of sensorimotor function in the spinal cord in multiple sclerosis. *Mult Scler* 19(4): 427-435.

Oleen-Burkey, M., Castelli-Haley, J., Lage, M. J. &Johnson, K. P. (2012). Burden of a multiple sclerosis relapse: the patient's perspective. *Patient* 5(1): 57-69.

Olney, J. W. (1969). Brain lesions, obesity, and other disturbances in mice treated with monosodium glutamate. *Science* 164(3880): 719-721.

Olney, J. W. (1971). Glutamate-induced neuronal necrosis in the infant mouse hypothalamus. An electron microscopic study. *J Neuropathol Exp Neurol* 30(1): 75-90.

Olney, J. W., Adamo, N. J. &Ratner, A. (1971). Monosodium glutamate effects. *Science* 172(3980): 294.

Olney, J. W. &Sharpe, L. G. (1969). Brain lesions in an infant rhesus monkey treated with monsodium glutamate. *Science* 166(3903): 386-388.

Olsen, J. A. &Akirav, E. M. (2014). Remyelination in multiple sclerosis: Cellular mechanisms and novel therapeutic approaches. *J Neurosci Res*.

Oppenheimer, D. R. (1978). The cervical cord in multiple sclerosis. *Neuropathol Appl Neurobiol* 4(2): 151-162.

Ota, M., Ishikawa, M., Sato, N., Hori, H., Sasayama, D., Hattori, K., Teraishi, T., Nakata, Y. &Kunugi, H. (2012). Glutamatergic changes in the cerebral white matter associated with schizophrenic exacerbation. *Acta Psychiatr Scand*.

Ourselin, S., Roche, A., Prima, S. &Ayache, N. (2000).Block Matching: A General Framework to Improve Robustness of Rigid Registration of Medical Images. In *Medical Image Computing and Computer-Assisted Intervention – MICCAI 2000*, Vol. 1935, 557-566 (Eds S. Delp, A. DiGoia and B. Jaramaz). Springer Berlin Heidelberg.

Ozcan, M. E., Ince, B., Bingol, A., Erturk, S., Altinoz, M. A., Karadeli, H. H., Kocer, A. &Asil, T. (2014). Association between smoking and cognitive impairment in multiple sclerosis. *Neuropsychiatr Dis Treat* 10: 1715-1719.

Ozinga, S. J. &Alberts, J. L. (2014). Quantification of postural stability in older adults using mobile technology. *Exp Brain Res* 232(12): 3861-3872.

Pachter, J. S., de Vries, H. E. &Fabry, Z. (2003). The blood-brain barrier and its role in immune privilege in the central nervous system. *J Neuropathol Exp Neurol* 62(6): 593-604.

Pampliega, O., Domercq, M., Villoslada, P., Sepulcre, J., Rodriguez-Antiguedad, A. &Matute, C. (2008). Association of an EAAT2 polymorphism with higher glutamate concentration in relapsing multiple sclerosis. *J Neuroimmunol* 195(1-2): 194-198.

Pan, J. W., Mason, G. F., Pohost, G. M. &Hetherington, H. P. (1996). Spectroscopic imaging of human brain glutamate by water-suppressed J-refocused coherence transfer at 4.1 T. *Magn Reson Med* 36(1): 7-12.

Patel, T. B. &Clark, J. B. (1979). Synthesis of N-acetyl-L-aspartate by rat brain mitochondria and its involvement in mitochondrial/cytosolic carbon transport. *Biochem J* 184(3): 539-546.

Patt, S. L. &Sykes, B. D. (1972). Water Eliminated Fourier Transform NMR Spectroscopy. *J Chem Phys* 56(6): 3182-3184.

Perneger, T. V. (1998). What's wrong with Bonferroni adjustments. *BMJ* 316(7139): 1236-1238.

Piani, D., Frei, K., Do, K. Q., Cuenod, M. &Fontana, A. (1991). Murine brain macrophages induced NMDA receptor mediated neurotoxicity in vitro by secreting glutamate. *Neurosci Lett* 133(2): 159-162.

Piani, D., Spranger, M., Frei, K., Schaffner, A. &Fontana, A. (1992). Macrophage-induced cytotoxicity of N-methyl-D-aspartate receptor positive neurons involves excitatory amino

acids rather than reactive oxygen intermediates and cytokines. *Eur J Immunol* 22(9): 2429-2436.

Pichiecchio, A., Tavazzi, E., Poloni, G., Ponzio, M., Palesi, F., Pasin, M., Piccolo, L., Tosello, D., Romani, A., Bergamaschi, R., Piccolo, G. &Bastianello, S. (2011). Advanced magnetic resonance imaging of neuromyelitis optica: a multiparametric approach. *Mult Scler.*

Pitt, D., Nagelmeier, I. E., Wilson, H. C. &Raine, C. S. (2003). Glutamate uptake by oligodendrocytes: Implications for excitotoxicity in multiple sclerosis. *Neurology* 61(8): 1113-1120.

Pitt, D., Werner, P. &Raine, C. S. (2000). Glutamate excitotoxicity in a model of multiple sclerosis. *Nat Med* 6(1): 67-70.

Pittas, F., Ponsonby, A. L., van der Mei, I. A., Taylor, B. V., Blizzard, L., Groom, P., Ukoumunne, O. C. &Dwyer, T. (2009). Smoking is associated with progressive disease course and increased progression in clinical disability in a prospective cohort of people with multiple sclerosis. *J Neurol* 256(4): 577-585.

Pittock, S. J., McClelland, R. L., Mayr, W. T., Jorgensen, N. W., Weinshenker, B. G., Noseworthy, J. &Rodriguez, M. (2004). Clinical implications of benign multiple sclerosis: a 20-year population-based follow-up study. *Ann Neurol* 56(2): 303-306.

Plaut, G. S. (1987). Effectiveness of amantadine in reducing relapses in multiple sclerosis. *J R Soc Med* 80(2): 91-93.

Polman, C. H., Reingold, S. C., Banwell, B., Clanet, M., Cohen, J. A., Filippi, M., Fujihara, K., Havrdova, E., Hutchinson, M., Kappos, L., Lublin, F. D., Montalban, X., O'Connor, P., Sandberg-Wollheim, M., Thompson, A. J., Waubant, E., Weinshenker, B. &Wolinsky, J. S. (2011). Diagnostic criteria for multiple sclerosis: 2010 revisions to the McDonald criteria. *Ann Neurol* 69(2): 292-302.

Polman, C. H., Reingold, S. C., Edan, G., Filippi, M., Hartung, H. P., Kappos, L., Lublin, F. D., Metz, L. M., McFarland, H. F., O'Connor, P. W., Sandberg-Wollheim, M., Thompson, A. J., Weinshenker, B. G. &Wolinsky, J. S. (2005). Diagnostic criteria for multiple sclerosis: 2005 revisions to the "McDonald Criteria". *Ann Neurol* 58(6): 840-846.

Poonawalla, A. H., Hou, P., Nelson, F. A., Wolinsky, J. S. &Narayana, P. A. (2008). Cervical Spinal Cord Lesions in Multiple Sclerosis: T1-weighted Inversion-Recovery MR Imaging with Phase-Sensitive Reconstruction. *Radiology* 246(1): 258-264.

Popescu, B. F. &Lucchinetti, C. F. (2012). Pathology of demyelinating diseases. *Annu Rev Pathol* 7: 185-217.

Popescu, B. F., Pirko, I. &Lucchinetti, C. F. (2013). Pathology of multiple sclerosis: where do we stand? *Continuum (Minneap Minn)* 19(4 Multiple Sclerosis): 901-921.

Poser, C. M., Paty, D. W., Scheinberg, L., McDonald, W. I., Davis, F. A., Ebers, G. C., Johnson, K. P., Sibley, W. A., Silberberg, D. H. &Tourtellotte, W. W. (1983). New diagnostic criteria for multiple sclerosis: guidelines for research protocols. *Ann Neurol* 13(3): 227-231.

Pouwels, P. J. &Frahm, J. (1998). Regional metabolite concentrations in human brain as determined by quantitative localized proton MRS. *Magn Reson Med* 39(1): 53-60.

Provencher, S. W. (1993). Estimation of metabolite concentrations from localized in vivo proton NMR spectra. *Magn Reson Med* 30(6): 672-679.

Provencher, S. W. (2001). Automatic quantitation of localized in vivo H-1 spectra with LCModel. *NMR Biomed* 14(4): 260-264.

Provencher, S. W. (2014).LCModel & LCMgui User's Manual. Vol. 2014http://s-provencher.com/pub/LCModel/manual/manual.pdf.

Purcell, E. M., Torrey, H. C. &Pound, R. V. (1946). Resonance Absorption by Nuclear Magnetic Moments in a Solid. *Physical Review* 69(1-2): 37-38.

Raftopoulos, R., Hickman, S., Toosy, A., Wheeler-Kingshott, C., Altmann, D., Mallik, S., Paling, D., Yiannakas, M., Schmierer, K. &Sharrack, B. (2014). OCT, Visual Function and MRI Measures in Acute Optic Neuritis: Baseline Data from a Clinical Trial (P2. 255). *Neurology* 82(10 Supplement): P2. 255-P252. 255.

Ramagopalan, S. V., Hoang, U., Seagroatt, V., Handel, A., Ebers, G. C., Giovannoni, G. &Goldacre, M. J. (2011). Geography of hospital admissions for multiple sclerosis in England and comparison with the geography of hospital admissions for infectious mononucleosis: a descriptive study. *J Neurol Neurosurg Psychiatry* 82(6): 682-687.

Ramagopalan, S. V., Maugeri, N. J., Handunnetthi, L., Lincoln, M. R., Orton, S. M., Dyment, D. A., Deluca, G. C., Herrera, B. M., Chao, M. J., Sadovnick, A. D., Ebers, G. C. &Knight, J. C. (2009). Expression of the multiple sclerosis-associated MHC class II Allele HLA-DRB1*1501 is regulated by vitamin D. *PLoS Genet* 5(2): e1000369.

Ramio-Torrenta, L., Sastre-Garriga, J., Ingle, G. T., Davies, G. R., Ameen, V., Miller, D. H. &Thompson, A. J. (2006). Abnormalities in normal appearing tissues in early primary progressive multiple sclerosis and their relation to disability: a tissue specific magnetisation transfer study. *J Neurol Neurosurg Psychiatry* 77(1): 40-45.

Rashid, W., Davies, G. R., Chard, D. T., Griffin, C. M., Altmann, D. R., Gordon, R., Thompson, A. J. &Miller, D. H. (2006). Increasing cord atrophy in early relapsing-remitting multiple sclerosis: a 3 year study. *J Neurol Neurosurg Psychiatry* 77(1): 51-55.

Raz, N., Lindenberger, U., Rodrigue, K. M., Kennedy, K. M., Head, D., Williamson, A., Dahle, C., Gerstorf, D. &Acker, J. D. (2005). Regional Brain Changes in Aging Healthy Adults: General Trends, Individual Differences and Modifiers. *Cereb Cortex* 15(11): 1676-1689.

Reich, D. S., Ozturk, A., Calabresi, P. A. &Mori, S. (2010). Automated vs. conventional tractography in multiple sclerosis: variability and correlation with disability. *Neuroimage* 49(4): 3047-3056.

Reynolds, R., Roncaroli, F., Nicholas, R., Radotra, B., Gveric, D. &Howell, O. (2011). The neuropathological basis of clinical progression in multiple sclerosis. *Acta Neuropathol* 122(2): 155-170.

Riederer, I., Karampinos, D. C., Settles, M., Preibisch, C., Bauer, J. S., Kleine, J. F., Muhlau, M. &Zimmer, C. (2014). Double Inversion Recovery Sequence of the Cervical Spinal Cord in Multiple Sclerosis and Related Inflammatory Diseases. *AJNR Am J Neuroradiol*.

Rijpkema, M., Schuuring, J., van der Meulen, Y., van der Graaf, M., Bernsen, H., Boerman, R., van der Kogel, A. &Heerschap, A. (2003). Characterization of oligodendrogliomas using short echo time 1H MR spectroscopic imaging. *NMR Biomed* 16(1): 12-18.

Robbins, S., Waked, E. &Mcclaran, J. (1995). Proprioception and Stability - Foot Position Awareness as a Function of Age and Footwear. *Age and Ageing* 24(1): 67-72.

Rothman, K. J. (1990). No Adjustments Are Needed for Multiple Comparisons. *Epidemiology* 1(1): 43-46.

Rothstein, J. D., Martin, L., Levey, A. I., Dykes-Hoberg, M., Jin, L., Wu, D., Nash, N. &Kuncl, R. W. (1994). Localization of neuronal and glial glutamate transporters. *Neuron* 13(3): 713-725.

Rothstein, J. D., Martin, L. J. &Kuncl, R. W. (1992). Decreased glutamate transport by the brain and spinal cord in amyotrophic lateral sclerosis. *N Engl J Med* 326(22): 1464-1468.

Ruggieri, S., Petracca, M., Farrell, C., Howard, J., Riley, C., Fabian, M., Lublin, F. &Inglese, M. (2015). Spinal Cord Atrophy and Clinical Disability in Primary-Progressive MS: A 1-Year Follow-Up Study (P6.167). *Neurology* 84(14 Supplement).

Runmarker, B. &Andersen, O. (1993). Prognostic factors in a multiple sclerosis incidence cohort with twenty-five years of follow-up. *Brain* 116 (Pt 1): 117-134.

Ruthel, G. &Hollenbeck, P. J. (2003). Response of mitochondrial traffic to axon determination and differential branch growth. *J Neurosci* 23(24): 8618-8624.

Sadovnick, A. D., Armstrong, H., Rice, G. P., Bulman, D., Hashimoto, L., Paty, D. W., Hashimoto, S. A., Warren, S., Hader, W., Murray, T. J. &et al. (1993). A population-based study of multiple sclerosis in twins: update. *Ann Neurol* 33(3): 281-285.

Sadovnick, A. D. &Baird, P. A. (1988). The familial nature of multiple sclerosis: age-corrected empiric recurrence risks for children and siblings of patients. *Neurology* 38(6): 990-991.

Sailasuta, N., Ernst, T. &Chang, L. (2008). Regional variations and the effects of age and gender on glutamate concentrations in the human brain. *Magn Reson Imaging* 26(5): 667-675.

Sarchielli, P., Greco, L., Floridi, A. &Gallai, V. (2003). Excitatory amino acids and multiple sclerosis: evidence from cerebrospinal fluid. *Arch Neurol* 60(8): 1082-1088.

Saritas, E. U., Cunningham, C. H., Lee, J. H., Han, E. T. &Nishimura, D. G. (2008). DWI of the spinal cord with reduced FOV single-shot EPI. *Magn Reson Med* 60(2): 468-473.

Sastre-Garriga, J., Ingle, G. T., Chard, D. T., Ramio-Torrenta, L., McLean, M. A., Miller, D. H. &Thompson, A. J. (2005). Metabolite changes in normal-appearing gray and white matter are linked with disability in early primary progressive multiple sclerosis. *Arch Neurol* 62(4): 569-573.

Saunders, D. E., Howe, F. A., van den Boogaart, A., Griffiths, J. R. &Brown, M. M. (1999). Aging of the adult human brain: in vivo quantitation of metabolite content with proton magnetic resonance spectroscopy. *J Magn Reson Imaging* 9(5): 711-716.

Sayao, A. L., Devonshire, V. &Tremlett, H. (2007). Longitudinal follow-up of "benign" multiple sclerosis at 20 years. *Neurology* 68(7): 496-500.

Scalfari, A., Neuhaus, A., Degenhardt, A., Rice, G. P., Muraro, P. A., Daumer, M. &Ebers, G. C. (2010). The natural history of multiple sclerosis: a geographically based study 10: relapses and long-term disability. *Brain* 133(Pt 7): 1914-1929.

Schneider, T., Ciccarelli, O., Kachramanoglou, C., Thomas, D. L. &Wheeler-Kingshott, C. A. M. (2011).Reliability of tract-specific q-space imaging metrics in healthy spinal cord. In *ISMRM*Montreal.

Schneider, T. &Wheeler-Kingshott, C. (2014).Q-Space Imaging: A Model-Free Approach. In *Quantitative MRI of the Spinal Cord*(Eds J. Cohen-Adad and C. Wheeler-Kingshott). Oxford: Elsevier.

Schousboe, A., Westergaard, N., Sonnewald, U., Petersen, S. B., Huang, R., Peng, L. &Hertz, L. (1993). Glutamate and glutamine metabolism and compartmentation in astrocytes. *Dev Neurosci* 15(3-5): 359-366.

Schubert, F., Gallinat, J., Seifert, F. &Rinneberg, H. (2004). Glutamate concentrations in human brain using single voxel proton magnetic resonance spectroscopy at 3 Tesla. *Neuroimage* 21(4): 1762-1771.

Schuff, N., Ezekiel, F., Gamst, A. C., Amend, D. L., Capizzano, A. A., Maudsley, A. A. &Weiner, M. W. (2001). Region and tissue differences of metabolites in normally aged brain using multislice 1H magnetic resonance spectroscopic imaging. *Magn Reson Med* 45(5): 899-907.

Sethi, V., Yousry, T. A., Muhlert, N., Ron, M., Golay, X., Wheeler-Kingshott, C., Miller, D. H. &Chard, D. T. (2012). Improved detection of cortical MS lesions with phase-sensitive inversion recovery MRI. *J Neurol Neurosurg Psychiatry* 83(9): 877-882.

Sharrack, B. &Hughes, R. A. (1996). Clinical scales for multiple sclerosis. *J Neurol Sci* 135(1): 1-9.

Shaw, P. J. &Ince, P. G. (1997). Glutamate, excitotoxicity and amyotrophic lateral sclerosis. *J Neurol* 244 Suppl 2: S3-14.

Silver, N. C., Good, C. D., Sormani, M. P., MacManus, D. G., Thompson, A. J., Filippi, M. &Miller, D. H. (2001). A modified protocol to improve the detection of enhancing brain and spinal cord lesions in multiple sclerosis. *J Neurol* 248(3): 215-224.

Sim, F. J., Zhao, C., Penderis, J. &Franklin, R. J. (2002). The age-related decrease in CNS remyelination efficiency is attributable to an impairment of both oligodendrocyte progenitor recruitment and differentiation. *J Neurosci* 22(7): 2451-2459.

Simmons, M. L., Frondoza, C. G. &Coyle, J. T. (1991). Immunocytochemical localization of N-acetyl-aspartate with monoclonal antibodies. *Neuroscience* 45(1): 37-45.

Siroky, M. B. (2004). The aging bladder. *Rev Urol* 6 Suppl 1: S3-7.

Smith, K. J. (2007). Sodium channels and multiple sclerosis: roles in symptom production, damage and therapy. *Brain Pathol* 17(2): 230-242.

Smith, S. A., Edden, R. A., Farrell, J. A., Barker, P. B. &Van Zijl, P. C. (2008). Measurement of T1 and T2 in the cervical spinal cord at 3 tesla. *Magn Reson Med* 60(1): 213-219.

Smith, S. A., Levante, T. O., Meier, B. H. &Ernst, R. R. (1994). Computer-Simulations in Magnetic-Resonance - an Object-Oriented Programming Approach. *Journal of Magnetic Resonance Series A* 106(1): 75-105.

Soher, B. J., van Zijl, P. C., Duyn, J. H. &Barker, P. B. (1996). Quantitative proton MR spectroscopic imaging of the human brain. *Magn Reson Med* 35(3): 356-363.

Song, S. K., Sun, S. W., Ramsbottom, M. J., Chang, C., Russell, J. &Cross, A. H. (2002). Dysmyelination revealed through MRI as increased radial (but unchanged axial) diffusion of water. *Neuroimage* 17(3): 1429-1436.

Srinivasan, R., Sailasuta, N., Hurd, R., Nelson, S. &Pelletier, D. (2005). Evidence of elevated glutamate in multiple sclerosis using magnetic resonance spectroscopy at 3 T. *Brain* 128(Pt 5): 1016-1025.

Stein, J., Narendran, K., McBean, J., Krebs, K. &Hughes, R. (2007). Electromyography-controlled exoskeletal upper-limb-powered orthosis for exercise training after stroke. *Am J Phys Med Rehabil* 86(4): 255-261.

Stejskal, E. O. &Tanner, J. E. (1965). Spin diffusion measurements - spin echoes in presence of a time-dependent field gradient. *J Chem Phys* 42: 5.

Stevenson, V. L., Gawne-Cain, M. L., Barker, G. J., Thompson, A. J. &Miller, D. H. (1997). Imaging of the spinal cord and brain in multiple sclerosis: a comparative study between fast FLAIR and fast spin echo. *J Neurol* 244(2): 119-124.

Stevenson, V. L., Leary, S. M., Losseff, N. A., Parker, G. J., Barker, G. J., Husmani, Y., Miller, D. H. &Thompson, A. J. (1998). Spinal cord atrophy and disability in MS: a longitudinal study. *Neurology* 51(1): 234-238.

Stevenson, V. L., Miller, D. H., Rovaris, M., Barkhof, F., Brochet, B., Dousset, V., Filippi, M., Montalban, X., Polman, C. H., Rovira, A., de Sa, J. &Thompson, A. J. (1999). Primary and transitional progressive MS: a clinical and MRI cross-sectional study. *Neurology* 52(4): 839-845.

Stover, J. F., Pleines, U. E., Morganti-Kossmann, M. C., Kossmann, T., Lowitzsch, K. &Kempski, O. S. (1997). Neurotransmitters in cerebrospinal fluid reflect pathological activity. *Eur J Clin Invest* 27(12): 1038-1043.

Stys, P. K. &Jiang, Q. (2002). Calpain-dependent neurofilament breakdown in anoxic and ischemic rat central axons. *Neurosci Lett* 328(2): 150-154.

Stys, P. K., Zamponi, G. W., van Minnen, J. &Geurts, J. J. (2012). Will the real multiple sclerosis please stand up? *Nat Rev Neurosci* 13(7): 507-514.

Su, K. G., Banker, G., Bourdette, D. &Forte, M. (2009). Axonal degeneration in multiple sclerosis: the mitochondrial hypothesis. *Curr Neurol Neurosci Rep* 9(5): 411-417.

Svens, B. &Lee, H. (2005). Intra- and inter-instrument reliability of Grip-Strength Measurements: GripTrack™ and Jamar® hand dynamometers. *The British Journal of Hand Therapy* 10(2): 47-55.

Tallantyre, E. C., Bø, L., Al-Rawashdeh, O., Owens, T., Polman, C. H., Lowe, J. S. &Evangelou, N. (2010). Clinico-pathological evidence that axonal loss underlies disability in progressive multiple sclerosis. *Mult Scler* 16(4): 406-411.

Tartaglia, M. C., Narayanan, S., De Stefano, N., Arnaoutelis, R., Antel, S. B., Francis, S. J., Santos, A. C., Lapierre, Y. &Arnold, D. L. (2002). Choline is increased in pre-lesional normal appearing white matter in multiple sclerosis. *J Neurol* 249(10): 1382-1390.

Tartaglino, L. M., Friedman, D. P., Flanders, A. E., Lublin, F. D., Knobler, R. L. &Liem, M. (1995). Multiple sclerosis in the spinal cord: MR appearance and correlation with clinical parameters. *Radiology* 195(3): 725-732.

Taylor, B. V., Pearson, J. F., Clarke, G., Mason, D. F., Abernethy, D. A., Willoughby, E. &Sabel, C. (2010). MS prevalence in New Zealand, an ethnically and latitudinally diverse country. *Mult Scler* 16(12): 1422-1431.

Tench, C. R., Morgan, P. S. &Constantinescu, C. S. (2005). Measurement of cervical spinal cord cross-sectional area by MRI using edge detection and partial volume correction. *J Magn Reson Imaging* 21(3): 197-203.

Thielen, K. R. &Miller, G. M. (1996). Multiple sclerosis of the spinal cord: magnetic resonance appearance. *J Comput Assist Tomogr* 20(3): 434-438.

Thompson, A. J., Kermode, A. G., MacManus, D. G., Kendall, B. E., Kingsley, D. P., Moseley, I. F. &McDonald, W. I. (1990). Patterns of disease activity in multiple sclerosis: clinical and magnetic resonance imaging study. *BMJ* 300(6725): 631-634.

Thompson, A. J., Montalban, X., Barkhof, F., Brochet, B., Filippi, M., Miller, D. H., Polman, C. H., Stevenson, V. L. &McDonald, W. I. (2000a). Diagnostic criteria for primary progressive multiple sclerosis: a position paper. *Ann Neurol* 47(6): 831-835.

Thompson, A. J., Montalban, X., Barkhof, F., Brochet, B., Filippi, M., Miller, D. H., Polman, C. H., Stevenson, V. L. &McDonald, W. I. (2000b). Diagnostic criteria for primary progressive multiple sclerosis:a position paper. *Ann Neurol* 47: 831-835.

Thompson, A. J., Polman, C. H., Miller, D. H., McDonald, W. I., Brochet, B., Filippi, M. M. X. &De Sa, J. (1997). Primary progressive multiple sclerosis. *Brain* 120 (Pt 6): 1085-1096.

Thorpe, J. W., Kidd, D., Kendall, B. E., Tofts, P. S., Barker, G. J., Thompson, A. J., MacManus, D. G., McDonald, W. I. &Miller, D. H. (1993). Spinal cord MRI using multi-array coils and fast spin echo. I. Technical aspects and findings in healthy adults. *Neurology* 43(12): 2625-2631.

Thorpe, J. W., Kidd, D., Moseley, I. F., Kenndall, B. E., Thompson, A. J., MacManus, D. G., McDonald, W. I. &Miller, D. H. (1996). Serial gadolinium-enhanced MRI of the brain and spinal cord in early relapsing-remitting multiple sclerosis. *Neurology* 46(2): 373-378.

Tiberio, M., Chard, D. T., Altmann, D. R., Davies, G., Griffin, C. M., McLean, M. A., Rashid, W., Sastre-Garriga, J., Thompson, A. J. &Miller, D. H. (2006). Metabolite changes in early relapsing-remitting multiple sclerosis. A two year follow-up study. *J Neurol* 253(2): 224-230.

Tkac, I., Andersen, P., Adriany, G., Merkle, H., Ugurbil, K. &Gruetter, R. (2001). In vivo 1H NMR spectroscopy of the human brain at 7 T. *Magn Reson Med* 46(3): 451-456.

Tkac, I., Starcuk, Z., Choi, I. Y. &Gruetter, R. (1999). In vivo H-1 NMR spectroscopy of rat brain at 1 ms echo time. *Magnetic Resonance in Medicine* 41(4): 649-656.

Todd, A. J. (2010). Neuronal circuitry for pain processing in the dorsal horn. *Nature Reviews Neuroscience* 11(12): 823-836.

Trapp, B. D. &Nave, K. A. (2008). Multiple sclerosis: an immune or neurodegenerative disorder? *Annu Rev Neurosci* 31: 247-269.

Trapp, B. D., Peterson, J., Ransohoff, R. M., Rudick, R., Mork, S. &Bo, L. (1998). Axonal transection in the lesions of multiple sclerosis. *N Engl J Med* 338(5): 278-285.

Trapp, B. D. &Stys, P. K. (2009). Virtual hypoxia and chronic necrosis of demyelinated axons in multiple sclerosis. *Lancet Neurol* 8(3): 280-291.

Tremlett, H., Yousefi, M., Devonshire, V., Rieckmann, P. &Zhao, Y. (2009). Impact of multiple sclerosis relapses on progression diminishes with time. *Neurology* 73(20): 1616-1623.

Trop, I., Bourgouin, P. M., Lapierre, Y., Duquette, P., Wolfson, C. M., Duong, H. D. &Trudel, G. C. (1998). Multiple sclerosis of the spinal cord: diagnosis and follow-up with contrast-enhanced MR and correlation with clinical activity. *AJNR Am J Neuroradiol* 19(6): 1025-1033.

Truckenmiller, M. E., Namboodiri, M. A., Brownstein, M. J. &Neale, J. H. (1985). N-Acetylation of L-aspartate in the nervous system: differential distribution of a specific enzyme. *J Neurochem* 45(5): 1658-1662.

Tuch, D. S., Reese, T. G., Wiegell, M. R., Makris, N., Belliveau, J. W. &Wedeen, V. J. (2002). High angular resolution diffusion imaging reveals intravoxel white matter fiber heterogeneity. *Magnetic Resonance in Medicine* 48(4): 577-582.

Tur, C., Wheeler-Kingshott, C. A., Altmann, D. R., Miller, D. H., Thompson, A. J. &Ciccarelli, O. (2014). Spatial variability and changes of metabolite concentrations in the cortico-spinal tract in multiple sclerosis using coronal CSI. *Hum Brain Mapp* 35(3): 993-1003.

Urenjak, J., Williams, S. R., Gadian, D. G. &Noble, M. (1993). Proton nuclear magnetic resonance spectroscopy unambiguously identifies different neural cell types. *J Neurosci* 13(3): 981-989.

Vaithianathar, L., Tench, C. R., Morgan, P. S. &Constantinescu, C. S. (2003). Magnetic resonance imaging of the cervical spinal cord in multiple sclerosis--a quantitative T1 relaxation time mapping approach. *J Neurol* 250(3): 307-315.

van Horssen, J., Witte, M. E. &Ciccarelli, O. (2012). The role of mitochondria in axonal degeneration and tissue repair in MS. *Mult Scler* 18(8): 1058-1067.

van Waesberghe, J. H., Kamphorst, W., De Groot, C. J., van Walderveen, M. A., Castelijns, J. A., Ravid, R., Lycklama a Nijeholt, G. J., van der Valk, P., Polman, C. H., Thompson, A. J. &Barkhof, F. (1999). Axonal loss in multiple sclerosis lesions: magnetic resonance imaging insights into substrates of disability. *Ann Neurol* 46(5): 747-754.

Vavasour, I., Laule, C., Hodgson, M., Li, D., Traboulsee, A., Maedler, B. &MacKay, A. (2011).Reversible NAA decreases in active MS lesions are not due solely to water content changes. In *Proc. Intl. Soc. Mag. Reson. Med*Montreal.

Vladimirova, O., O'Connor, J., Cahill, A., Alder, H., Butunoi, C. &Kalman, B. (1998). Oxidative damage to DNA in plaques of MS brains. *Mult Scler* 4(5): 413-418.

Vos, C. M., Geurts, J. J., Montagne, L., van Haastert, E. S., Bo, L., van der Valk, P., Barkhof, F. &de Vries, H. E. (2005). Blood-brain barrier alterations in both focal and diffuse abnormalities on postmortem MRI in multiple sclerosis. *Neurobiol Dis* 20(3): 953-960.

Vukusic, S., Van Bockstael, V., Gosselin, S. &Confavreux, C. (2007). Regional variations in the prevalence of multiple sclerosis in French farmers. *J Neurol Neurosurg Psychiatry* 78(7): 707-709.

Wandinger, K., Jabs, W., Siekhaus, A., Bubel, S., Trillenberg, P., Wagner, H., Wessel, K., Kirchner, H. &Hennig, H. (2000). Association between clinical disease activity and Epstein-Barr virus reactivation in MS. *Neurology* 55(2): 178-184.

Weinshenker, B. G. (1994). Natural history of multiple sclerosis. *Ann Neurol* 36 Suppl: S6-11.

Weinshenker, B. G., Bass, B., Rice, G. P., Noseworthy, J., Carriere, W., Baskerville, J. &Ebers, G. C. (1989). The natural history of multiple sclerosis: a geographically based study. I. Clinical course and disability. *Brain* 112 (Pt 1): 133-146.

Werner, P., Pitt, D. &Raine, C. S. (2000). Glutamate excitotoxicity--a mechanism for axonal damage and oligodendrocyte death in Multiple Sclerosis? *J Neural Transm Suppl* (60): 375-385.

Werner, P., Pitt, D. &Raine, C. S. (2001). Multiple sclerosis: altered glutamate homeostasis in lesions correlates with oligodendrocyte and axonal damage. *Ann Neurol* 50(2): 169-180.

Werring, D. J., Clark, C. A., Barker, G. J., Thompson, A. J. &Miller, D. H. (1999). Diffusion tensor imaging of lesions and normal-appearing white matter in multiple sclerosis. *Neurology* 52(8): 1626-1632.

Wheeler-Kingshott, C. A., Hickman, S. J., Parker, G. J., Ciccarelli, O., Symms, M. R., Miller, D. H. &Barker, G. J. (2002). Investigating cervical spinal cord structure using axial diffusion tensor imaging. *Neuroimage* 16(1): 93-102.

Wheeler-Kingshott, C. A., Stroman, P. W., Schwab, J. M., Bacon, M., Bosma, R., Brooks, J., Cadotte, D. W., Carlstedt, T., Ciccarelli, O., Cohen-Adad, J., Curt, A., Evangelou, N., Fehlings, M. G., Filippi, M., Kelley, B. J., Kollias, S., Mackay, A., Porro, C. A., Smith, S., Strittmatter, S. M., Summers, P., Thompson, A. J. &Tracey, I. (2014). The current state-of-the-art of spinal cord imaging: Applications. *Neuroimage* 84: 1082-1093.

Wheeler-Kingshott, C. A. M., Barker, G. J., Steens, S. C. A. &van Buchem, M. A. (2003).D: the Diffusion of Water

In *Quantitative MRI of the Brain*

(Ed P. Toft). Chichester, England: John Wiley & Sons Ltd.
Williams &Warwick *Gray's Anatomy*. Churchill Livingstone.

Wilm, B. J., Svensson, J., Henning, A., Pruessmann, K. P., Boesiger, P. &Kollias, S. S. (2007). Reduced field-of-view MRI using outer volume suppression for spinal cord diffusion imaging. *Magnetic Resonance in Medicine* 57(3): 625-630.

Witte, M. E., Bo, L., Rodenburg, R. J., Belien, J. A., Musters, R., Hazes, T., Wintjes, L. T., Smeitink, J. A., Geurts, J. J., De Vries, H. E., van der Valk, P. &van Horssen, J. (2009). Enhanced number and activity of mitochondria in multiple sclerosis lesions. *J Pathol* 219(2): 193-204.

Wolfson, L., Whipple, R., Amerman, P. &Tobin, J. N. (1990). Gait Assessment in the Elderly - a Gait Abnormality Rating-Scale and Its Relation to Falls. *Journals of Gerontology* 45(1): M12-M19.

Wood, E. T., Ronen, I., Techawiboonwong, A., Jones, C. K., Barker, P. B., Calabresi, P., Harrison, D. &Reich, D. S. (2012). Investigating axonal damage in multiple sclerosis by diffusion tensor spectroscopy. *J Neurosci* 32(19): 6665-6669.

Wu, Y. C., Field, A. S., Duncan, I. D., Samsonov, A. A., Kondo, Y., Tudorascu, D. &Alexander, A. L. (2011). High b-value and diffusion tensor imaging in a canine model of dysmyelination and brain maturation. *Neuroimage* 58(3): 829-837.

Yiannakas, M. C., Kearney, H., Samson, R. S., Chard, D. T., Ciccarelli, O., Miller, D. H. &Wheeler-Kingshott, C. A. (2012). Feasibility of grey matter and white matter segmentation of the upper cervical cord in vivo: A pilot study with application to magnetisation transfer measurements. *Neuroimage* 63(3): 1054-1059.

Zackowski, K. M., Smith, S. A., Reich, D. S., Gordon-Lipkin, E., Chodkowski, B. A., Sambandan, D. R., Shteyman, M., Bastian, A. J., van Zijl, P. C. &Calabresi, P. A. (2009). Sensorimotor dysfunction in multiple sclerosis and column-specific magnetization transfer-imaging abnormalities in the spinal cord. *Brain* 132(Pt 5): 1200-1209.

Zahr, N. M., Mayer, D., Pfefferbaum, A. &Sullivan, E. V. (2008). Low striatal glutamate levels underlie cognitive decline in the elderly: Evidence from in vivo molecular spectroscopy. *Cereb Cortex* 18(10): 2241-2250.

Zahr, N. M., Mayer, D., Rohlfing, T., Chanraud, S., Gu, M., Sullivan, E. V. &Pfefferbaum, A. (2013). In vivo glutamate measured with magnetic resonance spectroscopy: behavioral correlates in aging. *Neurobiol Aging* 34(4): 1265-1276.

Zeman, A. Z., Kidd, D., McLean, B. N., Kelly, M. A., Francis, D. A., Miller, D. H., Kendall, B. E., Rudge, P., Thompson, E. J. &McDonald, W. I. (1996). A study of oligoclonal band negative multiple sclerosis. *J Neurol Neurosurg Psychiatry* 60(1): 27-30.

Zivadinov, R., Weinstock-Guttman, B., Hashmi, K., Abdelrahman, N., Stosic, M., Dwyer, M., Hussein, S., Durfee, J. &Ramanathan, M. (2009). Smoking is associated with increased lesion volumes and brain atrophy in multiple sclerosis. *Neurology* 73(7): 504-510.

Zlotnik, A., Gruenbaum, B. F., Mohar, B., Kuts, R., Gruenbaum, S. E., Ohayon, S., Boyko, M., Klin, Y., Sheiner, E., Shaked, G., Shapira, Y. &Teichberg, V. I. (2011). The effects of estrogen and progesterone on blood glutamate levels: evidence from changes of blood glutamate levels during the menstrual cycle in women. *Biol Reprod* 84(3): 581-586.